

Eocene Potassic Magmatism of the Milk River Area, Southern Alberta (NTS 72E) and Sweet Grass Hills, Northern Montana: Overview and New Data on Mineralogy, Geochemistry, Petrology and Economic Potential

Eocene Potassic Magmatism of the Milk River Area, Southern Alberta (NTS 72E) and Sweet Grass Hills, Northern Montana: Overview and New Data on Mineralogy, Geochemistry, Petrology and Economic Potential

A.S. Rukhlov¹ and J.G. Pawlowicz²

¹ British Columbia Geological Survey
(formerly of Alberta Geological Survey)

² Energy Resources Conservation Board
Alberta Geological Survey

March 2012

©Her Majesty the Queen in Right of Alberta, 2012
ISBN 978-1-4601-0073-8

Energy Resources Conservation Board/Alberta Geological Survey (ERCB/AGS) and its employees and contractors make no warranty, guarantee or representation, express or implied, or assume any legal liability regarding the correctness, accuracy, completeness or reliability of this publication. Any software supplied with this publication is subject to its licence conditions. Any references to proprietary software in the documentation, and/or any use of proprietary data formats in this release, do not constitute endorsement by ERCB/AGS of any manufacturer's product.

If you use information from this publication in other publications or presentations, please give due acknowledgement to ERCB/AGS. We recommend the following reference format:

Rukhlov, A.S. and Pawlowicz, J.G. (2012): Eocene potassic magmatism of the Milk River area, southern Alberta (NTS 72E) and Sweet Grass Hills, northern Montana: overview and new data on mineralogy, geochemistry, petrology and economic potential; Energy Resources Conservation Board, ERCB/AGS Open File Report 2012-01, 88 p.

External author address:

British Columbia Geological Survey
5th Floor, 1810 Blanshard Street
Victoria, BC V8W 9N3

Published March 2012 by:

Energy Resources Conservation Board
Alberta Geological Survey
4th Floor, Twin Atria Building
4999 – 98th Avenue
Edmonton, AB T6B 2X3
Canada

Tel: 780.422.1927
Fax: 780.422.1918
E-mail: AGS-Info@ercb.ca
Website: www.ags.gov.ab.ca

Contents

Acknowledgements.....	vi
Abstract.....	vii
1 Introduction.....	1
2 Previous Studies.....	3
3 Geology and Tectonic Setting.....	4
3.1 Study Area.....	4
3.2 Regional Tectonic Setting.....	5
4 Analytical Methods.....	9
5 Sample Location and Description.....	9
5.1 Forty-Ninth Parallel Dike Swarm (Site SG01).....	9
5.2 Coulee 29 Vent Complex (Site SG02).....	11
5.3 Philp Coulee Dike (Site SG03).....	13
5.4 Black Butte Plug (Site SG04).....	13
5.5 Bear Creek Dike (Site SG05).....	13
5.6 Grassy Butte Felsite Breccia (Site SG06).....	14
5.7 Gold Butte Dike Swarm (Site SG07).....	17
6 Mineral Chemistry.....	17
6.1 Mica.....	17
6.2 Amphibole.....	21
6.3 Clinopyroxene.....	21
6.4 Feldspar.....	21
6.5 Analcime.....	23
6.6 Spinel.....	23
6.7 Ilmenite.....	23
6.8 Apatite.....	23
6.9 Other Minerals.....	24
7 Whole-Rock Geochemistry.....	24
7.1 Igneous Rocks.....	24
7.2 Geochemical Signatures of Mineralization.....	30
8 Discussion.....	33
8.1 Classification of Igneous Rocks.....	33
8.2 Mantle Sources and Primary Magmas.....	35
8.3 Fractional Crystallization and Crustal Assimilation.....	38
8.4 Economic Potential of Potassic Rocks of the Milk River Area.....	46
9 Conclusions.....	47
10 References.....	49
Appendices.....	58
Appendix 1 – Sample Locations and Descriptions.....	58
Appendix 2 – Whole-Rock Geochemical Analytical Methods.....	60
Appendix 3 – Whole-Rock Sample Preparation and Geochemical Data Quality.....	61
Appendix 4 – Whole-Rock Geochemical Data.....	63
Appendix 5 – Quantitative Mineralogical Analytical Techniques.....	77
Appendix 6 – Quantitative Mineralogical Data.....	78
Appendix 7 – Electron Microprobe Analytical Techniques.....	80
Appendix 8 – Electron Microprobe Data.....	81
Appendix 9 – Trace-Element Modelling Methodology.....	88

Tables

Table 1. Global Positioning System locations of sample sites in the Milk River area of southern Alberta and Sweet Grass Hills of northern Montana.....	10
Table 2. Representative whole-rock analyses of magmatic rocks from the Milk River area of southern Alberta and the Sweet Grass Hills of northern Montana.....	25
Table 3. Concentrations of selected elements in magmatic, hydrothermal and adjacent sedimentary rocks of the Milk River area, southern Alberta.....	31
Table 4. Concentrations of selected elements in Eocene intrusions and adjacent sedimentary rocks of the Sweet Grass Hills, northern Montana.....	32
Table 5. Least-squares, mass-balance models of fractional crystallization and crustal assimilation for the Sweet Grass Hills igneous complex.....	42
Table 6. Compilation of published trace-element mineral/melt distribution coefficients for potassic magmas.....	45

Figures

Figure 1. Simplified bedrock geology of the Milk River area in southern Alberta and the Sweet Grass Hills in northern Montana, showing rock-sample sites.....	2
Figure 2. Bedrock geology of the Coulee 29 vent-intrusive complex (site SG02) in the Milk River area...	6
Figure 3. Lithostratigraphic correlation chart of the Mississippian, Jurassic and Cretaceous strata exposed in the study area of southeastern Alberta and northern Montana.....	7
Figure 4. Forty-Ninth Parallel dike (site SG01).....	10
Figure 5. Coulee 29 vent-intrusive complex (site SG02).....	12
Figure 6. Black Butte plug (site SG04).....	14
Figure 7. Bear Creek dike (site SG05).....	15
Figure 8. Grassy Butte felsite breccia (site SG06), northern Montana.....	16
Figure 9. Gold Butte (site SG07), northern Montana.....	18
Figure 10. Analytical results for phlogopite-annite from the 49 th Parallel dike (sample 8151).....	19
Figure 11. Variations of Al ₂ O ₃ versus FeO _t and Al ₂ O ₃ versus TiO ₂ for phlogopite-annite in intrusive rocks of the Milk River area, compared with those of micas from lamproites, minettes and other ultrapotassic rocks.....	20
Figure 12. Compositions and nomenclature for pyroxene and feldspar from igneous rocks of the Milk River area and Sweet Grass Hills.....	22
Figure 13. Whole-rock concentrations of SiO ₂ , TiO ₂ , Al ₂ O ₃ , MnO, CaO, Na ₂ O, K ₂ O and P ₂ O ₅ versus Mg# for igneous rocks from the Milk River area and Sweet Grass Hills.....	27
Figure 14. Whole-rock concentrations of selected trace elements versus Mg# for igneous rocks from the Milk River area and Sweet Grass Hills.....	28
Figure 15. Normalized whole-rock patterns for representative analyses of igneous rocks from the Milk River area and Sweet Grass Hills.....	29
Figure 16. Whole-rock chemical classification of magmatic rocks in the Milk River area of southern Alberta and the Sweet Grass Hills of northern Montana.....	34
Figure 17. Plot of whole-rock Ni versus MgO for igneous rocks and ultramafic xenoliths of the Milk River area and Sweet Grass Hills.....	36
Figure 18. Normative compositions of igneous rocks from the Milk River area and Sweet Grass Hills projected onto the anhydrous base of the tetrahedron NaAlSiO ₄ -KAlSiO ₄ -SiO ₂ -H ₂ O.....	38
Figure 19. Compositions of igneous rocks from the Milk River area and Sweet Grass Hills plotted in terms of normative KAlSiO ₄ -Mg ₂ SiO ₄ -SiO ₂	40
Figure 20. Compositions of potassic igneous rocks from the Milk River area and Sweet Grass Hills projected from kalsilite onto the augite-olivine-sanidine pseudo-ternary plane in the system KAlSiO ₄ -Mg ₂ SiO ₄ -CaMgSi ₂ O ₆ -SiO ₂ -H ₂ O, with phase boundaries at various pressures.....	41

Figure 21. Two-stage, least-squares mass-balance model of fractional crystallization–crustal assimilation in the Sweet Grass Hills igneous complex.....43

Figure 22. Whole-rock concentration plots of Ni versus Co, Co versus Ce, Nb versus Ni and Rb versus Co for igneous rocks of the Milk River area and Sweet Grass Hills, showing calculated trends for two-stage fractional crystallization and assimilation–fractional crystallization processes.....46

Acknowledgements

We are grateful to P. Glombick, A.R. Chakhmouradian (University of Manitoba), S.V. Matveev (University of Alberta), R. Mussieux (Royal Alberta Museum), L.N. Smith (Montana Bureau of Mines and Geology) and L.B. Vanhill (Sandswamp Exploration Ltd.) for valuable discussions.

S.V. Matveev provided expertise and help with the microprobe analyses. A.P. Beaton provided management support and participated in the 2008 fieldwork. L. White helped with the literature and land-use search. D.K. Chao, K. Mckay and R. Elgr helped with the spatial data.

Alberta Tourism, Parks and Recreation granted the authors a Research and Collection Permit (RC-08SE-025) to carry out field investigations and sampling in the Milk River Natural Area in 2008. We also thank Pinhorn Grazing Association, C. Wallace of Milk River Management Society, J.A. Ross, B. Johnson, W. Brower, L. Finstad, R. Kunzli, C. Kunzli, R. Pearson, E. Fritz and M. Wickem for assistance and permissions to access private roads and lands. Constructive reviews of the report by D.I. Pană, G.J. Prior and K. Bell (Carleton University), and editorial handling by B. Davie of RnD Technical led to significant improvements.

Abstract

This report presents an overview of previous data and new whole-rock geochemical, quantitative mineralogical and electron-microprobe analyses for the Eocene potassic intrusions, related hydrothermal veins and Cretaceous sedimentary rocks adjacent to the magmatic bodies of the Milk River area of southern Alberta and the Sweet Grass Hills of northern Montana. The rock samples were collected during 2008 and 2009 fieldwork from five sites in the Milk River area and two sites in the Sweet Grass Hills. The outcrops examined in the Sweet Grass Hills are known metallic mineral occurrences associated with the Eocene intrusions. We discuss the geology, mineralogy, geochemistry, petrology and economic potential of these outcrops.

Based on new petrological, mineralogical and geochemical evidence, we suggest that the ultrapotassic peralkaline rock-forming dikes at the 49th Parallel locality in the Milk River area can be classified as sanidine-phlogopite lamproite. Lamproites have not been previously recognized in Alberta, although these rocks are known to be associated with lamprophyres and kimberlites in Montana, Wyoming, Colorado, Utah, Kansas and Arizona. Other potassic intrusions and volcanic rocks exposed in the Milk River area include alkali olivine minettes, diopside-phlogopite trachyte and amphibole latite. We propose a petrogenetic model in which latite, trachyte and high-K rhyolite of the Sweet Grass Hills igneous complex originate by fractional crystallization of parent olivine minette magma through settling of primary minerals observed as phenocrysts. Major-element mass-balance and trace-element models, coupled with published Sr, Pb and Nd isotopic data, rule out any significant assimilation of crustal material by the ultrapotassic magma at Sweet Grass Hills. In the Milk River area, olivine minettes and lamproite that is more enriched in incompatible elements represent primary magmas generated by partial melting of a heterogeneous mantle, enriched in potassium, rare-earth and other incompatible elements, in equilibrium with olivine, phlogopite and clinopyroxene.

Porphyry to epithermal-style mineralization related to the intermediate and felsic intrusions of the Sweet Grass Hills is associated with potassic, propylitic, argillic and supergene alteration, similar to metallic deposits related to alkalic intrusions elsewhere in Montana. The more primitive ultrapotassic rocks of the Milk River area are associated with weak alteration and erratic precious- and base-metal mineralization. The new results aid our understanding of the nature and origin of the potassic magmatism and its economic potential in the Milk River area of southern Alberta. Recognition of the first lamproite occurrence in Alberta is important because these magmas originate from specific mantle sources and can carry diamonds.

1 Introduction

The Energy Resources Conservation Board/Alberta Geological Survey (ERCB/AGS) initiated a project in 2008 to better understand the geology and mineral resources of southern Alberta. This study examines the Eocene igneous complex that straddles the Canada–United States border and comprises intermediate to felsic intrusions in the Sweet Grass Hills of northern Montana and seven known exposures of potassic dikes, small plugs and a vent-intrusive complex in the Milk River area of southern Alberta (e.g., Dawson, 1884; Kjarsgaard, 1994; Buhlmann et al., 2000). The Sweet Grass Hills igneous complex marks the northern extent of the Late Cretaceous–Oligocene (69–27 Ma) Montana alkaline province (Pirsson, 1905; Larsen, 1940; Currie, 1976; Hearn et al., 1978; Marvin et al., 1980; Irving and O’Brien, 1991; Irving and Hearn, 2003; Figure 1).

In addition to significant oil, gas and coal production on both sides of the border, precious-metal mining took place in the Sweet Grass Hills during the mid-1900s (Gavin, 1991; Lopez, 1995). Between 1934 and 1942, the Gold Butte placer-gold mine produced 42.3 kg of gold and 2.7 kg silver from the pediment and alluvial gravels derived from the northwestern flank of Middle Butte (Figure 1; Gavin, 1991; Lopez, 1995). In addition, about 1.8 tonnes of ore grading 64.8 ppm Au were produced from a lode-gold mine about 0.8 km to the east in 1932 (Lopez, 1995). More recent exploration identified the presence of several styles of porphyry to epithermal precious- and base-metal mineralization at East, Middle, West and Grassy buttes of the Sweet Grass Hills, with grades up to 157.7 ppm Au and Au:Ag ratios of about 1:1 (Gavin, 1991). Elsewhere in the Montana alkaline province, the Zortman and Landusky epithermal-gold mining camps associated with the Little Rocky Mountains syenite porphyry intrusive complex (Figure 1) produced about 38 880 kg of gold, with the current open-pit operation extracting about 10 million tonnes per year grading 0.5–0.7 ppm Au (Russell, 1991).

Despite the evidence for gold, silver, copper, lead, fluorite and magnetite associated with the Sweet Grass Hills intrusive complex and other igneous complexes of the Montana alkaline province, mineral potential of the coeval igneous rocks in southern Alberta remained unknown until the early 1990s. Although initial exploration indicated the presence of precious-metal mineralization associated with some of the Eocene intrusions in the Milk River area (Lau and Dudek, 1991), the subsequent exploration concentrated mainly on diamond potential (Burwash and Nelson, 1992; Williams, 1993; Walker, 1994).

Most of the potassic igneous rocks in the Milk River area are mica-rich lamprophyre, classified by Kjarsgaard (1994, 1997) as alkali and peralkaline minettes. However, ultrapotassic peralkaline dikes at the 49th Parallel locality (Figure 1) are quite different from other igneous rocks of the Milk River area, their mineral assemblages and whole-rock and mineral compositions being similar to those of lamproites. Kjarsgaard (1994, 1997) pointed out the problematic classification of these rocks, which cannot be discriminated from minettes based on their modal composition. However, lamproites can be positively distinguished from other potassic rocks on the basis of mineral proportions in conjunction with mineral chemistry, presence of diagnostic minerals and whole-rock geochemistry (Mitchell and Bergman, 1991; Peterson, 1996).

Buhlmann et al. (2000) proposed a model in which evolved minettes of the Milk River area could have derived from primitive olivine minette magma by high-pressure fractionation of an apatite-mica-clinopyroxene assemblage, observed in some of these rocks as ultramafic nodules, with removal of olivine at a lower pressure. However, this model does not explain 1) the origin of intermediate and felsic rocks in the Sweet Grass Hills igneous complex, 2) the differing mineralogy of the 49th Parallel dikes and the minettes, 3) the strong enrichment of the 49th Parallel dikes in light rare-earth and other incompatible elements relative to the minettes, and 4) the differing Sr, Pb and Nd isotopic ratios in the minettes and the 49th Parallel dikes.

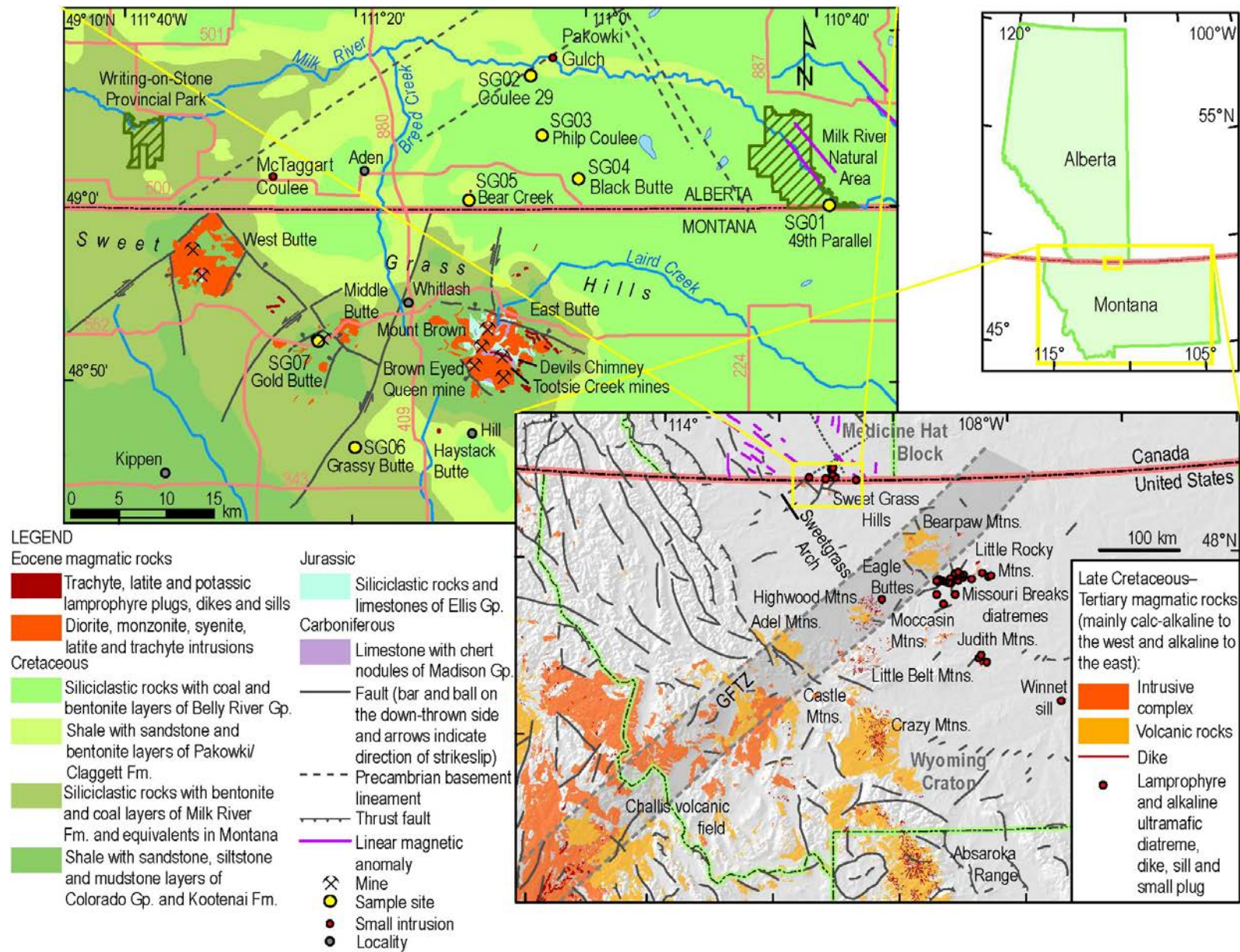


Figure 1. Simplified bedrock geology of the Milk River area in southern Alberta and the Sweet Grass Hills in northern Montana (modified from Okulitch et al., 1996; Hamilton et al., 1999; Lopez, 2002), showing rock-sample sites. Locations of the Sweet Grass Hills mines are after Gavin (1991) and Lopez (1995). Inset map shows the location of the study area (rectangle). The Late Cretaceous–Oligocene magmatic rocks, Precambrian basement, Great Falls Tectonic Zone (GFTZ) and other tectonic features of the northwestern United States and southwestern Canada are after Haites and van Hees (1962), Ozoray (1972), Herbaly (1974), O'Neill and Lopez (1985), Hearn (1989), Ross et al. (1991), Lopez (1995, 2002), Lemieux et al. (2005), Massey et al. (2005), Stoesser et al. (2005) and Vuke et al. (2007). Linear magnetic anomalies in southern Alberta are after Ross et al. (1997); shaded relief after United States Geological Survey (1996). See Table 1 and Appendix 1 for a list of all sites and samples, and Appendix 2 for types of analyses.

This report presents new whole-rock geochemical, quantitative mineralogical and electron-microprobe analyses of rock samples collected during 2008 and 2009 field programs from outcrops of the magmatic rocks, the related hydrothermally altered rocks, and the Cretaceous sedimentary rocks adjacent to the magmatic bodies of the Milk River area and Sweet Grass Hills (Appendices 1, 4, 6 and 8). We revise the nomenclature of the potassic rocks in this area on the basis of mineralogical and geochemical criteria (Mitchell and Bergman, 1991; Peterson, 1996) and discuss their petrogenesis and mineral potential in light of the previously published and new data.

2 Previous Studies

Eocene magmatic rocks of the Milk River area in southern Alberta were originally described, in the early 1870s (Dawson, 1884), as ‘mica traps’ subordinate to the intrusions of the Sweet Grass Hills in northern Montana. These rocks have received much attention during subsequent geological work in the area (e.g., Weed and Pirsson, 1895; Kemp and Billingsley, 1921; Williams and Dyer, 1930; Russell and Landes, 1940; Truscott, 1975; Currie, 1976; Hearn et al., 1978; Gavin, 1991; Burwash and Nelson, 1992; Ash, 1993; Cavell et al., 1993; Williams, 1993; Kjarsgaard, 1994, 1997; Kjarsgaard and Davis, 1994; 1996; Lopez, 1995, 2002; Carlson, 1999; Buhlmann et al., 2000). Various authors referred to mica-rich lamprophyres of the Milk River area as ‘minettes,’ ‘potassic olivine basalts,’ ‘lamproites’ and ‘rocks of lamproitic to kamafugitic affinity,’ reflecting a problematic classification of these rocks.

Kjarsgaard (1994) examined the geology, petrography, mineralogy and geochemistry of igneous rocks in the Milk River area and recognized volcanic and epiclastic rocks in a vent-intrusive complex at the Coulee 29 locality (Figure 1). He described the majority of the mica-rich rocks as alkali minettes, which are similar to olivine minettes of the Bearpaw and Highwood mountains in Montana (O’Brien et al., 1991, 1995; Macdonald et al., 1992). Kjarsgaard (1994, 1997) also classified the ultrapotassic dikes at the 49th Parallel locality (Figure 1) as ‘peralkaline minette,’ despite their distinctive mineralogical and geochemical attributes that are typical of lamproites.

Baadsgaard et al. (1961) reported a K-Ar date of 49.2 ± 2.5 Ma for minette from Black Butte, and Davis and Kjarsgaard (1994) obtained a similar Rb-Sr isochron date of 50.3 ± 0.5 Ma for an olivine minette dike from the Coulee 29 locality (Figure 1). More recently, Buhlmann et al. (2000) reported Rb-Sr isochron dates of 49.0 ± 0.8 Ma and 52.0 ± 1.7 Ma for mica clinopyroxenite inclusions, and a Rb-Sr model date of 50.0 ± 0.3 Ma for a late-stage minette dike from Coulee 29. These correspond, within the uncertainties, to the established radiometric age of 54–50 Ma for the Sweet Grass Hills intrusive complex (Currie, 1976; Hearn et al., 1978; Marvin et al., 1980).

Noranda Exploration Co. Ltd. performed the first reported metal exploration in the Milk River area, involving prospecting, magnetic and lithochemical surveys (Lau and Dudek, 1991). The results indicated erratic but highly anomalous Au concentrations (up to 5.70 ppm Au and 0.4 ppm Ag in a pan concentrate and 65 ppb Au in soil samples), along with evidence of hydrothermal brecciation, manganese and barium enrichment, and alteration of the Late Cretaceous calcareous mudstone near the Bear Creek locality (Figure 1) that are similar to epithermal systems elsewhere (Lau and Dudek, 1991).

Subsequent exploration, however, focused on diamond potential of the Eocene magmatic rocks in the Milk River area (Burwash and Nelson, 1992; Williams, 1993; Walker, 1994). This was due to the discoveries of diamondiferous kimberlites in Saskatchewan and Northwest Territories in the late 1980s to early 1990s, which led to a province-wide staking rush in Alberta (e.g., Dufresne et al., 1996). Kjarsgaard (1997) considered whole-rock and mineral chemistry of the Milk River minettes to be consistent with possible magma derivation from the diamond-stability field in the mantle. However, he pointed out that the inferred Middle Proterozoic tectonothermal and metasomatic overprinting of the lithospheric mantle beneath the Archean Medicine Hat and Wyoming basement (e.g., Dudás et al., 1987; Hearn et al., 1991;

Cavell et al., 1993; Davis et al., 1995; Buhlmann et al., 2000) might have affected diamond preservation (Kjarsgaard, 1997).

Consolidated Pine Channel Gold Corp. performed a soil lithochemical survey to investigate two separate ground-magnetic ‘bull’s-eye’ anomalies, previously identified by Noranda Exploration Co. Ltd., and analyzed three rock samples from a minette dike at Bear Creek (Figure 1; Williams, 1993). The results indicated slightly elevated concentrations of up to 11 ppm As, 6 ppm Sb and 0.8 ppm Cd for soil samples, and up to 165 ppm Zn, 105 ppm Cu, 86 ppm Pb, 0.9 ppm Ag, 8 ppm Sn, 5 ppm Sb and 1.0 ppm Cd for the dike (Williams, 1993).

Marum Resources Inc. carried out an exploration program in the Milk River area that involved an airborne geophysical survey, a lithochemical survey and diamond-indicator mineral studies (Walker, 1994). Whole-rock and mineral chemistry of some of the mica lamprophyre bodies were interpreted to be transitional between minettes and lamproites, with samples of magmatic and sedimentary host rocks containing up to 8 ppb Au, 198 ppm Zn, 126 ppm Cu, 125 ppm Pb, 41 ppm As, 4 ppm W and 1.5 ppm Sb (Walker, 1994). In addition, pyrite, pyrrhotite and rare visible gold grains were identified in the heavy-mineral concentrates from the Coulee 29 and Pakowki Gulch localities (Figure 1). A composite sample from the latter assayed up to 1.20 ppm Au, thus confirming the presence of erratic gold mineralization associated with the Eocene magmatic rocks in the Milk River area (Walker, 1994).

Kjarsgaard (1994) and Buhlmann et al. (2000) reported geochemical analyses of magmatic rocks and ultramafic xenoliths from the Milk River area that indicated low concentrations of precious metals, with maximum values of 6 ppb Au and 12 ppb Ir. However, the sedimentary rocks, adjacent to the magmatic bodies, were not analyzed. These publications also provide electron-microprobe and isotopic (C-O and Sr-Pb-Nd, respectively) analyses of rocks and minerals from the Milk River area.

3 Geology and Tectonic Setting

3.1 Study Area

Figure 1 shows the simplified bedrock geology of the Milk River area in southern Alberta and the Sweet Grass Hills in northern Montana, as well as major tectonic features on a regional scale. Bedrock exposure is restricted mainly to buttes of the Sweet Grass Hills and slopes of meltwater and modern drainage channels. Glacial sediments deposited from the Laurentide Ice Sheet cover much of the study area to an altitude of about 1460 m above sea level and form flat, undulating, hummocky and ridged topography. They are composed mainly of till up to 30 m thick and local water-sorted material (Shetsen, 1987; Lopez, 1995, 2002; Vuke et al., 2007). Fluvial deposits occur on floors and terraces of river valleys and meltwater channels. Pediment gravel deposits are common on buttes of the Sweet Grass Hills and landslide deposits occur in areas with steep slopes (Lopez, 1995).

The Eocene (54–49 Ma) Sweet Grass Hills igneous complex is emplaced into the Phanerozoic strata of the Western Canada Sedimentary Basin (WCSB) underlain by the Archean (3.28–2.61 Ga) Medicine Hat crystalline basement, to the east of the Cordilleran fold-and-thrust belt (Figure 1; Marvin et al., 1980; Ross et al., 1991; Villeneuve et al., 1993; Lopez, 1995; Buhlmann et al., 2000; Vuke et al., 2007). Most of the complex comprises partly eroded laccoliths and stocks, composed of porphyritic monzonite, diorite, syenite, trachyte and felsite breccia, that form the core of several prominent buttes in the Sweet Grass Hills of northern Montana. Numerous dikes, sills and small plugs of potassic lamprophyres, latites and trachytes crosscut the earlier intrusions and extend to the north, into the Milk River area of southern Alberta.

In the Milk River area, most of these intrusive rocks are phlogopite rich with variable proportions of calcite, analcime, apatite and oxides (\pm olivine \pm diopside \pm magnesite \pm sanidine phenocrysts). A feldspar- and hornblende-phyric latite, previously described as ‘porphyritic andesite,’ ‘diorite porphyry’ and

'benmoreite' (Williams and Dyer, 1930; Russell and Landes, 1940; Kjarsgaard, 1994, 1997; Buhlmann et al., 2000), forms a plug at McTaggart Coulee (Figure 1). Kjarsgaard (1994, 1997) classified the mica-rich rocks as alkali to peralkaline minettes and compared them with olivine minettes from the Bearpaw and Highwood mountains of Montana and the diamondiferous Akluilâk minette dike in the Northwest Territories.

Mineralogically hybrid latite-minette rocks occur at the Coulee 29 explosive pipe (vent)–intrusive complex in the Milk River area and form a sill at Middle Butte in the Sweet Grass Hills (Figure 1; Kemp and Billingsley, 1921; Burwash and Nelson, 1992; Kjarsgaard, 1994, 1997). Figure 2 shows the bedrock geology of the Coulee 29 vent-intrusive complex, comprising early latite-minette breccia, pyroclastic and epiclastic rocks, and at least two generations of late olivine minette dikes and sills (Dawson, 1884; Burwash and Nelson, 1992; Kjarsgaard, 1994, 1997; Walker, 1994; Buhlmann et al., 2000).

An airborne geophysical survey carried out by Marum Resources Inc. showed linear magnetic and resistivity anomalies over all of the exposed Eocene magmatic bodies (Black Butte, Coulee 29, Pakowki Gulch and Philp Coulee) in the surveyed area (Figure 1; Walker, 1994). The survey also revealed a similar linear magnetic-resistivity anomaly trending 029°, parallel to the Philp Coulee dike that is exposed about 2.1 km northeast of the centre of the anomaly. This magnetic-resistivity anomaly likely reflects an unexposed Eocene magmatic body just southwest of the Philp Coulee dike (Walker, 1994).

Based on a regional geophysical survey in southern Alberta, Ross et al. (1997) reported northwest- and north-northeast-trending linear magnetic anomalies that are interpreted to reflect subvertical Eocene dikes intruding the Phanerozoic sedimentary rocks (Figure 1). Pardasie (2003) carried out follow-up magnetic and seismic surveys over some of the anomalies and concluded that two northwest-trending (304°) magnetic anomalies are best explained as subparallel, steeply dipping (63°SW dip) dikes (4–20 m thick) 65–85 m below the surface. These studies suggested that the northern limit of the Eocene magmatism might extend to the Lethbridge area, although the features are perhaps too small to be confirmed using a seismic survey (Pardasie, 2003).

The Sweet Grass Hills intrusions dome and intrude Mississippian, Jurassic and Cretaceous marine and nonmarine strata comprising limestone, shale and siliciclastic rocks interlayered with bentonite, ironstone and coal beds (Figure 1). Figure 3 shows the lithostratigraphic correlation and nomenclature of sedimentary strata exposed at the surface in the study area of southern Alberta and northern Montana (Okulitch et al., 1996; Energy Resources Conservation Board, 2009).

In the Milk River area, exposed country rocks intruded by the Eocene dikes and sills include shale, mudstone and sandstone, interbedded with coal, bentonite and ironstone layers of the Late Cretaceous Pakowki and Judith River (equivalent to Foremost and Oldman) formations (Figure 1). The bedrock exposed at two examined sites in the Sweet Grass Hills of northern Montana comprises 1) Eagle Formation siliciclastic rocks and Claggett Formation shale (equivalent to Milk River and Pakowki formations, respectively) that are intruded, brecciated and hornfelsed by felsite breccia at Grassy Butte; and 2) faulted, brecciated and silicified mudstone and siltstone of the Colorado Group that are intruded by numerous minette and latite dikes and sills at Gold Butte (Figure 1).

3.2 Regional Tectonic Setting

The Sweet Grass Hills igneous complex, along with the Missouri Breaks, Eagle Buttes, Highwood Mountains and Bearpaw Mountains, mark the Eocene (55–49 Ma) peak of magmatic activity within the Late Cretaceous–Oligocene (69–27 Ma) Montana alkaline province (Figure 1; Pirsson, 1905; Larsen, 1940; Currie, 1976; Hearn et al., 1978; Marvin et al., 1980; Irving and O'Brien, 1991; Kjarsgaard, 1997; Irving and Hearn, 2003). Compositionally diverse alkaline and silica-undersaturated rocks (monzonites, syenites, shonkinites, latites, minettes, leucitites, theralites, monticellite peridotites, alnoites, kimberlites,

carbonatites and lamproites) of the Montana alkaline province are closely associated with shoshonitic and calcalkaline rocks of similar age (O'Brien et al., 1991, 1995). Extensive volumes of calcalkaline and shoshonitic rocks occur to the south and southwest in the Challis volcanic field, Absaroka Range, Castle Mountains and environs (Figure 1; e.g., Marvin et al., 1980; O'Brien et al., 1991, 1995; Feeley and Cosca, 2003; Vuke et al., 2007).

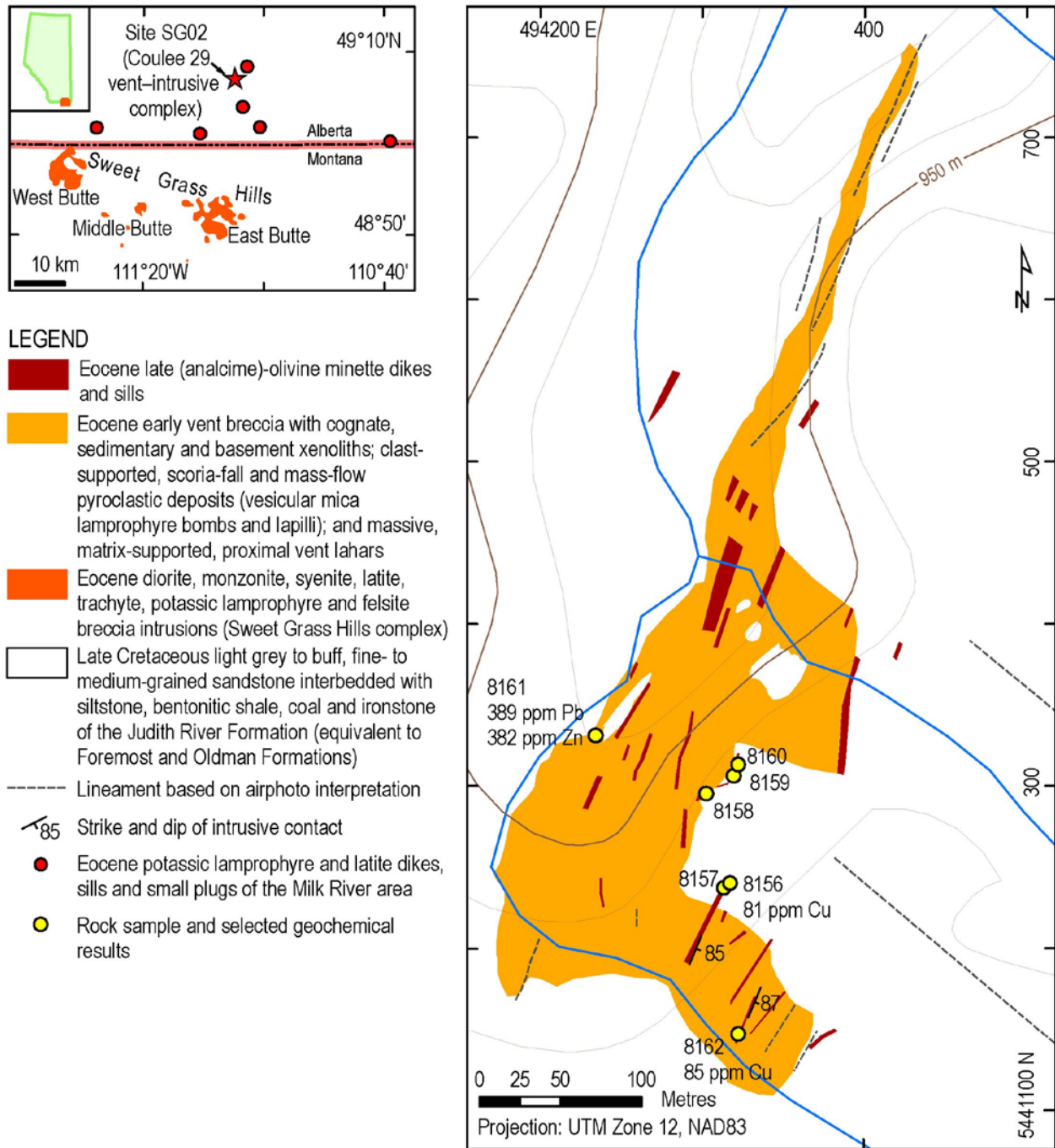


Figure 2. Bedrock geology of the Coulee 29 vent-intrusive complex (site SG02) in the Milk River area (modified after Burwash and Nelson, 1992; Kjarsgaard, 1994), southern Alberta (NTS area 72E/3), showing the locations of AGS rock samples and selected geochemical results. Contour interval is 10 m.

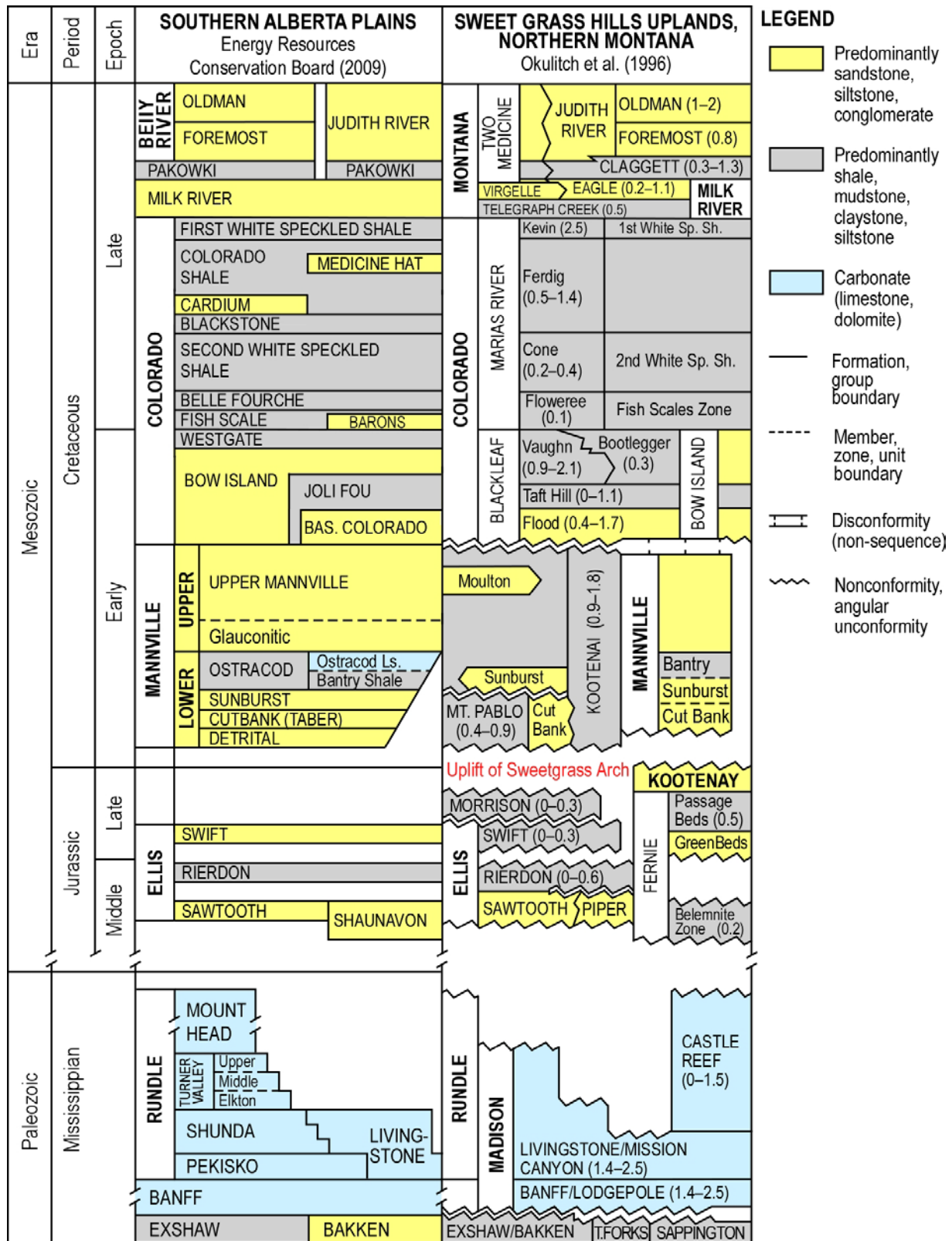


Figure 3. Lithostratigraphic correlation chart of the Mississippian, Jurassic and Cretaceous strata exposed in the study area of southeastern Alberta and northern Montana (after Okulitch et al., 1996; Energy Resources Conservation Board, 2009). Numbers in parentheses indicate thickness of the strata in hundreds of metres.

Recent tectonic models of the Late Cretaceous–Oligocene magmatism in western North America include

- break-off and roll-back of the subducted, low-angle Farallon Plate due to slowed convergence, resulting in convective upflow and decompression melting of the asthenospheric wedge that had been metasomatized by slab-derived fluids during the Late Cretaceous or contemporaneously with the magmatism (O'Brien et al., 1991, 1995);
- upwelling of hot asthenospheric mantle into the Kula-Farallon subducted slab window, coupled with regional crustal extension that triggered partial melting of the metasomatized lithospheric mantle beneath the Montana alkaline province (Thorkelson and Taylor, 1989; Dostal et al., 2003; Madsen et al., 2006); and
- upwelling of asthenospheric mantle due to back-arc extension and lithospheric thinning (decompression), related to subduction of the Farallon Plate, that provided the heat source and/or volatile influx required to induce partial melting in the lithospheric mantle beneath the Wyoming craton (Eggler et al., 1988; Dudás, 1991; Christiansen et al., 2002; Mirnejad and Bell, 2006).

All of these models involve interaction between ancient lithospheric mantle, inferred to have been metasomatized during the Proterozoic, and upwelling asthenospheric mantle during regional lithospheric extension, with modification of the mantle source by metasomatism shortly before or contemporaneously with the Late Cretaceous–Oligocene magmatism (Eggler et al., 1988; Dudás, 1991; Macdonald et al., 1992; O'Brien et al., 1991, 1995; Buhlmann et al., 2000; Christiansen et al., 2002; Dostal et al., 2003; Madsen et al., 2006; Mirnejad and Bell, 2006).

However, Macdonald et al. (1992) concluded that the evidence for a subduction component is equivocal in the Bearpaw Mountains rocks. Morris et al. (2000) argued against subduction in the petrogenesis of the calcalkaline Colville igneous complex, a part of the Eocene Magmatic Belt of the North American Cordilleran interior. Feeley and Cosca (2003) also concluded that geochemical variation in the Absaroka Range rocks does not require mantle processes involving a subducting slab.

On a regional scale, much of western and central Montana is underlain by the Mesoproterozoic Belt-Purcell Basin, thrust to the east by the Cordilleran Orogeny and offset by the dextral, northwest-trending Rocky Mountain Trench and the west-northwest-trending Lewis-Clark, Perry and Mesoproterozoic Montana-Tennessee lineaments (Vuke et al., 2007). Part of the Montana alkaline province and the coeval Challis calcalkaline volcanic field (49–44 Ma) to the southwest are coincident with the northeast-trending Great Falls Tectonic Zone (GFTZ) that separates the Medicine Hat basement of the Archean Hearn craton to the north from the Archean Wyoming craton to the south (Figure 1; O'Neill and Lopez, 1985; Ross et al., 1991; Vuke et al., 2007). The GFTZ represents a repeatedly reactivated zone of crustal weakness, interpreted to be either a cryptic Proterozoic suture or an intracontinental shear zone (O'Neill and Lopez, 1985; Ross et al., 1991; Boerner et al., 1998), parallel to the Dillon Suture–Shear Zone and Weldon-Brockton-Froid Fault Zone (Vuke et al., 2007). Based on geochemical evidence from mantle xenoliths and alkaline rocks, Cavell et al. (1993) and Buhlmann et al. (2000) rejected the idea of a Proterozoic suture for the GFTZ and proposed that the Medicine Hat basement could be a part of the Wyoming craton.

Mutschler et al. (1991) suggested that, during the Late Cretaceous–Eocene, the GFTZ might have acted as a transtensional zone between the large-scale, northwest-trending, right-lateral transcurrent faults due to oblique convergence of the Farallon Plate and North America. In this model, the transtensional zone would result in upwelling of hot asthenospheric mantle beneath the thinned lithosphere, decompression melting and magma ponding, thus producing the compositional diversity of the Late Cretaceous–Oligocene magmatic rocks of the northwestern United States (Mutschler et al., 1991).

However, the Sweet Grass Hills igneous complex is located to the north of the GFTZ apart from the main part of the Montana alkaline province. The complex is situated on the east flank of the Sweetgrass Arch and is offset by the northeast-trending strike-slip and normal faults and northwest-trending normal faults (Figure 1; Lopez, 1995). The Sweetgrass Arch has been interpreted to represent a forebulge of the Laramide Orogeny, although the area had been repeatedly uplifted since the Middle Proterozoic–Paleocene (Lorenz, 1982; Richards et al., 1994; Lopez, 1995).

The northwesterly alignment of the Sweet Grass Hills is oblique to the northeast trend of the GFTZ and the main part of the Montana alkaline province, consistent with the difference in structural grain between the Medicine Hat and Wyoming basement (Lopez, 1995). However, the northwest trend of the Sweet Grass Hills parallels the Lewis-Clark, Cat Creek and Lake Basin lineaments of western and central Montana (Vuke et al., 2007). Therefore, emplacement of the Sweet Grass Hills igneous complex during the regional Eocene extension might have been controlled by reactivation of a pre-existing, northwest-trending zone of crustal weakness that is reflected by the geophysical anomalies in the Medicine Hat basement and surface faults in the area (Lopez, 1995).

4 Analytical Methods

A total of 48 rock samples, including quality controls, were analyzed at Acme Analytical Laboratories Ltd. (Acme) in Vancouver, British Columbia (Appendix 1). All samples were analyzed using standard Acme methods (Appendix 2). Appendix 3 provides details on rock-sample crushing and quality control of the whole-rock geochemical analyses. Appendix 4 lists the analytical results by the different methods, along with the laboratory minimum detection limits (MDL) and estimated precision (reproducibility) and accuracy of the results.

To identify minerals and their relative proportions in some of the rock samples analyzed for whole-rock geochemistry, we performed quantitative Rietveld X-ray diffraction (XRD) and mineral-liberation analyses (MLA) on 12 samples at Activation Laboratories Ltd. (Actlabs) in Ancaster, Ontario (Appendix 5). Appendix 6 lists the analytical results by the Rietveld XRD and MLA methods.

Back-scattered-electron (BSE) images and elemental X-ray maps were obtained using a CAMECA SX 100 electron microprobe at the University of Alberta. Minerals were identified using energy-dispersive spectrometry (EDS), with the compositions of the minerals being determined by wavelength-dispersion spectrometry using a JEOL 8900 electron microprobe in the same laboratory (Appendix 7). Representative mineral analyses carried out on five polished thin sections are listed in Appendix 8.

5 Sample Location and Description

Table 1 lists the Global Positioning System (GPS) locations of the sample sites shown in Figure 1, and Appendix 1 provides sample locations and descriptions. The AGS examined and sampled outcrops of the Eocene magmatic rocks, and Late Cretaceous siliciclastic rocks adjacent to the magmatic bodies, from five sites in the Milk River area in 2008. Two additional sites, comprising known metallic mineral occurrences in the Sweet Grass Hills of northern Montana, were examined and sampled by the AGS in 2009. The sample sites are described below.

5.1 Forty-Ninth Parallel Dike Swarm (Site SG01)

Four subvertical, subparallel dikes (0.5–2 m thick) intermittently outcrop over >200 m along strike (051°–073°) near the 49th parallel in the Milk River valley (Figure 1; Kjarsgaard, 1994). These dikes cut sandstone, mudstone and shale, with coal layers, of the Belly River Group and form a series of en échelon offsets (Figure 4a). A branch of the main dike shows zeolite-chlorite-carbonate-smectite alteration

associated with centimetre-thick, rusty calcite veins (Figure 4b). We collected five rock samples at this locality (Appendix 1).

Table 1. Global Positioning System (GPS) locations of sample sites in the Milk River area of southern Alberta and Sweet Grass Hills of northern Montana. The locations are shown on Figure 1.

Site	Area	Location	UTM (Zone 12, NAD 83)		Elevation (m asl)	Month	Year	No. of Samples
			Easting	Northing				
SG01	S. Alberta	49th Parallel	525796	5427590	882	July	2008	5
SG02	S. Alberta	Coulee 29	494315	5441237	974	July	2008	7
SG03	S. Alberta	Philp Coulee	495533	5434938	1019	July	2008	4
SG04	S. Alberta	Black Butte	499355	5430347	1080	July	2008	3
SG05	S. Alberta	Bear Creek	487864	5428100	1133	July	2008	7
SG06	Montana	Grassy Butte	475822	5402056	1344	Aug	2009	4
SG07	Montana	Gold Butte	471950	5413300	1432	Aug	2009	12

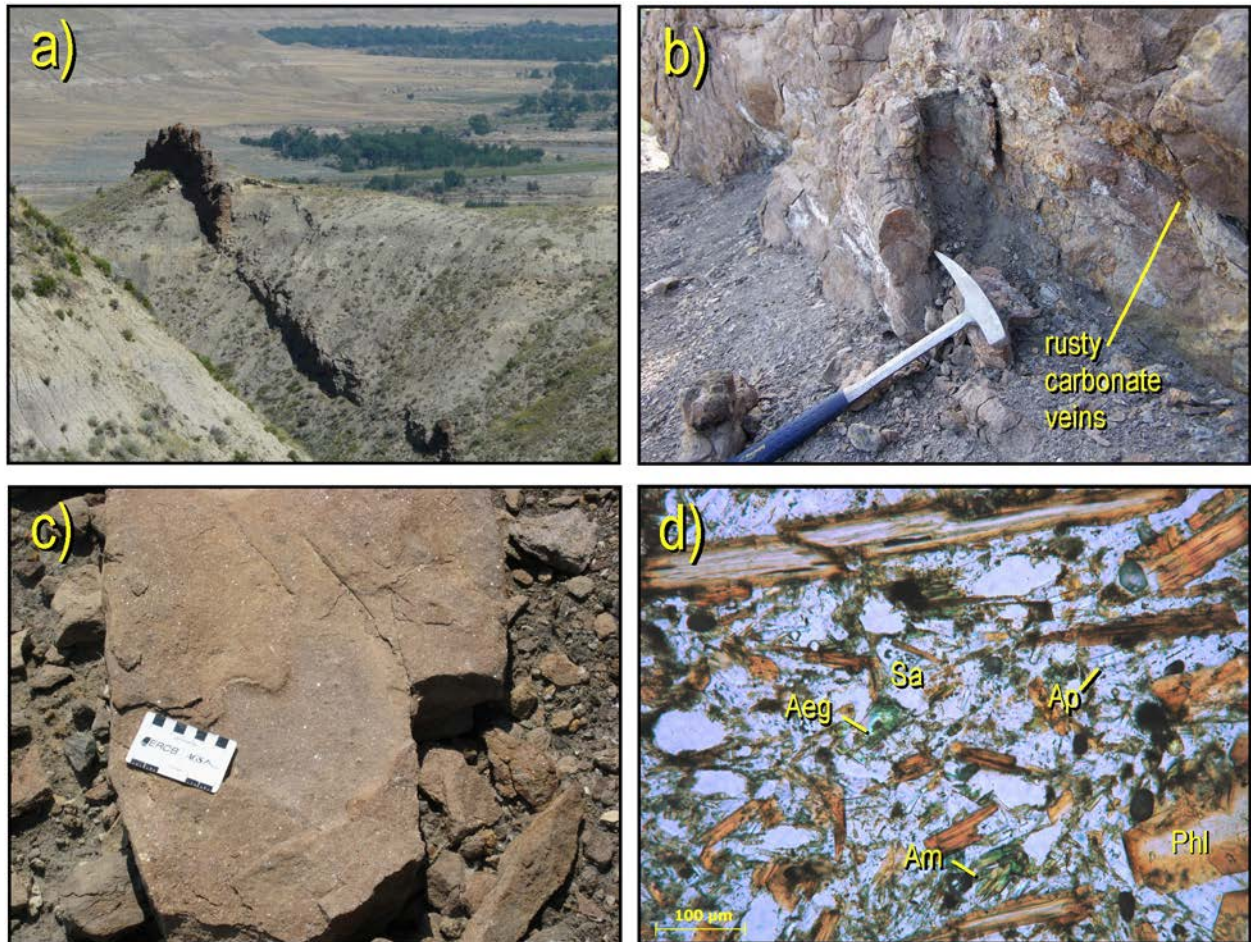


Figure 4. Forty-Ninth Parallel dike (site SG01): a) southeasterly view of the Milk River valley with the Eocene dike cutting siliciclastic rocks interbedded with coal of the Belly River Group; b) rusty-coloured carbonate veins along the contact of the dike branch with the enclosing mudstone; c) close-up of fresh dike rock with glistening phlogopite phenocrysts set in a brown dense groundmass; d) plane-polarized-light (PPL) photomicrograph of sample 8151, showing flow-aligned titanian phlogopite (Phil), Na-K-Ti-amphibole (Am), Na-clinopyroxene (Aeg), apatite (Ap) and sanidine (Sa).

The dikes are composed of light brown porphyritic rock with trachytoid texture and contain flow-aligned, zoned phenocrysts of pinkish-orange phlogopite mantled by Al-poor, Ti-rich phlogopite-annite (Figure 4c, d). Olivine (up to 5–7 vol. %) is pseudomorphed by chlorite, saponite and poorly crystalline smectite (Appendix 6). The fine-grained groundmass is composed of mainly poikilitic and plumose sanidine plates and euhedral Ti-rich phlogopite-annite (Figure 4d). Other identified minerals are abundant fluorapatite and minor to accessory La-Ce-rich strontian fluorapatite, ilmenite, Na-K-Ti-amphibole (potassic titanoferronyböite–ferrynyböite), strontian barite, barian celestine, pyrite and an unidentified Zr-Ti phase (Appendix 8). Optically identified Na-rich clinopyroxene was not analyzed by microprobe. Minor gypsum and jarosite were detected by the XRD in sample 8152 (Appendix 6). The MLA results also indicate traces of titanomagnetite, rutile, albite, clinozoisite, hematite, goethite and calcite. However, none of these minerals were detected by BSE-EDS and optical investigations of a fresh sample. Kjarsgaard (1994, 1997) reported possible analcime and significant calcite. However, we found no analcime and only minor calcite restricted to a secondary vein in our samples.

5.2 Coulee 29 Vent Complex (Site SG02)

The Coulee 29 vent complex outcrops in a deeply incised stream valley, approximately 3 km south of the Milk River (Figure 1; Burwash and Nelson, 1992; Kjarsgaard, 1994, 1997; Walker, 1994; Buhlmann et al., 2000). The complex is irregular and northeasterly elongated, and measures up to 225 m across its widest part and about 750 m in length (Figure 2). It intrudes siliciclastic rocks with coal layers of the Pakowki and Judith River formations and consists of the following distinct magmatic phases, in order of emplacement (Figure 5a; Kjarsgaard, 1994):

- 1) explosive-pipe (vent) breccia (Figure 5b) made up of latite and minette clasts, abundant xenoliths of sedimentary rocks (shale, sandstone and limestone), rare ultramafic to mafic (clinopyroxenite, glimmerite and mafic syenite) and basement tonalite-gneiss clasts (up to 1.5 m), and fragmented phenocrysts (hornblende, plagioclase, clinopyroxene and brown mica) set in a fine-grained groundmass of plagioclase, alkali feldspar, clinopyroxene, brown mica, magnetite and quartz
- 2) clast-supported, scoria-fall and mass-flow pyroclastic deposits (Figure 5c), consisting of brown vesicular minette bombs and lapilli, associated with massive, poorly sorted, matrix-supported proximal vent mudflows, both with fluvially reworked tops
- 3) at least two generations of alkali olivine minette dikes and sills (<1–6 m thick; Figure 5a, d)

Late-stage quartz-calcite veins (a few centimetres wide) were observed as float in talus along the southwestern margin of the complex. We collected seven rock samples at the Coulee 29 locality, including olivine minette dikes, quartz-calcite vein and baked sedimentary rocks engulfed by or adjacent to the magmatic rocks (Appendix 1).

The olivine minette dikes and sills form en échelon offsets and show porphyritic, massive or trachytoid textures (Figure 5e, f). Phenocrysts (up to 2 cm long) include euhedral to subhedral, normally and reversely zoned phlogopite, biotite (total mica 15–50 vol. %), diopside-augite (20–25 vol. %), pseudomorphed olivine (10–20 vol. %), titanomagnetite and analcime (Appendix 8). The fine-grained groundmass consists of the same minerals plus sanidine, devitrified glass mesostasis (up to 20 vol. %) and minor apatite and pyrite. Secondary phases include chlorite, saponite, poorly crystalline smectite and Mg-Fe-rich clays, and traces of albite, clinozoisite, quartz–amorphous silica, calcite, ankerite, sulphates and goethite (Appendix 6). Walker (1994) reported up to 80 vol. % of xenoliths, including sedimentary, basement and ultramafic rocks, in some of these dikes. However, we observed only sporadic ultramafic inclusions in the examined minette dikes (Figure 5d).

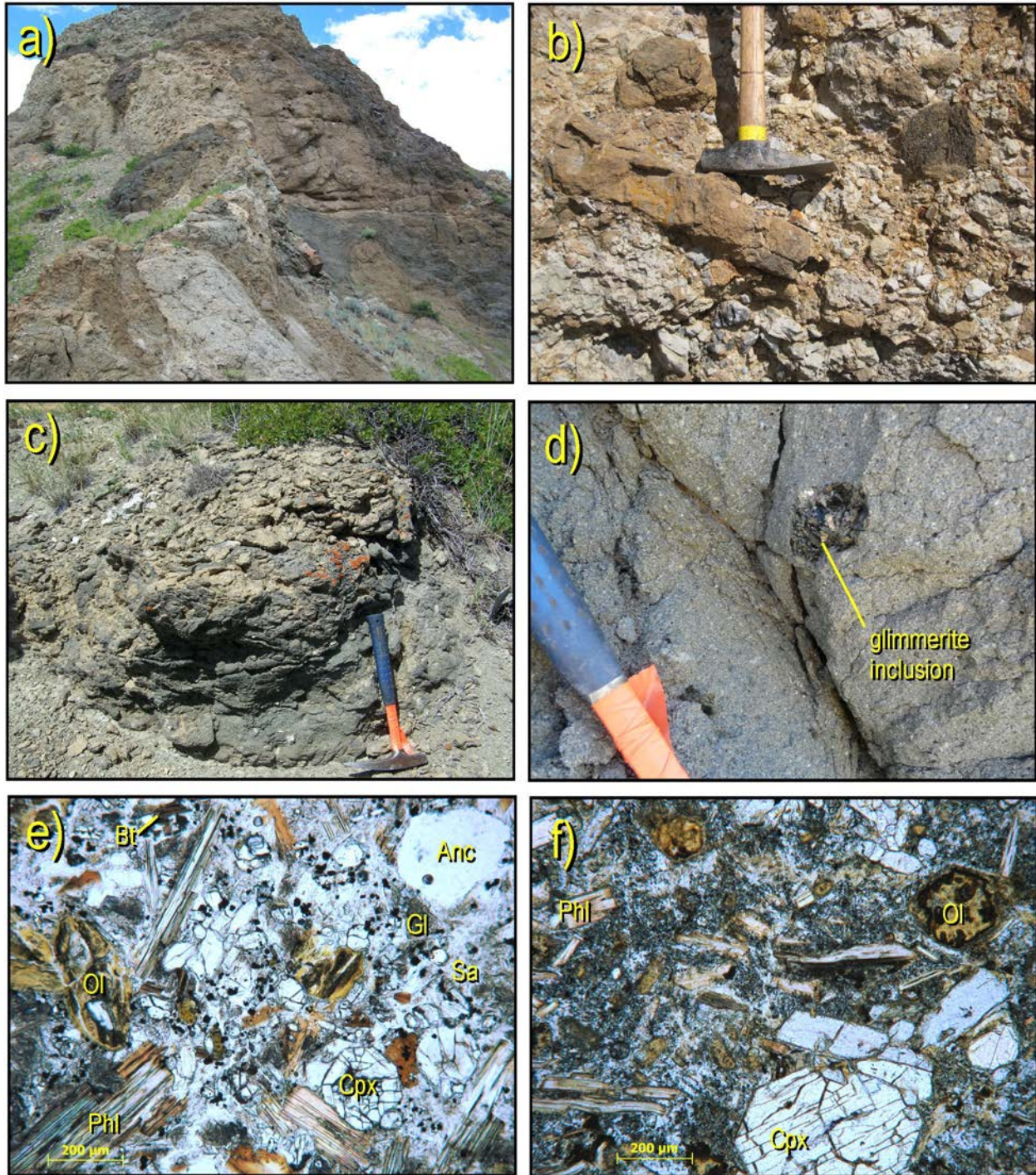


Figure 5. Coulee 29 vent-intrusive complex (site SG02): a) northeasterly view, showing crosscutting relationships between early breccia (tan), pyroclastic and epiclastic deposits, and brown and black olivine minette dikes; b) early breccia with clasts of magmatic and sedimentary rocks; c) proximal vent agglomerate consisting of vesicular minette bombs; d) close-up of the black olivine minette dike, showing abundant mica phenocrysts and glimmerite inclusion set in a dense groundmass; e) plane-polarized light (PPL) photomicrograph of the black olivine minette (sample 8156), showing phenocrysts of phlogopite (Phl), diopside-augite (Cpx), pseudomorphed olivine (Ol), analcime (Anc) and biotite (Bt), groundmass sanidine (Sa) and devitrified glass (Gl); f) PPL photomicrograph of the brown olivine minette (sample 8162), showing phenocrysts of diopside-augite (Cpx), pseudomorphed olivine (Ol) and flow-aligned phlogopite (Phl) in a very fine grained groundmass.

5.3 Philp Coulee Dike (Site SG03)

An alkali olivine minette dike (1.9–2.1 m thick) is intermittently exposed over 700 m and strikes 028°–039° at Philp Coulee, about 5 km south of the Coulee 29 vent complex (Figure 1). The dike forms a series of left-lateral en échelon offsets with subvertical dips, cutting the Oldman Formation light grey sandstone, clayey siltstone and shale. We analyzed four rock samples from the dike and adjacent sedimentary rocks (Appendix 1). The sedimentary rocks adjacent to the dike are baked, showing some textural reorganization. The dike has a dark brown colour and trachytoid texture due to the abundant flow-aligned phenocrysts of normally and reversely zoned phlogopite (up to 2.8 mm). It also contains pseudomorphed olivine, diopside-augite and biotite phenocrysts set in a fine-grained groundmass. The latter is composed of the same minerals plus poikilitic sanidine, chlorite, clay minerals, titanomagnetite, fluorapatite and minor to accessory aegirine-augite, calcite, dolomite-ankerite and perovskite (Appendix 6). Calcite and chlorite form rare amygdules. Kjarsgaard (1994) reported up to 5 vol. % of calcite and minor analcime in this dike. However, we did not find analcime.

5.4 Black Butte Plug (Site SG04)

Black Butte (Figure 1) comprises a northeast-trending, tear-shaped intrusive plug exposed over an area of about 400 by 200 m, rising up to 30 m above the surrounding plain (Figure 6a; Kjarsgaard; 1994). It intrudes crossbedded, light grey sandstone, clayey siltstone and grey and dark carbonaceous shales of the Oldman Formation. Three rock samples were collected along the long axis of the plug at approximately equal intervals (Appendix 1). The plug is made up of grey phlogopite trachyte in the centre and alkali olivine minette in the peripheral parts. The former contains sporadic euhedral phenocrysts of sanidine mantled by hyalophane (Figure 6c), whereas the latter contains rare pseudomorphed olivine. Both rock types contain normally zoned phenocrysts of inclusion-free and sieve phlogopite (up to 25 vol. %), reversely zoned diopside-augite (up to 2.4 mm), partially resorbed ferroan magnesite (up to 1.4 mm), skeletal titanomagnetite and fluorapatite in a dense groundmass (Figure 6c, d). The groundmass consists of hyalophane, Ti-Fe-rich phlogopite, diopside, aegirine-augite, poikilitic calcite (up to 5 vol. %), titanomagnetite and minor analcime and fluorapatite (Appendix 8). Titanomagnetite also forms euhedral inclusions in clinopyroxene and phlogopite phenocrysts. Sporadic chalcopyrite with secondary malachite staining occurs on the southwestern margin of the intrusion. Xenoliths (up to 40 cm) are common and include basement felsic granulite, ultramafic rocks (clinopyroxenite, phlogopite clinopyroxenite and glimmerite), mafic syenite, agpaitic calcite-sodalite(?) nepheline-aegirine syenite and carbonate-phlogopite-andradite rock (Figure 6b). Walker (1994) reported accessory chromite, spinel, ilmenite, picroilmenite, low-Al amphibole, picrotitanite and armalcolite recovered from heavy-mineral concentrate. However, we did not observe any of these minerals microscopically or during microprobe analyses.

5.5 Bear Creek Dike (Site SG05)

A 2.8 m thick dike is intermittently exposed over a total length of 1.1 km along a strike of 005°, standing as a resistant wall up to 2 m high to the east of Bear Creek and just north of the Canada–United States border (Figures 1 and 7a, b). The dike forms a series of left-lateral en échelon offsets with subvertical dips, intruding grey and dark carbonaceous shales, siltstone, grey and pale brown sandstones and coal seams of the Foremost Formation (Kjarsgaard, 1994). Five rock samples of the alkali olivine minette and baked sedimentary rocks adjacent to the dike were collected at this locality (Appendix 1). The dike is composed of brown, porphyritic, alkali olivine minette that is characterized by trachytoid texture due to abundant (25–40 vol. %), large (up to 4 by 1 cm), flow-aligned phenocrysts of normally zoned phlogopite (Figure 7c, d). The dike also contains phenocrysts of diopside-augite (3–10 vol. %), pseudomorphed olivine (up to 4 mm) and minor fluorapatite set in the aphanitic groundmass. The groundmass consists of Ti-rich phlogopite, poikilitic sanidine, Sr-bearing calcite, diopside, aegirine-augite, titanomagnetite, perovskite, analcime and minor devitrified glass (Appendix 8). Magnetite and pyrrhotite occur as

inclusions in some phlogopite phenocrysts. Primary calcite forms globules, composed of platy calcite crystals (Figure 7e), and encloses radial apatite aggregates (Figure 7f).

The XRD-MLA data also indicate traces of albite, ankerite, dolomite and ilmenite/leucoxene. Secondary phases include poorly crystalline clays, chlorite, clinozoisite, hematite, goethite, Fe-sulphate, gypsum, jarosite and amorphous silica (Appendix 6).

5.6 Grassy Butte Felsite Breccia (Site SG06)

Grassy Butte is a conical topographic feature located about 8 km south-southeast of Middle Butte in the Sweet Grass Hills of northern Montana (Figure 1). Light grey- to buff-weathered, pumice-like to scoriaceous felsite breccia, with abundant angular clasts of baked sandstone, siltstone and shale, is exposed on the north flank, near the top of Grassy Butte (Figure 8a, b). The felsite breccia forms an irregularly shaped pipe or stock (about 200 m in diameter) emplaced within the Montana Group siliciclastic rocks (Lopez, 1995). We collected four rock samples from the breccia and adjacent sedimentary rocks (Appendix 1). The breccia consists of optically unresolved, devitrified glass with flow-aligned polygonal cavities after argillitized euhedral phenocrysts (Figure 8c). The XRD-MLA identified

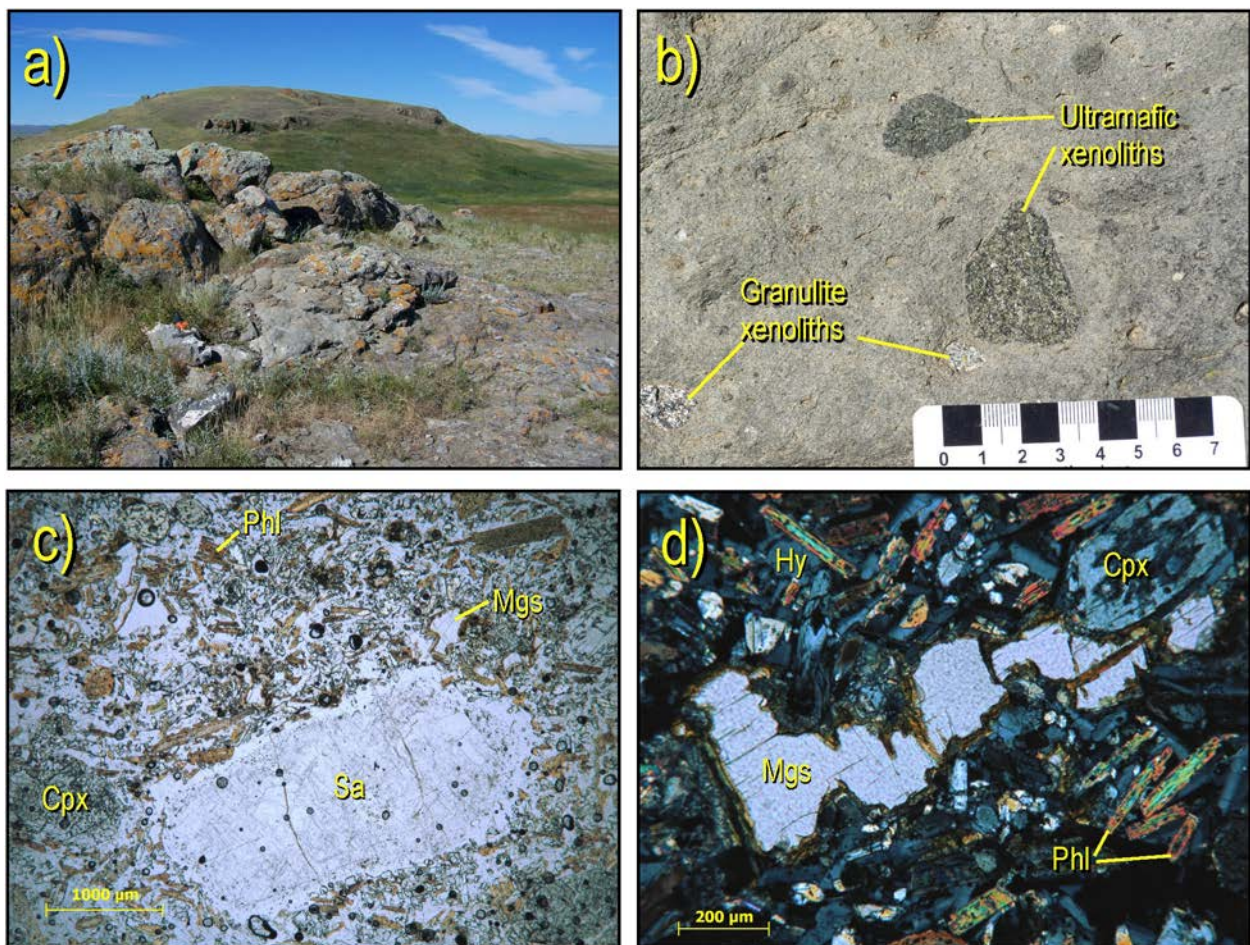


Figure 6. Black Butte plug (site SG04): a) southwesterly view of the intrusive plug; b) close-up of the massive minette with ultramafic and basement xenoliths; c) plane-polarized-light photomicrograph of phlogopite trachyte (sample 8168), showing phenocrysts of phlogopite (Phl), diopside-augite (Cpx), sanidine (Sa) and ferroan magnesite (Mgs) in the fine-grained groundmass; d) cross-polarized-light photomicrograph of the same sample showing resorbed ferroan magnesite (Mgs), flow-aligned phlogopite (Phl), diopside (Cpx) and hyalophane (Hy).

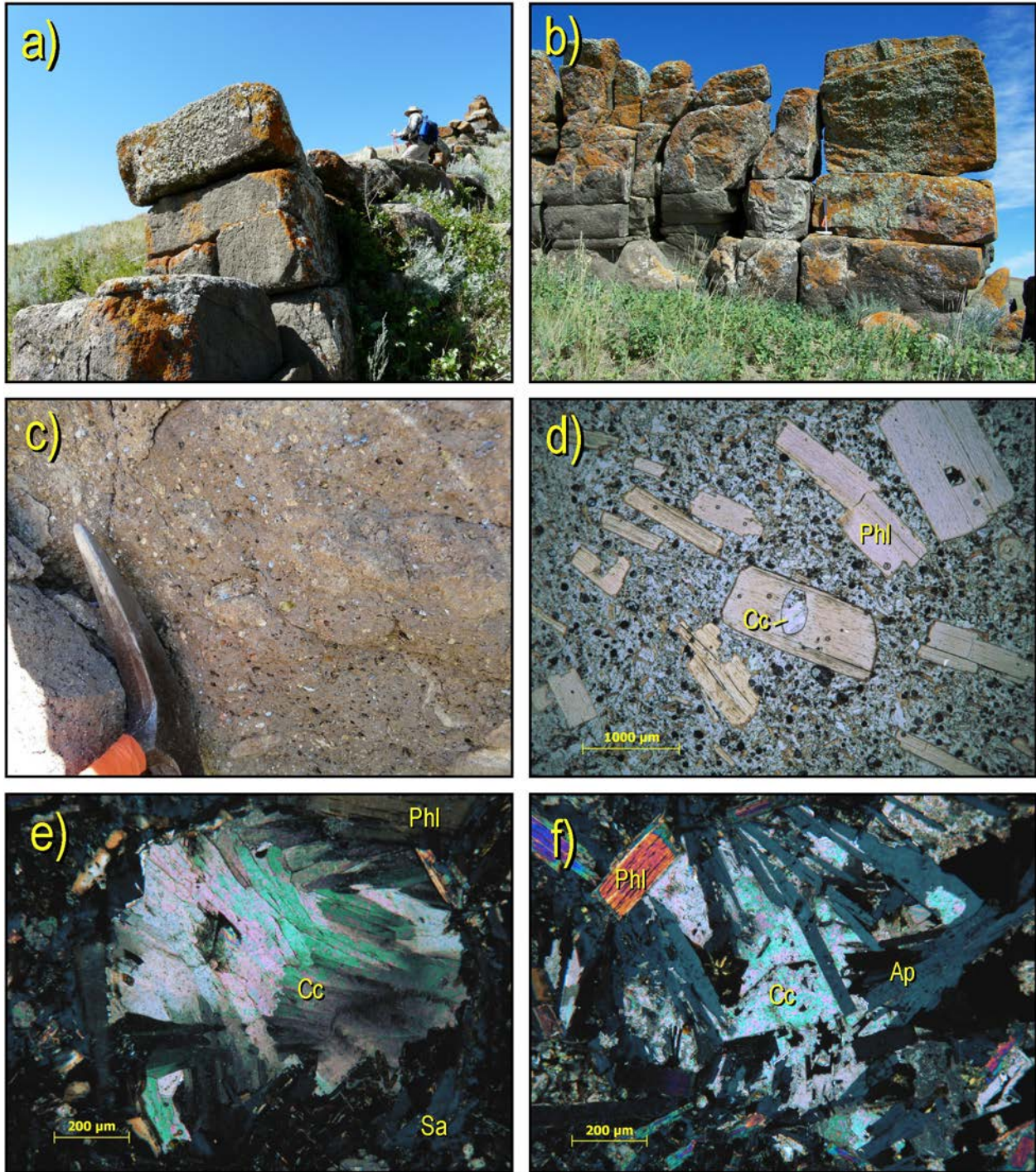


Figure 7. Bear Creek dike (site SG05): a) northwesterly view of the dike; b) easterly view of the dike; c) close-up of the dike, showing phlogopite phenocrysts in a brown groundmass; d) plane-polarized-light photomicrograph of sample 8171, showing trachytoid texture with flow-aligned phlogopite phenocrysts (Phl) and rounded calcite inclusion (Cc); e) cross-polarized-light (CPL) photomicrograph of the same sample showing a globule made up of platy calcite (Cc) and mantled by phlogopite (Phl) and sanidine (Sa); and f) CPL photomicrograph of the same sample showing radial apatite (Ap) enclosed by calcite (Cc) and euhedral phlogopite (Phl).

quartz, amorphous silica, K-feldspar, jarosite, Fe-sulphate and smectite as the main constituents, with traces of phosphates, rutile, illite, barite, goethite, Fe-rich cerussite and pyrite (Appendix 6). The Montana Group siliciclastic rocks adjacent to felsite breccia have been silicified and contact-metamorphosed to fine-grained hornfels (Figure 8d). The hornfels consists of a mosaic K-feldspar–quartz matrix, jarosite-epidote veins, Fe-sulphate, poorly crystalline smectite, and minor to trace pyrite, As-Fe–rich phosphate, galena, rutile, goethite, illite, chlorite, biotite and albite (Appendix 6). The paragenetic relationships of the secondary-mineral assemblages in the felsite breccia and adjacent country rocks indicate potassic and propylitic alteration overprinted by the intermediate argillic and supergene alteration.

Gavin (1991) reported gold mineralization associated with brecciation, silicification, pyritization and oxidation along the contact between felsite breccia and hornfelsed country rocks at Grassy Butte. Our BSE-EDS observations suggest that pyrite is likely to host gold, with most of the arsenic contained in phosphate and jarosite.

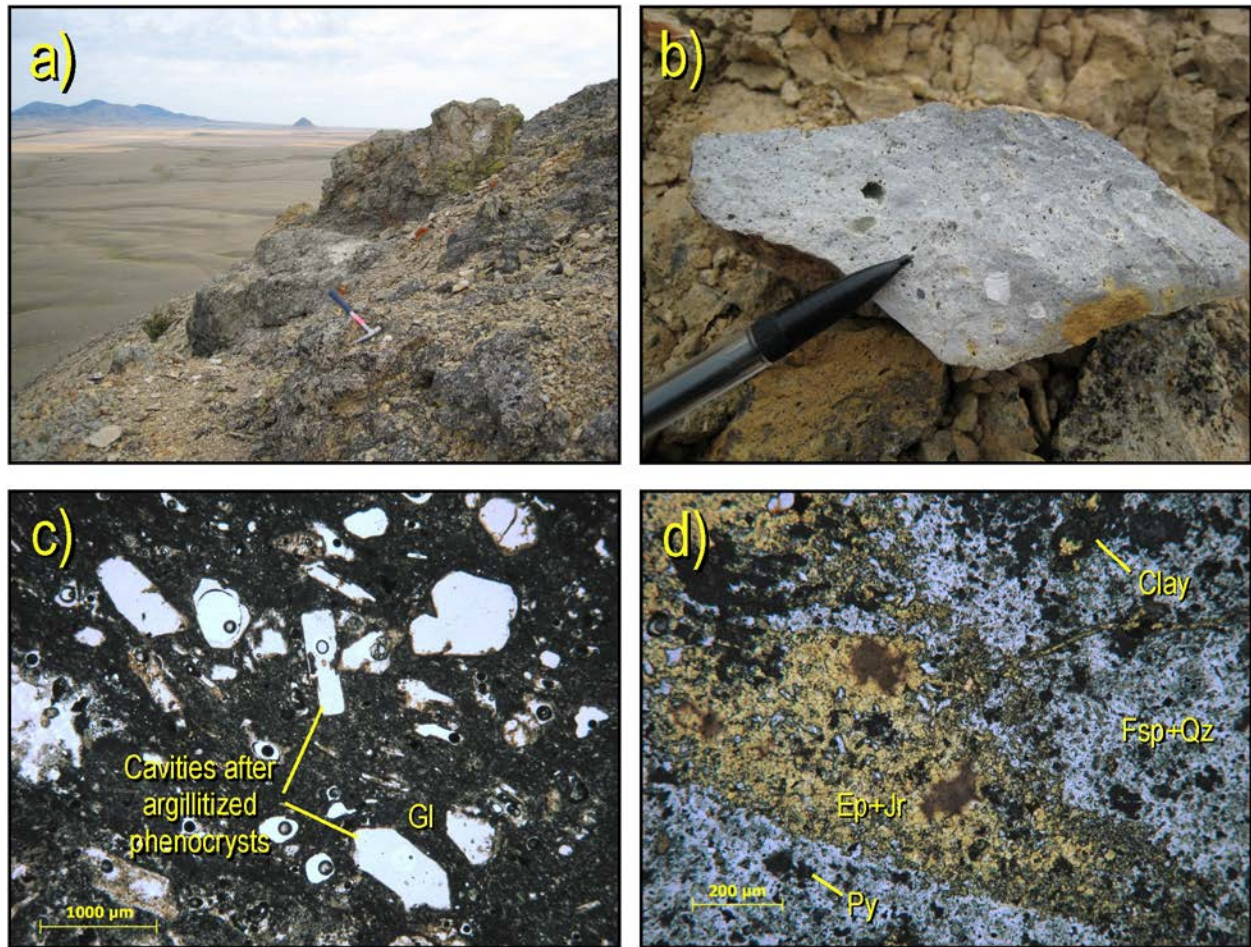


Figure 8. Grassy Butte felsite breccia (site SG06), northern Montana: a) easterly view of the breccia exposure; b) close-up of the breccia, showing porous texture and abundant angular clasts of the sedimentary country rocks; c) plane-polarized-light (PPL) photomicrograph of felsite breccia (sample 8230), showing flow-aligned polygonal cavities after argillitized euhedral phenocrysts in the devitrified glass (Gl) groundmass; and d) PPL photomicrograph of brecciated, contact-metamorphosed Montana Group shale (sample 8231), showing fine-grained K-feldspar–quartz matrix (Fsp+Qz), epidote-jarosite veins (Ep+Jr), clay and pyrite (Py).

5.7 Gold Butte Dike Swarm (Site SG07)

Gold Butte is on the southwest flank of Middle Butte in the Sweet Grass Hills of northern Montana (Figure 1). During the 1930s and 1940s, gold mining took place on the pediment gravel and alluvial deposits in the Eclipse Gulch valley and from the lode source immediately to the east of the placer workings at Gold Butte (Gavin, 1991; Lopez, 1995). An adit has been driven through silicified (veined) and pyritized hornfels breccia after black shales and siltstones of the Colorado Group, intruded and engulfed by minette, trachyte and latite dikes and sills (<1.5 m thick), and offset by a west-northwest-

trending, high-angle, gossanous shear zone about 0.3 m wide (Figure 9a, b). We collected 12 samples of intrusive rocks and adjacent sedimentary rocks from near the adit (Appendix 1).

A brown minette dike exposed at the entrance to the adit has a 2 cm thick quenched margin. The minette shows porphyritic texture due to the euhedral phenocrysts of phlogopite (7–40 vol. %), diopside (5–25 vol. %), brown hornblende (~1–8 vol. %), fluorapatite (<1–3 vol. %) and pseudomorphed olivine (~1 vol. %) in a dense trachytic groundmass (Figure 9c). The groundmass consists of flow-aligned sanidine and minor to accessory phlogopite-biotite, plagioclase, quartz, fluorapatite, titanite, rutile and titanomagnetite. Secondary minerals include albite, clinozoisite, actinolite-tremolite (uralite), amorphous silica, chlorite, smectite, Mn-oxides, Fe-sulphate, goethite, jarosite and hematite (Appendix 6).

Trachyte and latite dikes near the adit contain angular to subangular ultramafic and basement xenoliths (up to 4.5 cm long). They are light grey porphyritic rocks containing euhedral phenocrysts of sanidine, oligoclase-andesine (25–40 vol. % of total feldspar), diopside (5–20 vol. %), Ti-rich potassic magnesiohastingsite-hastingsite to potassic ferropargasite (2–15 vol. %), and fluorapatite (1–2 vol. %) in a trachytic groundmass (Figure 9e). The groundmass consists of sanidine and minor to accessory phlogopite-biotite, pyrite, quartz, titanomagnetite, titanite, rutile, galena and zircon. Secondary phases include tremolite-actinolite, epidote-clinozoisite, albite, amorphous silica, illite, chlorite, clays, calcite, hematite, goethite, jarosite, ankerite, Fe-sulphate and gypsum (Appendix 6). Chalcopyrite forms anhedral segregations (up to 5 vol. %) in some of these dikes (Figure 9f).

The Colorado Group siliciclastic rocks adjacent to the intrusions have been brecciated, hornfelsed, silicified and pyritized along the high-angle gossanous shear zone (Figure 9a, b, d). Crosscutting quartz veins (0.1–1 cm wide) form a dense stockwork along the shear zone. The hornfels breccia (Figure 9d) is made up of patchy, fine-grained, mosaic K-feldspar-quartz matrix, with segregations of euhedral pyrite (2–20 vol. %) up to 1.2 mm. Smectite-goethite (\pm epidote \pm chlorite) infills fractures. Other identified minerals include albite, illite, biotite, rutile, apatite, jarosite, Fe-sulphate and zircon (Appendix 6).

The secondary mineral assemblages indicate weak to strong propylitic alteration of the intrusions and potassic to propylitic alteration of the adjacent sedimentary rocks, overprinted by intermediate argillic and supergene alteration. Historical drilling in this area indicated grades of 0.34–157.7 ppm Au, with a Au:Ag ratio of about 1:1, across 3 m intervals (Gavin, 1991; Lopez, 1995).

6 Mineral Chemistry

This section describes the paragenesis and composition of minerals in igneous rocks of the study area. Appendix 8 lists the representative electron microprobe analyses and calculated structural formulas.

6.1 Mica

Mica of the phlogopite-annite solid-solution series occurs as euhedral to subhedral phenocrysts and in the groundmass of the 49th Parallel dikes (Figure 10) and minettes of the Milk River area, and forms glimmerite and mica-clinopyroxenite xenoliths in the latter (Kjarsgaard, 1994; Buhlmann et al., 2000).

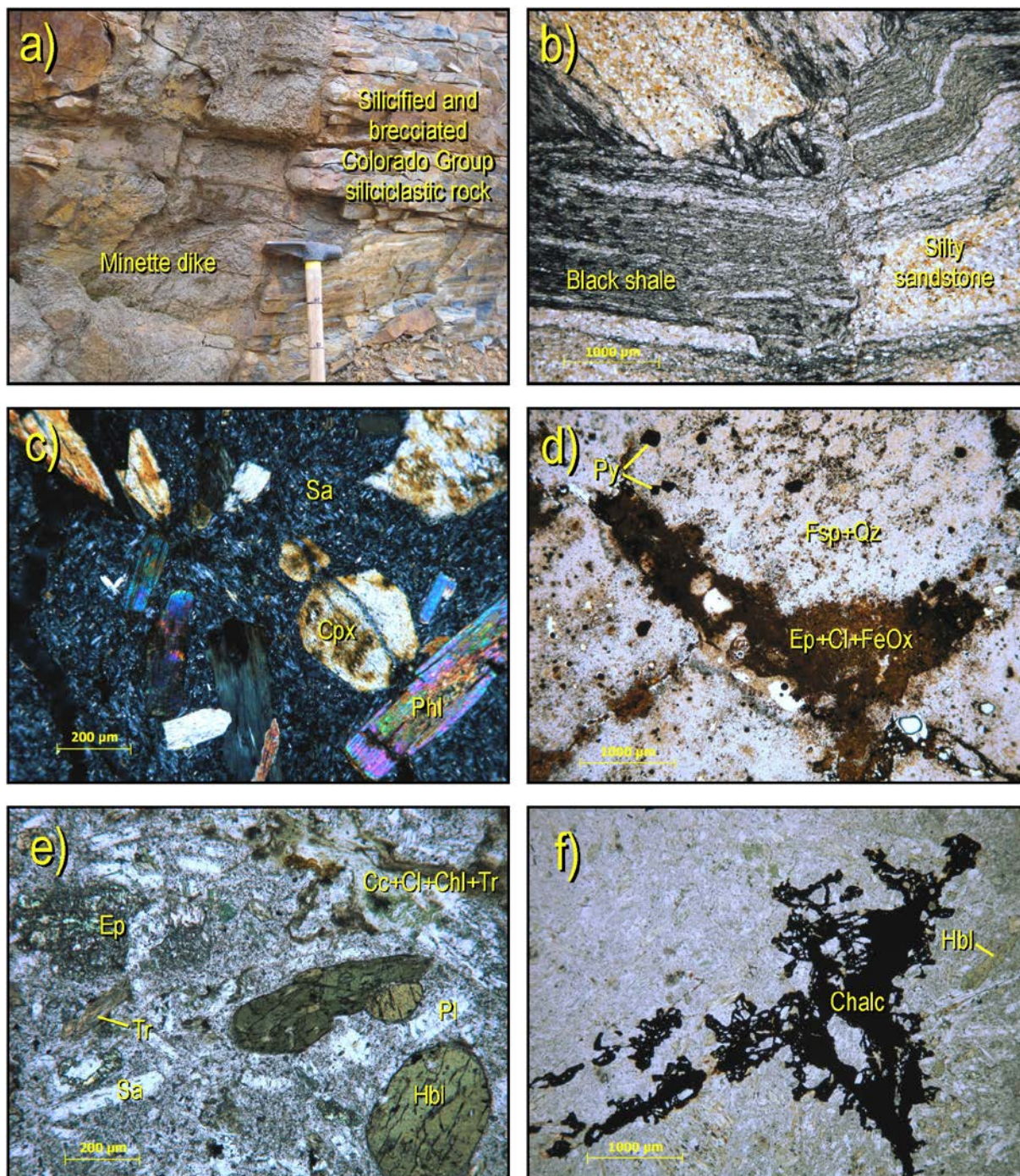


Figure 9. Gold Butte (site SG07), northern Montana: a) minette dike intruding brecciated and silicified Colorado Group siliciclastic rocks; b) plane-polarized-light (PPL) photomicrograph of brecciated Colorado Group black shale, interbedded with silty sandstone (sample 8241); c) cross-polarized-light (CPL) photomicrograph of propylitically altered minette dike (sample 8244), showing urutilized diopside (Cpx), phlogopite (Phl) and groundmass sanidine (Sa); d) PPL photomicrograph of brecciated, limonitized hornfels after Colorado Group shale (sample 8237), showing feldspar-quartz matrix (Fsp+Qz), pyrite (Py) and epidote-clay-goethite aggregate (Ep+Cl+FeOx); e) PPL photomicrograph of propylitically altered latite dike (sample 8242), showing sanidine (Sa), oligoclase-andesine (Pl), hastingsite-pargasite (Hbl), epidote (Ep), actinolite-tremolite (Tr) pseudomorphs after diopside, and calcite-clay-chlorite-tremolite veins (Cc+Cl+Chl+Trem); and f) PPL photomicrograph of the same latite sample, showing hastingsite-pargasite (Hbl) and segregations of chalcopyrite (Chalc).

It exhibits extensive compositional variation with respect to FeO_t (total iron expressed as FeO), TiO_2 and Al_2O_3 (Figure 11).

Phlogopite and Al_2O_3 -poor, TiO_2 -rich ferroan phlogopite-annite (10.2–13.1 wt. % Al_2O_3 , 1.14–6.71 wt. % TiO_2), with up to 0.243 atoms per formula unit of tetrahedral Fe^{3+} , in the 49th Parallel dike overlap the compositions of phenocryst and groundmass mica in lamproites (Figure 11).

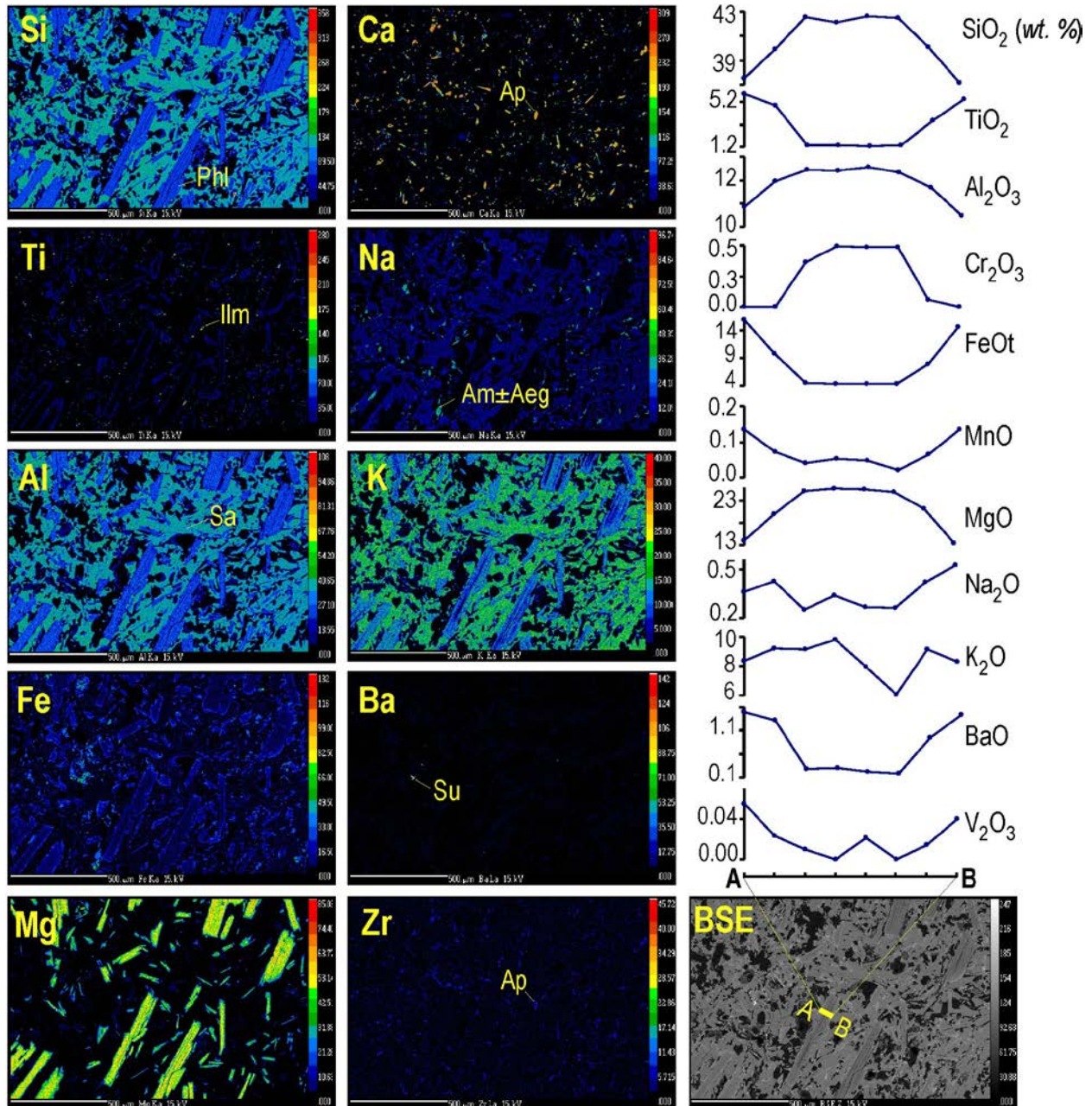
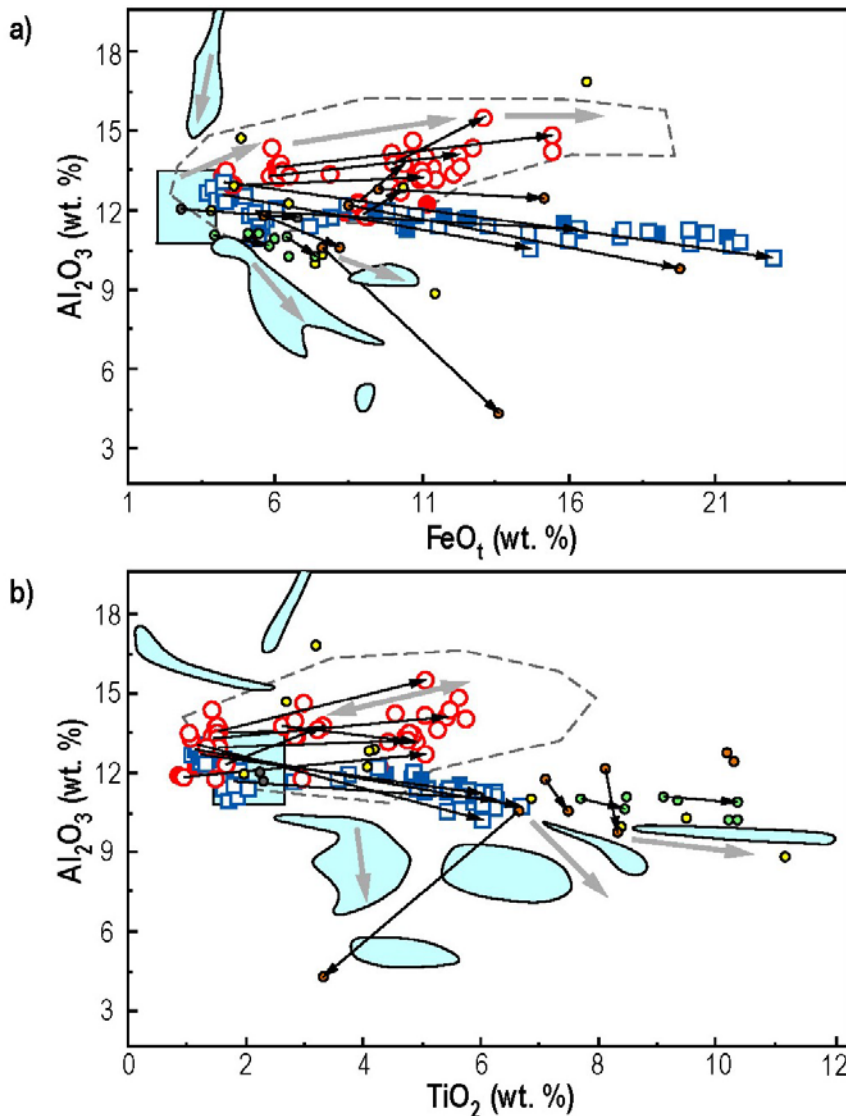


Figure 10. Analytical results for phlogopite-annite from the 49th Parallel dike (sample 8151): line-traverse electron microprobe analyses of 11 elements (wt. % oxides) across a phlogopite phenocryst; BSE image; and elemental X-ray maps for Si, Ti, Al, Fe, Mg, Ca, Na, K, Ba and Zr. The analyzed phenocryst is marked with a solid line (A–B) on the BSE image. The elemental maps highlight Na-clinopyroxene (Aeg), Na-Ti-K-amphibole (Am), apatite-group minerals (Ap), an unidentified Zr-Ti phase and ilmenite (Ilm), Ti-rich phlogopite-annite (Phl), sanidine (Sa) and Ba-Sr sulphate (Su).



This study

49th Parallel dike (sample 8151):

- Mica phenocrysts
- Groundmass micas

Milk River minettes (samples 8156, 8168 and 8171):

- Mica phenocrysts
- Groundmass micas
- Core-to-rim zonation trend

Compiled data from Mitchell and Bergman (1991)

- Micas from Spanish lamproite
- Micas from Sisimiut lamproite, Greenland
- Mica phenocrysts from Smoky Butte lamproite, Montana
- Mica phenocrysts from Francis lamproite, Utah
- Compositional fields of micas from Leucite Hills lamproite, Wyoming
- Compositional field of micas from worldwide minette and Roman Province-type lavas and leucite
- Mica-zonation trend

Figure 11. Variations of Al₂O₃ versus FeO₁ (a) and Al₂O₃ versus TiO₂ (b) for phlogopite-annite in intrusive rocks of the Milk River area, compared with those of micas from lamproites, minettes and other ultrapotassic rocks (Mitchell and Bergman, 1991). Black arrows indicate core-to-rim zonation trends in individual mica phenocrysts. Wide grey arrows indicate representative mica-zonation trends in minettes and lamproites.

Importantly, the mica core-to-rim zoning trends in the 49th Parallel dike display increasing FeO₁ and TiO₂ at decreasing Al₂O₃, similar to those of micas in lamproites (Mitchell and Bergman, 1991). In addition, SiO₂, Cr₂O₃ and MgO decrease as V₂O₃, MnO and BaO increase from core to rim in phlogopite phenocrysts from the 49th Parallel dike (Figure 10). In contrast, phlogopite in other potassic rocks of the study area overlaps the composition of minettes and shows zoning trends of increasing FeO₁ and TiO₂ at increasing Al₂O₃, consistent with those of micas in minettes (Mitchell and Bergman, 1991). Therefore, the compositions and zoning trends of mica distinguish the 49th Parallel dikes from minettes of the Milk River area. The former contain phlogopite-annite mica similar to that in lamproites, whereas the latter contain phlogopite, typical of minettes.

6.2 Amphibole

Prismatic Na-Ti-K-amphibole (6.53 wt. % TiO₂, 2.37 wt. % K₂O) occurs in the groundmass and is restricted to the 49th Parallel dikes (Figures 4d and 10), confirming petrographic observations by Kjarsgaard (1997). It contains 0.35 wt. % ZrO₂ and corresponds to potassic titanoferronyböite–ferrinyböite in the International Mineralogical Association (IMA) amphibole classification scheme (Leake et al., 2004). The absence of F and Cl, coupled with an oxide total of ~100% in the analysis of this amphibole (Appendix 8), suggest substitution of monovalent anions (OH, F, Cl) by O²⁻ accompanied by the occurrence of high-charge cations in the octahedral site. Based on the electroneutrality principle, calculated Fe³⁺/Fe²⁺ increases from zero (no substitution of OH⁻ by O²⁻) up to 2.3 (only O²⁻ anions). Oscillatory-zoned, euhedral calcic amphibole phenocrysts, ranging in composition from Ti-rich, potassic magnesiohastingsite-hastingsite to potassic ferropargasite (1.68–2.35 wt. % TiO₂, 2.02–2.13 wt. % K₂O), occur in trachyte and latite dikes at Gold Butte (Figure 9e).

6.3 Clinopyroxene

Clinopyroxene of diopside and augite composition (Figure 12a), occurs as euhedral phenocrysts and in the groundmass of minettes, latites and trachytes of the Milk River area and Sweet Grass Hills, and forms ultramafic xenoliths hosted by these rocks (Kjarsgaard, 1994; Buhlmann et al., 2000). Pleochroic aegirine-augite occurs in the groundmass of the 49th Parallel dikes (Figures 4d and 10) and mantles the edges of groundmass diopside and augite prisms in the Black Butte diopside-phlogopite trachyte and olivine minette dikes at Philp Coulee and Bear Creek.

The phenocrysts show normal, reverse and oscillatory zoning, with solid solution toward enstatite or hedenbergite (Figure 12a). Diopside phenocrysts with resorbed or sieved cores (Figure 6c, d) occur in diopside-phlogopite trachyte at Black Butte (sample 8168). The majority of diopside and augite phenocrysts in olivine minettes of the Milk River area are poor in TiO₂ (0.15–0.81 wt. %), Al₂O₃ (0.34–2.20 wt. %), MnO (0.10–0.36 wt. %), Cr₂O₃ (0.00–0.59 wt. %) and Na₂O (0.16–0.93 wt. %), with Mg/Fe ranging between 2.9 and 9.0. Green Al-diopside cores (2.46–2.69 wt. % Al₂O₃) in some of the phenocrysts have lower Mg/Fe (2.1–2.7). Diopside phenocrysts in latite at Gold Butte (sample 8232) contain higher MnO (0.39–0.76 wt. %) but have Mg/Fe (2.0–3.4) partly overlapping that of normally zoned phenocryst rims in diopside-phlogopite trachyte (sample 8168) and Al-diopside phenocryst cores in olivine minettes of the Milk River area (Figure 12a). Our data are consistent with the interpretation that the complex zoning patterns in the clinopyroxene phenocrysts reflect multiple mixing of evolved and more primitive batches of potassic magma (Macdonald et al., 1992; Buhlmann et al., 2000).

6.4 Feldspar

Rare euhedral sanidine (Or_{73–79}Ab_{20–27}An_{0–1}) phenocrysts occur in diopside-phlogopite trachyte at Black Butte (Figure 6c). Latite and trachyte dikes at Gold Butte contain both oligoclase-andesine (Ab_{59–62}An_{28–31}Or_{7–12}) and sanidine phenocrysts (Figure 9e), with the former containing 0.61–0.66 wt. % SrO. Hyalophane (3.58–4.73 wt. % BaO), containing 0.31–0.35 wt. % SrO, mantles sanidine phenocrysts and occurs in the groundmass of the Black Butte diopside-phlogopite trachyte (Appendix 8). All igneous

rocks studied contain groundmass sanidine (Figure 12b). Highly potassic sanidine in the groundmass of the 49th Parallel dikes forms plumose poikilitic plates and slender prisms, and contains significant BaO (0.79–1.36 wt. %) and TiO₂ (0.15–0.25 wt. %), minor Na₂O (1.15–2.65 wt. %) and FeO_t (0.02–0.07 wt. %), and negligible CaO (0.00–0.01 wt. %). It is compositionally similar to sanidine in some lamproites (Mitchell and Bergman, 1991). In contrast, groundmass sanidine and hyalophane in olivine minettes and diopside-sanidine trachyte of the Milk River area contain higher amounts of Na₂O (2.23–3.44 wt. %) and CaO (0.04–0.25 wt. %), and lower TiO₂ (0.00–0.16 wt. %) and FeO_t (0.00–0.03 wt. %). Therefore, sanidine composition further distinguishes the 49th Parallel dikes from other potassic rocks of the Milk River area (Figure 12b).

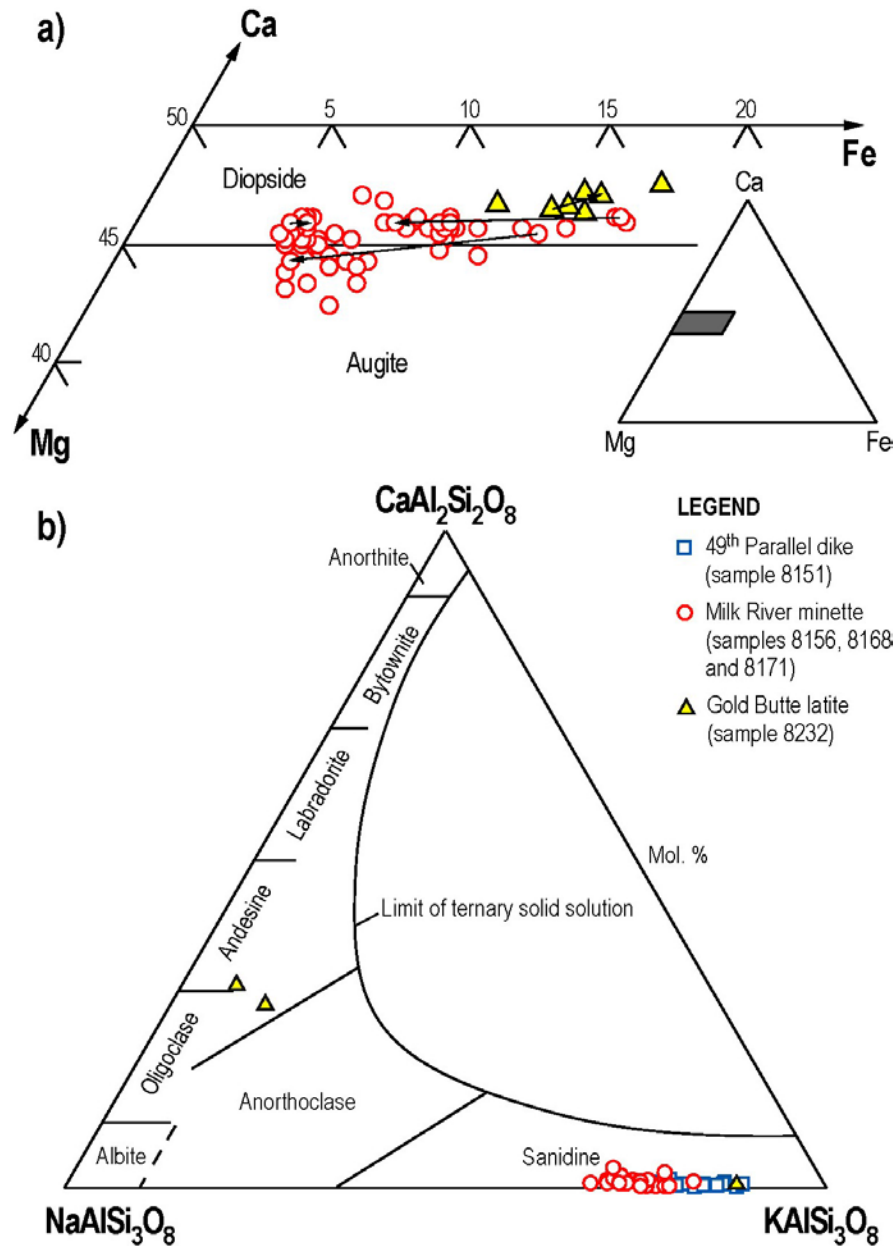


Figure 12. Compositions and nomenclature for pyroxene and feldspar from igneous rocks of the Milk River area and Sweet Grass Hills: a) clinopyroxenes plotted on a Mg-Ca-Fe (mol. %) diagram (Morimoto et al., 1988) and b) feldspars plotted on a NaAlSi₃O₈-CaAl₂Si₂O₈-KAlSi₃O₈ (mol. %) diagram (Deer et al., 1996). Arrows indicate core-to-rim zoning trends in clinopyroxene phenocrysts.

6.5 Analcime

Analcime is a minor constituent of olivine minettes in the Milk River area (Kjarsgaard, 1994, 1997). It forms rare euhedral phenocrysts (Figure 5e) and rounded crystals in the groundmass. Based on a few microprobe analyses (Appendix 8C), the analcime is SiO₂ rich and contains traces of PbO (0.00–0.15 wt. %), K₂O and CaO (both 0.02–0.04 wt. %). Kjarsgaard (1994) suggested that analcime in the olivine minettes of the Milk River area might have pseudomorphed primary leucite microphenocrysts. O'Brien et al. (1991) and Macdonald et al. (1992) documented fresh primary leucite and textural evidence of its replacement by secondary analcime in compositionally similar minettes of the Bearpaw and Highwood mountains in Montana. Similarly, Wallace and Carmichael (1989) interpreted analcime in minette lavas of the western Mexican Volcanic Belt to be the product of leucite conversion in the presence of aqueous NaCl solution at low temperature. Based on the mineralogical and whole-rock geochemical data, we agree with the interpretation that analcime in the Milk River area minettes is perhaps a subsolidus mineral.

6.6 Spinel

Spinel-group minerals occur as euhedral, skeletal and atoll groundmass crystals (up to 103 µm but mostly <50 µm) and as inclusions in phlogopite and clinopyroxene in olivine minettes and diopside-phlogopite trachyte of the Milk River area. The majority are titanomagnetite with 3.05–8.47 wt. % TiO₂, 0.00–3.64 wt. % Cr₂O₃, 0.50–2.74 wt. % MgO, 0.35–2.38 wt. % Al₂O₃, 0.41–0.99 wt. % MnO, 0.06–0.12 wt. % ZnO and 78.9–86.1 wt. % FeO_t (Appendix 8), making them compositionally similar to those in minettes elsewhere (Mitchell and Bergman, 1991). Our results are consistent with the compositional range of titanomagnetite in minettes of the Milk River area reported by Buhlmann et al. (2000). Kjarsgaard (1997) and Buhlmann et al. (2000) also reported Cr-rich spinel in glomeroporphyritic clusters with olivine and phlogopite and as inclusions in pseudomorphed olivine, respectively. However, we did not find Cr-rich spinel.

6.7 Ilmenite

Groundmass ilmenite grains (<40 µm) are relatively common in the 49th Parallel dikes (Figure 10). Microprobe analyses indicate 0.78–1.95 wt. % MnO, 0.26–1.43 wt. % BaO, 0.03–0.91 wt. % ZrO₂ and 0.05–0.19 wt. % MgO (Appendix 8), similar to ilmenite compositions in lamproites (Mitchell and Bergman, 1991). Notably, ilmenite is absent in olivine minettes and other potassic rocks of the Milk River area and at Gold Butte. Thus, the presence of ilmenite, coupled with the lack of titanomagnetite, further discriminates the 49th Parallel dikes from the minettes.

6.8 Apatite

Apatite-group minerals occur as euhedral or rounded phenocrysts, as microphenocrysts and in the groundmass of all studied magmatic rocks. Both fluorapatite and strontian fluorapatite are ubiquitous in the 49th Parallel dikes, with the latter being restricted to these rocks (Figure 10). The fluorapatite contains 2.83–3.60 wt. % F, 0.67–1.82 wt. % SrO, 0.61–1.70 wt. % SO₃, 0.00–0.56 wt. % BaO, 0.24–0.42 wt. % Ce₂O₃ and 0.07–0.21 wt. % La₂O₃. The strontian fluorapatite has significantly higher SrO (17.5–25.2 wt. %), Ce₂O₃ (2.86–3.34 wt. %), La₂O₃ (1.56–1.59 wt. %) and Na₂O (1.05–1.61 wt. %), and lower F (1.95–1.99 wt. %). Both minerals are poor in Cl (0.02–0.13 wt. %) and Y₂O₃ (0.01–0.13 wt. %), with elemental X-ray maps indicating the presence of some Zr in them (Figure 10). A single microprobe analysis returned 0.16 wt. % ZrO₂ in fluorapatite from the 49th Parallel dike (Appendix 8). Compositionally similar, Ba-rich, Cl-poor fluorapatite and strontian fluorapatite have been reported in lamproites and other strongly peralkaline rocks (Mitchell and Bergman, 1991; Chakhmouradian et al., 2002). Mitchell and Bergman (1991) pointed out that Ba-rich apatite is unique to lamproites.

In contrast, fluorapatite in minettes and other potassic rocks of the study area has negligible BaO (0.00–0.01 wt. %), higher Cl (0.18–0.76 wt. %) and lower rare-earth element (REE), FeO₁ and SO₃ contents

(Appendix 8). Therefore, the composition and paragenesis of the apatite-group minerals further separate the 49th Parallel dikes from minettes and other potassic rocks in the study area.

6.9 Other Minerals

Strontian barite (38.8–44.1 wt. % BaO, 16.3–22.1 wt. % SrO) and barian celestine (40.4–48.7 wt. % SrO, 5.8–20.7 wt. % BaO) occur as inclusions in phlogopite and as groundmass phases in the 49th Parallel dikes (Appendix 8). Mitchell and Bergman (1991) attributed barite in lamproites to a replacement of pre-existing Ba-bearing oxides and silicates.

Euhedral titanite crystals occur in latite and trachyte dikes at Gold Butte. Analyses indicate 1.89–3.73 wt. % FeO_t, 0.33–1.75 wt. % ZrO₂, 0.71–1.30 wt. % Ce₂O₃, 0.26–0.51 wt. % NiO and 0.02–0.17 wt. % Cl (Appendix 8).

Ferroan magnesite (30.0–37.6 wt. % MgO, 17.0–26.8 wt. % FeO_t, 1.81–1.96 wt. % CaO, 0.17–0.58 wt. % MnO) occurs as resorbed phenocrysts in the Black Butte diopside-phlogopite trachyte (Figure 6c, d). The phenocrysts show normal zoning, with increasing FeO_t (17.0–26.8 wt. %) and decreasing MgO (30.0–37.6 wt. %) from core to rim (Appendix 8). Primary calcite occurs as rounded inclusions in phlogopite phenocrysts (Figure 7d) and as groundmass globules made up of platy or poikilitic crystals (Figure 7e, f) in the Bear Creek olivine minette dike. It contains 50.5–56.0 wt. % CaO, 1.89–1.99 wt. % FeO_t, 0.32–1.99 wt. % MgO, 0.41–0.42 wt. % MnO and 0.11–0.12 wt. % SrO (Appendix 8).

Rounded grains (<20 µm) of an unidentified Zr-Ti phase occur in the groundmass of the 49th Parallel dikes (Figure 10). Microprobe analyses indicate 76.7–88.0 wt. % TiO₂, 2.12–7.24 wt. % ZrO₂, 1.33–3.97 wt. % SiO₂, 1.49–3.02 wt. % FeO_t, 0.29–1.49 wt. % MgO, 0.33–1.29 wt. % Al₂O₃, 0.55–1.01 wt. % V₂O₅ and low amounts (<1 wt. %) of CaO, K₂O, NiO, Na₂O, Cr₂O₃, BaO, SO₃ and F (Appendix 8). Low totals of the analyses perhaps reflect the presence of 3–4 wt. % H₂O. The presence of the Zr-Ti phase distinguishes the 49th Parallel dikes from minettes and other potassic rocks in the study area. Mitchell and Bergman (1991) suggested a possible secondary origin for Cr- and Fe-bearing TiO₂ polymorphs in some lamproites. At present, we are not sure whether the Zr-Ti phase in the 49th Parallel dikes is primary or secondary, replacing pre-existing Zr-Ti phase(s).

7 Whole-Rock Geochemistry

7.1 Igneous Rocks

Appendix 4 presents complete whole-rock geochemical analyses of magmatic rocks from the Milk River area (15 samples) of southern Alberta and the Sweet Grass Hills (8 samples) of northern Montana; the results are discussed in this section. Table 2 lists the representative analyses, CIPW norms and geochemical ratios. Minettes and other phlogopite-rich rocks of the Milk River area contain 38.4–51.4 wt. % SiO₂, 0.88–1.72 wt. % TiO₂, 9.60–12.97 wt. % Al₂O₃, 4.00–13.16 wt. % MgO, 2.62–12.73 wt. % CaO, 0.77–2.24 wt. % Na₂O, 4.34–10.68 wt. % K₂O and 1.05–1.83 wt. % P₂O₅. In terms of trace elements, these rocks have 404–1218 ppm Cr, 122–189 ppm V, 64–438 ppm Ni, 133–406 ppm Rb, 3095–5970 ppm Ba, 898–2162 ppm Sr, 162–451 ppm Zr and 144–638 ppm total REE. They are potassic to ultrapotassic (molar K₂O/Na₂O of 1.8–7.0) but not perpotassic (molar K₂O/Al₂O₃ of 0.49–0.91), and are rich in volatiles, with 2.9–10.8 wt. % total loss-on-ignition (LOI), 0.23–0.49 wt. % F and 0.03–2.23 wt. % total C (equivalent to 0.11–8.50 wt. % CO₂).

The atomic 100Mg/(Mg+Fe²⁺) ratio (Mg#) ranges from 57 to 78. All of these rocks are silica undersaturated, characterized by the presence of normative olivine (ol; 0.8–24.8 wt. %), nepheline (ne; 1.5–9.8 wt. %) and leucite (lc; 0.0–41.2 wt. %). The molar (Na₂O+K₂O)/Al₂O₃ ratio ranges from 0.8 to 1.1, with the peralkaline rocks containing normative acmite (ac; 1.9–6.1 wt. %). The presence of up to 14.1 wt. % normative larnite (cs) reflects the significant calcite that occurs in some of these rocks.

Table 2. Representative whole-rock analyses of magmatic rocks from the Milk River area of southern Alberta and the Sweet Grass Hills of northern Montana.

Sample No.	8151	8152	8156	8162	8165	8167	8171	8230	8234	8242	8244
Petrographic Type:	LR	LR	OM	OM	OM	OM	OM	R	LT	LT	M
SiO ₂ (wt %)	49.39	41.54	46.86	47.40	48.38	48.15	40.15	74.41	55.26	55.93	53.72
TiO ₂	1.72	1.45	0.98	1.03	1.05	0.88	1.08	1.66	0.69	0.70	0.75
Al ₂ O ₃	12.97	11.60	9.60	10.12	10.39	10.19	11.36	10.50	15.89	15.33	14.06
Fe ₂ O ₃ total	8.49	7.80	9.14	9.59	8.20	6.86	7.50	0.70	7.98	6.36	8.83
MnO	0.07	0.06	0.14	0.14	0.14	0.12	0.15	<0.01	0.12	0.08	1.25
MgO	6.13	4.94	13.16	11.01	9.44	8.59	9.80	0.09	2.79	3.15	4.08
CaO	2.62	8.65	7.42	7.95	6.65	8.50	9.70	0.16	5.26	5.37	2.84
Na ₂ O	1.63	1.23	1.59	1.52	1.84	2.24	1.04	1.42	4.98	3.86	3.87
K ₂ O	10.68	9.20	4.34	5.55	6.64	6.37	7.98	6.86	4.11	5.36	4.63
P ₂ O ₅	1.83	1.65	1.06	1.20	1.09	1.05	1.07	0.13	0.54	0.54	0.71
SrO	0.26	0.23	0.11	0.15	0.18	0.23	0.15	0.16	0.12	0.14	0.07
BaO	0.57	0.50	0.35	0.39	0.40	0.48	0.43	0.39	0.29	0.49	0.42
Cr ₂ O ₃	0.08	0.07	0.13	0.10	0.10	0.07	0.18	0.08	<0.01	0.01	0.03
V ₂ O ₃	0.03	0.02	0.03	0.03	0.02	0.02	0.03	0.01	0.02	0.02	0.03
ZrO ₂	0.06	0.03	0.03	0.03	0.04	0.04	0.02	0.03	0.02	0.02	0.02
Rb ₂ O	0.04	0.03	0.01	0.02	0.02	0.02	0.03	0.02	0.01	0.01	0.01
NiO	0.01	0.01	0.06	0.04	0.03	0.02	0.04	<0.01	<0.01	<0.01	0.06
CoO	0.01	<0.01	0.01	0.01	<0.01	<0.01	0.01	<0.01	<0.01	<0.01	0.04
LOI	3.30	10.80	4.80	3.50	5.20	6.00	9.17	3.30	1.80	2.50	4.40
Total	99.89	99.82	99.80	99.77	99.82	99.83	99.87	99.92	99.89	99.89	99.82
C	0.09	0.42	0.03	0.32	0.82	1.43	1.75	0.14	0.04	0.25	0.03
F	0.49	0.46	0.23	0.23	0.27	0.25	0.33	0.03	0.07	0.11	0.14
S	0.21	3.18	0.02	0.05	<0.02	<0.02	0.06	0.24	<0.02	1.71	<0.02
CIPW norm (wt %)											
Q	-	-	-	-	-	-	-	40.57	-	0.39	-
C	-	-	-	-	-	-	-	0.38	-	-	-
Z	0.09	0.05	0.05	0.05	0.07	0.06	0.04	0.05	0.03	0.03	0.03
or	53.21	6.61	27.19	34.31	41.70	37.72	-	41.92	24.92	32.11	28.88
ab	-	-	11.49	4.72	5.24	-	-	12.41	39.54	33.08	34.50
an	-	-	6.62	4.60	0.48	-	3.04	1.19	9.15	8.89	7.84
ne	3.99	4.91	1.49	4.72	6.11	9.78	5.25	-	1.97	-	-
lc	9.60	41.22	-	-	-	2.02	40.97	-	-	-	-
ac	6.07	1.97	-	-	-	1.94	-	-	-	-	-
di	0.32	26.82	20.06	23.20	21.79	30.81	14.89	-	12.35	12.50	2.24
hy	-	-	-	-	-	-	-	0.23	-	3.93	16.65
ol	16.51	0.76	24.75	19.58	15.95	10.94	19.58	-	6.07	-	2.56
cs	-	-	-	-	-	-	7.38	-	-	-	-
cm	0.12	0.11	0.20	0.15	0.16	0.11	0.28	0.11	-	0.02	0.05
hm	-	0.76	-	-	-	-	-	0.23	-	-	-
mt	0.37	1.18	3.02	3.13	3.06	1.61	2.60	-	3.17	2.50	3.61
il	3.38	2.99	1.97	2.04	2.12	1.79	2.27	0.30	1.34	1.35	1.50
ru	-	-	-	-	-	-	-	1.56	-	-	-
ap	4.89	4.36	2.71	3.03	2.81	2.73	2.84	0.46	1.34	1.34	1.87
fr	0.78	0.73	0.31	0.27	0.39	0.36	0.55	0.05	0.05	0.14	0.18
pr	0.41	6.46	0.04	0.10	-	-	0.13	0.46	-	3.24	-
Mg#	66	63	78	74	75	77	77	26	49	57	55
P.I.	1.10	1.03	0.76	0.84	0.98	1.04	0.91	0.93	0.80	0.79	0.81
K ₂ O/Al ₂ O ₃ molar	0.89	0.86	0.49	0.59	0.69	0.68	0.76	0.71	0.28	0.38	0.36
K ₂ O/Na ₂ O molar	4.3	4.9	1.8	2.4	2.4	1.9	5.1	3.2	0.5	0.9	0.8
ΣREE	511	638	193	211	262	252	152	217	177	187	220
(La/Yb) _{CN}	42	51	20	20	22	25	18	44	14	15	17
(Ce/Yb) _{CN}	35	49	17	17	19	21	14	30	12	13	13
(La/Sm) _{CN}	4.3	3.7	3.2	3.0	3.4	3.4	3.0	9.8	3.1	3.1	3.4
(Gd/Yb) _{CN}	4.6	6.4	3.7	3.7	3.7	4.1	3.5	1.4	2.4	2.7	2.9
Eu ^{CN} /Eu*	0.81	0.83	0.92	0.91	0.92	0.89	0.97	1.24	1.04	1.09	0.87
K/U	7336	2349	16561	17161	15375	16147	39931	11086	16637	16094	10945
Rb/Cs	203	244	37	74	58	73	112	94	19	86	19
Rb/Zr	0.92	1.49	0.62	0.76	0.57	0.64	1.56	0.63	0.50	0.58	0.89
Ba/La	49	39	83	87	70	87	130	59	75	130	83
Ba/Nb	212	203	284	316	212	311	382	35	294	448	413
Ba/Th	104	113	418	409	273	432	657	137	359	607	522
La/Nb	4.3	5.2	3.4	3.6	3.0	3.6	2.9	0.6	3.9	3.4	5.0
Nb/U	1.9	0.6	4.7	3.9	4.4	4.0	5.4	19	4.2	3.5	2.5
Ce/Pb	4.9	8.5	4.0	3.5	3.8	3.0	2.7	2.3	1.5	5.4	25
Th/Ta	38	25	15	12	10	8.3	11	6.0	6.1	18	6.0
Th/Yb	29	26	6.0	6.2	8.4	7.4	5.3	28	4.3	4.7	3.9
Zr/Nb	18	10	20	21	19	20	18	2	18	16	17
Y/Nb	0.9	1.2	1.5	1.6	1.2	1.3	1.5	0.1	2.2	1.9	3.2

Abbreviations: LR, sanidine-phlogopite lamproite (±olivine); OM, olivine minette (±carbonate±analcime); R, high-K rhyolite (felsite breccia); LT, hornblende-diopside latite; M, propylitically altered minette (±olivine); LOI, loss on ignition at 1000°C; Mg#, atomic 100 Mg/(Mg + Fe²⁺) using Fe³⁺/Fe²⁺ ratios according to Middlemost (1989); P.I., Peralkalinity Index = molar (Na₂O + K₂O)/Al₂O₃; ΣREE, total rare earth elements; CN, normalized to CI carbonaceous chondrite (McDonough and Sun, 1995). CIPW norms calculated by IUGSTAS code (Le Maitre et al., 2002) using (oxides+S+F) totals normalized to 100% on H₂O- and CO₂-free basis and Fe²⁺/Fe³⁺ ratios according to Middlemost (1989). * measure of Eu-anomaly on chondrite-normalized REE plot.

The 49th Parallel dikes are distinguished from minettes and other potassic rocks of the Milk River area by the higher TiO₂, K₂O, P₂O₅, S, F, Rb, Nb, Th, U and REE concentrations, higher K₂O/Al₂O₃, Ce/Yb, La/Sm, Gd/Yb, Rb/Cs, Ce/Pb, Th/Ta and Th/Yb ratios, and lower Mg#, Eu/Eu*, Ba/La, Ba/Th and Nb/U (Table 2).

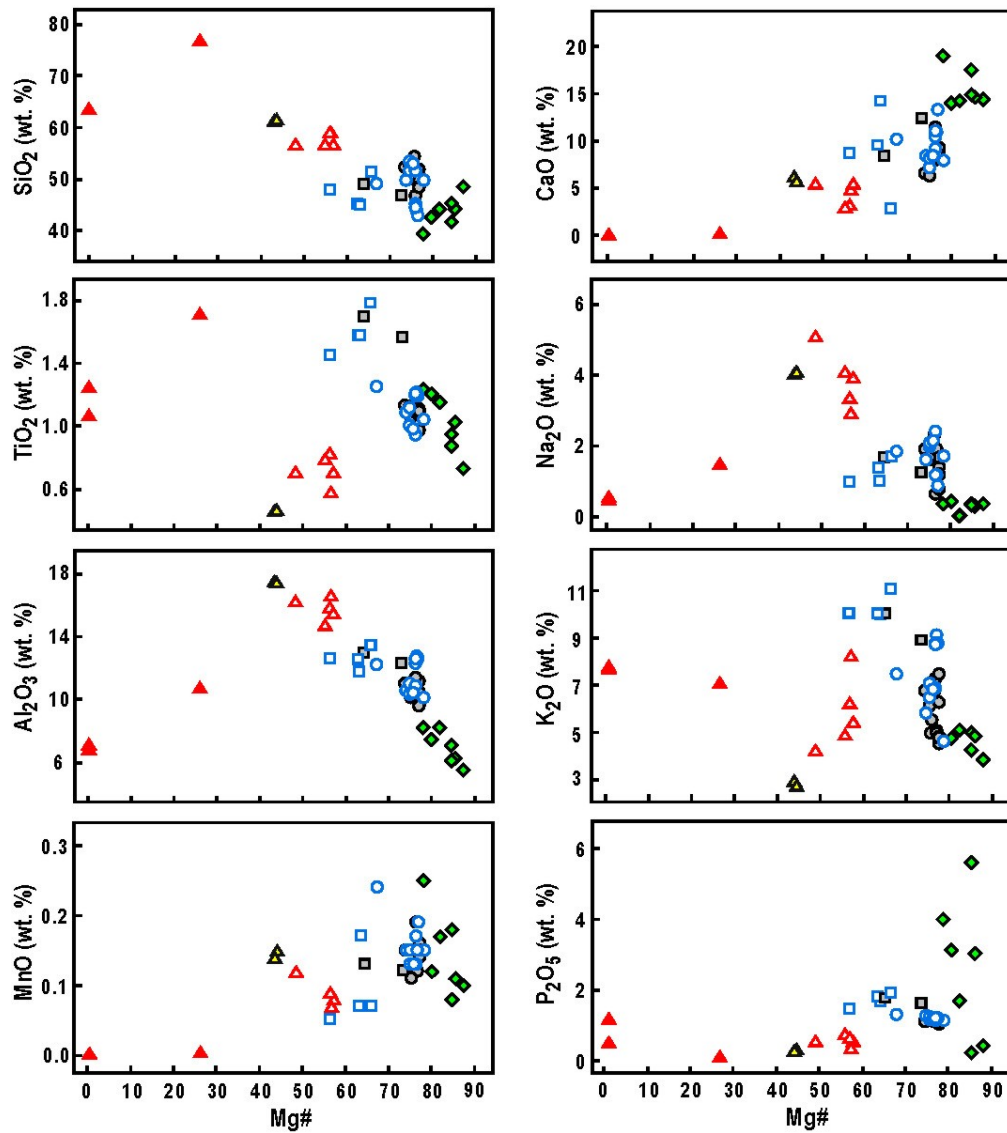
The Gold Butte minettes, latites and trachytes, and the Grassy Butte felsite breccia contain 53.7–74.4 wt. % SiO₂, 0.57–1.66 wt. % TiO₂, 6.06–16.41 wt. % Al₂O₃, 0.02–4.08 wt. % MgO, 0.04–5.37 wt. % CaO, 0.43–4.98 wt. % Na₂O, 4.11–8.09 wt. % K₂O and 0.13–1.03 wt. % P₂O₅. Compared to olivine minettes and other phlogopite-rich rocks of the Milk River area, these have a greater concentration range of volatiles (1.8–15.3 wt. % LOI), and lower F (0.03–0.15 wt. %) and total C (0.03–0.25 wt. %; equivalent to 0.04–0.92 wt. % CO₂). Trace-element concentrations also have large ranges: 26–666 ppm Cr, 54–215 ppm V, 11–488 ppm Ni, 79–155 ppm Rb, 2241–4431 ppm Ba, 560–1381 ppm Sr, 47–280 ppm Zr and 177–293 ppm REE. The majority of these rocks have Mg# in the range 26–57 and are mildly potassic (molar K₂O/Na₂O of 0.5–3.2; molar K₂O/Al₂O₃ of 0.28–0.71), with molar (Na₂O+K₂O)/Al₂O₃ of 0.8–0.9 (Table 2). They are silica oversaturated, with normative quartz (Q; 0.4–40.6 wt. %) and/or hypersthene (hy; 0.2–16.7 wt. %), to mildly undersaturated, with nepheline and/or olivine (ol; 2.6–6.1 wt. %) in their norms. Two altered samples of the Grassy Butte felsite breccia have very low Mg# (0.36–0.38) and are perpotassic (molar K₂O/Al₂O₃ of 1.15–1.22) and peralkaline, with molar (Na₂O+K₂O)/Al₂O₃ of 1.3 and K₂O/Na₂O of 9.3–10.5.

Figures 13 and 14 show whole-rock major- and trace-element concentrations, respectively, plotted against Mg# in the magmatic rocks of the Milk River area and Sweet Grass Hills. The new results are compared with published data for the Milk River intrusions and ultramafic xenoliths (mica-clinopyroxenite and glimmerite), interpreted to be cumulate crystallized from the minette magmas (Kjarsgaard, 1994, 1997; Buhlmann et al., 2000).

Our new whole-rock data overlap and extend the compositional range of the published data. Both major and trace elements display large variations from olivine minettes of the Milk River area to more felsic latites, trachytes and felsite breccia of the Sweet Grass Hills, with increasing SiO₂ concentrations at decreasing Mg#, MnO, CaO, Cr, Ni, V and Co, suggesting a fractional crystallization process. Variations of TiO₂, K₂O, P₂O₅, Rb, Ba, Sr, Nb, Th, Zr, Y and REE show inversions, with enrichment from olivine minettes of the Milk River area to the 49th Parallel dikes and depletion in the latites and trachytes. Concentrations of Al₂O₃ and Na₂O increase from the olivine minettes to the latites and trachytes but are depleted in the Grassy Butte felsite breccia. The latter are enriched in TiO₂, Cr, Nb and Th, depleted in Y and have similar concentrations of K₂O, P₂O₅, Rb, Ba, Sr, Zr and Ce, relative to the latites and trachytes. The ultramafic xenoliths have higher CaO, P₂O₅ and Mg#, and similar or lower SiO₂, TiO₂, Al₂O₃, Na₂O, Cr, Ni and incompatible elements, relative to the host olivine minettes.

Representative whole-rock analyses of igneous rocks from the Milk River area and Sweet Grass Hills are plotted on chondrite-normalized REE diagrams (Figure 15a) and primitive mantle-normalized incompatible-element diagrams (Figure 15b). Our data are compared with published compositions of coeval minettes from the Montana alkaline province (O'Brien et al., 1991, 1995; Macdonald et al., 1992) and with lamproites from Wyoming, Colorado and southeastern Spain (Mitchell and Steele, 1992; Toscani et al., 1995; Thompson et al., 1997; Benito et al., 1999; Toscani, 1999; Turner et al., 1999; Mirnejad and Bell, 2006).

Overall, the analyzed samples are characterized by their REE enrichment (by a factor of 5 to 500) relative to chondritic abundances, with fractionated, light REE (LREE)-enriched patterns (La_N/Yb_N of 14–51) and weak to moderate Eu anomalies (Eu_N/Eu* of 0.81–1.24). Primitive mantle-normalized incompatible-element patterns indicate that Th, Ta, Nb and Ti are less enriched than Ba, K, REE, Sr and P.



LEGEND

Milk River area, southern Alberta:

- Minette and phlogopite trachyte
- Minette (Kjarsgaard, 1994; Buhlmann et al., 2000)
- 49th Parallel dikes
- 49th Parallel dikes (Kjarsgaard, 1994; Buhlmann et al., 2000)
- ▲ McTaggart Coulee latite (Kjarsgaard, 1994; Buhlmann et al., 2000)
- ◆ Mica-clinopyroxenite xenoliths (Buhlmann et al., 2000)

Sweet Grass Hills, northern Montana:

- ▲ Gold Butte minette, latite and trachyte
- ▲ Grassy Butte felsite breccia

Figure 13. Whole-rock concentrations of SiO₂, TiO₂, Al₂O₃, MnO, CaO, Na₂O, K₂O and P₂O₅ (wt. %) versus Mg# (100Mg/[Mg+Fe₂₊]; Fe³⁺/Fe²⁺ ratios adjusted after Middlemost, 1989) for igneous rocks from the Milk River area and Sweet Grass Hills.

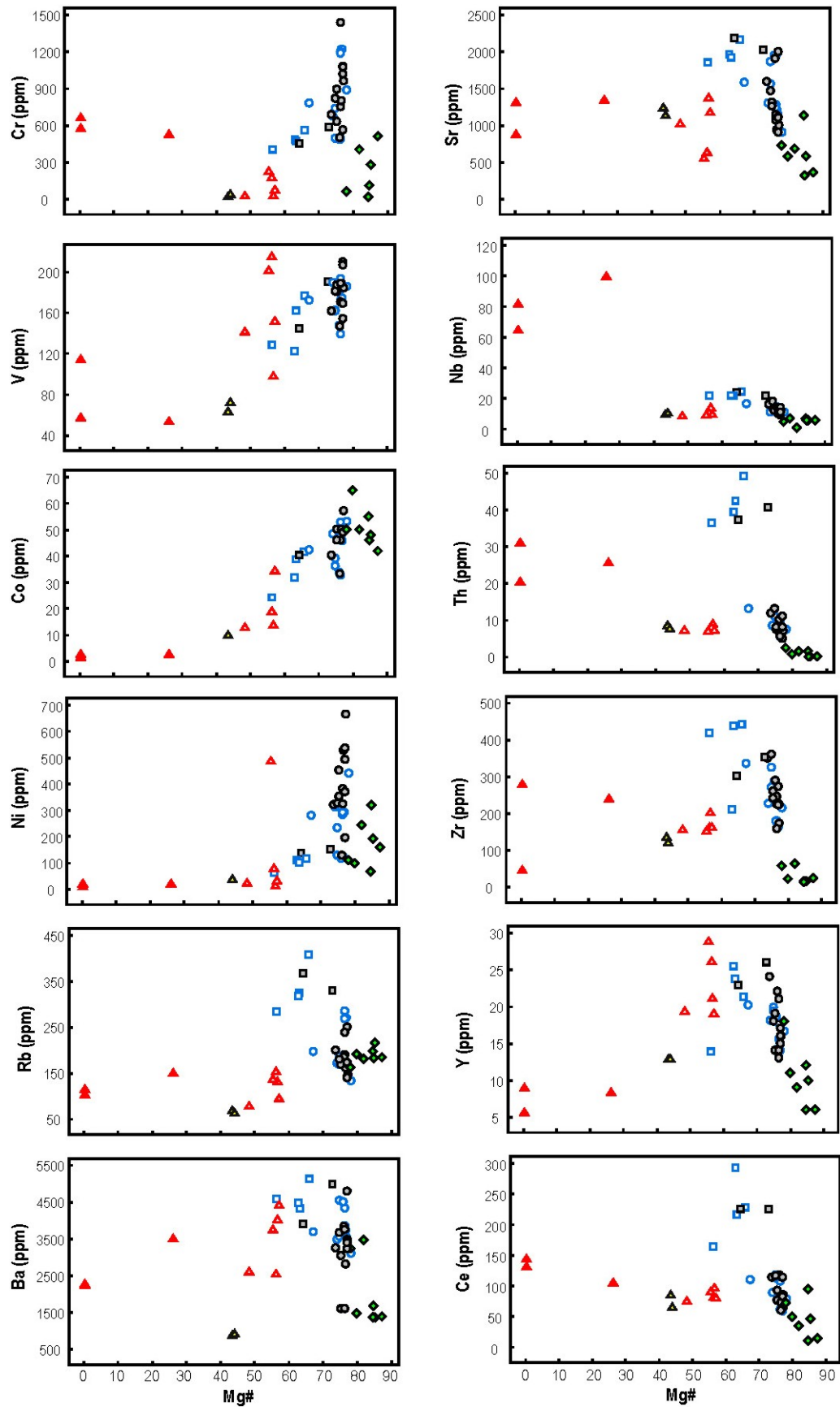


Figure 14. Whole-rock concentrations of selected trace elements (ppm) versus Mg# ($100\text{Mg}/[\text{Mg}+\text{Fe}^{2+}]$; $\text{Fe}^{3+}/\text{Fe}^{2+}$ ratios adjusted after Middlemost, 1989) for igneous rocks from the Milk River area and Sweet Grass Hills.

See Figure 13 for explanation of symbols.

Compared to minettes and other potassic rocks of the Milk River area, the 49th Parallel dikes have the highest Ti, K, P, Rb, Nb, Th, U, Zr, Hf and REE concentrations and more fractionated, LREE-enriched patterns, similar to the Spanish and North American lamproites. In contrast, the Milk River minettes have REE and incompatible-element patterns similar to minettes of the Bearpaw and Highwood mountains (Figure 15).

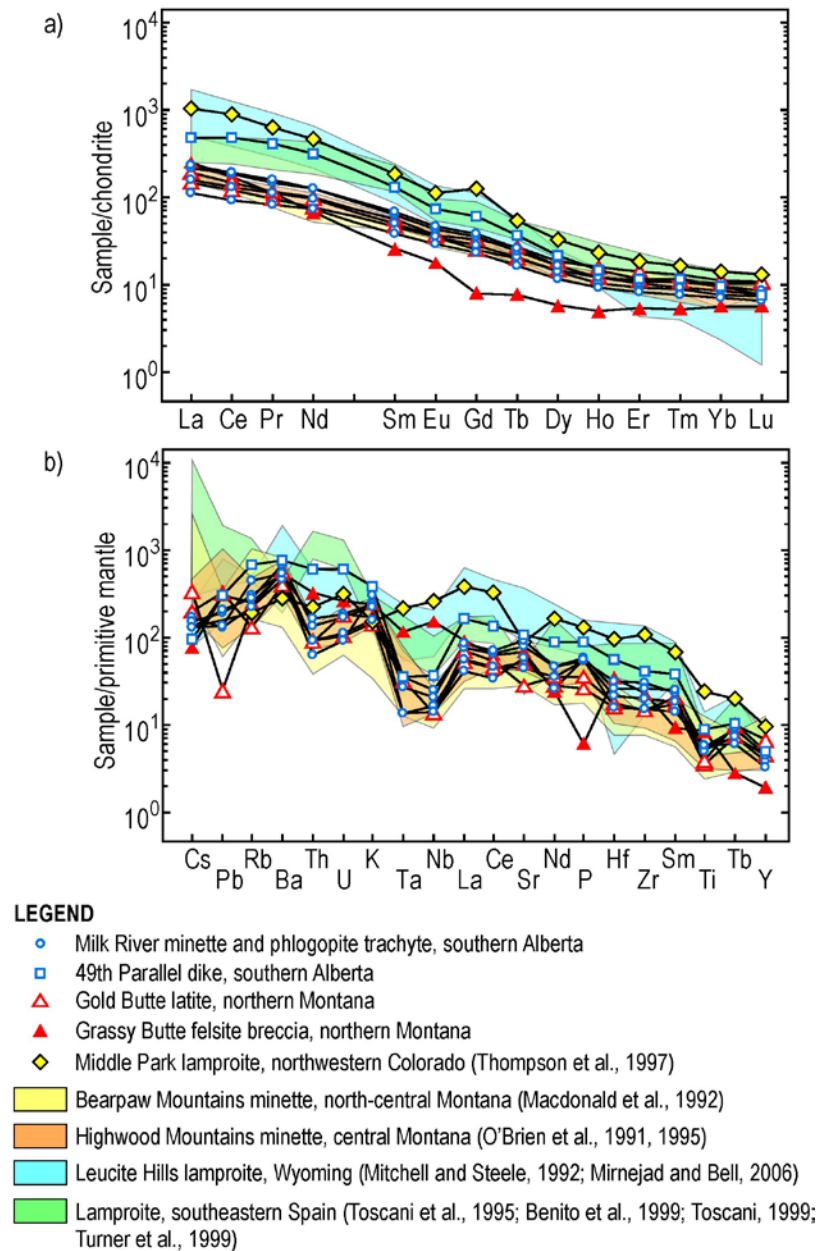


Figure 15. Normalized whole-rock patterns for representative analyses of igneous rocks from the Milk River area and Sweet Grass Hills: a) chondrite-normalized rare-earth element plots, and b) primitive mantle-normalized incompatible-element diagrams. Shown for comparison are the compositions of minettes from the Bearpaw and Highwood mountains (Montana), and lamproites from Middle Park (northwestern Colorado), Leucite Hills (Wyoming) and southeastern Spain. Normalization values are from McDonough and Sun (1995).

The Gold Butte latites and trachytes display REE and incompatible-element patterns similar to the Milk River minettes, with the former having slightly higher Cs and Y, and lower Rb, Ba, Sr, P and Ti abundances. The Grassy Butte felsite breccia is distinguished from other potassic rocks of the study area by higher Ta and Nb concentrations and La/Sm and Eu/Eu* ratios, coupled with lower Cs, P, Y, middle REE (MREE), heavy REE (HREE) and Gd/Yb (Figure 15).

7.2 Geochemical Signatures of Mineralization

Whole-rock concentrations, with highlighted anomalous values, of selected elements in magmatic rocks, hydrothermal veins, and adjacent sedimentary rocks in the Milk River area and the Sweet Grass Hills are listed in Tables 3 and 4, respectively.

In the Milk River area, lamproite and minette intrusions contain erratic elevated concentrations of Ag (up to 2.8 ppm), Cu (up to 182 ppm), Mo (up to 59 ppm), Pd (up to 17 ppb), Pt, Ce, Th, U, Co, Cr, Ni, Ba, Sr, Zr and F. The increased concentrations of metals appear to correlate with locally abundant quartz-carbonate veins and weak propylitic, argillic and supergene alteration, manifested by secondary carbonate, clinozoisite, chlorite, albite, clay minerals, sulphates, goethite and jarosite. Sporadic copper sulphides occur within the Black Butte minette-trachyte plug. Bleached and hornfelsed sedimentary rocks of the Belly River Group and Pakowki Formation, adjacent to the magmatic bodies, contain erratic elevated concentrations of Au (up to 9 ppb), Ag (up to 0.8 ppm), Mn (up to 0.17 wt. %), Cd, Pd and Re. A carbonate vein crosscutting the Coulee 29 vent returned anomalous concentrations of Pb (402 ppm), Zn (491 ppm) and Mn (3752 ppm), coupled with increased values of Ag, Cd, Cr, Ni, Pd and Pt (Table 3).

In comparison with the Milk River area, intermediate to felsic intrusions and adjacent sedimentary rocks at Grassy and Gold buttes of the Sweet Grass Hills display strong potassic and/or propylitic alteration, overprinted by intermediate argillic alteration and oxidation. Alteration minerals include K-feldspar, quartz, albite, epidote, clinozoisite, tremolite-actinolite, chlorite, illite, clays, pyrite, sulphates, calcite, hematite, goethite, jarosite and Mn-oxides. At Grassy Butte, argillitized and oxidized felsite breccia and adjacent brecciated and hornfelsed siliciclastic rocks of the Montana Group contain highly anomalous concentrations of Au (235–959 ppb), As (0.21–0.25 wt. %), W (184–432 ppm), Tl (27–72 ppm), Sb (25–46 ppm), Se (1.5–1.8 ppm) and Hg (0.5–1.3 ppm), along with erratic anomalous values of Ba (up to 0.4 wt. %), Cr, Ge, platinum-group elements (PGE), Sn and Th (Table 4). The felsite breccia-related Au–As–W–Tl–Sb–Hg–Se±Ba±Cr±PGE geochemical signature and associated potassic to intermediate argillic alteration indicate epithermal mineralization.

At Gold Butte, propylitized and argillitized trachyte, latite and minette dikes and sills contain anomalous concentrations of Au (26–100 ppb), Ba (0.4–0.5 wt. %), Cu (251–290 ppm), W (10–32 ppm) and Bi (1.0–2.3 ppm), along with erratic anomalous concentrations of Mn (up to 1.0 wt. %), Zn (up to 270 ppm), Ag (up to 0.6 ppm), Ni (up to 488 ppm), Co (up to 287 ppm), Se (up to 4.5 ppm), Cd, Cr, Mo, PGE, As, Sb, Te and Tl (Table 4). Chalcopyrite is abundant in some of these dikes, forming centimetre-size blebs (Figure 9f). The adjacent silicified and pyritized hornfels breccias after siliciclastic rocks of the Colorado Group contain anomalous concentrations of Au (18–25 ppb), Ba (0.22–0.43 wt. %) and As (26–35 ppm), coupled with erratic increased values of W (up to 75 ppm), Sn (up to 31 ppm), Ce, K, Rb, Re, Sb, U and V (Table 4). The intermediate intrusion-hosted Au–Ag–Cu–W–Ba–Bi±Ag±Zn±PGE±Mn±As±Se signature and the related, hornfels-hosted Au–As±Ba±W±Sb±Sn signature, associated with strong potassic, propylitic and intermediate argillic alteration, indicate porphyry- to epithermal-style mineralization at Gold Butte.

Table 3. Concentrations of selected elements in magmatic, hydrothermal and adjacent sedimentary rocks of the Milk River area, southern Alberta. Site numbers (in parentheses) are as in Table 1; elevated values are in bold.

Location	49th Parallel (SG01)		Coulee 29 (SG02)			Philp Coulee (SG03)		Black Butte (SG04)	Bear Creek (SG05)	
	Lithology	Lamproite	BR mdst.	Minette	Calcite vein	PF/BR sh., ss., co.	Minette	BR calc. ss., sh.	Minette	Minette
Ag (ppb)	2800	50	55	800	800	2500	123	59	200	33
As	4.0	4.0	1.3	3.7	16	1.5	12	1.9	3.2	21
Au (ppb)	3.0	9.0	5.0	3.0	5.0	0.7	4.0	2.0	3.0	0.3
Ba	5970	720	4017	1175	880	4162	801	4800	4296	850
Bi	0.20	0.50	0.10	0.15	0.43	0.12	0.20	0.20	0.10	0.12
Cd	0.40	0.23	0.30	1.8	0.40	0.60	1.1	0.30	0.30	0.10
Ce	300	89	88	34	78	112	48	117	64	43
Co	42	10	53	17	10	42	18	36	53	10
Cr	561	57	883	287	56	780	91	490	1218	90
Cu	182	27	100	44	26	54	57	75	94	20
F	4910	1100	2330	850	1190	2830	450	3030	3460	640
Ge	0.3	<0.1	0.2	<0.1	0.1	0.1	<0.1	0.2	0.2	<0.1
Hg (ppb)	20	10	<5	<5	9	7	<5	<5	14	14
K (wt %)	8.9	2.5	4.6	1.6	3.1	5.6	1.5	5.5	6.8	1.5
Mn	1215	160	1167	3752	800	1821	1657	1065	1420	1588
Mo	59	3.3	1.1	3.3	8.0	2.6	1.6	0.7	5.0	3.0
Ni	116	26	438	128	28	278	49	127	294	26
Pb	46	20	25	402	23	32	15	42	25	10
Pd (ppb)	17	<0.5	12	2.5	<0.5	<0.5	0.6	16	12	4.2
Pt (ppb)	5.0	<0.1	5.7	1.8	0.9	3.0	0.5	4.9	5.9	0.8
Rb	406	132	172	56	164	195	65	182	284	69
Re (ppb)	4	11	<1	<1	14	<1	2	1	<1	4
S (wt %)	3.70	0.13	0.05	0.05	0.03	<0.02	0.04	<0.02	0.13	0.20
Sb	0.4	0.6	0.6	0.5	2.4	0.4	1.3	0.2	0.2	0.5
Se	0.8	0.2	0.4	0.3	0.6	0.4	0.6	0.3	0.6	0.5
Sn	3.1	3.0	2.0	1.3	3.0	2.3	1.2	1.9	2.0	1.2
Sr	2162	149	1298	1086	411	1579	362	1947	1275	668
Te	0.11	<0.02	<0.02	0.10	0.07	0.03	0.05	0.08	0.06	0.06
Th	49	13	8.5	2.8	13	13	6.4	11	6.7	6.0
Tl	1.22	0.36	0.72	0.21	0.68	0.60	0.06	0.42	1.01	0.16
C (wt %)	2.32	0.24	0.32	9.26	8.11	1.51	5.58	1.43	2.16	6.94
U	35	4.9	3.1	1.0	6.4	3.9	3.6	3.5	2.2	2.3
V	176	93	189	77	99	172	127	161	193	126
W	3.9	3.0	0.3	0.7	2.9	2.0	1.6	0.6	4.0	1.5
Y	26	35	18	11	28	20	22	19	16	19
Zn	120	89	100	491	93	100	120	110	87	110
Zr	451	201	230	69	194	351	161	286	185	167

Concentrations in parts per million (ppm) unless otherwise indicated

Lithology abbreviations: **co.**, coal; **calc.**, calcareous; **mdst.**, mudstone; **sh.**, shale; **ss.**, sandstone; **sts.**, siltstone; **BR**, Belly River Group; **PF**, Pakowki Formation

Table 4. Concentrations of selected elements in Eocene intrusions and adjacent sedimentary rocks of the Sweet Grass Hills, northern Montana. Site numbers (in parentheses) are as in Table 1; elevated values are in bold.

Location	Grassy Butte (SG06)		Gold Butte (SG07)			
	Felsite breccia	Hornfelsed MG siliciclastics	Latite	Minette	Hornfelsed CG siliciclastics	Silicified CG blk. sh., mdst., ss.
Ag (ppb)	99	21	617	200	27	200
As	2506	2116	4.7	54	35	26
Au (ppb)	235	959	26	100	25	18
Ba	4000	240	5000	4300	4300	2200
Bi	0.05	0.13	2.3	0.97	0.25	0.39
Cd	0.03	0.02	0.90	1.9	0.20	0.10
Ce	144	9.1	100	91	213	85
Co	3.1	0.8	35	287	13	8.3
Cr	666	88	81	230	120	120
Cu	39	15	251	290	31	37
F	310	80	1120	1470	340	930
Ge	1.3	0.4	0.2	0.3	0.2	0.1
Hg (ppb)	501	1296	<5	6	<5	<5
K (wt %)	5.7	2.5	6.7	4.9	10.7	3.8
Mn	28	22	930	9933	657	232
Mo	1.0	0.7	2.6	15	4.7	5.0
Ni	23	4	35	488	56	47
Pb	46	20	70	5.5	28	12
Pd (ppb)	4.5	<0.5	1.1	4.0	2.0	1.6
Pt (ppb)	4.1	0.2	1.0	8.0	1.2	0.6
Rb	151	42	140	160	220	158
Re (ppb)	3	3	2	<1	1	7
S (wt %)	4.00	2.80	1.92	<0.02	<0.02	0.07
Sb	25	46	0.6	1.5	2.7	0.6
Se	1.5	1.8	4.5	0.4	0.3	0.5
Sn	16	1.6	3.2	2.1	31	2.0
Sr	1351	52	1381	640	418	727
Te	0.03	0.06	0.35	0.18	0.13	0.14
Th	31	2.0	9.1	8.3	14	13
Tl	72	27	0.36	7.8	0.47	0.83
C (wt %)	0.19	0.25	0.25	0.03	0.16	0.58
U	5.4	1.7	3.5	4.3	15	6.4
V	115	44	152	215	206	249
W	432	184	10	32	75	6.0
Y	9.0	1.1	21	29	26	32
Zn	5.0	2.2	270	110	100	78
Zr	280	30	203	164	160	197

Concentrations in parts per million (ppm) unless otherwise indicated

Lithology abbreviations: **blk.**, black; **mdst.**, mudstone; **sh.**, shale; **ss.**, sandstone; **MG**, Montana Group; **CG**, Colorado Group

8 Discussion

8.1 Classification of Igneous Rocks

Kjarsgaard (1994, 1997) pointed out that whole-rock geochemistry or modal mineralogy alone might be insufficient to categorize potassic rocks of the Milk River area. Here, we classify these rocks on the basis of both whole-rock geochemical and mineralogical criteria using a hybrid approach proposed by Mitchell and Bergman (1991).

In the total alkalis versus silica (TAS) diagram (Le Bas et al., 1986), the majority of the whole-rock compositions fall into the alkaline field, with the Milk River minettes and other phlogopite-rich rocks plotting into the fields of potassic trachybasalt, shoshonite, tephrite or basanite, foidite, phonotephrite, tephriphonolite and latite (Figure 16a). Analyses of the McTaggart Coulee ‘diorite porphyry’ or ‘benmoreite’ from Kjarsgaard (1994) and Buhlmann et al. (2000), respectively, correspond to latite. The Gold Butte feldspar-phyric rocks and minettes fall into the fields of latite and trachyte. Data points for the Grassy Butte felsite breccia plot within the fields of trachyte and high-K rhyolite.

All of the rocks are potassic, having $K_2O > (Na_2O - 2)$ after Le Maitre et al. (2002). In the Milk River area, the majority are ultrapotassic rocks, with $MgO > 3$ wt. %, molar $K_2O/Na_2O > 2$, and $K_2O > 3$ wt. % (Figure 16b), based on the criteria proposed by Foley et al. (1987). However, only the 49th Parallel and Bear Creek dikes have molar $K_2O/Na_2O > 3$, as required for ultrapotassic designation according to Le Maitre et al. (2002).

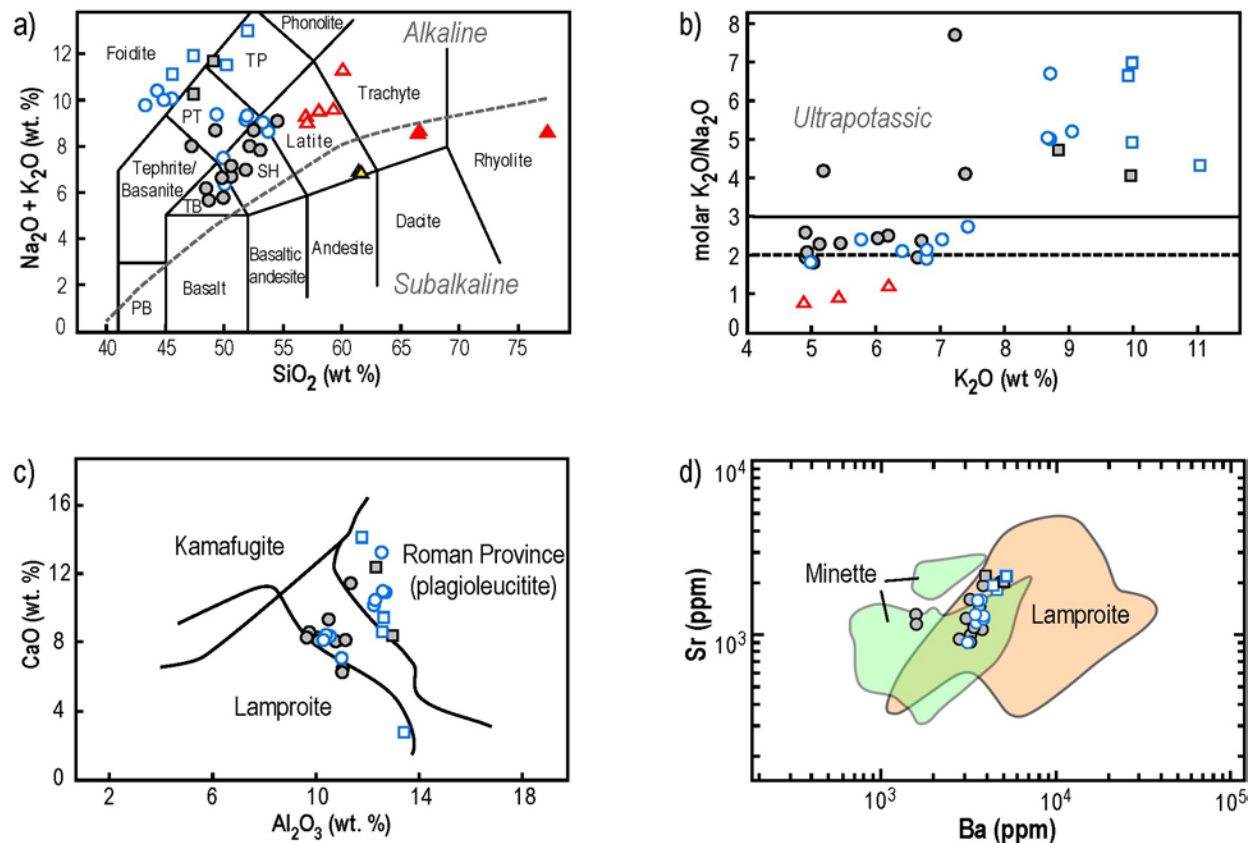
The TAS classification appears to be satisfactory for latites, trachytes and felsite breccia of the study area. However, it is unsuitable for the Milk River phlogopite-rich rocks because the assigned root names suggest inappropriate modal mineralogy and obscure the petrogenetic relationships between these rocks (Mitchell and Bergman, 1991).

Foley et al. (1987) subdivided ultrapotassic rocks into three groups based on major elements. They also recognized compositionally transitional rocks associated with two of the three groups. In the CaO versus Al_2O_3 classification (Foley et al., 1987; Foley, 1992), the Milk River ultrapotassic rocks appear to scatter between the fields of lamproites and Roman Province plagioclitites (Figure 16c). Therefore, the CaO versus Al_2O_3 classification fails to categorize the ultrapotassic rocks of the Milk River area.

Mitchell and Bergman (1991) discriminated worldwide lamproites from other potassic rocks using trace elements. On their Sr versus Ba diagram, the 49th Parallel dikes fall into the field of lamproite, whereas the majority of other potassic rocks of the Milk River area plot in the area of overlap between minette and lamproite (Figure 16d).

Normalized REE and incompatible-element diagrams provide more conclusive discrimination for potassic rocks of the Milk River area (Figure 15). As discussed above, the 49th Parallel dikes have a more fractionated distribution of REE, characterized by stronger enrichment in LREE, and incompatible-element patterns similar to lamproites. In contrast, the distribution of REE and incompatible elements in olivine minettes of the Milk River area is similar to that in minettes of the Bearpaw and Highwood mountains in Montana (O’Brien et al., 1991, 1995; Macdonald et al., 1992).

Kjarsgaard (1997) previously described the 49th Parallel dikes as “peralkaline minette” and other ultrapotassic rocks of the Milk River area as “alkali olivine minette” and “alkali minette.” He compared the “peralkaline minette” to the diamondiferous Akluilâk lamprophyre dike of the Gibson Lake area in the Northwest Territories, which resembles lamproite in several respects (MacRae et al., 1996; Peterson, 1996). However, our data indicate that the 49th Parallel dikes contains lower Al_2O_3 , CaO and Ba , and higher TiO_2 , MgO , total Fe_2O_3 , K_2O , Cr , Ni and Sr contents relative to the Akluilâk dike.



LEGEND

Milk River area, southern Alberta:

- Minette and phlogopite trachyte
- Minette (Kjarsgaard, 1994; Buhlmann et al., 2000)
- 49th Parallel dikes
- 49th Parallel dikes (Kjarsgaard, 1994; Buhlmann et al., 2000)
- ▲ McTaggart Coulee latite (Kjarsgaard, 1994; Buhlmann et al., 2000)

Sweet Grass Hills, northern Montana:

- ▲ Gold Butte minette, latite and trachyte
- ▲ Grassy Butte felsite breccia

Figure 16. Whole-rock chemical classification of magmatic rocks in the Milk River area of southern Alberta and the Sweet Grass Hills of northern Montana: a) total alkalis versus silica diagram after Le Bas et al. (1986), with the subdivision of the alkaline from subalkaline rocks (dashed line) after Irvine and Baragar (1971); b) molar K_2O/Na_2O versus K_2O (wt. %) plot for rocks with $MgO > 3$ wt. %, showing the subdivision of ultrapotassic from potassic rocks after Foley et al. 1987; dashed line) and Le Maitre et al. (2002; solid line); c) CaO versus Al_2O_3 (wt. %) plot for ultrapotassic rocks, showing the compositional fields of lamproites, kamafugites and Roman Province plagiocleucitites after Foley et al. (1987) and Foley (1992); and d) Sr versus Ba (ppm) plot showing the worldwide compositional fields of lamproites and minettes after Mitchell and Bergman (1991). Abbreviations: PT, phonotephrite; SH, shoshonite; TB, potassic trachybasalt; TP, tephriphonolite.

In addition, the latter contains Al₂O₃-rich, TiO₂-poor mica, whereas the 49th Parallel dikes have Al₂O₃-poor, TiO₂-rich phlogopite-annite, similar to mica in lamproites.

Mitchell and Bergman (1991) argued that a successful discrimination between rock types requires consideration of compositions of minerals in conjunction with their modal proportions; the presence of characteristic, often accessory, phases; and whole-rock geochemistry. Using this hybrid genetic approach, we propose to reclassify the 49th Parallel dikes as sanidine-phlogopite lamproite based on their compositional and mineralogical attributes, which are characteristic of the lamproite clan as defined by Mitchell and Bergman (1991).

In summary, the 49th Parallel lamproite dikes are more enriched in Ti, K, P, Rb, Nb, Th, U, Zr, Hf and LREE than olivine minettes of the Milk River area. The lamproite contains Al-poor and Ti-rich phlogopite-annite, Na-poor sanidine, Ba-rich and Cl-poor fluorapatite and LREE-rich strontian fluorapatite, Na-Ti-K-amphibole, ilmenite, strontian barite, barian celestine and an unidentified Zr-Ti phase, possibly after primary Zr-Ti silicate(s). Notably, the 49th Parallel lamproite lacks any magnetite and primary carbonates. In contrast, olivine minettes of the Milk River area contain ubiquitous titanomagnetite and primary magnesite and calcite without any ilmenite.

The whole-rock geochemistry and modal mineralogy, coupled with the compositions of sanidine, apatite and mica, mica-zonation trends and the absence of Al-rich clinopyroxene are diagnostic of the lamproite clan and distinguish the 49th Parallel dikes from olivine minettes of the Milk River area. These mineralogical and geochemical differences indicate a mantle source for the 49th Parallel lamproite magma that is reduced, CO₂ poor and more enriched in LREE and other incompatible elements, unlike the source of the olivine minettes, which are less enriched in LREE and incompatible elements, oxidized and carbonated.

8.2 Mantle Sources and Primary Magmas

Primary magmas have undergone little or no modification during ascent from their source region. The more primitive, Mg-rich olivine minettes of the Milk River area satisfy the compositional criteria commonly used to identify primary mantle-derived magmas, namely high Mg# (>65) and Ni contents between 235 and 400 ppm (Sato, 1977; Frey et al., 1978; Clague and Frey, 1982). These criteria assume that primary melts form in equilibrium with an olivine-bearing mantle. However, presence of olivine as a major or residual phase may not be required in the sources of all mantle-derived magmas.

Sekine and Wyllie (1982) presented experimental evidence for generation of a phlogopite-clinopyroxene-orthopyroxene assemblage by reaction between hydrous siliceous melts rising from the subducting slab and peridotite of the overlying mantle in subduction zones. Partial melting of this assemblage due to lithospheric extension produces alkaline magmas at convergent margins (Sekine and Wyllie, 1982). Based on high-pressure experiments, Lloyd et al. (1985) also showed that phlogopite-clinopyroxene nodules in highly potassic lavas of southwestern Uganda could represent their source region in the subcontinental mantle. In addition, the olivine-free mantle xenoliths, rich in phlogopite, amphibole, clinopyroxene and Ti-oxide minerals, that are found in some kimberlites have been interpreted to represent cumulate or metasomatic rocks formed in the subcontinental mantle by kimberlite, Mg-rich lamproite or orangeite melts, or by alkaline hydrous vapour (Dawson and Smith, 1977; Sweeney et al., 1993; Grégoire et al., 2002). Olivine-free glimmerite and phlogopite-clinopyroxenite nodules are common in the Milk River minettes (Kjarsgaard, 1994, 1997; Walker, 1994, Buhlmann et al., 2000). These rocks have been interpreted to represent cumulate materials crystallized at depth from parent minette magmas (Buhlmann et al., 2000).

The presence of olivine phenocrysts, coupled with high MgO, Cr and Ni concentrations, in the Milk River minettes suggests that they are derived from an olivine-bearing mantle source. In an MgO versus Ni plot

(Figure 17), the position of whole-rock compositions for the Milk River lamproites and minettes with MgO <12 wt. % is consistent with derivation by olivine fractionation from a range of primary magmas in equilibrium with an olivine-bearing mantle (Hart and Davis, 1978; Clague and Frey, 1982). Rocks with MgO >12 wt. % might have accumulated olivine phenocrysts or derived from an unusually Ni-rich mantle (Hart and Davis, 1978). The presence of abundant phenocrysts suggests that olivine is likely accumulated in some of the minettes.

The olivine minette dike (sample 8156) at the Coulee 29 vent complex represents the most primitive composition for the Milk River area and Sweet Grass Hills that falls within the field of primary magmas (Figure 17). Some of the Bearpaw Mountains minettes (Macdonald et al., 1992) and the most primitive minette from the Highwood Mountains, with 14 wt. % MgO and 335 ppm Ni (O'Brien et al., 1991), also satisfy the compositional criteria commonly accepted for primary magmas (Sato, 1977; Frey et al., 1978; Clague and Frey, 1982).

The position of the 49th Parallel lamproite compositions in the Ni-MgO plot (Figure 17) suggests that these rocks could represent either a more evolved magma than that of the olivine minettes, or a primary magma with lower MgO and Ni contents. The contrasting normalized REE and incompatible-element patterns (Figure 15), coupled with the different Rb/Cs, Ba/La, Ba/Th, Nb/U, Th/Ta, Ce/Pb and Th/Yb ratios (Table 2), suggest that the 49th Parallel lamproite and olivine minettes of the Milk River area are more likely to represent the distinct primary magmas.

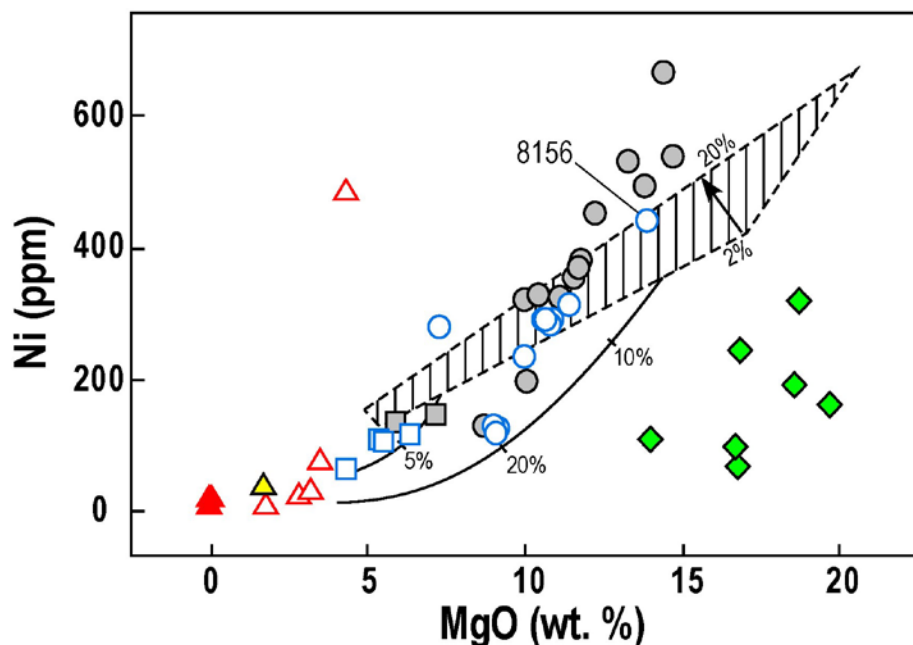


Figure 17. Plot of whole-rock Ni (ppm) versus MgO (wt. %) for igneous rocks and ultramafic xenoliths of the Milk River area and Sweet Grass Hills. Hatched field shows compositions of primary melts formed by 2%–20% partial melting of a model mantle with 70% olivine, 15%–20% orthopyroxene, 10% clinopyroxene, and 0%–5% garnet, and containing 2000–2500 ppm Ni (Hart and Davis, 1978; Clague and Frey, 1982). Curves are olivine-fractionation trends for the primary liquids, with cross-ticks indicating the percentage of olivine crystallized from the melts (modified after Macdonald et al., 1992). Olivine minette sample 8156 represents the most primitive primary magma in the Sweet Grass Hills igneous complex. Other symbols are as in Figure 13.

Buhlmann et al. (2000) presented Sr, Pb and Nd isotopic data for the Eocene magmatic rocks and ultramafic nodules of the Milk River area. Overall, the isotopic data for potassic rocks of the Milk River area indicate strongly nonradiogenic initial $^{143}\text{Nd}/^{144}\text{Nd}$ (-12.4 to $-19.4 E_{\text{Nd}}$ units) and $^{206}\text{Pb}/^{204}\text{Pb}$ (16.96–17.69) ratios, and a moderately radiogenic initial $^{87}\text{Sr}/^{86}\text{Sr}$ (0.7051–0.7075) ratio relative to bulk Earth composition (Buhlmann et al., 2000). On a regional scale, the isotopic data from potassic rocks of the Milk River area fall approximately in the centre of a broad, fan-shaped field defined by isolated and partially overlapping data fields from other igneous complexes of the Montana alkaline province, the Absaroka Range and the Leucite Hills lamproites (e.g., O'Brien et al., 1995; Mirnejad and Bell, 2006). These isotopic data fields from several alkaline complexes scatter from the bulk Earth composition well into the enriched quadrant, encompassing the EM-1 (enriched mantle) isotopic end member, in the Sr-Nd isotopic space and plot to the left of the Pb-Pb geochron (Rollinson, 1993).

The 49th Parallel lamproite has more radiogenic initial $^{87}\text{Sr}/^{86}\text{Sr}$ and $^{208}\text{Pb}/^{204}\text{Pb}$ ratios, a lower initial $^{143}\text{Nd}/^{144}\text{Nd}$ ratio and similar initial $^{206}\text{Pb}/^{204}\text{Pb}$ and $^{207}\text{Pb}/^{204}\text{Pb}$ ratios, compared with the olivine minettes and latites of the Milk River area. A sample of the McTaggart Coulee latite has less radiogenic initial $^{87}\text{Sr}/^{86}\text{Sr}$, $^{207}\text{Pb}/^{204}\text{Pb}$ and $^{208}\text{Pb}/^{204}\text{Pb}$ ratios and similar initial $^{206}\text{Pb}/^{204}\text{Pb}$ and $^{143}\text{Nd}/^{144}\text{Nd}$ ratios, relative to the minettes and lamproite (Buhlmann et al., 2000). These isotopic data suggest either an open-system behaviour during magmatic evolution or an isotopically heterogeneous mantle source of the minette and lamproite magmas.

Kjarsgaard (1997) pointed out that the C and O isotopic compositions of carbonates in igneous rocks of the Milk River area might indicate some post-magmatic alteration, perhaps as a result of interaction with meteoric water. Based on the geochemical and Sr-Pb-Nd isotopic evidence, Buhlmann et al. (2000) argued against any significant crustal assimilation by potassic magmas of the Milk River area. Therefore, the Sr-Pb-Nd isotopic systematics indicate higher time-integrated Rb/Sr and Th/Pb ratios, lower Sm/Nd ratio and similar U/Pb ratio in the source region of the 49th Parallel lamproite, compared with the mantle source of the Milk River minettes and latite. Moreover, variations of initial Sr, Pb and Nd isotopic ratios displayed by the minettes (Buhlmann et al., 2000) suggest that these rocks represent discrete partial melts from isotopically heterogeneous mantle. On a regional scale, the Sr-Pb-Nd isotopic data from the Montana alkaline province, the Absaroka Range and the Leucite Hills lamproites do not rule out mixing between at least three distinct mantle end members: a more depleted component, similar to bulk Earth; and two enriched components with different Sr/Nd and Sr/Pb ratios.

The geochemical and isotopic data, therefore, are consistent with the derivation of lamproite and olivine-minette primary magmas of the Milk River area from the subcontinental mantle, heterogeneously enriched in K, LREE and other incompatible elements. Similar geochemical and isotopic signatures of other Late Cretaceous–Oligocene alkaline rocks of southwestern Canada and northwestern United States have been interpreted in favour of an involvement of at least three distinct components in their mantle sources: 1) lithospheric mantle enriched in LREE and depleted in high-field-strength elements (HFSE) during the Proterozoic; 2) asthenospheric mantle; and 3) young metasomatism, with enrichment in K, Rb, Ba and other large-ion lithophile elements (LILE), and depletion in Ta, Nb and Ti, contemporaneous with or slightly predating derivation of the alkaline magmas (Eggler et al., 1988; Dudás, 1991; O'Brien et al., 1991, 1995; Macdonald et al., 1992; Buhlmann et al., 2000; Christiansen et al., 2002; Dostal et al., 2003; Madsen et al., 2006; Mirnejad and Bell, 2006).

Buhlmann et al. (2000) proposed that magmatic evolution of the minettes might have involved settling of the phlogopite-clinopyroxenite cumulate at high pressures, followed by olivine precipitation at lower pressures. In the following section, we discuss the magmatic evolution in the Sweet Grass Hills igneous complex using phase-equilibrium data and the least-squares mass-balance and trace-element models.

8.3 Fractional Crystallization and Crustal Assimilation

Notably, compositions of magmatic rocks in the Milk River area and Sweet Grass Hills define an evolutionary trend in the Ni-MgO plot (Figure 17) controlled by the removal of olivine from the parent olivine minette magma. Extensive variations of major- and trace-element concentrations between the primitive olivine minettes and the more felsic latites, trachytes and high-K rhyolite (Figures 13 and 14) are consistent with fractional crystallization involving primary minerals observed as phenocrysts in these rocks (Truscott, 1975; Buhlmann et al., 2000).

Phase relations in the synthetic $\text{NaAlSi}_3\text{O}_8\text{-KAlSi}_3\text{O}_8\text{-SiO}_2\text{-H}_2\text{O}$ system at 1 kb pressure (Figure 18; see figure caption for citations) can be extrapolated to the evolution of potassic magmas in the Sweet Grass Hills igneous complex. The normative compositions of the Milk River lamproites and minettes, projected onto the anhydrous base of the tetrahedron, plot along the fractional crystallization paths, suggesting fractionation of leucite followed by feldspar or nepheline (or perhaps analcime). Compositions of the Highwood and Bearpaw minettes (O'Brien et al., 1991; Macdonald et al., 1992) and the Leucite Hills lamproites (Mitchell and Steele, 1992; Mirnejad and Bell, 2006), plotted for comparison, follow crystallization paths similar to those of the Milk River minettes and lamproites (Figure 18). Although leucite was not observed in the Milk River rocks, we agree with Kjarsgaard's (1994) interpretation that primary leucite might have been pseudomorphed by analcime. Analcimization of leucite was documented in similar minettes of the Bearpaw and Highwood mountains (O'Brien et al., 1991; Macdonald et al., 1992) and the Mexican Volcanic Belt (Wallace and Carmichael, 1989).

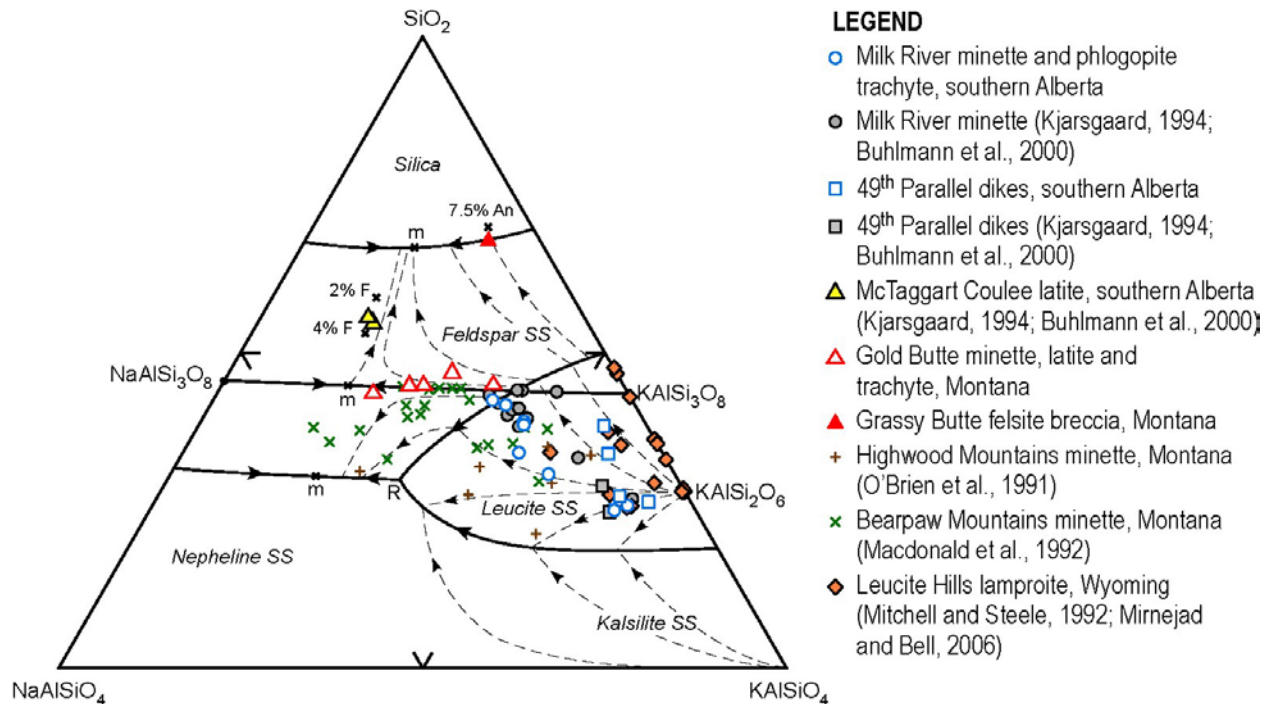


Figure 18. Normative compositions of igneous rocks from the Milk River area and Sweet Grass Hills projected onto the anhydrous base of the tetrahedron $\text{NaAlSi}_3\text{O}_8\text{-KAlSi}_3\text{O}_8\text{-SiO}_2\text{-H}_2\text{O}$ (wt. %). Liquidus relationships, minima (m), peritectic (R) and fractional crystallization paths (dashed lines with arrows) at $P_{\text{H}_2\text{O}}$ of 1 kb are after Tuttle and Bowen (1958), Fudali (1963) and Hamilton and MacKenzie (1965); piercing point for the plane 7.5% anorthite after James and Hamilton (1969); and F-bearing minimum (2% F) and eutectic (4% F) after Manning (1981). Shown for comparison are the compositions of minettes from the Highwood and Bearpaw mountains (Montana) and lamproites from the Leucite Hills (Wyoming). Abbreviation: SS, solid solution.

Compositions of the latites and trachytes evolve from the minettes toward the feldspar minimum (Tuttle and Bowen, 1958; Fudali, 1963; Hamilton and MacKenzie, 1965) and the F-bearing quartz-feldspar minima or eutectic (Manning, 1981). The Grassy Butte felsite breccia plots near the anorthite-bearing piercing point (James and Hamilton, 1969). The crystallization sequence inferred from phase relations in the $\text{NaAlSi}_3\text{O}_8\text{-KAlSi}_3\text{O}_8\text{-SiO}_2\text{-H}_2\text{O}$ system is consistent with our petrographic observations that crystallization of analcime (perhaps pseudomorphed leucite) preceded that of sanidine in these rocks.

Phase relations in the synthetic $\text{KAlSi}_3\text{O}_8\text{-Mg}_2\text{SiO}_5\text{-SiO}_2$ system provide further insights on the origin and evolution of the potassic magmas because it contains the liquidus fields of both mafic and salic phases (Wallace and Carmichael, 1989). Figure 19a shows phase relations in this system at $P_{\text{H}_2\text{O}}$ of 2 kb after Luth (1967), and Figure 19b shows approximate phase boundaries constructed by Wallace and Carmichael (1989) from H_2O -saturated and -undersaturated experiments at pressures between 4 and 20 kb by Ruddock and Hamilton (1978) and Sekine and Wyllie (1982). The compositions of igneous rocks from the Milk River area and Sweet Grass Hills are plotted in terms of their normative kalsilite (KAlSi_3O_8), olivine (Mg_2SiO_4) and silica, along with the compositions of Highwood and Bearpaw minettes and Leucite Hills lamproites for comparison (O'Brien et al., 1991; Macdonald et al., 1992; Mitchell and Steele, 1992; Mirnejad and Bell, 2006).

An important observation from the phase relationships is that, with increasing pressure and activity of water ($a_{\text{H}_2\text{O}}$), the stability field of phlogopite expands at the expense of leucite (Wallace and Carmichael, 1989). Most of the minettes and lamproites, however, plot within the forsterite liquidus field. If the synthetic-system topology were applicable to the natural system, this would indicate equilibrium of the minette and lamproite magmas with olivine. The ubiquitous phlogopite phenocrysts in these magmas, however, imply that the phlogopite liquidus volume must have been much greater in the natural system than in the synthetic-system topology (Macdonald et al., 1992).

Foley (1992) presented a possible explanation to this problem based on experiments in the $\text{KAlSi}_3\text{O}_8\text{-Mg}_2\text{SiO}_5\text{-SiO}_2$ system in the presence of volatiles at different pressure-redox conditions. Foley's (1992) results show that, with increasing pressure, the position of the peritectic point forsterite+phlogopite+enstatite+melt in this system moves away from the $\text{KAlSi}_3\text{O}_8\text{-SiO}_2$ joint. However, the composition of the volatile phase, depending on the redox conditions, affects the position of the peritectic point in the transverse direction to the pressure trend. At 28 kb pressure, the stability field of olivine appears to be reduced in the presence of CO_2 -rich, oxidized volatiles (Foley, 1992). Extrapolating these results to the Milk River minettes and lamproites, the former magmas might have originated in more oxidized conditions in the presence of a CO_2 -rich fluid, consistent with the presence of abundant titanomagnetite and magnesite phenocrysts, and primary calcite, in the minettes and phlogopite trachytes (Figures 6c, d, 7e, f). On the other hand, the 49th Parallel lamproites might have formed in more reduced conditions in equilibrium with a F-rich fluid, consistent with the presence of ubiquitous ilmenite and notable absence of magnetite in these rocks.

To better understand the phase relations involving phlogopite, clinopyroxene and olivine, the compositions of igneous rocks of the Milk River area and Sweet Grass Hills have been projected from kalsilite onto the augite-olivine-sanidine pseudo-ternary plane in the system $\text{KAlSi}_3\text{O}_8\text{-Mg}_2\text{SiO}_5\text{-CaMgSi}_2\text{O}_6\text{-SiO}_2\text{-H}_2\text{O}$ (Figure 20). Compositions of Highwood and Bearpaw minettes and Leucite Hills lamproites (O'Brien et al., 1991; Macdonald et al., 1992; Mitchell and Steele, 1992; Mirnejad and Bell, 2006) are plotted for comparison. Wallace and Carmichael (1989) constructed phase boundaries in this projection using the experimental results of Esperança and Holloway (1987) at various pressures, and extrapolated the phase relations for 30 kb pressure. Comparison of the natural compositions with the experimental phase relations shows that the Milk River minettes could have been in equilibrium with olivine, phlogopite and clinopyroxene at pressures greater than 15 kb, with the composition of the most primitive olivine minette (sample 8156) corresponding to the olivine+clinopyroxene+phlogopite peritectic (triple junction) at 30 kb pressure (Buhlmann et al., 2000). Similarly, minettes from the Bearpaw and

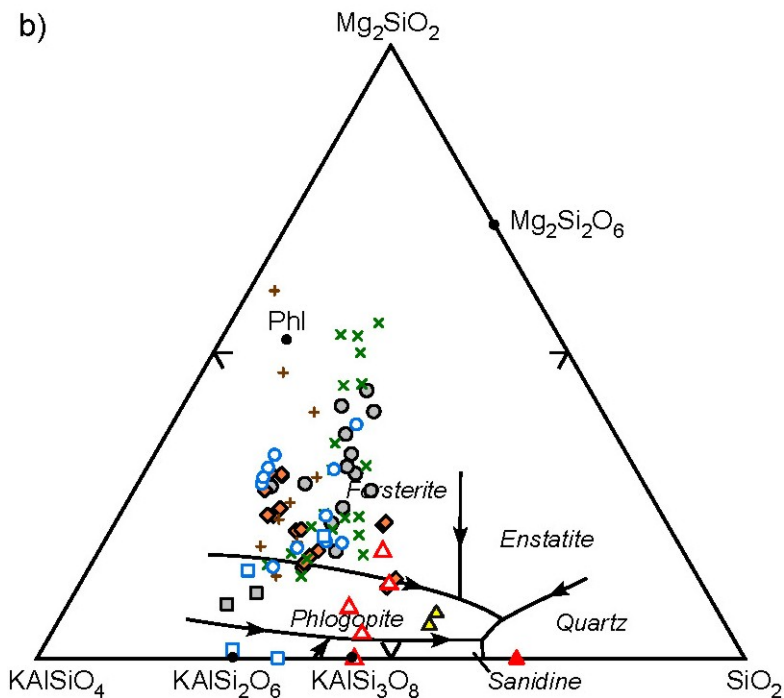
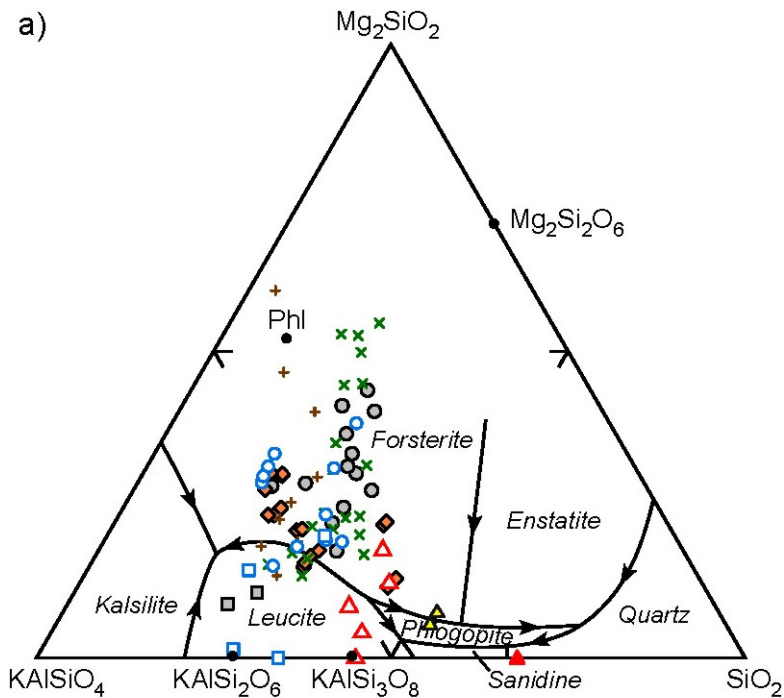


Figure 19. Compositions of igneous rocks from the Milk River area and Sweet Grass Hills plotted in terms of normative KAlSiO_4 - Mg_2SiO_4 - SiO_2 (wt. %): a) phase relationships at $P_{\text{H}_2\text{O}}$ of 2 kb after Luth (1967); and b) approximate phase boundaries constructed by Wallace and Carmichael (1989) from H_2O -saturated and -undersaturated experiments at pressures between 4 and 20 kb after Ruddock and Hamilton (1978) and Sekine and Wyllie (1982). Kalsilite and silica have been calculated to include leucite, nepheline, orthoclase and albite normative components; Phl, anhydrous phlogopite composition. Shown for comparison are the compositions of minettes from the Highwood and Bearpaw mountains (Montana) and lamproites from the Leucite Hills (Wyoming). Symbols as in Figure 18.

Highwood mountains might have been in equilibrium with olivine and phlogopite at 30 kb, and with clinopyroxene and phlogopite at lower pressures due to the reaction of olivine with melt.

Wallace and Carmichael (1989), however, cautioned that the phase relations in the augite-olivine-sanidine plane may be inappropriate for more silica-undersaturated, leucite-normative compositions because phlogopite-phase volume constricts with decreasing kalsilite/silica ratio. This might be the case for a group of leucite-normative minettes and lamproites, which scatter along the KAlSiO_4 - $\text{CaMgSi}_2\text{O}_6$ joint (Figure 20). Nonetheless, extrapolating the phase relations to the 49th Parallel lamproites suggests that these melts might have been in equilibrium with olivine and phlogopite at lower pressures (~10–15 kb). The position of the Gold Butte latites and trachytes in the augite-olivine-sanidine plane (Figure 20) is consistent with their origin by fractional crystallization of the parent olivine minette magmas.

To test the fractional-crystallization process, we modelled crystal settling of observed phenocrysts in these rocks using ten major-element oxides by the least-squares mass-balance method of Stormer and Nicholls (1978) and the Petrograph computer program (Petrelli et al., 2005). Average chemical compositions of phenocrysts (except cores of reversely zoned diopside and phlogopite) in the olivine minettes and latites were used in the mass-balance calculations (Table 5).

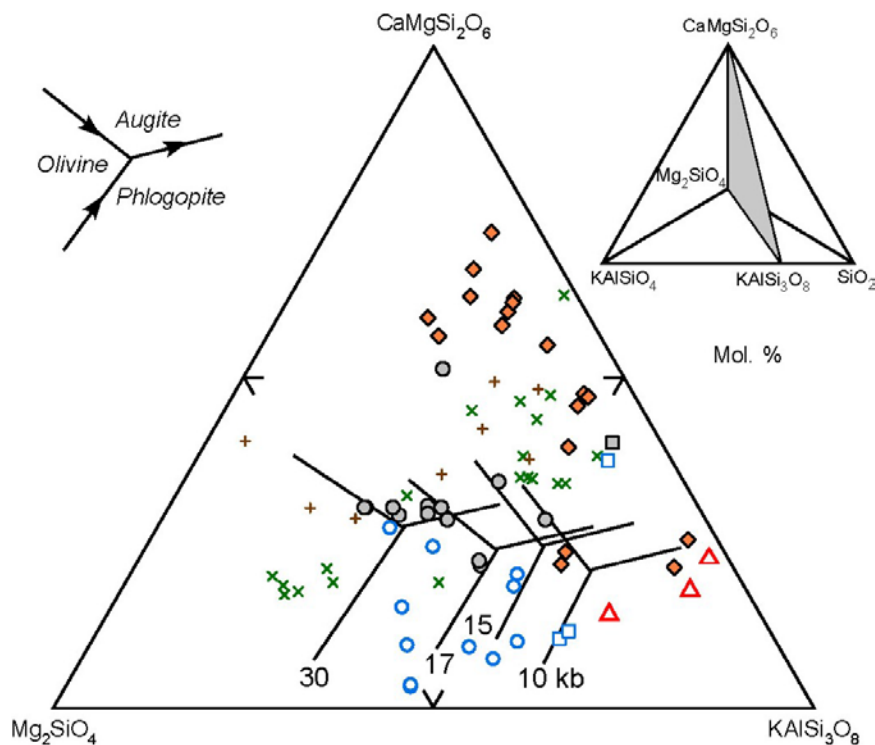


Figure 20. Compositions of potassic igneous rocks from the Milk River area and Sweet Grass Hills projected from kalsilite onto the augite-olivine-sanidine pseudo-ternary plane (mol %) in the system KAlSiO_4 - Mg_2SiO_4 - $\text{CaMgSi}_2\text{O}_6$ - SiO_2 - H_2O , with phase boundaries at various pressures (Esperança and Holloway, 1987; Wallace and Carmichael, 1989). Insets show liquidus relations at the olivine + melt \leftrightarrow clinopyroxene + phlogopite peritectic point and location of the Mg_2SiO_4 - $\text{CaMgSi}_2\text{O}_6$ - SiO_2 plane in the KAlSiO_4 - Mg_2SiO_4 - $\text{CaMgSi}_2\text{O}_6$ - SiO_2 tetrahedron. Molecular norms were calculated using $\text{Fe}^{2+} = 0.85(\text{total Fe})$ after Wallace and Carmichael (1989) and Macdonald et al. (1992). Shown for comparison are the compositions of minettes from the Highwood and Bearpaw mountains (Montana) and lamproites from the Leucite Hills (Wyoming). Symbols as in Figure 18.

Table 5. Least-squares, mass-balance models of fractional crystallization and crustal assimilation for the Sweet Grass Hills igneous complex, calculated using the Petrograph program (Petrelli et al., 2005) and following the method of Stormer and Nicholls (1978). See text for details.

Stage 1: Initial olivine minette (8156) to latite (MR92-01 ⁽¹⁾ or 8242) - models A1 and B1, respectively									
Oxide (wt. %)	Whole-rock compositions			Compositions of phenocryst phases and assumed assimilant (LCC)					
	8156	MR92-01	8242	Di	Phl	Olivine ⁽²⁾	Ap	TiMgt	LCC
SiO ₂	50.18	61.58	58.23	54.50	42.82	40.70	0.22	0.63	53.37
TiO ₂	1.05	0.46	0.73	0.28	1.64	0.00	0.00	6.78	0.82
Al ₂ O ₃	10.28	17.67	15.96	0.83	14.22	0.06	0.01	1.10	16.94
FeO _{total}	8.82	5.03	5.96	4.75	6.27	11.26	0.12	88.71	8.57
MnO	0.15	0.14	0.08	0.14	0.04	0.20	0.07	0.81	0.10
MgO	14.09	1.60	3.28	16.85	24.50	47.70	0.14	1.65	7.24
CaO	7.95	6.28	5.59	22.31	0.03	0.08	55.90	0.16	9.59
Na ₂ O	1.70	4.05	4.02	0.33	0.41	0.00	0.12	0.09	2.65
K ₂ O	4.65	2.92	5.58	0.01	10.07	0.00	0.01	0.08	0.61
P ₂ O ₅	1.13	0.28	0.57	0.00	0.00	0.00	43.40	0.00	0.10
Total	100.00	100.00	100.00	100.00	100.00	100.00	100.00	100.00	100.00
Model A1	Fractionated phases and assimilated LCC (wt %)			36.8	48.0	6.9	2.1	6.1	-
$\sum r^2 = 1.108$	Total cumulate = 64.1 %								
Model B1	Fractionated phases and assimilated LCC (wt %)			37.8	36.7	16.6	3.0	5.9	up to 2.7
$\sum r^2 = 0.177$	Total cumulate: 53.9 %								
Stage 2: latite (MR92-01 or 8242) to high-K rhyolite (8230) - models A2 and B2, respectively									
Oxide (wt. %)	Whole-rock compositions			Compositions of phenocryst phases and assumed assimilant (LCC)					
	MR92-01	8242	8230	Amph	Di	Ap	Sa	An	LCC
SiO ₂	61.58	58.23	77.63	40.34	52.77	0.32	65.50	60.76	53.37
TiO ₂	0.46	0.73	1.73	2.18	0.27	0.00	0.01	0.05	0.82
Al ₂ O ₃	17.67	15.96	10.95	13.94	1.35	0.01	18.58	24.65	16.94
FeO _{total}	5.03	5.96	0.66	18.71	8.87	0.20	0.01	0.01	8.57
MnO	0.14	0.08	0.00	0.30	0.61	0.08	0.01	0.02	0.10
MgO	1.60	3.28	0.09	8.93	13.03	0.07	0.03	0.03	7.24
CaO	6.28	5.59	0.17	11.20	22.56	56.05	0.04	5.90	9.59
Na ₂ O	4.05	4.02	1.49	2.30	0.51	0.05	2.52	7.05	2.65
K ₂ O	2.92	5.58	7.15	2.10	0.02	0.03	13.30	1.52	0.61
P ₂ O ₅	0.28	0.57	0.13	0.00	0.00	43.18	0.00	0.00	0.10
Total	100.00	100.00	100.00	100.00	100.00	100.00	100.00	100.00	100.00
Model A2	Fractionated phases and assimilated LCC (wt %)			30.0	3.7	0.6	-	65.7	up to 5.0
$\sum r^2 = 1.684$	Total cumulate: 69.5 %								
Model B2	Fractionated phases and assimilated LCC (wt %)			37.5	3.8	1.1	29.8	27.8	-
$\sum r^2 = 1.103$	Total cumulate: 80.1 %								

⁽¹⁾ Composition of 'benmoreite' (reclassified as latite here) from McTaggart Coulee plug of the Milk River area (after Buhlmann et al., 2000)

⁽²⁾ Average composition of cores of olivine phenocrysts in olivine minettes of the Bearpaw Mountains (after Macdonald et al., 1992)

Abbreviations: **Amph**, amphibole (potassian magnesiohastingsite); **An**, andesine; **Ap**, fluorapatite; **Di**, diopside; **LCC**, average composition of the lower continental crust (Rudnick and Fountain, 1995); **Phl**, phlogopite; **Sa**, sanidine; **TiMgt**, titanomagnetite; **FeO_{total}**, total iron expressed as FeO; $\sum r^2$, sum of the squares of the residuals (i.e. difference between the observed and calculated derivative rock compositions)

Because fresh olivine was not found in the studied samples of olivine minettes from the Milk River area, we used the average composition of cores of olivine phenocrysts ($Fe_{0.4}$) in compositionally similar olivine minettes of the Bearpaw Mountains (Macdonald et al., 1992). This olivine composition approaches the median of the reported range of olivine compositions (Fe_{89-91}) recovered from heavy-mineral concentrates of the Milk River minettes (Kjarsgaard, 1997). We also tested the feasibility of crustal assimilation by addition of the average composition of the lower continental crust (LCC; after Rudnick and Fountain, 1995) in the mass-balance models.

Because the primitive olivine minettes and the intermediate latites have different mineral assemblages and chemical compositions for the phenocryst phases, we considered a two-stage model of magmatic evolution in the Sweet Grass Hills igneous complex (Figure 21). During stage 1, fractional crystallization of the parent olivine-minette magma (sample 8156) generated the intermediate latite liquid by crystal settling of phlogopite, diopside, olivine, titanomagnetite and fluorapatite. During stage 2, further fractionation of the intermediate latite magma by crystal settling of amphibole (potassic magnesiohastingsite), andesine, sanidine, diopside and fluorapatite led to the final residual liquid, represented by the Grassy Butte high-K rhyolite (sample 8230).

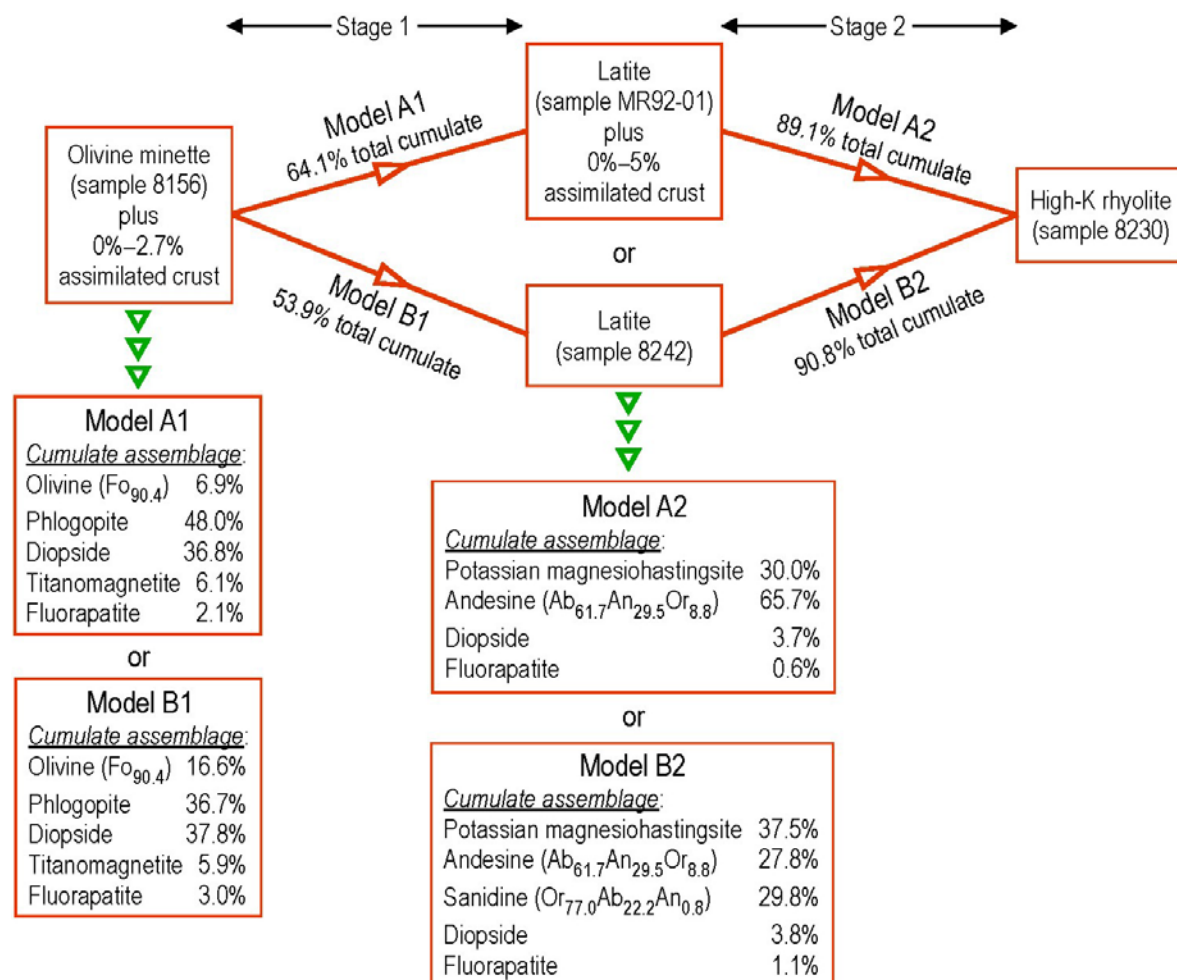


Figure 21. Two-stage, least-squares mass-balance model of fractional crystallization–crustal assimilation in the Sweet Grass Hills igneous complex (Table 5). Two alternative scenarios for each stage involve compositionally different intermediate latites of the Milk River area (models A1 and A2) and Gold Butte (models B1 and B2), respectively. The calculated total cumulate percentages (relative to the parent olivine minette magma) and the cumulate assemblages are given for both scenarios. See text for details.

Although both diopside and fluorapatite were fractionating phases throughout the magmatic evolution, their chemical compositions were different in the parent olivine minettes and in the intermediate latites (Table 5).

To account for the compositional variation between the intermediate latites (Mg# of 44–57), we modelled two alternative scenarios involving a) the more evolved latite at McTaggart Coulee (sample MR92-01 after Buhlmann et al., 2000), and b) the more MgO-rich latite at Gold Butte (our sample 8242). Therefore, models A1 and A2 represent stage 1 (olivine minette to latite) and stage 2 (latite to rhyolite), respectively, for the former scenario, and likewise models B1 and B2 for the latter scenario. The best mass-balance solutions for stage 1 call for fractional crystallization of 54%–64% of the parent olivine minette magma, with the cumulate assemblage consisting of about 37%–48% phlogopite, 37%–38% diopside, 7%–17% olivine, 6% titanomagnetite and 2%–3% fluorapatite. The calculated cumulate assemblage is consistent with the observed phenocryst proportions in the olivine minettes.

For stage 2, fractional crystallization of the intermediate latite magma generates a high-K rhyolite as a 10% residual melt relative to the parent olivine minette magma, with the cumulate assemblage consisting of 30–38% potassic magnesiohastingsite, 28–66% andesine, 0–30% sanidine, 4% diopside and 1% fluorapatite (Table 5; Figure 21). The calculated cumulate assemblage is consistent with modal compositions of some plutonic monzonites, syenites and diorites of the Sweet Grass Hills (Lopez, 1995).

The mass-balance solutions allow, but do not require, up to 5% assimilation of crustal material by the olivine-minette or latite magmas. To further evaluate the least-squares mass-balance results, we modelled the behaviour of trace elements during the two-stage fractional crystallization (FC) and assimilation–fractional crystallization (AFC) processes using published mineral/melt trace-element distribution coefficients (Table 6). Appendix 9 provides details on the methodology of the trace-element modelling.

Figure 22 shows whole-rock concentration plots of Ni versus Co, Co versus Ce, Nb versus Ni and Rb versus Co for igneous rocks of the Milk River area and Sweet Grass Hills, with calculated trends of the FC and AFC processes. The two-stage FC models (curves A1, A2, B1 and B2) are plotted for the two alternative intermediate latite compositions. To illustrate the effect of crustal assimilation, the AFC trends are shown only for the high rate of assimilation to fractional crystallization (0.8), since the AFC trends approximate those of the FC process at the lower rates.

The FC models are consistent with the observed trace-element trends from the parent olivine minette through the intermediate latites to the final high-K rhyolite. Although the Ni-Co, Nb-Ni and Rb-Co plots do not discriminate between the AFC and FC processes, the AFC model does not fit the observed whole-rock trend in the Ce-Co diagram. Therefore, a fractional crystallization process must have controlled the liquid line of descent, comprising the parent olivine minette and the derivative latites, trachytes and high-K rhyolite of the Sweet Grass Hills igneous complex. The mass-balance and trace-element models preclude any major assimilation of crustal materials by these magmas, consistent with the isotopic evidence (Buhlmann et al., 2000).

Interestingly, neither FC nor AFC models fit the observed compositional variations between the Milk River minettes and the 49th Parallel lamproites, particularly their enrichment in REE, Rb and other incompatible elements relative to the most primitive olivine minette (Figure 22) and the Sr-Pb-Nd isotopic systematics (Buhlmann et al., 2000). The least-squares mass-balance and trace-element models, coupled with the mineralogical, geochemical and isotopic evidence, rule out derivation of olivine minettes of the Milk River area and the 49th Parallel lamproite as residual liquids from a common parent magma represented by the most primitive olivine minette. Therefore, the geochemical and isotopic variations displayed by olivine minettes and lamproite of the Milk River area suggest that all these rocks perhaps represent distinct primary magma batches generated by low-degree partial melting of a metasomatized (veined?) mantle containing hydrous minerals and heterogeneously enriched in CO₂ and incompatible

Table 6. Compilation of published trace-element mineral/melt distribution coefficients for potassic magmas.

Model	Element:		Co		Ni		Nb		Ce		Rb	
	Mineral	Kd	Source	Kd	Source	Kd	Source	Kd	Source	Kd	Source	
Stage 1 (olivine minette to latite)	Cpx	1.89	Foley and Jenner (2004)	11.8	Foley and Jenner (2004)	0.0042	Foley and Jenner (2004)	0.265	Foley and Jenner (2004)	0.022	Foley and Jenner (2004)	
	Mica	2.68	Adam and Green (2006)	73.7	Adam and Green (2006)	0.085	Foley et al. (1996)	0.0078	Foley et al. (1996)	5.18	Foley et al. (1996)	
	Olivine	6.43	Foley and Jenner (2004)	82	Foley and Jenner (2004)	0.0001	Foley and Jenner (2004)	0.0001	Foley and Jenner (2004)	0.0004	Foley and Jenner (2004)	
	Mgt	21	Mahood and Stimac (1990)	29	Esperança et al. (1997)	0.115	Nielsen and Beard (2000)	0.07	Mahood and Stimac (1990)	0.01	Lemarchand et al. (1987)	
	Apatite	0.2	Mahood and Stimac (1990)	N/A		0.005	Klemme (2003)	23	Larsen (1979)	0.4	Mahood and Stimac (1990)	
Stage 2 (latite to high-K rhyolite)	Cpx	5.38	Villemant (1988)	25	Villemant (1988)	0.03	Marks et al. (2004)	0.585	Marks et al. (2004)	0.03	Marks et al. (2004)	
	Amph	16.7	Lemarchand et al. (1987)	6.0	Liotard et al. (1982)	1.05	Marks et al. (2004)	0.73	Liotard et al. (1982)	0.14	Lemarchand et al. (1987)	
	Apatite	0.2	Mahood and Stimac (1990)	N/A		0.005	Klemme (2003)	31	Mahood and Stimac (1990)	0.4	Mahood and Stimac (1990)	
	Plag	0.03	Villemant (1988)	0.14	Villemant (1988)	0.135	Ewart and Griffin (1994)	0.0178	Mahood and Stimac (1990)	0.835	Villemant (1988)	
	KFsp	0.24	Mahood and Hildreth (1983)	1.44	Ewart and Griffin (1994)	0.004	Larsen (1979)	0.039	Larsen (1979)	0.32	Larsen (1979)	

Abbreviations: **Amph**, amphibole; **Cpx**, clinopyroxene; **KFsp**, potassium feldspar; **Mgt**, magnetite; **Plag**, plagioclase.

elements (Dudás et al., 1987; Hearn et al., 1991; Foley, 1992; Cavell et al., 1993; O'Brien et al., 1995; Buhlmann et al., 2000; Mirnejad and Bell, 2006).

In summary, based on the geochemical and Sr-Pb-Nd isotopic heterogeneity, the 49th Parallel lamproite and each of the five olivine minette localities in the Milk River area perhaps represent discrete partial melts of a metasomatized mantle. Compositions of intermediate and felsic rocks within the Sweet Grass Hills igneous complex can be predicted by the mass-balance and trace-element models involving a fractional crystallization process using any of the Milk River olivine minettes as an initial composition. Such magma batches must have seen recharge in crustal chambers, as evidenced by reverse- and oscillatory-zoned clinopyroxene, mica and feldspar phenocrysts in the olivine minettes, latites and trachytes. Therefore, mixing of isotopically distinct primary magma batches cannot be ruled out. However, the 49th Parallel lamproite could not have been a parent magma for any of these rocks.

8.4 Economic Potential of Potassic Rocks of the Milk River Area

Rock's (1991) summary of the relationships between the precious-metal deposits and lamprophyres shows that some of these rocks may have the potential for economic deposits. Of importance to the economic potential of the Milk River area are the epithermal to porphyry-type precious- and base-metal deposits related to the intermediate and felsic intrusions and potassic lamprophyres in the adjacent Sweet

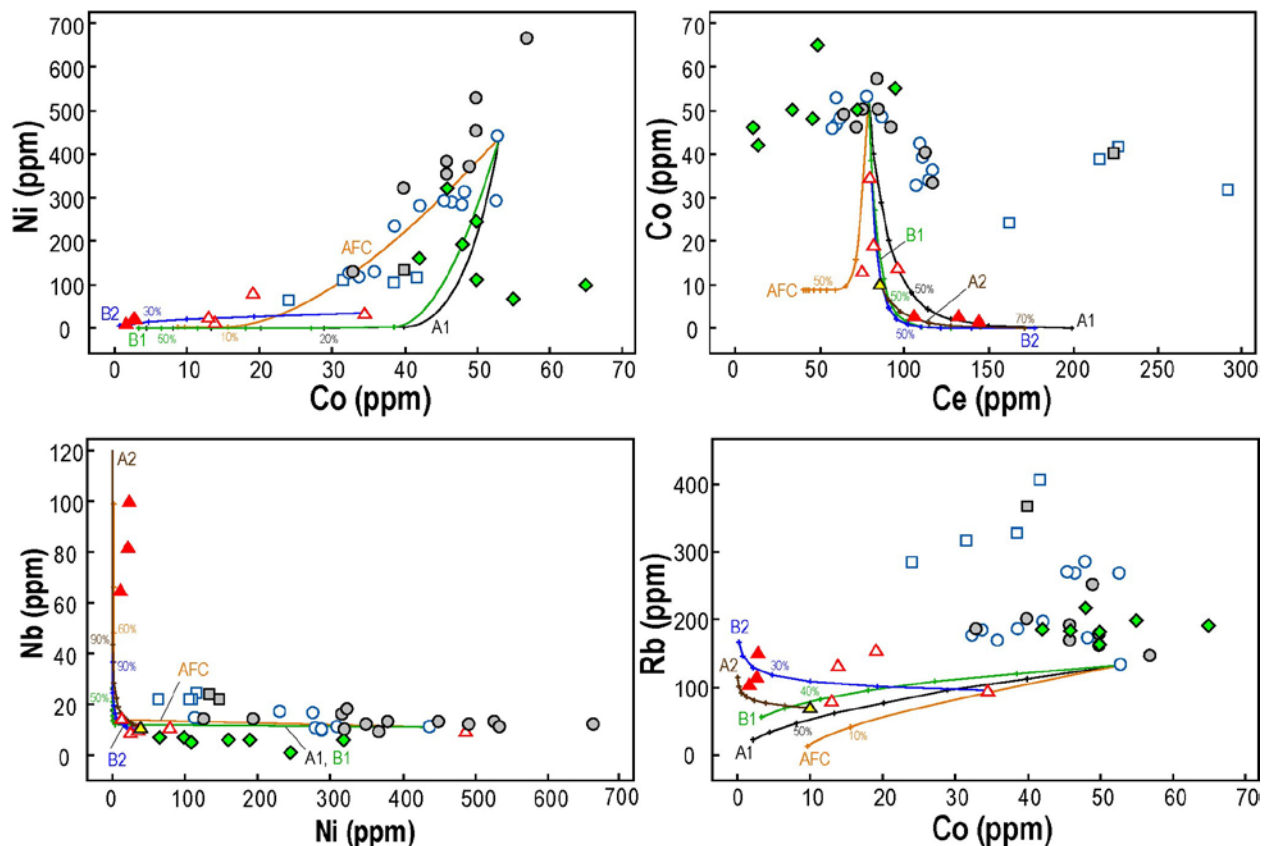


Figure 22. Whole-rock concentration plots of Ni versus Co, Co versus Ce, Nb versus Ni and Rb versus Co for igneous rocks of the Milk River area and Sweet Grass Hills, showing calculated trends for two-stage fractional crystallization (A1, A2, B1 and B2) and assimilation–fractional crystallization (AFC) processes. Ticks indicate percentage of fractionation of the initial olivine minette (models A1 and B1) and intermediate latite (models A2 and B2) magmas and concurrent assimilation of the lower continental crust (Rudnick and Fountain, 1995). See text for details. Symbols as in Figure 13.

Grass Hills of northern Montana (Gavin, 1991; Lopez, 1995; Carlson, 1999). They described several styles of mineralization at Sweet Grass Hills:

- Gold (1.41–5.07 ppm) associated with gypsum, barite, hematite, iron hydroxides, pyrite and other sulphides across a 12.5 m interval in silicified marble breccias of the Mississippian Madison Group adjacent to a propylitized and strongly argillitized syenite porphyry intrusion at the Tootsie Creek mine (Figure 1)
- Gold (1.03–3.43 ppm) associated with tellurium in a quartz-fluorite-pyrite (\pm calcite \pm chlorite) stockwork in a syenite intrusion with vein-proximal, propylitic and moderate argillic alteration over a 6.1 m interval at the Devils Chimney mine (Figure 1)
- Silver-gold in chalcocite-galena veins (porphyry type) associated with brecciated shear zones in syenite porphyry at the Brown Eyed Queen mine, East Butte (Figure 1)
- Gold (0.34–157.71 ppm) associated with discontinuous pyritization, silicification and bleaching across a 3 m interval in a high-angle shear zone that offsets hornfelsed Colorado Group shales intruded and engulfed by propylitically altered dikes, sills and irregular masses of mafic syenite, diorite and potassic lamprophyres at the Gold Butte mine (Figure 1)
- An estimated geological resource of 0.36 million tonnes of 1.65 ppm Au, with grades up to 3.09 ppm Au across a drilled interval of 46 m, associated with minor pyritization (<1 vol. %), limonitization, silicification, potassic alteration, minor propylitization and argillitization along the contact of felsite breccia and hornfelsed country rocks of the Montana Group at Grassy Butte (Figure 1)
- Gold-lead-silver and fine-grained fluorite along shear zones within pyritized, propylitized and weakly to strongly argillitized intrusive-breccia pipes associated with latite, trachyte, phonolite and tephrite laccolithic domes emplaced into mudstones and shales of the Colorado and Montana groups at West Butte (Figure 1)

Our results confirm the presence of porphyry to epithermal Au–As \pm Cu \pm Ag \pm Zn \pm W \pm Sb \pm Hg \pm Se mineralization associated with felsite breccia at Grassy Butte and intermediate intrusions at Gold Butte. The mineralization is associated with potassic, propylitic and intermediate argillic alteration.

Compared with the Sweet Grass Hills, ultrapotassic rocks of the Milk River area presently have low potential to host economic concentrations of metals (Lau and Dudek, 1991; Kjarsgaard, 1994; Walker, 1994). On the other hand, because the lamproite-hosted Argyle deposit in northern Australia is the world's largest producer of diamonds (Peterson, 1996), identification of the 49th Parallel lamproites implies that the Milk River area may have diamond potential (Kjarsgaard, 1997). However, Kjarsgaard (1997) pointed out that the Proterozoic reworking of the Wyoming lithosphere may have destroyed the diamonds.

9 Conclusions

Based on a review of previous data and new field and laboratory studies, we revised the nomenclature of igneous rocks of the Milk River area in southern Alberta and proposed a new petrogenetic model for the Eocene Sweet Grass Hills igneous complex. Our findings are summarized as follows:

- Magmatic rocks of the Milk River area include sanidine-phlogopite lamproite (previously classified as 'peralkaline minette'), latite (previously classified as 'benmoreite' or 'diorite porphyry'), diopside-phlogopite trachyte and alkali olivine minettes.
- The lamproite and minettes of the Milk River area represent distinct primary magmas generated by partial melting of an olivine-bearing, hydrous mantle, heterogeneously enriched in CO₂, K, Rb, REE and other incompatible elements.

- The latites, trachytes and high-K rhyolite (felsite breccia) form a liquid line of descent from the parent olivine minette magmas that is controlled by fractional crystallization concurrent with negligible, if any, assimilation of crustal materials.
- The intermediate and felsic rocks of the Sweet Grass Hills are associated with porphyry- to epithermal-style metallic mineralization and potassic, propylitic and argillic alteration of the magmatic and adjacent sedimentary rocks.
- The minettes and lamproites in the Milk River area presently have low potential for economic metallic deposits but may have potential for diamonds.

10 References

- Adam, J. and Green, T. (2006): Trace element partitioning between mica- and amphibole-bearing garnet lherzolite and hydrous basanitic melt: 1. Experimental results and the investigation of controls on partitioning behaviour; *Contributions to Mineralogy and Petrology*, v. 152, p. 1–17.
- Allegre, C.J., Treuil, M., Minster, J-F., Minster, B. and Albarede, F. (1977): Systematic use of trace elements in igneous processes, part I: fractional crystallization processes in volcanic suites; *Contributions to Mineralogy and Petrology*, v. 60, p. 57–75.
- Ash, W.M. (1993): Property evaluation report of the JD-1 (Black Butte) lamproite diatreme, Milk River area, southeastern Alberta, Ash & Associates Consulting Limited; Alberta Energy, Mineral Assessment Report 19950022, 18 p.
- Baadsaard, H., Folinsbee, R.E. and Lipson, J. (1961): Potassium-argon dates of biotites from Cordilleran granites; *Geological Society of America Bulletin*, v. 72, p. 689–701.
- Benito, R., López-Ruiz, J., Cebriá, J.M., Hertogen, J., Doblas, M., Oyarzun, R. and Demaiffe, D. (1999): Sr and O isotope constraints on source and crustal contamination in the high-K calc-alkaline and shoshonitic Neogene volcanic rocks of SE Spain; *Lithos*, v. 46, no. 4, p. 773–802.
- Boerner, D.E., Craven, J.A., Kurtz, R.D., Ross, G.M. and Jones, F.W. (1998): The Great Falls Tectonic Zone: suture or intracontinental shear zone?; *Canadian Journal of Earth Sciences*, v. 35, p. 175–183.
- Buhlmann, A.L., Cavell, P., Burwash, R.A., Creaser, R.A. and Luth, R.W. (2000): Minette bodies and cognate mica-clinopyroxenite xenoliths from the Milk River area, southern Alberta: records of a complex history of the northernmost part of the Archean Wyoming craton; *Canadian Journal of Earth Sciences*, v. 37, p. 1629–1650.
- Burwash, R.A. and Nelson, D.B. (1992): Report on exploration permit 6890010001 in the Milk River region of southern Alberta; Alberta Research Council, Alberta Energy, Mineral Assessment Report 19920003, 18 p.
- Burwash, R.A., Chacko, T., Muehlenbachs, K. and Bouzidi, Y. (2000): Oxygen isotope systematics of the Precambrian basement of Alberta: implications for Paleoproterozoic and Phanerozoic tectonics in northwestern Alberta; *Canadian Journal of Earth Sciences*, v. 37, no. 11, p. 1611–1628.
- Carlson, J.C. (1999): Geology and mineralization of the West Butte intrusive complex, Sweet Grass Hills, northern-central Montana; M.Sc. thesis, University of Montana, 179 p.
- Cavell, P.A., Burwash, R.A. and Nelson, D.B. (1993): Enriched mantle beneath southern Alberta: isotopic evidence for a northern extension of the Wyoming block into southern Alberta; *Geological Association of Canada–Mineralogical Association of Canada, Joint Annual Meeting, Edmonton, Alberta, May 17–18, 1993, Program with Abstracts*, v. 18, p. A17.
- Chakhmouradian, A.R., Reguir, E.P. and Mitchell, R.H. (2002): Strontium-apatite: new occurrences, and the extent of Sr-for-Ca substitution in apatite-group minerals; *The Canadian Mineralogist*, v. 40, p. 121–136.
- Christiansen, R.L., Foulger, G.R. and Evans, J.R. (2002): Upper-mantle origin of the Yellowstone hotspot; *Geological Society of America Bulletin*, v. 114, p. 1245–1256.
- Clague, D.A. and Frey, F.A. (1982): Petrology and trace element geochemistry of the Honolulu Volcanics, Oahu: implications for the oceanic mantle beneath Hawaii; *Journal of Petrology*, v. 23, p. 447–504.
- Currie, K.L. (1976): The alkaline rocks of Canada; Geological Survey of Canada, Bulletin 239, 228 p.

- Davis, W.J. and Kjarsgaard, B.A. (1994): A Rb-Sr phlogopite-whole rock isochron age for olivine minette from the Milk River area, southern Alberta; in Radiogenic age and isotopic studies: report 8, Current Research 1994-F, Geological Survey of Canada, p. 11–14.
- Davis, W.J., Berman, R. and Kjarsgaard, B.A. (1995): U-Pb geochronology and isotopic studies of crustal xenoliths from the Archean Medicine Hat Block, northern Montana and southern Alberta: Paleoproterozoic reworking of Archean crust; *in* 1995 Alberta Basement Transects Workshop, G.M. Ross (ed.), LITHOPROBE Secretariat, University of British Columbia, LITHOPROBE Report 47, p. 329–334.
- Dawson, G.M. (1884): Report on the region in the vicinity of the Bow and Belly rivers, North-West Territory: embracing the country from the base of the Rocky Mountains eastward to longitude 110° 45', and from the 49th Parallel northward to latitude 51° 20'; *in* Reports and maps of investigations and surveys 1882–83–84, Geological and Natural History Survey and Museum of Canada, Report of Progress 1882–83–84, p. 16–17 and 45–47.
- Dawson, J.B. and Smith, J.V. (1977): The MARID (mica-amphibole-rutile-ilmenite-diopside) suite of xenoliths in kimberlite; *Geochimica et Cosmochimica Acta*, v. 41, p. 309–323.
- Deer, W.A., Howie, R.A. and Zussman, J. (1996): An introduction to the rock-forming minerals, 2nd edition; Longman, London, United Kingdom, 696 p.
- DePaolo, D.J. (1981): Trace element and isotopic effects of combined wallrock assimilation and fractional crystallization; *Earth and Planetary Science Letters*, v. 53, p. 189–202.
- Dostal, J., Breitsprecher, K., Church, B.N., Thorkelson, D. and Hamilton, T.S. (2003): Eocene melting of Precambrian lithospheric mantle: analcime-bearing volcanic rocks from the Challis-Kamloops belt of south central British Columbia; *Journal of Volcanology and Geothermal Research*, v. 126, p. 303–326.
- Droop, G.T.R. (1987): A general equation for estimating Fe³⁺ concentrations in ferromagnesian silicates and oxides from microprobe analyses, using stoichiometric criteria; *Mineralogical Magazine*, v. 51, no. 3, p. 431–435.
- Dudás, F.Ö. (1991): Geochemistry of igneous rocks from the Crazy Mountains, Montana, and tectonic models for the Montana alkalic province; *Journal of Geophysical Research*, v. 96, p. 13261–13277.
- Dudás, F.Ö., Carlson, R.W. and Egglar, D.H. (1987): Regional Middle Proterozoic enrichment of the subcontinental mantle source of igneous rocks from central Montana; *Geology*, v. 15, p. 22–25.
- Dufresne, M.B., Eccles, D.R., McKinstry, B., Schmitt, D.R., Fenton, M.M., Pawlowicz, J.G. and Edwards, W.A.D. (1996): The diamond potential of Alberta; Alberta Energy and Utilities Board, EUB/AGS Bulletin 63, 158 p., URL <http://www.ags.gov.ab.ca/publications/abstracts/BUL_063.html> [May 2010].
- Egglar, D.H., Meen, J.K., Welt, F., Dudás, F.Ö., Furlong, K.P., McCallum, M.E. and Carlson, R.W. (1988): Tectonomagmatism of the Wyoming Province; *in* Cenozoic volcanism in the southern Rocky Mountains revisited: a tribute to Rudy C. Epis, Part 3, J.W. Drexler and E.E. Larson (ed.), Colorado School of Mines Quarterly, v. 88, p. 25–40.
- Energy Resources Conservation Board (2009): Table of formations, Alberta; ERCB Information Services, Calgary, Alberta, URL <<http://www.ercb.ca/docs/products/catalog/TOF.pdf>> [October 2010].
- Esperança, S. and Holloway, J.R. (1987): On the origin of some mica-lamprophyres: experimental evidence from a mafic minette; *Contributions to Mineralogy and Petrology*, v. 95, p. 207–216.
- Esperança, S., Carlson, R.W., Shirey, S.B. and Smith, D. (1997): Dating crust-mantle separation: Re-Os isotopic study of mafic xenoliths from central Arizona; *Geology*, v. 25, p. 651–654.

- Ewart, A. and Griffin, W.L. (1994): Application of proton-microprobe data to trace-element partitioning in volcanic rocks; *Chemical Geology*, v. 117, p. 251–284.
- Feeley, T.C. and Cosca, M.A. (2003): Time vs. composition trends of magmatism at Sunlight volcano, Absaroka volcanic province, Wyoming; *Geological Society of America Bulletin*, v. 115, p. 714–728.
- Foley, S. (1992): Petrological characterization of the source components of potassic magmas: geochemical and experimental constraints; *Lithos*, v. 28, p. 187–204.
- Foley, S. and Jenner, G. (2004): Trace element partitioning in lamproitic magmas—the Gausberg olivine leucite; *Lithos*, v. 75, p. 19–38.
- Foley, S.E., Venturelli, G., Green, D.H. and Toscani, L. (1987): The ultrapotassic rocks: characteristics, classification, and constraints for petrogenetic models; *Earth-Science Reviews*, v. 24, p. 81–134.
- Foley, S.F., Jackson, S.E., Fryer, B.J., Greenough, J.D. and Jenner, G.A. (1996): Trace element partition coefficients for clinopyroxene and phlogopite in an alkaline lamprophyre from Newfoundland by LAM-ICP-MS; *Geochimica et Cosmochimica Acta*, v. 60, no. 4, p. 629–638.
- Frey, F.A., Green, D.H. and Roy, S.D. (1978): Integrated models of basalt petrogenesis: a study of quartz tholeiites to olivine melilitites from southeastern Australia; *Journal of Petrology*, v. 19, p. 463–513.
- Fudali, R.F. (1963): Experimental studies bearing on the origin of pseudoleucite and associated problems of alkalic rock systems; *Geological Society of America Bulletin*, v. 74, p. 1101–1126.
- Gavin, B. (1991): Precious-metal mineralization in the Sweet Grass Hills, north-central Montana; *in* Guidebook of the Central Montana Alkalic Province: geology, ore deposits and origin, D. Baker and R.B. Berg (ed.), Tobacco Root Geological Society, 16th Annual Field Conference, August 14–17, 1991, Great Falls, Montana, Montana Bureau of Mines and Geology, Special Publication 100, p. 55–62.
- Grégoire, M., Bell, D.R. and Le Roex, A.P. (2002): Trace element geochemistry of phlogopite-rich mafic mantle xenoliths: their classification and their relationship to phlogopite-bearing peridotites and kimberlites revisited; *Contributions to Mineralogy and Petrology*, v. 142, p. 603–625.
- Haites, T.B., and van Hees, H. (1962): The origin of some anomalies in the plains of western Canada; *Journal of the Alberta Society of Petroleum Geologists*, v. 10, p. 511–533.
- Hamilton, D.L. and MacKenzie, W.S. (1965): Phase equilibria studies in the system NaAlSi₃O₈ (nepheline)–KAlSi₃O₈ (kalsilite)–SiO₂–H₂O; *Mineralogical Magazine*, v. 34, p. 214–231.
- Hamilton, W.N., Price, M.C. and Langenberg, C.W., comp. (1999): Geological map of Alberta; Alberta Energy and Utilities Board, EUB/AGS Map 236, scale 1:1 000 000, URL <http://www.ags.gov.ab.ca/publications/abstracts/MAP_236.html> [August 2010].
- Hart, S.R. and Davis, K.E. (1978): Nickel partitioning between olivine and silicate melt; *Earth and Planetary Science Letters*, v. 40, p. 203–219.
- Hearn, B.C., Jr. (1989): Alkalic ultramafic magmas in north-central Montana, USA: genetic connections of alnöite, kimberlite and carbonatite; *in* Kimberlites and related rocks: their composition, occurrence, origin and emplacement, J. Ross, A.L. Jaques, J. Ferguson, D.H. Green, S.Y. O’Reilly, R.V. Danchin and A.J.A. Janse (ed.), *Australian Journal of Earth Sciences*, Special Publication 14, v. 1, p. 109–119.
- Hearn, B.C., Jr., Marvin, R.F., Zartman, R.E. and Naeser, C.W. (1978): Ages of alkalic activity in north-central Montana; *United States Geological Survey, Professional Paper P1100*, p. 59–60.
- Hearn, B.C., Jr., Upton, B.C.J. and MacDonald, R.A. (1991): Ancient and enriched upper mantle beneath north-central Montana; *in* Guidebook of the Central Montana Alkalic Province: geology, ore deposits

- and origin, D. Baker and R.B. Berg (ed.), Tobacco Root Geological Society, 16th Annual Field Conference, August 14–17, 1991, Great Falls, Montana, Montana Bureau of Mines and Geology, Special Publication 100, p. 133–135.
- Herbaly, E.L. (1974): Petroleum geology of Sweetgrass Arch, Alberta; American Association of Petroleum Geologists Bulletin, v. 58, p. 2227–2244.
- Irvine, T.N. and Baragar, W.R.A. (1971): A guide to the chemical classification of the common volcanic rocks; Canadian Journal of Earth Sciences, v. 8, p. 523–548.
- Irving, A.J. and Hearn, B.C., Jr. (2003): Alkalic rocks of Montana: kimberlites, lamproites, and related magmatic rocks; *in* Montana Field Trip Guidebook, 8th International Kimberlite Conference, June 16–21, 2003, B.A. Kjarsgaard (ed.), Geological Survey of Canada, Ottawa, 44 p.
- Irving, A.J. and O'Brien, H.E. (1991): Isotopic and trace element characteristics of Late Cretaceous to Oligocene mafic volcanics from west-central Montana: implications for Tertiary tectonics and magma genesis; *in* Guidebook of the Central Montana Alkalic Province: geology, ore deposits and origin, D. Baker and R.B. Berg (ed.), Tobacco Root Geological Society, 16th Annual Field Conference, August 14–17, 1991, Great Falls, Montana, Montana Bureau of Mines and Geology, Special Publication 100, p. 140–142.
- James, R.S. and Hamilton, D.L. (1969): Phase relations in the system $\text{NaAlSi}_3\text{O}_8$ – KAlSi_3O_8 – $\text{CaAl}_2\text{Si}_2\text{O}_8$ – SiO_2 at 1 kilobar water vapour pressure; Contributions to Mineralogy and Petrology, v. 21, p. 111–141.
- Kemp, J.F. and Billingsley, P. (1921): Sweet Grass Hills, Montana; Geological Society of America Bulletin, v. 32, p. 437–478.
- Kjarsgaard, B.A. (1994): Potassic magmatism in the Milk River area, southern Alberta: petrology and economic potential; *in* Current Research 1994-B, Geological Survey of Canada, p. 59–68.
- Kjarsgaard, B.A. (1997): Diamonds in Alberta: studies of potential host rocks of deep-seated origin and applications of indicator mineral exploration techniques; *in* Exploring for minerals in Alberta, Geological Survey of Canada geoscience contributions, Canada-Alberta Agreement on Mineral Development (1992–1995), R.W. Macqueen (ed.), Geological Survey of Canada, Bulletin 500, p. 185–207.
- Kjarsgaard, B.A. and Davis, W.J. (1994): Eocene magmatism in the Sweet Grass Hills, and its tectonic significance; *in* 1994 Alberta Basement Transects Workshop, G.M. Ross (ed.), LITHOPROBE Secretariat, University of British Columbia, LITHOPROBE Report 47, p. 234–237.
- Kjarsgaard, B.A. and Davis, W.J. (1996): Sweet Grass minettes, Alberta; *in* Searching for diamonds in Canada, A.N. LeCheminant, D.G. Richardson, R.N.W. DiLabio and K.A. Richardson (ed.), Geological Survey of Canada, Open File 3228, p. 111–114.
- Klemme, S. (2003): Trace element partitioning between apatite and carbonatite melt; American Mineralogist, v. 88, p. 639–646.
- Larsen, E.S. (1940): Petrographic province of central Montana; Geological Society of America Bulletin, v. 51, p. 887–948.
- Larsen, L.M. (1979): Distribution of REE and other trace elements between phenocrysts and peralkaline undersaturated magmas, exemplified by rocks from the Gardar igneous province, south Greenland; Lithos, v. 12, no. 4, p. 303–315.
- Lau, S. and Dudek, D. (1991): Geology report on the Sweet Grass area, southern Alberta, metallic mineral exploration permit area W4M-R9-T1, W4M-R9-T3, W4M-R10-T1, November 1990, NTS 72E/3,

- project 1748, Noranda Exploration Company Limited; Alberta Energy, Mineral Assessment Report 19910001, 198 p.
- Leake, B.E., Woolley, A.R., Birch, W.D., Burke, E.A.J., Ferraris, G., Grice, J.D., Hawthorne, F.C., Kisch, H.J., Krivovichev, V.G., Schumacher, J.C., Stephenson, N.C.N. and Whittaker, E.J.W. (2004): Nomenclature of amphiboles: additions and revisions to the International Mineralogical Association's amphibole nomenclature; *Canadian Mineralogist*, v. 41, 1355–1370.
- Le Bas, M.J., Le Maitre, R.W., Streckeisen, A. and Zanettin, B. (1986): A chemical classification of volcanic rocks based on the total alkali–silica diagram; *Journal of Petrology*, v. 27, p. 745–750.
- Le Maitre, R.W., Streckeisen, A., Zanettin, B., Le Bas, M.J., Bonin, B., Bateman, P., Bellieni, G., Dudek, A., Efremova, S., Keller, J., Lameyre, J., Sabine, P.A., Schmid, R., Sorensen, H. and Woolley, A.R., ed. (2002): *Igneous rocks: a classification and glossary of terms, recommendations of the International Union of Geological Sciences Subcommission on the Systematics of Igneous Rocks*, 2nd edition, Cambridge University Press, Cambridge, United Kingdom, 256 p.
- Lemarchand, F., Benoit, V. and Calais, G. (1987): Trace element distribution coefficients in alkaline series; *Geochimica et Cosmochimica Acta*, v. 51, p. 1071–1081.
- Lemieux, S. (1999): Seismic reflection expression and tectonic significance of Late Cretaceous extensional faulting of the Western Canadian Sedimentary Basin in southern Alberta; *Bulletin of Canadian Petroleum Geology*, v. 47, p. 375–390.
- Liotard, J.M., Dupuy, C., Dostal, J. and Cornen, G. (1982): Geochemistry of the volcanic island of Annobon, Gulf of Guinea; *Chemical Geology*, v. 35, p. 115–138.
- Lloyd, F.E., Arima M. and Edgar, A.D. (1985): Partial melting of a phlogopite-clinopyroxenite nodule from south-west Uganda: an experimental study bearing on the origin of highly potassic continental rift volcanics; *Contributions to Mineralogy and Petrology*, v. 91, p. 321–329.
- Lopez, D.A. (1995): *Geology of the Sweet Grass Hills, north-central Montana*; Montana Bureau of Mines and Geology, Memoir 68, 35 p.
- Lopez, D.A. (2002): *Geologic map of the Sweet Grass Hills 30' x 60' quadrangle, north-central Montana*; Montana Bureau of Mines and Geology, Open File Report MBMG 443, 17 p., Plate 1, scale 1:100 000, URL <<http://www.mbm.g.mtech.edu/gis/gis-datalinks.asp>> [October 2010].
- Lorenz, J.C. (1982): Lithospheric flexure and the history of the Sweetgrass Arch in northwestern Montana; *in* *Geologic studies of the Cordilleran Thrust Belt*, R.B. Powers (ed.), Rocky Mountain Association of Geologists, Denver, Colorado, p. 77–89.
- Ludington, S., Moring, B.C., Miller, R.J., Flynn, K., Hopkins, M.J., Stone, P., Bedford, D.R. and Haxel, G.A. (2005): Preliminary integrated geologic map databases for the United States western states: California, Nevada, Arizona, Washington, Oregon, Idaho and Utah [version 1.3]; United States Geological Survey, Open-File Report 2005–1305, 44 p., scale 1:500 000, URL <<http://pubs.usgs.gov/of/2005/1305>> [October, 2010].
- Lukie, T.D., Dalrymple, R.W., Ardies, G.W. and Zaitlin, B.A. (2002): Alluvial architecture of the Horsefly unit (Basal Quartz) in southern Alberta and northern Montana: influence of accommodation changes and contemporaneous faulting; *Bulletin of Canadian Petroleum Geology*, v. 50, p. 73–91.
- Luth, W.C. (1967): Studies in the system $KAlSiO_4$ – Mg_2SiO_4 – SiO_2 – H_2O : part 1, inferred phase relations and petrographic applications; *Journal of Petrology*, v. 8, p. 372–416.
- Macdonald, R., Upton, B.G.J., Collerson, K.D., Hearn, B.C., Jr. and James, D. (1992): Potassic mafic lavas of the Bearpaw Mountains, Montana: mineralogy, chemistry, and origin; *Journal of Petrology*, v. 33, no. 2, p. 305–346.

- MacRae, N.D., Armitage, A.E., Miller, A.R., Roddick, J.C., Jones, A.L. and Mudry, M.P. (1996): The diamondiferous Akluilâk lamprophyre dyke, Gibson Lake area, N.W.T.; *in* Searching for diamonds in Canada, A.N. LeCheminant, D.G. Richardson, R.N.W. DiLabio and K.A. Richardson (ed.), Geological Survey of Canada, Open File 3228, p. 101–107.
- Madsen, J.K., Thorkelson, D.J., Friedman, R.M. and Marshall, D.D. (2006): Cenozoic to Recent plate configurations in the Pacific Basin: ridge subduction and slab window magmatism in western North America; *Geosphere*, v. 2, p. 11–34.
- Mahood, G.A. and Hildreth, E.W. (1983): Large partition coefficients for trace elements in high-silica rhyolites; *Geochimica et Cosmochimica Acta*, v. 47, p. 11–30.
- Mahood, G.A. and Stimac, J.A. (1990): Trace-element partitioning in pantellerites and trachytes; *Geochimica et Cosmochimica Acta*, v. 54, p. 2257–2276.
- Manning, D.A.C. (1981): The effect of fluorine on liquidus phase relationships in the system Qz-Ab-Or with excess water at 1 kb; *Contributions to Mineralogy and Petrology*, v. 76, p. 206–215.
- Marks, M., Halama, R., Wenzel, T. and Markl, G. (2004): Trace element variations in clinopyroxene and amphibole from alkaline to peralkaline syenites and granites: implications for mineral-melt trace-element partitioning; *Chemical Geology*, v. 211, p. 185–215.
- Marvin, R.F., Hearn, B.C., Jr., Mehnert, H.H., Naeser, C.W., Zartman, R.E. and Lindsley, D.A. (1980): Late Cretaceous–Paleocene–Eocene igneous activity in north-central Montana; *Isochron West*, no. 29, p. 5–25.
- Massey, N.W.D., MacIntyre, D.G., Desjardins, P.J. and Cooney, R.T. (2005): Digital geology map of British Columbia: whole province; British Columbia Ministry of Energy and Mines, Geofile 2005-1, scale 1:250 000, URL <http://www.empr.gov.bc.ca/Mining/Geoscience/PublicationsCatalogue/GeoFiles/Pages/2005-1.aspx> [October 2010].
- McDonough, W.F. and Sun, S.S. (1995): Composition of the Earth; *Chemical Geology*, v. 120, p. 223–253.
- McIntire, W.L. (1963): Trace element partition coefficients—a review of theory and applications to geology; *Geochimica et Cosmochimica Acta*, v. 27, p. 1209–1264.
- Middlemost, E.A.K. (1989): Iron oxidation ratios, norms and the classification of volcanic rocks; *Chemical Geology*, v. 77, p. 19–26.
- Mirnejad, H. and Bell, K. (2006): Origin and source evolution of the Leucite Hills lamproites: evidence from Sr-Nd-Pb-O isotopic compositions; *Journal of Petrology*, v. 47, no. 12, p. 2463–2489.
- Mitchell, R.H. and Bergman, S.C. (1991): *Petrology of lamproites*; Plenum Press, New York, 447 p.
- Mitchell, R.H. and Steele, I. (1992): Potassian zirconium and titanium silicates and strontian cerian perovskite in lamproites from the Leucite Hills, Wyoming; *Canadian Mineralogist*, v. 30, p. 1153–1159.
- Morimoto, N., Fabries, J., Ferguson, A.K., Ginzburg, I.V., Ross, M., Seifert, F.A., Zussman, J., Aoki, K. and Gottardi, G. (1988): Nomenclature of pyroxenes; *Mineralogical Magazine*, v. 52, p. 535–550.
- Morris, G.A., Larson, P.B. and Hooper, P.R. (2000): ‘Subduction style’ magmatism in a non-subduction setting: the Colville igneous complex, NE Washington State, USA; *Journal of Petrology*, v. 41, p. 43–67.
- Mutschler, F.E., Johnson, D.C. and Mooney, T.C. (1991): A speculative plate kinematic model for the central Montana alkalic province and related gold deposits; *in* Guidebook of the Central Montana

- Alkalic Province: geology, ore deposits and origin, D. Baker and R.B. Berg (ed.), Tobacco Root Geological Society, 16th Annual Field Conference, August 14–17, 1991, Great Falls, Montana, Montana Bureau of Mines and Geology, Special Publication 100, p. 121–124.
- Nielsen, R.L. and Beard, J.S. (2000): Magnetite-melt HFSE partitioning; *Chemical Geology*, v. 164, p. 21–34.
- O'Brien, H.E., Irving, A.J. and McCallum, I.S. (1991): Eocene potassic magmatism in the Highwood Mountains, Montana: petrology, geochemistry, and tectonic implications; *Journal of Geophysical Research*, v. 96, no. B8, p. 13237–13260.
- O'Brien, H.E., Irving, A.J., McCallum, I.S. and Thirlwall, M.F. (1995): Strontium, neodymium and lead isotopic evidence for the interaction of post-subduction asthenospheric potassic mafic magmas of the Highwood Mountains, Montana, USA, with ancient Wyoming craton lithospheric mantle; *Geochimica et Cosmochimica Acta*, v. 59, p. 4539–4556.
- Okulitch, A.V., Lopez, D.A. and Jerzykiewicz, T., comp. (1996): *Geology, Lethbridge, Alberta-Saskatchewan-Montana*; Geological Survey of Canada, National Earth Science Series, Geological Atlas, Map NM-12-G, scale 1:1 000 000.
- O'Neill, J.M. and Lopez, D.A. (1985): Character and regional significance of Great Falls Tectonic Zone, east-central Idaho and west-central Montana; *American Association of Petroleum Geologists Bulletin*, v. 69, no. 3, p. 437–447.
- Ozoray, G. (1972): Structural control of morphology in Alberta; *Albertan Geographer*, v. 8, p. 35–42.
- Pardasie, W. (2003): High resolution geophysical survey over a Sweetgrass dyke, Milk River, south Alberta; M.Sc. thesis, University of Alberta, 101 p.
- Peterson, T.D. (1996): Lamproites; *in* Searching for diamonds in Canada, A.N. LeCheminant, D.G. Richardson, R.N.W. DiLabio and K.A. Richardson (ed.), Geological Survey of Canada, Open File 3228, p. 79–86.
- Petrelli, M., Poli, G., Perugini, D. and Peccerillo, A. (2005): Petrograph: a new software to visualize, model, and present geochemical data in igneous petrology; *Geochemistry, Geophysics, Geosystems*, v. 6, doi:10.1029/2005GC000932, URL <<http://www.unipg.it/~maurip/SOFTWARE.htm>> [December 2010].
- Pirsson, L.V. (1905): The petrographic province of central Montana; *American Journal of Science*, Fourth Series, v. 20, p. 35–49.
- Richards, B.C., Barclay, J.E., Bryan, D., Hartling, A., Henderson, C.M. and Hinds, R.C. (1994): Carboniferous strata of the Western Canada Sedimentary Basin; Chapter 14 *in* Geological atlas of the Western Canada Sedimentary Basin, G.D. Mossop and I. Shetsen (comp.), Canadian Society of Petroleum Geologists and Alberta Research Council, p. 221–250, URL <http://www.ags.gov.ab.ca/publications/wcsb_atlas/a_ch14/ch_14.html> [March 2011].
- Rock, N.M.S. (1991): Lamprophyres; Blackie & Son Ltd., Glasgow, United Kingdom, 285 p.
- Rollinson, H.R. (1993): Using geochemical data: evaluation, presentation, interpretation; Longman Scientific and Technical, London, United Kingdom, Geochemistry Series, 352 p.
- Ross, G.M., Parrish, R.R., Villeneuve, M.E. and Bowring, S.A. (1991): Geophysics and geochronology of the crystalline basement of the Alberta Basin, Western Canada; *Canadian Journal of Earth Sciences*, v. 28, p. 512–522.
- Ross, G.M., Mariano, J., Dumont, R., Kjarsgaard, B.A. and Teskey, D. (1997): Was Eocene magmatism widespread in the subsurface of southern Alberta? evidence from new aeromagnetic anomaly data; *in* Exploring for minerals in Alberta, Geological Survey of Canada geoscience contributions, Canada-

- Alberta Agreement on Mineral Development (1992–1995), R.W. Macqueen (ed.), Geological Survey of Canada, Bulletin 500, p. 235–246.
- Ruddock, D.I. and Hamilton, D.L. (1978): Stability of carbonate in a simple potassium-rich rock model: experimental studies in the system $\text{Lc}_{60}\text{Di}_5\text{Si}_{35}\text{-CO}_2\text{-H}_2\text{O}$; *in* Progress in experimental petrology: fourth progress report of research supported by N.E.R.C., 1975–1978, W.S. MacKenzie (ed.), Natural Environment Research Council, London, United Kingdom, Publication D, no. 11, p. 28–31.
- Rudnick, R.L., and Fountain, D.M. (1995): Nature and composition of the continental crust—a lower crustal perspective; *Reviews in Geophysics*, v. 33, p. 267–309.
- Russell, L.S. and Landes, R.W. (1940): Geology of the southern Alberta Plains; Geological Survey of Canada, Memoir 221, 223 p.
- Russell, C.W. (1991): Cold mineralization in the Little Rocky Mountains; *in* Guidebook of the Central Montana Alkalic Province: geology, ore deposits and origin, D. Baker and R.B. Berg (ed.), Tobacco Root Geological Society, 16th Annual Field Conference, August 14–17, 1991, Great Falls, Montana, Montana Bureau of Mines and Geology, Special Publication 100, p. 1–18.
- Sato, H. (1977): Nickel contents of basaltic magmas: identification of primary magma and a measure of the degree of olivine fractionation; *Lithos*, v. 10, p. 113–120.
- Sekine, T. and Wyllie, P.J. (1982): Phase relationships in the system $\text{KAlSiO}_4\text{-Mg}_2\text{SiO}_4\text{-SiO}_2\text{-H}_2\text{O}$ as a model for hybridization between hydrous siliceous melts and peridotite; *Contributions to Mineralogy and Petrology*, v. 79, p. 368–374.
- Shetsen, I. (1987): Quaternary geology, southern Alberta; Alberta Research Council, Alberta Geological Survey, Map 207, scale 1:500 000, URL http://www.ags.gov.ab.ca/publications/abstracts/MAP_207.html [October 2010].
- Stoeser, D.B., Green, G.N., Morath, L.C., Heran, W.D., Wilson, A.B., Moore, D.W. and van Gosen, B.S., comp. (2005): Preliminary integrated geologic map databases for the United States central states: Montana, Wyoming, Colorado, New Mexico, North Dakota, South Dakota, Nebraska, Kansas, Oklahoma, Texas, Iowa, Missouri, Arkansas and Louisiana [version 1.2]; United States Geological Survey, Open-File Report 2005-1351, 44 p., scale 1:500 000, URL <http://pubs.usgs.gov/of/2005/1351> [October 2010].
- Stormer, J.C. and Nicholls, J. (1978): XLFRAC: a program for the interactive testing of magmatic differentiation models; *Computers and Geosciences*, v. 4, p. 143–159.
- Sun, S.S. and McDonough, W.F. (1989): Chemical and isotopic systematics of oceanic basalts: implications for mantle composition and processes; *in* Magmatism in ocean basins, A.D. Saunders and M.J. Norry (ed.), Geological Society of London, Special Publication 42, p. 313–345.
- Sweeney, R.J., Thompson, A.B. and Ulmer, P. (1993): Phase relations of a natural MARID composition and implications for MARID genesis, lithospheric melting and mantle metasomatism; *Contributions to Mineralogy and Petrology*, v. 115, p. 225–241.
- Thompson, R.N., Velde, D., Leat, P.T., Morrison, M.A., Mitchell, J.G., Dickin, A.P. and Gibson, S.A. (1997): Oligocene lamproite containing an Al-poor, Ti-rich biotite, Middle Park, northwest Colorado, USA; *Mineralogical Magazine*, v. 61, no. 4, p. 557–572.
- Thorkelson, D.J. and Taylor, R.P. (1989): Cordilleran slab windows; *Geology*, v. 17, p. 833–836.
- Toscani, L. (1999): Magmatic gold grains in the El Tale lamproite, Fortuna, SE Spain; *Mineralogical Magazine*, v. 63, no. 4, p. 595–602.
- Toscani, L., Contini, S. and Ferrarini, M. (1995): Lamproitic rocks from Cabezo Negro de Zeneta: brown micas as a record of magma mixing; *Mineralogy and Petrology*, v. 55, p. 281–292.

- Truscott, M.G. (1975): Petrology and geochemistry of igneous rocks of East Butte, Sweet Grass Hills, Montana; Ph.D. dissertation, University of Saskatchewan, 174 p.
- Turner, S.P., Platt, J.P., George, R.M.M., Kelley, S.P., Pearson, D.G. and Nowell, G.M. (1999): Magmatism associated with orogenic collapse of the Betic–Alboran domain, SE Spain; *Journal of Petrology*, v. 40, no. 6, p. 1011–1036.
- Tuttle, O.F. and Bowen, N.L. (1958): The origin of granite in the light of experimental studies in the system $\text{NaAlSi}_3\text{O}_8\text{-KAlSi}_3\text{O}_8\text{-SiO}_2\text{-H}_2\text{O}$; Geological Society of America, *Memoir* 74, 153 p.
- United States Geological Survey (1996): North America shaded relief (grid): Global 30-arc second elevation data set (GTOPO30); United States Geological Survey, Earth Resources Observation and Science (EROS) Center, Sioux Falls, South Dakota, scale 1:3 000 000, URL <http://eros.usgs.gov/#/Find_Data/Products_and_Data_Available/gtopo30_info> [October 2010].
- Villemant, B. (1988): Trace-element evolution in the Phlegrean Fields (central Italy)—fractional crystallization and selective enrichment; *Contributions to Mineralogy and Petrology*, v. 98, p. 169–183.
- Villeneuve, M.E., Ross, G.M., Parrish, R.R., Theriault, R.J., Miles, W. and Broome, J. (1993): Geophysical subdivision, U-Pb geochronology and Sm-Nd isotope geochemistry of the crystalline basement of the Western Canada Sedimentary Basin, Alberta and northeastern British Columbia; Geological Survey of Canada, *Bulletin* 447, 86 p.
- Vuke, S.M., Porter, K.W., Lonn, J.D. and Lopez, D.A., comp. (2007): Geologic map of Montana—information booklet; Montana Bureau of Mines and Geology, *Geologic Map* 62D, 67 p., URL <http://www.mbmgs.mtech.edu/mbmgcat/public/ListCitation.asp?pub_id=30081&> [December 2010].
- Walker, R.T. (1994): Report on the Pinhorn diamond/gold property, Milk River area, Alberta, Marum Resources Incorporated; Alberta Energy, *Mineral Assessment Report* 19940008, 173 p.
- Wallace, P. and Carmichael, I.S.E. (1989): Minette lavas and associated leucitites from the Western Front of the Mexican Volcanic Belt: petrology, chemistry, and origin; *Contributions to Mineralogy and Petrology*, v. 103, p. 470–492.
- Weed, W.H. and Pirsson, L.V. (1895): On the igneous rocks of the Sweet Grass Hills, Montana; *American Journal of Science—Third Series*, v. L, no. 298, p. 309–313.
- Williams, M.Y. and Dyer, W.S. (1930): Geology of southern Alberta and southwestern Saskatchewan; Geological Survey of Canada, *Memoir* 163, 160 p.
- Williams, T.M. (1993): Sweet Grass Project, Bear Creek Property, First Phase Exploration, Milk River area, southeastern Alberta, Permit No. 6890100010, NTS 72E/03, Latitude 49°00'30"N, Longitude 111°11'00"W, Consolidated Pine Channel Gold Corporation; Alberta Energy, *Mineral Assessment Report* 19930002, 45 p.
- Ziegler, A.C. and Combs, L.J. (1997): Base line data-collection and quality-control protocols and procedures for the Equus Beds ground-water recharge demonstration project near Wichita, Kansas, 1995–96; United States Geological Survey, *Open File Report* 97-0235, 57 p.
- Zimmerman, L.R., Strahan, A.P. and Thurman, E.M. (2001): Method of analysis and quality-assurance practices by the U.S. Geological Survey Organic Geochemistry Research Group: determination of four selected mosquito insecticides and a synergist in water using liquid-liquid extraction and gas chromatography/mass spectrometry; United States Geological Survey, *Open File Report* 01-0273, 11 p.

Appendices

Appendix 1 – Sample Locations and Descriptions

Legend	
Count:	number of samples
Sample:	AGS sample number
Lab-wt_kg:	weight of sample submitted to lab (in kilograms)
QC:	quality-control samples – duplicate (dup), triplicate (trip) or standard (std)
Site:	sample site
Month:	month sample collected
Year:	year sample collected
Zn_UTM:	UTM zone
E_UTM83:	UTM easting coordinate in NAD83 datum (from field GPS)
N_UTM83:	UTM northing coordinate in NAD83 datum (from field GPS)
Elev_m:	approximate elevation in metres above sea level (from field GPS)
Area:	general map area
Location:	local geographic location
Formation:	geological formation or equivalent
Lithology:	lithology of sample
Remarks:	descriptive comments

Count	Sample	Lab-wt_kg	QC	Site	Month	Year	Zn_UTM	E_UTM83	N_UTM83	Elev_m	Area	Location	Formation	Lithology	Remarks
1	8151	0.24		SG01	July	2008	12	525796	5427590	882	S Alberta	49th Parallel	Sweetgrass Intrusive Complex	Sa-Phl lamproite	dike, groundmass aegirine-augite and/or K-Na amphibole (?), analcime (?)
2	8152	0.48		SG01	July	2008	12	525729	5427576	888	S Alberta	49th Parallel	Sweetgrass Intrusive Complex	Sa-Phl lamproite	dike, oxidized carbonate veins, analcime (?)
3	8153	0.41		SG01	July	2008	12	525662	5427498	922	S Alberta	49th Parallel	Sweetgrass Intrusive Complex	Altered Sa-Phl lamproite	wedge termination of en-echelon dike, carbonatization
4	8154	0.66		SG01	July	2008	12	525659	5427498	920	S Alberta	49th Parallel	Oldman/Foremost	Silicified mudstone	between wedge terminations of en-echelon dike, brecciated
5	8155	0.57		SG01	July	2008	12	525624	5427469	934	S Alberta	49th Parallel	Sweetgrass Intrusive Complex	Altered Sa-Phl lamproite	dike apophysis, argillic alteration, zeolite-chlorite-carbonate veins
6	8156	0.53		SG02	July	2008	12	494315	5441237	974	S Alberta	Coulee 29	Sweetgrass Intrusive Complex	Olivine minette	black dike, the latest intrusive phase, analcime, devitrified glass mesostasis
7	8157	0.45		SG02	July	2008	12	494319	5441240	974	S Alberta	Coulee 29	Oldman/Foremost	Shale/sandy mudstone	light grey, laminated, hornfelsed, 0-20 cm from dike
8	8158	0.48		SG02	July	2008	12	494304	5441295	963	S Alberta	Coulee 29	Oldman/Foremost	Black sandy mudstone	baked, engulfed lense between dikes, carbonaceous
9	8159	0.55		SG02	July	2008	12	494321	5441306	966	S Alberta	Coulee 29	Oldman/Foremost	Sandstone	white, baked, 1.5 m above dike
10	8160	0.74		SG02	July	2008	12	494322	5441316	969	S Alberta	Coulee 29	Oldman/Foremost	Coaly shale	at the contact with grey mudflow, 1m from brown dike
11	8161	0.52		SG02	July	2008	12	494233	5441334	944	S Alberta	Coulee 29	Sweetgrass Intrusive Complex	Vuggy calcite vein	talus float sample, rhombohedral calcite crystals, cuts vent breccia or agglomerate
12	8162	0.70		SG02	July	2008	12	494324	5441147	953	S Alberta	Coulee 29	Sweetgrass Intrusive Complex	Olivine minette	brown dike, up to 2 cm phlogopite phenocrysts
13	8163	0.72		SG03	July	2008	12	495533	5434938	1019	S Alberta	Philp Coulee	Sweetgrass Intrusive Complex	Olivine minette	dike, left-horizontal offset of en-echelon dike, poikilitic groundmass calcite
14	8164	0.72		SG03	July	2008	12	495653	5435159	1001	S Alberta	Philp Coulee	Oldman	Calcareous sandstone	hornfelsed, adjacent to the dike
15	8165	1.24		SG03	July	2008	12	495654	5435163	1003	S Alberta	Philp Coulee	Sweetgrass Intrusive Complex	Olivine minette	dike, fresh, poikilitic groundmass calcite (3%-5%), perovskite (?)
16	8166	0.58		SG03	July	2008	12	495659	5435169	1005	S Alberta	Philp Coulee	Oldman	Shale	baked, 0-30 cm from dike
17	8167	0.56		SG04	July	2008	12	499355	5430347	1080	S Alberta	Black Butte	Sweetgrass Intrusive Complex	Olivine minette	plug (SW extent), poikilitic groundmass calcite (~5%), stubby apatite
18	8168	0.56		SG04	July	2008	12	499524	5430530	1103	S Alberta	Black Butte	Sweetgrass Intrusive Complex	Phlogopite trachyte	plug (middle), sanidine and magnesite phenocrysts, Phl-Di (±carbonate) inclusions
19	8169	0.59		SG04	July	2008	12	499640	5430589	1090	S Alberta	Black Butte	Sweetgrass Intrusive Complex	Minette	plug (NE extent), analcime, aegirine-nepheline-potassium feldspar-carbonate inclusions
20	8170	0.44		SG05	July	2008	12	487864	5428100	1133	S Alberta	Bear Creek	Oldman	Calcareous siltstone	grey, hornfelsed, 0-30 cm from dike
21	8171	0.59		SG05	July	2008	12	487865	5428123	1135	S Alberta	Bear Creek	Sweetgrass Intrusive Complex	Olivine minette	dike, phlogopite >1 cm, calcite, analcime, devitrified glass, Cr-spinel (?)
22	8172	0.53		SG05	July	2008	12	487966	5429100	1130	S Alberta	Bear Creek	Oldman	Shale	light grey, 0-10 cm from dike
23	8173	0.73		SG05	July	2008	12	487968	5429102	1131	S Alberta	Bear Creek	Sweetgrass Intrusive Complex	Olivine minette	dike, left-horizontal offset, abundant carbonate
24	8174	0.56		SG05	July	2008	12	487969	5429111	1137	S Alberta	Bear Creek	Oldman	Calcareous sandstone	yellow, 0-60 cm from dike
25	8183	0.03	Std		Sept	2008							Diabase		CCRMP TDB-1 certified reference material, ~30 grams
26	8184	0.41	8171 dup	SG05	July	2008	12	487865	5428123	1135	S Alberta	Bear Creek	Sweetgrass Intrusive Complex	Olivine minette	duplicate to 8171
27	8185	0.03	Std		Sept	2008							Diabase		CCRMP TDB-1 certified reference material, ~30 grams
28	8188	0.03	Std		Sept	2008							Diabase		CCRMP TDB-1 certified reference material, ~30 grams
29	8219	0.51	8171 trip	SG05	July	2008	12	487865	5428123	1135	S Alberta	Bear Creek	Sweetgrass Intrusive Complex	Olivine minette	triplicate to 8171
30	8229	0.46		SG06	Aug	2009	12	475822	5402056	1344	N. Montana	Grassy Butte	Sweetgrass Intrusive	Altered felsite breccia	pipe, yellow-stained, shale xenoliths, potassic, propylitic and argillic alteration
31	8230	0.41		SG06	Aug	2009	12	475825	5402064	1342	N. Montana	Grassy Butte	Sweetgrass Intrusive	Glassy felsite breccia	pipe, porous, high-K rhyolite
32	8231	0.47		SG06	Aug	2009	12	475825	5402067	1342	N. Montana	Grassy Butte	Montana Group	Hornfels	brecciated, silicified, epidote veins, carbonate, potassic and argillic alteration
33	8232	0.23		SG07	Aug	2009	12	471950	5413300	1432	N. Montana	Gold Butte	Sweetgrass Intrusive	Trachyte	dike, diopside and green hornblende phenocrysts, 2%-5% sulphides
34	8233	0.37		SG06	Aug	2009	12	475815	5402063	1344	N. Montana	Grassy Butte	Sweetgrass Intrusive	Altered felsite breccia	pipe, yellow-stained, shale xenoliths, potassic, propylitic and argillic alteration
35	8234	0.48		SG07	Aug	2009	12	471787	5413429	1402	N. Montana	Gold Butte	Sweetgrass Intrusive	Latite	dike, diopside and green hornblende phenocrysts, ultramafic inclusions
36	8235	0.69		SG07	Aug	2009	12	471945	5413305	1432	N. Montana	Gold Butte	Colorado Group	Black shale/sandstone	
37	8236	0.46		SG07	Aug	2009	12	471945	5413306	1432	N. Montana	Gold Butte	Colorado Group	Black mudstone	
38	8237	0.49		SG07	Aug	2009	12	471957	5413304	1435	N. Montana	Gold Butte	Colorado Group	Pyritized hornfels breccia	silicified, limonitized, carbonatization, epidotization, potassic and argillic alteration
39	8238	0.53		SG07	Aug	2009	12	471955	5413303	1435	N. Montana	Gold Butte	Sweetgrass Intrusive	Altered minette	sill, composite sample, argillic and propylitic alteration
40	8239	0.42		SG07	Aug	2009	12	471955	5413303	1435	N. Montana	Gold Butte	Colorado Group	Hornfels	silicified, limonitized shear zone, argillic alteration
41	8240	0.61		SG07	Aug	2009	12	471955	5413303	1435	N. Montana	Gold Butte	Colorado Group	Black shale/mudstone	laminated, silicification stockwork, 0-30 cm above minette sill
42	8241	0.49		SG07	Aug	2009	12	471955	5413303	1435	N. Montana	Gold Butte	Colorado Group	Silty sandstone/shale	brecciated, silicified, 0.5 m from shear zone, 1m above minette sill
43	8242	0.33		SG07	Aug	2009	12	471955	5413303	1435	N. Montana	Gold Butte	Sweetgrass Intrusive	Latite	dike, hornblende and diopside phenocrysts, propylitic alteration, 5% sulphides
44	8243	0.33		SG07	Aug	2009	12	471955	5413303	1435	N. Montana	Gold Butte	Colorado Group	Pyritized hornfels breccia	silicified, limonitized, carbonatization, epidotization, potassic and argillic alteration
45	8244	0.47		SG07	Aug	2009	12	471955	5413303	1435	N. Montana	Gold Butte	Sweetgrass Intrusive	Altered minette	dike, quenched margin, brecciated, limonitized, propylitic alteration
46	8306	0.07	Std		Sept	2008							Diabase		CCRMP TDB-1 certified reference material, 71.9 grams
47	8307	0.07	Std		Sept	2008							Diabase		CCRMP TDB-1 certified reference material, 71.3 grams
48	8308	0.07	Std		Sept	2008							Diabase		CCRMP TDB-1 certified reference material, 67.3 grams

Abbreviations: Di, diopside; Sa, sanidine; Phl, phlogopite

Appendix 2 – Whole-Rock Geochemical Analytical Methods

All analyses carried out by Acme Analytical Laboratories Ltd.

Method Code	Method Description
3B03	Lead-collection fire-assay fusion of 15 g sample splits, followed by dilute HNO ₃ digestion of the Ag dore bead and inductively coupled plasma–mass spectrometry (ICP-MS) analysis of the solution for Au, Pt and Pd.
4A	Sample splits of 0.2 g are weighed into graphite crucibles and fused with LiBO ₂ flux in a muffle furnace for 15 minutes at 1050°C. The molten mixtures are then poured into 100 mL of 5% HNO ₃ . The solutions are shaken for 2 hours, then an aliquot is poured into a polypropylene test tube and analyzed using inductively coupled plasma–atomic emission spectrometry (ICP-AES) for SiO ₂ , Al ₂ O ₃ , Fe ₂ O ₃ , MgO, CaO, Na ₂ O, K ₂ O, TiO ₂ , P ₂ O ₅ , MnO, Cr ₂ O ₃ , Ni and Sc. In addition, loss-on-ignition (LOI) is determined gravimetrically after ignition of 1 g sample splits at 1000°C, and total C and S are analyzed using 0.1 g sample splits by a LECO carbon-sulphur analyzer.
4B	The same fusion-HNO ₃ digestion as in the 4A method is followed by ICP-MS analysis of the solution for 31 elements (Ba, Be, Co, Cs, Ga, Hf, Nb, Rb, Sn, Sr, Ta, Th, U, V, W, Zr, Y, La, Ce, Pr, Nd, Sm, Eu, Gd, Tb, Dy, Ho, Er, Tm, Yb and Lu). The determinations are considered total.
1DX	As a supplement to the 4B group, sample splits of 0.5 g are leached for 1 hour in 95°C aqua regia (HCl-HNO ₃ -H ₂ O mixture) using an aqua regia/sample ratio of 6 mL/g, then diluted to a 20:1 mL/g final ratio and analyzed in solution by ICP-MS for 14 elements (Mo, Cu, Pb, Zn, Ni, As, Cd, Sb, Bi, Ag, Au, Hg, Tl and Se). Some minerals will not dissolve completely in aqua regia, which results in partial concentrations for some elements. Au solubility can be limited in refractory and graphitic samples.
1F04	The same aqua-regia leaching as in the 1DX procedure is followed by solution analysis by ICP-AES and ICP-MS. ICP-AES values may be reported if concentrations exceed laboratory-determined crossover values; otherwise, ICP-MS results are reported for 53 elements (Mo, Cu, Pb, Zn, Ag, Ni, Co, Mn, Fe, As, U, Au, Th, Sr, Cd, Sb, Bi, V, Ca, P, La, Cr, Mg, Ba, Ti, B, Al, Na, K, W, Sc, Tl, S, Hg, Se, Te, Ga, Cs, Ge, Hf, Nb, Rb, Sn, Ta, Zr, Y, Ce, In, Re, Be, Li, Pd and Pt). As with the 1DX method, only partial concentrations are determined for some elements due to incomplete sample digestion.
1EX	Sample splits of 0.25 g are weighed into Teflon test tubes, a 10 mL aliquot of the 2:2:1:1 H ₂ O-HF-HClO ₄ -HNO ₃ mixture is added, and this is heated until fuming on a hot plate and then taken to dryness. A 7.5 mL aliquot of 50% HCl is then added to the residue and heated in a hot-water bath (~95°C) for 30 minutes. After cooling, the solutions are transferred to polypropylene test tubes, made up to a 10 mL volume with 5% HCl and analyzed by ICP-AES and ICP-MS for 41 elements (Mo, Cu, Pb, Zn, Ag, Ni, Co, Mn, Fe, As, U, Au, Th, Sr, Cd, Sb, Bi, V, Ca, P, La, Cr, Mg, Ba, Ti, Al, Na, K, W, Zr, Ce, Sn, Y, Nb, Ta, Be, Sc, Li, S, Rb and Hf). The four-acid digestion is only partial for some Cr and Ba minerals and some oxides of Al, Hf, Mn, Sn, Ta and Zr. Volatilization during fuming may result in some loss of As, Sb and Au.
5A	Instrumental neutron activation analysis (INAA) involves irradiation of 5–30 g sample splits in a nuclear reactor followed by gamma-ray analysis at Becquerel Laboratories Ltd. for total determination of 35 elements (Sb, As, Ba, Br, Ca, Ce, Cs, Cr, Co, Eu, Au, Hf, Ir, Fe, La, Lu, Hg, Mo, Nd, Ni, Rb, Sm, Sc, Se, Ag, Na, Sr, Ta, Tb, Th, Sn, W, U, Yb and Zn). The Mo results are affected by the interference from Mo produced by the U fission. Other interferences may result in the higher minimum detection limits for some samples.
2A	Sample splits of 0.2 g are fused with NaOH, followed by fluorine analysis by specific-ion electrode.

Appendix 3 – Whole-Rock Sample Preparation and Geochemical Data Quality

All rock samples were crushed and split, and 250 g portions pulverized to –200 mesh using a mild-steel mill (Acme preparation method code R200-250). The mill was washed with glass between each pulverization to minimize cross-contamination by mineralized samples.

The laboratory performed analyses of several certified reference materials, random duplicate splits of pulverized samples, grinder wash-glass samples and blanks. The analyses of wash glass and blanks were used to monitor contamination during sample preparation and analysis. For internal data-quality control, we analyzed six aliquots of the Canadian Certified Reference Materials Project (CCRMP) TDB-1 certified reference material. The six aliquots (30–72 g) of TDB-1 were weighed into plastic vials at the AGS and inserted in sample sets before sending them to the laboratory. In addition, we made three splits of one of the dike samples, which were analyzed as blind triplicates (sample numbers 8171, 8184 and 8219) to check the reproducibility of the analyses.

We estimated precision or reproducibility of the analyses in terms of average relative percentage difference (RPD) based on multiple duplicate sample pairs (e.g., Ziegler and Combs, 1997; Zimmerman et al., 2001). The RPD for a duplicate pair is defined by

$$\text{RPD} = 100 \times [\text{absolute value } (C1 - C2)] / CX,$$

where (C1 – C2) is the concentration difference between duplicate results, and CX is the average of the two results. The duplicate pairs include triplicate sample splits prepared by the AGS before pulverization and duplicate analyses of pulverized samples by Acme. Table headers in Appendix 4 indicate the total number of duplicate pairs used to calculate the average RPD values for each element. A lower average RPD value indicates higher analytical precision.

Accuracy of the analyses was estimated in terms of average percentage recovery (APR; Ziegler and Combs, 1997), based on the analyses of the CCRMP TDB-1 certified reference material. The APR is defined by

$$\text{APR} = 100 \times \text{CM}/\text{CA},$$

where CM is the average measured concentration in the TDB-1 based on our results and CA is the expected concentration in the TDB-1 reported in the CCRMP Certificate of Analysis.

However, the accuracy estimate has an uncertainty that depends on both the precision of our analyses of TDB-1 and the error of the expected concentration reported in the CCRMP Certificate of Analysis. We estimated the 95.5%-confidence precision of our analyses of the TDB-1 in terms of relative standard deviation multiplied by a factor of two (2RSD) as

$$2\text{RSD} = \text{SD}/\text{CM} \times 200,$$

where SD is the standard deviation and CM is the average measured concentration in the TDB-1 based on our analyses.

If the error of the expected concentration in TDB-1 is reported in the CCRMP Certificate of Analysis, it is combined with the 2RSD according to the expression

$$\text{APR error} = \sqrt{(2\text{RSD}^2 + \text{EA}^2)},$$

where APR error (%) is the total relative uncertainty of the accuracy estimate (APR), 2RSD is two times the relative standard deviation or the 95.5%-confidence precision (%) of our TDB-1 results, and EA is the relative error (%) of the expected concentration in TDB-1 reported in the CCRMP Certificate of Analysis.

Therefore, if the error of the expected concentration in TDB-1 is not provided in the Certificate of Analysis, the total APR error simply equals the 95.5%-confidence precision of our TDB-1 analyses (i.e., 2RSD). In this case, the APR error should be regarded as the minimum uncertainty of the accuracy estimate because it does not include the analytical uncertainty of the expected concentration.

The APR values of about 100% within the uncertainty (i.e., \pm APR error %) indicate an accurate result. It should be emphasized that the APR error (i.e., the measure of the uncertainty of the accuracy estimate) applies only to the TDB-1 results, whereas the average RPD value based on duplicate pairs for many different samples characterizes analytical precision or reproducibility of the method applied to all of the samples.

The calculated RPD, APR and APR error values for each element are listed in the table headers in Appendix 4, with the minimum APR error values (i.e., APR error = 2RSD) highlighted in yellow. When more than 50% of the TDB-1 results returned '<MDL,' the APR is assigned an '<MDL' value.

Appendix 4 – Whole-Rock Geochemical Data

Legend

Element:	element analyzed
Method:	analytical method code (Acme Analytical Laboratories Ltd.)
Units:	units of measure in parts per million (ppm), parts per billion (ppb) or percent (%)
MDL:	minimum detection limit
RPD %:	average relative percentage difference between duplicate pairs
RPD count:	number of duplicate pairs used to calculate the RPD values
APR %:	average percentage recovery relative to the CCRMP TDB-1 certified reference material
APR error %:	relative 95.5%-confidence uncertainty (%) of the APR values
Sample:	AGS sample number
<:	less than the minimum detection limit
>:	greater than the maximum detection limit
NA:	not analyzed

Note: APR values are based on six samples of the CCRMP TDB-1 certified reference material analyzed along with other samples by Acme Analytical Laboratories Ltd. APR error values are based on two times relative standard deviation (2RSD) of the CCRMP TDB-1 results quadratically combined with the relative error of expected concentration in this reference material. When the error of expected concentration is not reported in the CCRMP TDB-1 Certificate of Analysis, minimum APR error values (equal to the 2RSD) are highlighted in yellow. Elements not reported in the TDB-1 Certificate of Analysis are denoted with 'NA'. See text for details on calculating the RPD, APR and APR error values.

Appendix 4A

Element:	Au	Pt	Pd
Method:	3BMS	3BMS	3BMS
Units:	ppb	ppb	ppb
MDL:	1	0.1	0.5
RPD %:	30.8	16.7	17.0
RPD count:	9	19	16
APR %:	74.1	78.7	88.6
APR error %:	38.4	27.7	29.4
Sample			
8151	2	1.9	0.8
8152	3	2.4	2.3
8153	3	1.8	1.5
8154	9	<0.1	<0.5
8155	2	2.2	<0.5
8156	5	5.7	2.9
8157	5	<0.1	<0.5
8158	3	0.9	<0.5
8159	<1	0.2	<0.5
8160	3	0.5	<0.5
8161	1	1.8	2.5
8162	<1	5.4	4.4
8163	<1	0.3	<0.5
8164	<1	0.3	0.6
8165	<1	0.3	<0.5
8166	2	0.5	0.6
8167	2	4.3	3.5
8168	<1	4.9	2.9
8169	<1	4.4	2.3
8170	<1	<0.1	<0.5
8171	<1	5.9	3.6
8172	<1	0.8	4.2
8173	3	3.8	5.3
8174	<1	<0.1	<0.5
8183	5	5.5	23.7
8184	<1	2.9	2.9
8185	<1	4.1	16.7
8188	<1	4.3	15.4
8219	<1	4.2	2.6
8229	200	2.2	2.7
8230	65	4.1	4.5
8231	850	0.2	<0.5
8232	22	0.4	<0.5
8233	31	2.8	3.3
8234	17	0.2	<0.5
8235	6	0.6	0.9
8236	5	0.6	1.6
8237	25	1.2	2.0
8238	17	2.0	2.1
8239	5	0.8	1.0
8240	18	0.5	1.1
8241	5	0.6	1.2
8242	20	1.0	1.1
8243	6	0.9	1.2
8244	13	8.0	4.0
8306	4	4.1	20.1
8307	4	4.8	20.5
8308	6	4.7	23.0

Appendix 4B

Element:	SiO ₂	Al ₂ O ₃	Fe ₂ O ₃	MgO	CaO	Na ₂ O	K ₂ O	TiO ₂	P ₂ O ₅	MnO	Cr ₂ O ₃	Ni	Sc	LOI	Sum	Ba
Method:	4A-4B	4A-4B	4A-4B	4A-4B	4A-4B	4A-4B	4A-4B	4A-4B	4A-4B	4A-4B	4A-4B	4A-4B	4A-4B	4A-4B	4A-4B	4A-4B
Units:	%	%	%	%	%	%	%	%	%	%	%	ppm	ppm	%	%	ppm
MDL:	0.01	0.01	0.04	0.01	0.01	0.01	0.01	0.01	0.01	0.01	0.002	20	1	0.1	0.01	1
RPD %:	0.7	1.2	1.3	1.7	7.5	2.6	2.3	1.0	5.9	6.4	3.5	3.6	4.1	11.9		5.1
RPD count:	25	25	25	24	25	25	25	25	25	21	24	16	24	25		25
APR %:	99.1	101.5	96.1	100.0	102.3	97.6	96.6	101.0	122.8	94.1	98.1	99.6	104.2	161.1		94.3
APR error %:	1.2	4.3	4.6	6.3	7.5	6.2	9.7	7.2	25.5	6.4	7.2	8.5	8.8	71.3		13.4
Sample																
8151	49.39	12.97	8.49	6.13	2.62	1.63	10.68	1.72	1.83	0.07	0.079	116	19	3.3	98.90	5109
8152	41.54	11.60	7.80	4.94	8.65	1.23	9.20	1.45	1.65	0.06	0.071	110	9	10.8	99.02	4460
8153	40.41	10.64	7.28	5.03	12.73	0.89	8.96	1.42	1.54	0.15	0.065	105	21	9.9	99.03	4333
8154	67.20	14.93	4.53	1.80	0.88	1.18	3.03	0.58	0.16	0.02	0.007	23	11	5.5	99.81	720
8155	44.31	11.68	8.02	4.00	7.95	0.87	9.28	1.35	1.34	0.05	0.059	64	15	10.1	99.06	4578
8156	46.86	9.60	9.14	13.16	7.42	1.59	4.34	0.98	1.06	0.14	0.127	438	22	4.8	99.23	3095
8157	64.93	15.14	5.42	3.42	1.12	1.23	3.73	0.55	0.12	0.06	0.008	28	12	4.1	99.79	800
8158	67.09	14.90	4.31	1.83	1.93	1.48	3.28	0.55	0.10	0.02	0.007	27	11	4.3	99.77	878
8159	62.08	10.18	2.23	3.05	8.21	1.89	2.64	0.33	0.11	0.10	0.004	<20	6	9.0	99.81	614
8160	58.79	13.89	3.91	1.88	0.99	0.97	2.65	0.49	0.05	0.02	0.006	<20	11	16.2	99.81	674
8161	15.52	3.36	4.47	6.08	33.64	0.33	1.87	0.35	0.38	0.45	0.042	128	9	33.0	99.51	1175
8162	47.40	10.12	9.59	11.01	7.95	1.52	5.55	1.03	1.20	0.14	0.098	310	24	3.5	99.16	3475
8163	44.65	11.20	8.14	6.69	9.23	1.65	6.80	1.14	1.17	0.22	0.114	278	20	8.1	99.16	3680
8164	37.62	8.05	3.94	1.56	24.55	1.60	1.07	0.34	0.14	0.20	0.008	<20	7	20.8	99.83	633
8165	48.38	10.39	8.20	9.44	6.65	1.84	6.64	1.05	1.09	0.14	0.100	232	19	5.2	99.16	3543
8166	61.77	14.15	5.68	2.16	3.05	2.20	1.75	0.64	0.16	0.11	0.013	48	14	8.1	99.78	801
8167	48.15	10.19	6.86	8.59	8.50	2.24	6.37	0.88	1.05	0.12	0.071	124	19	6.0	99.01	4316
8168	51.37	9.98	7.58	8.76	7.81	1.97	6.21	0.97	1.19	0.13	0.068	126	21	3.0	99.02	4538
8169	50.98	10.10	7.24	8.83	8.09	2.04	6.58	0.95	1.13	0.13	0.071	114	20	2.9	99.01	4496
8170	43.10	8.82	3.28	0.68	22.26	1.76	1.25	0.34	0.28	0.18	0.007	<20	7	17.9	99.82	729
8171	39.56	11.51	7.49	9.91	9.80	1.04	8.19	1.09	1.07	0.14	0.178	287	21	9.2	99.18	3727
8172	66.66	13.62	5.26	2.09	2.66	2.19	1.86	0.62	0.15	0.04	0.013	25	12	4.6	99.79	797
8173	38.41	11.29	7.09	9.53	11.84	0.77	7.83	1.07	1.05	0.17	0.178	290	21	10.0	99.23	3527
8174	27.02	7.03	5.52	1.74	29.81	1.24	1.03	0.31	0.43	0.19	0.008	<20	7	25.4	99.76	832
8183	50.08	13.60	14.03	5.85	9.65	2.24	0.91	2.35	0.22	0.19	0.037	95	38	0.5	99.68	239
8184	40.91	11.18	7.58	9.86	9.42	1.04	7.92	1.08	1.05	0.15	0.175	281	21	8.8	99.16	3853
8185	50.15	13.56	14.03	5.82	9.71	2.26	0.91	2.37	0.22	0.19	0.036	88	38	0.4	99.67	240
8188	49.80	13.73	13.98	5.93	9.89	2.26	0.91	2.37	0.23	0.20	0.037	91	38	0.3	99.67	241
8219	39.97	11.40	7.44	9.64	9.88	1.03	7.84	1.08	1.08	0.15	0.173	290	19	9.5	99.18	3841
8229	55.85	6.32	13.41	0.02	0.04	0.47	6.73	0.94	1.03	<0.01	0.080	<20	10	14.6	99.45	2287
8230	74.41	10.50	0.70	0.09	0.16	1.42	6.86	1.66	0.13	<0.01	0.075	23	4	3.3	99.31	3514
8231	75.80	1.94	8.85	<0.01	0.03	0.05	2.88	0.17	0.05	<0.01	0.012	<20	<1	10.1	99.90	236
8232	57.99	16.41	3.85	1.76	4.75	2.86	8.09	0.57	0.34	0.07	0.003	<20	10	2.5	99.19	4034
8233	55.46	6.06	13.76	0.02	0.04	0.43	6.80	1.09	0.46	<0.01	0.095	<20	2	15.3	99.46	2241
8234	55.26	15.89	7.98	2.79	5.26	4.98	4.11	0.69	0.54	0.12	0.003	26	15	1.8	99.43	2618
8235	66.68	16.68	1.92	1.70	3.18	2.77	3.58	0.73	0.21	0.03	0.015	47	15	2.1	99.60	1696
8236	70.01	16.40	2.47	1.18	0.31	0.55	3.66	0.78	0.20	<0.01	0.016	30	16	4.2	99.73	1025
8237	61.64	16.93	2.84	0.08	0.37	4.31	8.10	0.72	0.19	0.07	0.014	52	17	4.4	99.63	2023
8238	56.34	15.20	6.93	3.34	3.03	3.21	5.94	0.79	0.62	0.09	0.026	80	22	3.9	99.45	2552
8239	62.85	16.68	2.92	0.08	0.33	0.97	12.94	0.72	0.23	0.08	0.014	56	13	1.6	99.39	3747
8240	68.31	15.79	2.04	1.54	2.31	2.58	4.15	0.71	0.20	0.02	0.014	34	14	2.0	99.63	1554
8241	68.41	15.83	1.80	1.57	2.01	2.04	4.57	0.72	0.21	0.02	0.015	36	15	2.4	99.59	1927
8242	55.93	15.33	6.36	3.15	5.37	3.86	5.36	0.70	0.54	0.08	0.011	35	16	2.5	99.21	4431
8243	64.45	17.39	2.31	0.11	0.46	4.70	7.57	0.74	0.20	0.05	0.015	47	18	1.5	99.53	2746
8244	53.72	14.06	8.83	4.08	2.84	3.87	4.63	0.75	0.71	1.25	0.031	488	19	4.4	99.26	3756
8306	49.39	13.55	14.57	5.72	9.70	2.20	0.88	2.37	0.23	0.19	0.035	91	37	0.8	99.66	215
8307	49.61	13.62	14.59	5.76	9.75	2.22	0.88	2.35	0.23	0.19	0.035	91	37	0.4	99.65	213
8308	49.58	13.62	14.52	5.75	9.72	2.24	0.89	2.34	0.22	0.19	0.036	94	37	0.5	99.64	216

Appendix 4B

Element:	Be	Co	Cs	Ga	Hf	Nb	Rb	Sn	Sr	Ta	Th	U	V	W	Zr	Y	La
Method:	4A-4B	4A-4B	4A-4B	4A-4B	4A-4B	4A-4B	4A-4B	4A-4B	4A-4B								
Units:	ppm	ppm	ppm	ppm	ppm	ppm	ppm	ppm	ppm								
MDL:	1	0.2	0.1	0.5	0.1	0.1	0.1	1	0.5	0.1	0.2	0.1	8	0.5	0.1	0.1	0.1
RPD %:	16.1	10.4	6.0	3.6	7.5	5.0	4.8	20.7	5.6	14.7	8.8	7.5	4.9	13.6	3.8	3.6	4.0
RPD count:	19	25	25	25	25	25	25	24	25	23	25	25	25	17	25	25	25
APR %:	66.7	97.0	NA	100.5	93.3	115.3	92.4	125.0	101.0	95.8	98.1	100.0	104.5	<MDL	104.0	96.9	93.3
APR error %:	0.0	11.7		15.9	21.2	14.7	10.1	66.5	13.5	28.4	13.6	20.5	10.5		16.8	14.3	14.1
Sample																	
8151	3	41.7	2.0	19.2	14.4	24.1	405.6	3	2162.2	1.1	43.3	12.5	176	2.0	440.0	21.3	104.7
8152	4	31.6	1.3	18.0	7.8	22.0	316.7	3	1951.5	0.9	38.3	35.3	122	2.2	212.3	25.5	115.1
8153	6	38.6	2.4	14.5	12.7	21.8	326.9	3	1918.8	0.9	40.5	13.5	161	2.7	435.6	23.7	94.6
8154	3	9.4	9.6	19.4	5.7	15.3	131.7	3	149.2	1.1	12.3	4.4	93	2.7	200.9	34.6	42.8
8155	6	24.0	2.6	15.8	11.2	21.7	284.1	3	1851.0	0.9	37.2	14.1	128	3.9	417.7	13.8	77.3
8156	4	53.0	3.6	12.9	6.2	10.9	132.6	2	897.5	0.5	7.4	2.3	185	<0.5	212.6	16.6	37.1
8157	3	9.9	9.6	17.8	4.9	13.9	157.1	3	163.5	1.0	12.2	4.4	99	2.4	164.6	27.7	33.0
8158	3	8.8	7.3	17.5	5.4	15.0	150.2	3	411.2	1.2	12.9	4.3	94	2.9	193.8	25.5	37.5
8159	2	4.5	2.5	10.6	5.1	8.3	79.6	2	372.3	0.6	7.6	2.6	43	1.4	189.6	21.9	24.8
8160	3	8.0	9.8	18.2	5.9	13.5	145.3	3	210.7	1.0	11.5	6.4	85	3.0	191.1	22.4	29.8
8161	2	17.3	0.9	5.2	2.0	3.4	56.4	<1	1086.3	<0.1	2.8	1.0	77	0.7	68.8	11.0	16.1
8162	3	48.3	2.3	15.3	6.0	11.0	170.9	2	1298.4	0.5	8.5	2.8	189	<0.5	225.7	18.1	39.9
8163	4	42.2	3.6	15.7	9.1	16.5	195.2	2	1578.6	0.8	12.4	3.9	172	0.8	333.9	20.2	50.8
8164	1	6.7	1.1	8.6	2.3	4.9	28.1	<1	361.5	0.3	3.0	1.3	59	0.9	90.3	13.1	12.4
8165	5	38.8	3.2	15.1	8.8	16.7	185.1	3	1559.2	0.8	12.3	3.8	162	0.6	324.7	19.8	50.4
8166	2	17.6	3.7	15.8	3.9	9.4	59.9	1	331.9	0.6	6.4	3.6	127	1.1	160.9	22.0	23.3
8167	6	32.5	2.4	13.5	7.2	13.9	175.9	2	1928.1	0.7	9.8	3.5	139	0.5	274.3	17.8	49.6
8168	6	36.0	2.8	14.5	7.5	13.7	167.0	2	1863.4	0.6	10.5	3.5	161	0.6	270.3	19.3	55.4
8169	6	33.8	2.5	13.7	8.1	14.4	182.2	2	1946.9	0.7	11.1	3.1	147	<0.5	285.8	18.5	53.3
8170	1	8.3	0.9	9.5	3.0	5.6	30.9	<1	482.8	0.2	3.9	1.6	74	0.9	105.1	17.5	15.3
8171	3	46.6	2.4	14.0	4.4	9.6	267.5	1	1214.9	0.4	5.5	1.9	173	1.1	167.5	14.3	28.4
8172	2	9.5	3.2	14.5	4.4	9.0	67.7	1	320.6	0.6	5.9	2.3	126	1.5	166.7	16.6	20.5
8173	4	45.6	2.7	13.5	4.5	9.4	269.7	1	1156.8	0.5	5.1	1.9	174	<0.5	161.6	14.0	26.9
8174	1	6.2	1.1	7.7	2.4	4.4	31.3	<1	667.8	0.4	2.8	1.5	71	0.8	106.0	18.8	18.6
8183	1	46.4	0.5	22.6	5.2	12.6	21.9	3	240.3	0.7	2.7	1.1	510	<0.5	171.5	35.8	16.4
8184	4	48.1	2.4	15.0	4.9	10.5	284.0	2	1275.2	0.5	6.1	1.8	193	0.9	178.4	15.6	29.1
8185	<1	46.8	0.5	22.0	5.1	13.3	21.8	3	240.7	0.8	2.6	1.0	511	<0.5	170.4	36.5	16.0
8188	1	47.2	0.4	22.3	4.8	13.2	21.3	3	241.9	0.8	2.8	0.9	519	<0.5	168.6	36.5	16.6
8219	3	52.7	2.5	15.2	5.1	9.8	267.4	1	1233.8	<0.1	6.7	1.8	183	1.1	178.9	14.2	30.1
8229	4	2.7	1.1	11.9	2.5	81.6	115.5	2	1319.0	2.0	20.4	5.3	115	318.8	47.0	5.7	83.5
8230	3	2.9	1.6	13.4	9.8	100.0	150.8	16	1350.7	3.5	25.7	5.3	54	269.2	239.9	8.4	59.7
8231	<1	0.8	0.5	3.5	1.2	16.4	38.1	2	52.0	0.3	2.0	1.4	44	178.7	29.7	1.1	5.9
8232	2	13.9	0.7	19.5	6.2	14.5	132.4	2	1380.9	0.7	8.9	3.2	98	1.0	203.3	21.2	40.9
8233	2	1.7	1.1	12.8	11.0	64.6	105.0	2	884.7	2.4	30.7	2.5	58	416.7	279.5	9.0	70.6
8234	2	13.1	4.2	18.9	4.5	8.9	78.8	<1	1026.3	0.6	7.1	2.1	142	8.0	157.7	19.4	34.7
8235	2	4.6	4.9	18.3	4.9	15.7	126.6	<1	726.7	1.1	13.0	6.4	226	3.6	172.1	24.4	36.2
8236	2	8.0	5.7	19.1	6.0	17.7	157.5	2	109.2	1.2	13.2	4.9	249	1.9	197.0	32.2	42.7
8237	1	9.0	0.6	20.2	5.2	20.5	145.4	2	214.2	1.3	11.0	3.8	206	11.4	157.3	24.6	45.6
8238	2	19.1	4.5	21.1	4.7	10.9	154.6	2	640.1	0.5	8.0	4.0	215	16.6	164.3	26.2	42.1
8239	1	11.9	1.2	19.0	4.5	17.9	210.3	2	417.7	1.0	14.1	13.0	173	74.9	145.9	25.7	104.4
8240	2	4.7	5.1	17.4	4.9	15.7	139.3	<1	598.7	1.0	11.3	5.1	225	5.5	167.1	23.0	29.6
8241	2	4.9	5.2	17.7	5.1	16.9	144.9	<1	535.8	1.1	11.2	5.6	239	3.3	163.8	23.1	31.2
8242	3	34.6	1.1	20.0	4.8	9.9	95.1	3	1186.3	0.4	7.6	2.8	152	5.4	163.3	19.1	34.0
8243	1	4.5	0.7	19.5	4.5	20.4	142.0	31	348.4	1.2	13.3	4.1	199	12.6	159.5	23.7	51.6
8244	2	285.5	7.1	19.6	4.2	9.1	136.7	2	560.1	0.4	6.9	3.7	202	31.2	153.7	28.9	45.3
8306	<1	42.1	0.5	19.5	4.5	11.4	20.5	2	218.3	0.8	2.6	1.1	466	<0.5	154.2	33.2	15.2
8307	1	45.6	0.5	20.0	4.2	11.8	21.2	2	225.9	0.7	2.7	0.9	478	<0.5	155.5	33.4	15.1
8308	1	45.3	0.5	20.2	4.2	13.8	20.8	2	226.7	0.8	2.5	1.0	470	0.6	153.0	33.8	15.9

Appendix 4B

Element:	Ce	Pr	Nd	Sm	Eu	Gd	Tb	Dy	Ho	Er	Tm	Yb	Lu	TOT/C	TOT/S	F
Method:	4A-4B	2A Leco	2A Leco	2A												
Units:	ppm	%	%	ppm												
MDL:	0.1	0.02	0.3	0.05	0.02	0.05	0.01	0.05	0.02	0.03	0.01	0.05	0.01	0.02	0.02	10
RPD %:	4.5	3.4	3.7	3.8	4.5	5.2	3.3	3.0	5.7	6.4	5.7	3.3	4.3	10.3	31.8	4.4
RPD count:	25	25	25	25	25	25	25	25	25	25	25	25	25	23	23	27
APR %:	93.6	88.3	103.8	99.3	93.2	91.1	92.1	78.8	99.7	89.0	87.5	92.3	91.7	NA	80.0	95.0
APR error %:	11.0	8.3	10.4	10.7	10.6	9.1	11.0	14.1	32.0	2.8	17.8	12.9	12.3		45.6	25.8
Sample																
8151	226.5	28.89	112.9	15.37	3.22	9.61	1.02	4.36	0.68	1.74	0.27	1.69	0.23	0.09	0.21	4910
8152	291.3	38.12	146.1	19.47	4.15	12.06	1.32	5.31	0.81	1.87	0.29	1.53	0.19	0.42	3.18	4630
8153	215.9	28.24	114.6	16.05	3.40	10.13	1.08	4.85	0.74	1.78	0.28	1.57	0.22	2.32	0.50	4780
8154	88.0	10.64	40.0	7.50	1.45	6.65	1.07	6.00	1.19	3.32	0.56	3.24	0.49	0.24	0.13	1100
8155	162.7	19.85	77.9	10.50	2.16	6.19	0.69	2.98	0.43	1.12	0.16	0.93	0.13	0.08	3.37	3560
8156	78.7	10.46	43.6	7.38	1.96	5.71	0.74	3.48	0.56	1.48	0.22	1.23	0.18	0.03	<0.02	2330
8157	68.0	8.26	30.1	5.68	1.06	5.10	0.83	4.47	0.92	2.75	0.45	2.82	0.42	0.09	<0.02	1190
8158	77.9	9.13	32.9	6.18	1.16	5.28	0.85	4.53	0.86	2.57	0.41	2.54	0.38	0.65	<0.02	800
8159	52.4	6.20	23.9	4.30	0.90	3.95	0.65	3.57	0.75	2.21	0.36	2.21	0.31	1.85	<0.02	390
8160	60.9	7.39	27.4	4.75	0.83	4.25	0.65	3.49	0.74	2.29	0.38	2.45	0.38	8.11	0.03	720
8161	34.2	4.55	19.4	3.47	1.11	2.98	0.40	1.78	0.32	0.85	0.12	0.73	0.10	9.26	0.02	850
8162	87.6	11.45	46.4	8.33	2.15	6.30	0.81	3.75	0.62	1.68	0.23	1.37	0.20	0.32	0.05	2280
8163	109.8	13.98	57.4	9.62	2.40	6.86	0.88	3.80	0.70	1.73	0.26	1.66	0.22	1.51	<0.02	2830
8164	24.8	3.02	11.7	2.26	0.63	2.17	0.36	2.11	0.43	1.30	0.20	1.33	0.21	5.58	<0.02	310
8165	111.7	13.88	57.4	9.29	2.42	7.03	0.88	4.08	0.67	1.74	0.27	1.54	0.21	0.82	<0.02	2690
8166	46.0	5.97	23.9	4.68	1.23	4.47	0.72	3.83	0.76	2.32	0.35	2.16	0.34	2.45	0.04	450
8167	107.3	13.59	55.2	9.09	2.30	6.84	0.84	3.71	0.60	1.54	0.22	1.35	0.18	1.43	<0.02	2530
8168	117.3	14.57	58.2	10.16	2.58	7.65	0.93	4.09	0.65	1.65	0.23	1.36	0.19	0.44	<0.02	2630
8169	114.8	14.57	59.3	9.74	2.50	7.30	0.89	4.01	0.65	1.53	0.22	1.36	0.19	0.65	<0.02	3030
8170	29.5	3.70	15.0	2.82	0.76	2.75	0.42	2.48	0.52	1.61	0.26	1.73	0.28	4.86	0.19	630
8171	60.0	7.75	33.4	5.89	1.65	4.64	0.60	2.89	0.48	1.23	0.18	1.11	0.16	1.33	0.04	3170
8172	40.9	4.99	20.9	3.75	0.90	3.38	0.51	2.94	0.61	1.80	0.27	1.86	0.28	0.63	<0.02	420
8173	57.8	7.57	33.2	5.72	1.63	4.62	0.60	2.91	0.50	1.33	0.19	1.14	0.16	2.16	0.04	3430
8174	33.7	4.18	16.9	3.23	0.86	3.28	0.52	2.94	0.59	1.75	0.25	1.62	0.24	6.94	0.12	640
8183	39.5	5.48	25.0	6.33	2.02	6.57	1.14	6.49	1.30	3.52	0.54	3.12	0.48	0.03	0.03	400
8184	62.5	8.16	33.7	6.30	1.76	4.72	0.64	3.09	0.55	1.32	0.19	1.16	0.17	1.89	0.02	3310
8185	38.7	5.51	24.4	6.16	2.04	6.63	1.13	6.36	1.35	3.58	0.54	3.15	0.49	0.03	0.03	400
8188	38.9	5.48	24.7	6.19	2.04	6.66	1.15	6.53	1.37	3.65	0.54	3.10	0.48	0.03	0.02	460
8219	60.5	8.22	35.3	6.48	1.79	4.98	0.65	2.90	0.54	1.57	0.18	1.05	0.16	2.02	0.13	3460
8229	132.1	11.84	32.0	3.77	0.81	1.28	0.21	1.05	0.17	0.46	0.06	0.37	0.05	0.19	3.40	310
8230	106.0	10.32	30.6	3.83	1.00	1.60	0.28	1.42	0.27	0.86	0.13	0.92	0.14	0.14	0.24	250
8231	9.1	0.67	1.9	0.27	0.06	0.17	0.03	0.20	0.03	0.10	0.02	0.11	0.02	0.25	2.43	80
8232	96.6	11.36	40.5	7.44	2.31	5.52	0.83	3.95	0.72	1.97	0.30	1.94	0.28	0.14	1.24	320
8233	144.3	15.12	49.4	5.76	1.19	2.11	0.35	1.71	0.30	0.92	0.15	1.00	0.14	0.04	3.58	280
8234	75.6	8.93	35.2	6.95	2.00	5.02	0.73	3.59	0.67	1.79	0.27	1.68	0.26	0.04	<0.02	710
8235	71.2	8.49	31.9	5.67	1.26	4.29	0.75	4.10	0.82	2.40	0.37	2.51	0.40	0.13	0.07	720
8236	85.1	9.77	36.4	6.49	1.34	4.98	0.90	4.95	1.02	3.05	0.45	2.95	0.48	0.58	0.03	610
8237	87.6	9.68	34.3	6.01	1.70	4.61	0.81	4.33	0.89	2.60	0.39	2.67	0.41	0.08	<0.02	230
8238	82.2	9.89	39.2	7.11	1.59	5.36	0.86	4.24	0.82	2.24	0.32	2.06	0.30	<0.02	<0.02	1470
8239	212.9	21.45	67.8	9.83	2.23	5.38	0.87	4.28	0.81	2.21	0.34	2.33	0.36	0.16	<0.02	140
8240	58.2	7.10	26.8	4.95	0.97	3.67	0.65	3.72	0.74	2.29	0.36	2.35	0.37	0.16	0.03	760
8241	60.4	7.26	26.9	4.79	0.96	3.68	0.64	3.44	0.72	2.29	0.36	2.34	0.36	0.26	0.04	930
8242	80.2	9.76	39.2	6.99	2.16	5.30	0.79	3.61	0.65	1.80	0.26	1.56	0.22	0.25	1.71	1120
8243	105.6	10.64	38.9	6.28	1.64	4.39	0.76	4.03	0.81	2.41	0.39	2.42	0.39	0.05	<0.02	340
8244	91.0	10.78	45.2	8.37	2.10	6.54	0.98	4.63	0.86	2.30	0.32	1.83	0.27	0.03	<0.02	1430
8306	37.5	5.02	23.1	5.67	1.81	5.99	1.06	6.06	1.22	3.53	0.51	3.01	0.46	0.03	<0.02	340
8307	36.9	5.10	22.0	5.72	1.90	6.08	1.07	6.05	1.26	3.52	0.51	3.25	0.47	0.03	0.02	340
8308	38.8	5.19	24.0	5.66	1.93	6.33	1.08	6.32	1.28	3.55	0.51	3.20	0.48	0.03	0.02	340

Appendix 4C

Element	Mo	Cu	Pb	Zn	Ni	As	Cd	Sb	Bi	Ag	Au	Hg	Tl	Se
Method	1DX	1DX	1DX	1DX	1DX	1DX	1DX	1DX	1DX	1DX	1DX	1DX	1DX	1DX
Units	ppm	ppm	ppm	ppm	ppm	ppm	ppm	ppm	ppm	ppm	ppb	ppm	ppm	ppm
MDL	0.1	0.1	0.1	1	0.1	0.5	0.1	0.1	0.1	0.1	0.5	0.01	0.1	0.5
RPD %	17.6	9.6	13.3	5.8	12.0	29.2	24.2	27.1	18.5	6.7	34.0	30.2	13.5	12.8
RPD count	94	94	95	95	95	84	29	49	39	16	20	16	48	3
APR %	54.2	97.6	101.9	58.5	31.1	82.0	45.8	55.0	<MDL	20.0	65.1	NA	NA	<MDL
APR error %	49.8	8.7	20.9	11.9	12.7	54.9	44.5	55.3		0.0	28.9			
Sample														
8151	7.7	68.3	51.0	79	105.3	2.5	<0.1	0.1	0.2	<0.1	0.6	0.01	1.2	<0.5
8152	43.2	176.2	36.6	72	89.1	2.4	<0.1	<0.1	0.1	<0.1	<0.5	0.01	0.8	<0.5
8153	9.6	92.0	37.0	70	86.1	2.6	0.2	0.2	0.2	<0.1	0.6	0.02	0.4	<0.5
8154	3.0	19.9	17.1	84	22.1	3.7	0.4	0.1	0.5	<0.1	0.8	<0.01	0.3	<0.5
8155	14.6	40.1	30.0	46	55.8	3.5	<0.1	0.3	0.1	<0.1	<0.5	0.01	0.3	0.7
8156	0.8	92.5	21.7	68	335.8	0.9	<0.1	<0.1	<0.1	<0.1	<0.5	<0.01	0.6	<0.5
8157	1.6	21.1	17.0	73	26.5	4.1	0.3	0.2	0.2	<0.1	1.0	<0.01	0.6	<0.5
8158	2.4	27.3	2.9	60	22.2	0.8	<0.1	0.1	0.4	<0.1	<0.5	<0.01	0.3	<0.5
8159	0.6	3.6	6.3	34	7.9	3.2	<0.1	<0.1	0.1	<0.1	0.5	<0.01	0.1	<0.5
8160	4.1	24.9	23.6	51	18.6	15.1	0.4	0.9	0.4	0.1	<0.5	0.01	<0.1	<0.5
8161	3.2	47.1	375.1	404	102.3	6.6	1.8	0.4	0.2	0.4	<0.5	<0.01	0.2	<0.5
8162	0.9	98.7	25.1	70	235.7	1.5	0.1	<0.1	<0.1	<0.1	<0.5	<0.01	0.6	<0.5
8163	2.1	52.2	32.9	76	224.5	1.3	0.2	<0.1	0.1	<0.1	<0.5	0.01	0.5	<0.5
8164	1.3	10.5	4.1	34	18.1	7.2	0.1	0.1	<0.1	<0.1	<0.5	<0.01	<0.1	<0.5
8165	0.9	51.4	32.2	69	188.5	1.7	<0.1	<0.1	0.1	<0.1	<0.5	0.01	0.6	<0.5
8166	1.1	63.4	12.2	90	46.5	10.5	1.3	0.4	0.2	0.1	<0.5	<0.01	<0.1	<0.5
8167	0.3	77.7	37.3	56	94.7	1.3	<0.1	<0.1	0.1	<0.1	<0.5	<0.01	0.3	<0.5
8168	0.4	78.4	34.3	59	95.2	1.2	<0.1	<0.1	0.1	<0.1	1.6	<0.01	0.4	<0.5
8169	0.3	55.4	45.5	66	93.3	0.6	<0.1	<0.1	0.1	<0.1	0.9	<0.01	0.4	<0.5
8170	1.9	5.9	5.5	38	14.5	10.9	<0.1	0.2	<0.1	<0.1	<0.5	<0.01	<0.1	<0.5
8171	2.5	81.0	23.3	62	212.1	3.2	0.1	<0.1	<0.1	<0.1	<0.5	<0.01	0.9	<0.5
8172	0.8	15.7	7.0	71	23.3	3.7	<0.1	<0.1	0.1	<0.1	<0.5	<0.01	0.1	<0.5
8173	0.6	80.9	22.9	59	220.4	1.4	<0.1	<0.1	<0.1	<0.1	<0.5	<0.01	0.6	<0.5
8174	1.6	7.9	4.9	37	14.2	22.9	<0.1	0.4	<0.1	<0.1	<0.5	0.01	0.2	<0.5
8183	0.8	303.7	17.1	88	27.1	2.4	0.2	0.6	<0.1	0.1	3.5	<0.01	<0.1	<0.5
8184	1.4	84.8	22.4	62	217.2	2.7	<0.1	<0.1	<0.1	<0.1	<0.5	<0.01	0.8	<0.5
8185	0.8	304.8	17.3	93	26.8	2.3	0.2	0.6	<0.1	0.1	3.8	<0.01	<0.1	<0.5
8188	1.0	333.4	19.0	98	29.3	2.8	0.2	0.7	<0.1	0.1	4.9	<0.01	<0.1	0.6
8219	2.6	87.9	25.1	71	262.7	4.0	<0.1	<0.1	<0.1	<0.1	<0.5	<0.01	1.0	<0.5

Appendix 4D

Element:	Mo	Cu	Pb	Zn	Ag	Ni	Co	Mn	Fe	As	U	Au	Th	Sr	Cd	Sb	Bi	V
Method:	1F	1F	1F	1F	1F	1F	1F	1F	1F	1F	1F	1F	1F	1F	1F	1F	1F	1F
Units	ppm	ppm	ppm	ppm	ppb	ppm	ppm	ppm	%	ppm	ppm	ppb	ppm	ppm	ppm	ppm	ppm	ppm
MDL:	0.01	0.01	0.01	0.1	2	0.1	0.1	1	0.01	0.1	0.1	0.2	0.1	0.5	0.01	0.02	0.02	2
RPD %:	15.6	7.3	13.6	12.4	8.2	7.9	10.9	6.7	3.0	17.2	6.5	20.4	6.8	9.9	27.7	12.8	13.4	6.0
RPD count:	27	27	27	27	27	27	27	27	27	27	27	10	27	27	27	25	27	26
APR %:	50.3	100.6	95.9	60.0	27.4	31.3	34.1	26.3	38.0	75.3	65.0	77.5	64.8	22.8	42.9	37.8	7.7	50.9
APR error %:	49.2	12.3	20.7	17.6	16.2	11.5	14.0	12.5	3.8	53.8	27.6	27.3	16.3	26.6	39.3	92.4	13.2	14.4
Sample																		
8151	7.64	66.62	46.04	81.6	83	107.6	40.9	406	4.30	1.4	9.2	0.2	26.0	1433.6	0.02	0.08	0.17	125
8152	47.74	181.07	34.42	80.3	77	100.1	30.8	388	4.17	1.3	29.2	<0.2	21.0	1174.8	0.14	0.09	0.14	71
8153	9.37	85.60	33.77	73.7	63	97.8	35.7	1130	3.67	0.6	6.9	0.2	21.6	1165.4	0.15	0.16	0.17	117
8154	2.39	16.97	14.90	73.6	50	23.3	7.6	140	2.35	3.0	2.3	<0.2	9.0	57.3	0.23	0.04	0.47	34
8155	14.97	36.59	28.44	51.3	43	63.1	21.3	347	4.12	2.9	8.8	<0.2	15.9	990.1	0.03	0.20	0.12	83
8156	0.79	82.74	19.66	67.9	38	365.1	38.3	686	4.60	0.7	1.1	1.4	4.5	291.2	0.09	<0.02	0.09	130
8157	1.75	20.44	15.99	72.9	52	27.8	9.2	370	3.28	3.6	1.2	<0.2	8.0	79.0	0.26	0.06	0.24	73
8158	2.40	23.28	2.71	59.5	13	21.4	7.5	163	2.21	0.6	1.6	<0.2	7.6	132.8	0.04	0.03	0.32	33
8159	0.76	3.12	6.19	36.2	11	9.4	4.3	713	1.14	2.3	0.6	<0.2	5.3	211.1	0.09	0.04	0.09	25
8160	3.48	20.50	21.05	50.7	148	20.1	7.7	102	1.93	13.1	2.2	<0.2	7.0	113.2	0.34	0.20	0.43	16
8161	2.61	40.62	372.28	416.7	473	116.3	16.5	3558	2.78	3.7	0.4	0.6	1.4	746.3	1.56	0.21	0.15	58
8162	0.92	93.04	23.18	75.2	55	278.0	35.2	651	4.98	1.1	1.9	0.6	6.5	302.2	0.09	<0.02	0.10	129
8163	2.23	47.86	30.40	82.2	63	259.8	36.2	1546	4.25	0.9	1.7	0.4	8.2	528.1	0.12	0.06	0.12	128
8164	0.85	7.74	3.68	31.1	21	18.9	5.8	1557	2.34	4.9	0.7	<0.2	1.8	139.8	0.13	0.06	0.06	40
8165	0.89	46.42	28.31	66.4	39	203.3	28.6	675	3.67	1.5	2.8	<0.2	10.1	404.3	0.10	0.04	0.12	101
8166	0.86	53.67	11.28	85.6	123	45.9	15.5	784	3.29	8.7	1.5	<0.2	3.8	89.7	0.99	0.11	0.19	57
8167	0.25	68.62	32.28	52.1	39	97.4	23.5	554	2.77	0.9	2.6	<0.2	7.9	759.2	0.06	0.02	0.10	77
8168	0.38	65.55	29.78	54.9	44	95.0	22.6	499	3.00	1.1	2.4	<0.2	5.5	725.9	0.07	0.02	0.10	83
8169	0.26	48.65	38.15	60.0	59	94.5	23.6	546	2.92	0.7	2.3	0.4	7.8	811.4	0.07	<0.02	0.12	81
8170	1.59	5.45	5.16	40.8	23	15.5	7.2	1419	1.90	8.4	0.7	<0.2	2.5	187.4	0.04	0.06	0.04	30
8171	2.85	76.58	21.76	65.6	49	250.8	42.2	1069	4.24	2.4	1.4	0.8	3.9	427.8	0.08	0.03	0.08	141
8172	0.69	13.23	7.00	69.8	29	23.8	8.7	279	3.04	3.4	0.6	<0.2	3.5	67.4	0.06	<0.02	0.12	68
8173	0.66	73.62	19.80	65.9	44	241.2	40.9	1271	3.90	0.8	1.0	0.8	3.5	377.3	0.07	<0.02	0.07	139
8174	1.65	7.44	4.58	38.3	33	15.9	5.8	1538	3.49	18.8	0.8	0.3	2.0	434.5	0.07	0.17	0.06	51
8183	0.72	299.29	15.70	83.1	129	27.8	15.3	388	3.89	1.8	0.8	4.0	1.7	54.0	0.13	0.21	0.06	223
8184	1.60	80.76	21.63	65.2	51	251.4	43.3	1027	4.25	2.0	1.3	<0.2	3.6	423.6	0.09	<0.02	0.08	140
8185	0.72	306.89	15.41	83.7	124	26.5	14.7	387	3.86	1.8	0.7	4.9	1.8	52.3	0.13	0.22	0.06	217
8188	0.73	322.36	17.78	96.9	156	29.7	16.8	449	4.02	2.1	0.6	5.4	1.9	64.2	0.19	0.28	0.07	239
8219	2.13	72.38	21.28	67.6	51	271.7	38.3	1051	4.06	1.8	1.3	0.9	2.8	437.5	0.11	0.02	0.07	129
8229	0.73	15.81	20.29	2.4	40	12.2	1.8	14	9.45	2301.9	2.8	198.3	10.8	396.7	0.03	5.97	0.05	36
8230	0.15	4.89	25.78	2.0	99	6.4	1.1	17	0.36	28.6	1.5	42.2	9.7	132.1	0.02	0.27	0.03	11
8231	0.62	14.00	19.18	2.2	21	2.9	0.6	19	5.92	2017.0	0.7	747.9	1.6	42.2	0.02	14.66	0.13	24
8232	1.01	250.82	65.67	235.7	617	11.8	12.8	239	1.96	3.0	1.0	8.8	2.9	101.0	0.80	0.37	0.22	32
8233	0.55	34.50	32.01	1.4	56	5.7	1.1	18	9.67	469.9	1.7	25.7	17.0	361.5	0.03	0.62	0.02	29
8234	2.28	29.93	48.89	43.5	100	12.1	6.1	246	3.98	1.4	0.2	11.5	2.8	119.1	0.08	0.05	0.03	94
8235	3.28	21.52	6.30	17.4	55	39.3	4.3	185	1.25	7.0	1.8	<0.2	7.6	178.6	0.03	0.20	0.18	152
8236	0.47	33.11	4.50	11.1	19	23.5	7.4	63	1.50	10.2	1.6	<0.2	10.2	32.8	0.02	0.12	0.25	24
8237	0.85	30.99	1.79	38.6	10	52.3	9.4	532	1.98	31.0	0.8	15.1	7.8	15.2	0.12	0.61	0.18	80
8238	2.05	102.95	4.39	42.0	143	73.3	18.8	599	3.95	14.6	1.3	10.0	4.3	103.6	0.08	0.24	0.97	118
8239	4.00	21.88	21.05	65.1	27	50.6	12.0	657	1.98	18.9	9.8	4.1	11.1	29.1	0.10	1.90	0.25	74
8240	3.76	25.27	3.99	18.6	74	33.7	4.8	178	1.38	15.0	1.3	0.7	6.2	108.3	0.03	0.13	0.39	131
8241	2.54	32.12	11.31	23.3	138	26.0	4.3	117	1.11	23.9	1.7	<0.2	6.8	116.4	0.08	0.11	0.30	130
8242	2.20	25.81	11.35	23.3	102	24.3	31.7	264	2.68	1.6	0.6	18.1	3.0	94.5	0.06	0.15	2.28	40
8243	0.62	17.61	1.89	30.6	11	36.4	3.6	439	1.52	14.4	1.1	5.3	9.7	18.6	0.11	0.35	0.08	59
8244	13.53	290.48	1.14	79.1	74	473.0	252.9	9933	4.80	39.2	1.6	10.9	2.4	87.1	1.86	0.48	0.67	125
8306	0.91	338.20	15.96	99.1	142	29.4	16.9	418	4.01	2.7	0.6	5.2	1.8	47.4	0.18	0.50	0.06	256
8307	0.89	344.78	16.91	96.0	136	29.2	15.9	416	3.94	1.4	0.6	5.3	1.6	47.7	0.21	0.54	0.06	250
8308	0.86	337.87	16.09	98.9	136	30.1	16.6	428	3.98	1.5	0.6	4.5	1.7	48.4	0.19	0.52	0.06	253

Appendix 4D

Element:	Ca	P	La	Cr	Mg	Ba	Ti	B	Al	Na	K	W	Sc	Tl	S	Hg	Se	Te	Ga
Method:	1F	1F	1F	1F	1F	1F	1F	1F	1F	1F	1F	1F	1F	1F	1F	1F	1F	1F	1F
Units	%	%	ppm	ppm	%	ppm	%	ppm	%	%	%	ppm	ppm	ppm	%	ppb	ppm	ppm	ppm
MDL:	0.01	0.001	0.5	0.5	0.01	0.5	0.001	20	0.01	0.001	0.01	0.1	0.1	0.02	0.02	5	0.1	0.02	0.1
RPD %:	13.0	8.9	4.7	9.6	6.4	12.1	14.5	12.5	6.9	12.5	8.7	33.3	5.2	5.2	8.6	35.0	29.4	45.2	6.1
RPD count:	27	27	27	27	27	27	27	4	27	27	27	2	27	15	24	13	27	8	27
APR %:	20.1	115.4	75.0	16.2	17.9	17.3	20.7	<MDL	28.9	21.0	29.2	<MDL	9.2	NA	100.0	NA	59.5	17.5	37.5
APR error %:	30.0	34.8	19.3	13.6	13.6	9.6	11.1		27.0	20.3	14.2		21.2		0.0		36.1	84.3	12.2
Sample																			
8151	1.87	0.434	111.1	484.9	3.37	1676.5	0.035	<20	1.72	0.130	2.17	<0.1	7.6	1.22	0.26	20	0.2	0.03	7.1
8152	6.01	0.412	103.8	451.1	2.63	67.1	0.039	<20	1.65	0.075	1.83	<0.1	3.2	0.82	3.16	17	0.5	0.03	7.5
8153	8.56	0.396	87.9	359.7	2.54	962.3	0.077	<20	1.39	0.087	1.62	<0.1	11.2	0.43	0.59	20	0.2	0.11	5.0
8154	0.45	0.050	35.9	25.1	0.75	159.2	0.022	<20	1.93	0.055	0.59	<0.1	3.3	0.36	0.06	<5	0.2	<0.02	8.3
8155	4.86	0.335	49.0	364.8	2.05	27.2	0.124	<20	1.24	0.075	1.30	<0.1	7.5	0.40	3.48	13	0.8	0.03	5.9
8156	1.13	0.358	32.7	422.3	5.34	2020.1	0.405	<20	2.50	0.501	1.27	<0.1	2.5	0.67	0.02	<5	0.3	<0.02	8.3
8157	0.57	0.045	26.8	41.6	1.78	363.1	0.136	<20	3.14	0.259	1.30	0.2	6.6	0.68	0.02	<5	0.2	<0.02	9.0
8158	0.85	0.024	16.5	21.7	0.84	141.3	0.008	<20	1.48	0.038	0.34	<0.1	3.1	0.19	0.02	<5	0.4	0.07	6.6
8159	5.24	0.040	18.8	16.4	1.62	86.2	0.028	<20	1.50	0.185	0.23	<0.1	2.8	0.12	<0.02	<5	0.2	0.05	5.2
8160	0.55	0.020	26.6	10.4	0.69	141.1	0.002	<20	1.18	0.032	0.26	<0.1	2.0	<0.02	0.02	9	0.4	<0.02	3.9
8161	23.24	0.152	12.8	202.1	3.29	538.7	0.113	<20	0.73	0.028	0.55	<0.1	6.8	0.21	0.05	<5	0.3	0.10	2.6
8162	1.83	0.391	36.4	359.8	4.36	1248.0	0.303	<20	2.07	0.261	1.59	<0.1	5.6	0.72	0.05	<5	0.4	<0.02	7.0
8163	4.90	0.433	48.9	448.5	2.89	1598.4	0.286	<20	1.67	0.071	1.02	<0.1	8.7	0.60	<0.02	7	0.4	0.03	5.8
8164	16.58	0.052	8.4	23.5	0.72	194.3	0.031	<20	1.50	0.179	0.11	<0.1	4.9	0.05	0.03	<5	0.1	0.05	3.8
8165	1.74	0.374	45.1	359.2	3.81	1527.5	0.359	<20	1.23	0.080	1.15	<0.1	4.2	0.57	<0.02	6	0.3	<0.02	4.1
8166	1.45	0.055	18.2	40.2	1.00	133.2	0.014	<20	2.17	0.302	0.20	<0.1	5.4	0.06	<0.02	<5	0.3	0.04	6.2
8167	2.91	0.364	44.1	341.3	3.04	632.3	0.290	<20	1.01	0.126	1.12	<0.1	5.7	0.30	<0.02	<5	0.2	0.08	4.2
8168	1.34	0.254	46.9	299.6	2.51	697.3	0.089	<20	1.15	0.119	1.16	<0.1	3.2	0.41	<0.02	<5	0.2	<0.02	4.6
8169	2.04	0.351	45.2	350.0	2.92	809.7	0.285	<20	1.26	0.139	1.54	<0.1	4.0	0.42	<0.02	<5	0.3	0.02	4.7
8170	15.34	0.110	10.5	17.3	0.31	133.2	0.009	<20	1.17	0.139	0.12	<0.1	5.2	0.07	0.20	9	0.5	0.03	3.0
8171	6.57	0.296	27.5	980.3	4.81	1959.1	0.246	<20	2.59	0.077	2.61	0.2	13.1	1.01	0.07	<5	0.6	<0.02	6.6
8172	1.13	0.049	16.2	37.4	1.01	207.5	0.035	<20	2.26	0.169	0.48	<0.1	5.0	0.14	<0.02	<5	<0.1	<0.02	7.1
8173	7.44	0.312	26.4	973.4	4.47	1512.3	0.275	<20	2.72	0.070	2.39	<0.1	12.5	0.54	<0.02	<5	0.4	<0.02	7.5
8174	21.14	0.168	15.9	24.8	0.90	409.2	0.031	<20	1.63	0.111	0.21	<0.1	6.1	0.16	0.13	14	0.2	0.06	4.3
8183	1.22	0.078	11.8	41.7	0.59	40.1	0.283	<20	1.88	0.342	0.21	<0.1	3.4	<0.02	0.03	<5	0.3	0.04	7.8
8184	5.86	0.266	28.3	974.8	5.02	1985.6	0.222	<20	2.61	0.083	2.70	0.1	13.2	0.85	0.04	6	0.3	0.06	7.0
8185	1.21	0.078	11.4	40.0	0.60	39.1	0.280	<20	1.84	0.347	0.21	<0.1	3.5	<0.02	0.03	8	0.4	0.05	7.6
8188	1.75	0.101	12.7	44.8	0.70	43.3	0.314	<20	2.59	0.427	0.24	<0.1	3.8	<0.02	0.03	9	0.4	<0.02	8.4
8219	6.04	0.217	27.1	906.7	4.72	1969.3	0.126	<20	2.78	0.079	2.69	<0.1	12.4	0.92	0.06	14	0.2	<0.02	6.5
8229	0.03	0.404	50.4	156.3	<0.01	26.5	0.018	<20	0.22	0.040	1.94	77.8	8.2	72.20	3.61	501	1.5	0.03	4.8
8230	0.06	0.024	35.2	29.9	0.02	1565.0	0.011	<20	0.10	0.017	0.13	1.8	0.4	1.36	0.24	<5	0.2	<0.02	0.6
8231	<0.01	0.020	4.9	38.6	<0.01	99.8	0.001	<20	0.07	0.002	1.31	59.2	<0.1	27.27	2.66	1296	1.8	0.06	1.9
8232	1.01	0.143	21.7	8.0	0.34	114.1	0.122	<20	0.35	0.069	0.15	0.4	2.5	0.36	1.47	<5	4.5	0.04	1.7
8233	0.03	0.176	56.1	230.2	<0.01	28.7	0.020	<20	0.24	0.033	2.18	>100	0.4	39.01	3.80	<5	0.3	<0.02	6.8
8234	0.91	0.235	23.0	16.8	0.36	371.9	0.085	<20	1.63	0.741	0.15	3.0	2.2	0.07	<0.02	<5	<0.1	0.02	4.0
8235	1.22	0.071	16.4	70.5	0.87	197.9	0.092	<20	3.01	0.459	0.81	0.1	8.3	0.72	0.07	<5	0.3	0.08	9.6
8236	0.20	0.087	44.4	11.5	0.48	206.7	0.005	<20	1.59	0.039	0.44	<0.1	1.4	0.26	<0.02	<5	0.3	0.08	3.4
8237	0.22	0.075	47.0	28.6	0.03	89.6	0.003	<20	0.22	0.076	0.12	0.2	12.2	0.34	<0.02	<5	0.3	0.13	0.8
8238	0.98	0.275	37.3	120.9	1.17	400.8	0.152	<20	1.30	0.098	0.49	0.3	12.0	0.65	<0.02	<5	0.4	0.16	5.5
8239	0.19	0.080	94.9	30.7	0.03	110.0	0.009	<20	0.15	0.013	0.17	0.6	7.8	0.47	<0.02	<5	0.3	0.07	0.9
8240	0.60	0.071	20.0	61.4	0.79	282.4	0.063	<20	1.91	0.237	0.75	<0.1	6.8	0.69	0.03	<5	0.2	0.14	6.6
8241	0.75	0.068	20.5	62.9	0.77	371.8	0.053	<20	2.37	0.280	0.78	<0.1	6.4	0.83	0.04	<5	0.5	0.13	7.9
8242	1.61	0.221	21.2	20.0	0.52	116.0	0.122	<20	0.42	0.087	0.15	0.7	2.9	0.12	1.92	<5	2.9	0.35	2.7
8243	0.22	0.078	49.8	28.1	0.04	95.9	0.004	<20	0.22	0.073	0.10	0.1	11.1	0.29	<0.02	<5	0.1	0.04	0.8
8244	0.99	0.222	28.4	156.0	1.53	1730.8	0.063	<20	1.33	0.073	0.52	1.6	9.0	7.81	<0.02	6	0.1	0.18	5.3
8306	1.38	0.098	13.8	40.7	0.63	42.7	0.290	<20	2.03	0.354	0.23	<0.1	3.1	0.02	0.03	26	0.5	0.02	8.0
8307	1.32	0.100	13.6	37.5	0.62	42.1	0.285	<20	1.97	0.334	0.23	<0.1	3.0	<0.02	0.03	15	0.5	0.03	7.6
8308	1.32	0.099	13.2	38.7	0.62	42.5	0.288	<20	2.00	0.340	0.23	<0.1	3.0	<0.02	0.03	15	0.4	<0.02	7.8

Appendix 4D

Element:	Cs	Ge	Hf	Nb	Rb	Sn	Ta	Zr	Y	Ce	In	Re	Be	Li	Pd	Pt
Method:	1F	1F	1F	1F	1F	1F	1F	1F	1F	1F	1F	1F	1F	1F	1F	1F
Units	ppm	ppm	ppm	ppm	ppm	ppm	ppm	ppm	ppm	ppm	ppm	ppb	ppm	ppm	ppb	ppb
MDL:	0.02	0.1	0.02	0.02	0.1	0.1	0.05	0.1	0.01	0.1	0.02	1	0.1	0.1	10	2
RPD %:	10.3	19.2	29.4	8.5	11.3	29.3	<MDL	12.8	3.4	4.4	34.3	18.2	19.4	7.3	24.5	45.0
RPD count:	27	16	27	16	27	26	27	27	27	27	20	7	22	27	7	4
APR %:	NA	12.0	4.1	0.3	53.8	54.2	<MDL	4.7	35.3	63.9	14.2	NA	11.7	71.6	91.5	<MDL
APR error %:		74.5	69.9	28.0	40.8	51.9		70.8	17.7	15.8	53.1		109.4	30.3	43.1	
Sample																
8151	1.03	0.3	0.06	0.04	140.6	1.1	<0.05	3.3	11.01	233.9	0.06	2	1.3	23.8	<10	5
8152	0.79	0.2	0.06	0.06	124.0	1.0	<0.05	3.9	19.25	277.2	0.05	4	1.6	13.1	<10	3
8153	1.33	0.1	0.11	0.08	106.3	1.3	<0.05	6.9	14.57	192.9	0.06	4	2.9	12.8	17	3
8154	2.79	<0.1	0.13	0.04	40.1	0.7	<0.05	4.3	12.49	67.1	0.03	11	2.4	13.2	<10	<2
8155	1.31	0.1	0.25	0.11	84.7	1.2	<0.05	9.6	6.24	104.3	0.04	4	1.9	13.0	<10	4
8156	2.69	0.2	0.12	0.11	68.6	1.0	<0.05	10.0	7.83	62.4	<0.02	<1	3.8	15.3	<10	<2
8157	6.47	<0.1	0.14	0.06	98.0	1.6	<0.05	3.7	8.20	50.2	0.05	<1	1.1	17.3	<10	<2
8158	3.07	0.1	0.15	<0.02	31.5	0.5	<0.05	6.2	8.84	34.0	0.02	2	1.4	36.3	<10	<2
8159	1.28	<0.1	0.14	0.02	16.1	0.7	<0.05	3.5	10.92	36.6	<0.02	<1	0.7	10.6	<10	<2
8160	1.02	<0.1	0.10	0.10	20.5	0.4	<0.05	2.4	6.08	50.0	0.02	14	1.2	12.8	<10	<2
8161	0.59	<0.1	0.05	0.05	28.0	1.3	<0.05	4.7	6.96	26.0	<0.02	<1	1.3	4.2	<10	<2
8162	1.75	0.2	0.06	0.12	87.5	0.8	<0.05	5.8	10.93	71.0	<0.02	<1	2.7	23.6	12	3
8163	2.36	<0.1	0.08	0.10	59.7	0.9	<0.05	7.1	12.74	92.0	0.06	<1	2.1	19.9	<10	3
8164	0.51	<0.1	0.14	<0.02	6.1	0.3	<0.05	6.2	7.91	15.8	<0.02	<1	1.2	6.2	<10	<2
8165	2.06	0.1	0.21	0.20	59.3	0.5	<0.05	10.5	11.88	86.3	<0.02	<1	2.8	15.1	<10	3
8166	0.95	<0.1	0.17	0.03	13.6	0.4	<0.05	4.2	11.14	34.3	0.04	2	1.7	19.3	<10	<2
8167	1.34	0.1	0.20	0.06	55.6	0.5	<0.05	13.5	10.78	82.8	<0.02	1	2.4	11.5	16	3
8168	1.46	<0.1	0.12	0.16	55.9	0.6	<0.05	7.4	10.58	85.7	<0.02	<1	2.6	19.8	<10	4
8169	1.45	0.2	0.04	0.04	74.4	1.1	<0.05	5.7	10.50	83.5	<0.02	<1	2.6	12.3	<10	4
8170	0.34	<0.1	0.09	0.05	5.3	0.5	<0.05	2.8	11.03	18.9	0.03	4	0.9	3.4	<10	<2
8171	1.43	0.2	0.06	0.04	132.3	0.7	<0.05	3.1	10.14	53.2	0.05	<1	3.3	10.1	12	5
8172	1.07	<0.1	0.15	<0.02	24.1	0.4	<0.05	3.6	6.44	29.8	0.03	1	1.9	14.7	<10	<2
8173	1.89	0.1	0.05	0.03	132.3	0.8	<0.05	2.3	9.18	51.0	0.04	<1	2.4	18.8	<10	2
8174	0.83	<0.1	<0.02	0.03	13.2	0.4	<0.05	1.4	13.31	26.5	<0.02	<1	0.8	9.1	<10	<2
8183	0.37	0.1	0.09	<0.02	9.8	1.0	<0.05	3.7	11.61	24.2	0.04	<1	0.3	9.9	26	3
8184	1.63	0.2	0.07	0.04	141.5	0.8	<0.05	3.0	10.00	54.8	0.03	<1	2.9	10.7	11	3
8185	0.36	0.2	0.15	0.03	9.4	1.0	<0.05	5.3	11.59	24.0	0.02	<1	<0.1	9.9	21	<2
8188	0.41	<0.1	0.21	0.03	11.5	1.2	<0.05	6.6	13.63	27.3	0.03	<1	0.2	11.7	19	<2
8219	1.51	0.2	0.10	0.04	134.3	0.9	<0.05	3.8	9.88	52.3	0.04	<1	2.9	10.4	<10	3
8229	0.32	0.9	0.03	0.61	20.7	1.8	<0.05	3.3	1.95	62.5	0.05	<1	0.2	2.8	<10	2
8230	0.13	0.2	0.22	0.44	2.6	0.7	<0.05	5.1	1.55	47.3	<0.02	<1	<0.1	1.2	<10	<2
8231	0.11	0.4	0.04	0.17	5.9	1.4	<0.05	0.7	0.31	6.0	<0.02	3	<0.1	0.4	<10	<2
8232	0.11	<0.1	0.21	0.58	3.7	0.9	<0.05	11.4	7.95	42.5	<0.02	2	0.2	3.2	<10	<2
8233	0.19	1.3	0.34	0.48	11.6	1.1	<0.05	6.7	1.71	94.8	0.02	3	0.1	0.5	<10	<2
8234	3.32	0.1	0.13	0.21	8.6	0.2	<0.05	4.3	7.34	43.1	<0.02	<1	0.4	11.6	<10	<2
8235	3.18	0.1	0.22	0.02	70.7	0.1	<0.05	8.7	8.60	28.1	<0.02	7	1.0	23.2	<10	<2
8236	1.56	<0.1	0.06	<0.02	24.2	0.2	<0.05	2.6	7.28	70.4	<0.02	1	0.9	18.7	<10	<2
8237	0.09	0.1	0.13	<0.02	2.9	0.2	<0.05	5.0	14.19	73.4	<0.02	<1	0.1	0.5	<10	<2
8238	3.86	0.2	0.17	0.07	61.8	0.5	<0.05	9.3	14.98	57.0	0.04	<1	0.6	32.0	<10	<2
8239	0.17	0.2	0.11	0.03	4.5	0.4	<0.05	8.2	13.32	163.9	<0.02	1	0.3	1.0	<10	<2
8240	3.54	<0.1	0.24	<0.02	64.7	0.1	<0.05	8.8	7.80	32.6	<0.02	5	0.7	24.9	<10	<2
8241	3.14	<0.1	0.18	<0.02	62.6	0.3	<0.05	7.7	7.41	33.6	<0.02	<1	1.0	24.2	<10	<2
8242	0.59	0.2	0.37	0.27	5.5	0.9	<0.05	15.7	6.50	37.9	0.04	<1	0.4	7.8	<10	<2
8243	0.11	0.1	0.15	<0.02	2.9	0.2	<0.05	6.4	12.78	82.5	<0.02	<1	0.1	0.8	<10	<2
8244	6.12	0.3	0.04	0.02	63.6	0.4	<0.05	1.5	15.83	55.1	0.06	<1	1.1	36.3	<10	7
8306	0.56	0.1	0.26	0.03	14.3	1.1	<0.05	9.2	13.20	27.3	0.03	2	0.1	11.2	25	<2
8307	0.45	0.1	0.27	0.04	14.4	1.1	<0.05	9.7	13.02	26.9	0.02	<1	<0.1	10.4	17	<2
8308	0.41	0.1	0.24	0.03	14.9	1.1	<0.05	9.8	13.17	27.4	0.03	1	0.1	11.3	15	<2

Appendix 4E

Element:	Mo	Cu	Pb	Zn	Ag	Ni	Co	Mn	Fe	As	U	Au	Th	Sr	Cd
Method:	1EX	1EX	1EX	1EX	1EX	1EX	1EX	1EX	1EX	1EX	1EX	1EX	1EX	1EX	1EX
Units:	ppm	ppm	ppm	ppm	ppm	ppm	ppm	ppm	%	ppm	ppm	ppm	ppm	ppm	ppm
MDL	0.1	0.1	0.1	1	0.1	0.1	0.2	1	0.01	1	0.1	0.1	0.1	1	0.1
RPD %:	28.1	6.4	11.5	11.1	23.2	6.8	10.8	4.8	2.3	29.4	11.6	<MDL	4.8	4.4	23.9
RPD count:	27	27	27	27	22	27	27	27	27	25	27	27	27	27	23
APR %:	68.8	103.4	97.8	98.2	40.0	100.3	99.8	101.6	92.0	120.0	88.6	<MDL	99.5	97.3	82.1
APR error %:	69.9	6.1	21.9	13.9	0.0	9.3	11.0	5.7	3.5	58.0	34.5		15.6	10.8	29.7
Sample															
8151	8.0	62.0	42.2	93	0.8	108.1	37.4	517	5.76	2	11.7	<0.1	42.0	2081	0.4
8152	49.2	182.0	33.6	92	2.8	102.9	31.8	426	5.09	2	31.2	<0.1	28.5	1551	0.3
8153	9.9	93.2	35.4	88	0.1	102.4	36.6	1215	4.91	2	11.9	<0.1	37.0	1720	0.4
8154	3.3	26.7	19.7	89	<0.1	25.6	10.2	160	2.95	4	3.8	<0.1	11.6	141	0.2
8155	17.8	52.4	30.7	66	<0.1	67.4	23.1	362	5.18	4	12.6	<0.1	24.3	1437	0.4
8156	0.9	85.0	19.8	88	<0.1	419.5	47.7	1167	6.21	<1	2.2	<0.1	6.8	863	0.3
8157	1.8	24.3	18.3	79	<0.1	27.7	9.5	415	3.62	2	2.9	<0.1	10.9	153	0.3
8158	2.8	25.0	18.2	89	0.8	25.3	10.3	186	2.90	<1	3.1	<0.1	11.6	397	0.3
8159	0.5	4.4	9.5	40	<0.1	9.2	6.0	800	1.37	2	1.8	<0.1	7.4	355	0.1
8160	5.5	25.5	22.6	63	<0.1	20.4	8.4	122	2.62	16	5.6	<0.1	11.3	201	0.4
8161	3.3	43.8	402.1	491	0.8	117.6	16.5	3752	3.02	2	0.9	<0.1	2.5	978	1.8
8162	1.1	99.6	25.2	90	<0.1	303.6	46.2	1113	6.44	1	2.7	<0.1	7.9	1206	0.3
8163	2.6	54.3	31.8	92	<0.1	277.9	40.7	1821	5.43	<1	3.4	<0.1	11.7	1577	0.3
8164	1.6	11.7	6.7	38	<0.1	21.9	7.4	1657	2.65	5	1.3	<0.1	2.7	346	0.1
8165	1.1	52.1	29.2	84	2.5	238.5	36.6	1168	5.68	<1	3.3	<0.1	11.5	1530	0.6
8166	1.4	57.1	14.5	96	0.1	49.0	16.4	831	3.81	10	3.2	<0.1	5.7	321	1.1
8167	0.5	68.6	35.2	71	<0.1	116.8	31.7	1007	4.62	<1	2.9	<0.1	9.3	1809	0.3
8168	0.7	72.0	30.9	74	<0.1	127.1	35.4	1065	5.10	<1	2.8	<0.1	9.4	1705	0.2
8169	0.4	48.3	39.9	75	<0.1	110.6	29.4	1060	4.75	<1	2.9	<0.1	9.4	1812	0.1
8170	2.3	6.8	7.0	50	<0.1	17.7	9.5	1463	2.17	7	1.2	<0.1	3.6	421	<0.1
8171	3.3	86.8	22.2	71	<0.1	279.6	49.0	1216	5.21	1	1.8	<0.1	5.2	1244	0.3
8172	1.0	19.6	10.0	86	<0.1	26.1	10.2	293	3.46	4	1.8	<0.1	5.1	295	0.1
8173	0.9	83.4	20.6	78	<0.1	293.7	45.9	1420	4.78	<1	1.7	<0.1	5.0	1096	0.2
8174	2.1	9.7	5.9	43	<0.1	14.7	8.5	1588	3.64	14	1.2	<0.1	2.7	607	0.1
8183	1.5	334.5	18.7	167	0.2	95.9	47.7	1596	9.42	4	1.1	<0.1	2.7	222	0.3
8184	1.7	94.4	23.6	76	0.1	275.3	48.3	1210	5.20	3	1.7	<0.1	5.2	1158	0.3
8185	1.2	331.7	15.5	161	0.2	90.7	45.6	1596	9.56	4	0.9	<0.1	2.5	225	0.3
8188	1.3	335.0	16.8	155	0.2	87.4	44.2	1605	9.42	3	0.9	<0.1	2.5	227	0.3
8219	2.6	81.2	21.8	82	0.2	284.4	43.8	1218	5.06	3	1.9	<0.1	5.2	1151	0.2
8229	1.0	17.6	21.4	3	<0.1	21.7	2.9	16	9.38	2506	5.4	0.2	14.2	1147	<0.1
8230	0.5	11.8	46.2	5	<0.1	18.7	3.1	28	0.48	65	5.4	<0.1	24.9	1230	<0.1
8231	0.7	14.7	19.5	1	<0.1	3.5	0.8	22	6.38	2116	1.4	0.8	1.7	50	<0.1
8232	1.2	225.0	69.6	243	0.6	12.4	13.7	546	2.65	3	2.4	<0.1	6.2	1233	0.9
8233	0.7	39.2	35.2	1	<0.1	11.0	1.8	23	9.75	524	2.7	<0.1	25.2	803	<0.1
8234	2.6	29.5	48.3	65	0.1	18.7	15.7	924	5.32	2	1.4	<0.1	5.1	965	0.2
8235	3.8	21.6	7.0	18	<0.1	40.0	5.0	213	1.25	12	4.8	<0.1	9.4	607	<0.1
8236	0.7	36.9	4.3	18	<0.1	25.4	8.3	69	1.67	12	3.5	<0.1	9.7	90	<0.1
8237	1.1	30.5	3.9	36	<0.1	55.4	10.6	511	2.00	35	2.8	<0.1	8.9	191	0.2
8238	2.1	98.8	5.5	47	0.2	78.3	21.1	755	4.73	15	2.7	0.1	5.8	580	0.1
8239	4.7	22.9	28.4	68	<0.1	53.0	12.9	628	2.00	22	12.5	<0.1	11.9	332	0.2
8240	4.7	25.8	5.8	20	<0.1	37.4	5.2	179	1.34	16	3.9	<0.1	8.4	523	<0.1
8241	3.3	35.0	12.1	24	0.2	28.6	5.2	121	1.16	26	4.5	<0.1	9.2	477	0.1
8242	2.2	26.0	14.8	39	0.1	27.2	34.8	585	4.25	2	2.1	<0.1	5.0	985	0.1
8243	1.1	17.9	4.7	29	<0.1	37.9	4.0	422	1.53	19	3.2	<0.1	10.7	279	0.1
8244	14.1	271.3	3.7	89	<0.1	471.2	280.8	9826	5.99	54	2.8	<0.1	5.2	532	1.6
8306	1.3	336.7	16.8	149	0.2	94.5	48.9	1613	9.81	2	1.0	<0.1	2.7	219	0.3
8307	0.9	344.6	15.5	143	0.2	93.8	46.6	1638	9.65	2	0.7	<0.1	2.7	221	0.4
8308	0.7	333.1	16.5	143	0.2	89.5	46.8	1558	9.50	3	0.9	<0.1	2.8	225	0.4

Appendix 4E

Element:	Sb	Bi	V	Ca	P	La	Cr	Mg	Ba	Ti	Al	Na	K	W	Zr
Method:	1EX	1EX	1EX	1EX	1EX	1EX	1EX	1EX	1EX	1EX	1EX	1EX	1EX	1EX	1EX
Units:	ppm	ppm	ppm	%	%	ppm	ppm	%	ppm	%	%	%	%	ppm	ppm
MDL	0.1	0.1	1	0.01	0.001	0.1	1	0.01	1	0.001	0.01	0.001	0.01	0.1	0.1
RPD %:	6.6	21.5	2.3	10.3	5.0	6.9	5.7	2.0	6.0	3.7	4.5	5.2	10.1	21.4	4.5
RPD count:	26	12	27	27	27	27	27	27	27	27	27	27	27	27	27
APR %:	75.7	<MDL	103.7	102.3	124.3	98.4	80.4	97.1	98.3	110.4	102.1	99.2	97.8	52.4	94.8
APR error %:	42.4		11.1	12.4	25.7	13.3	8.1	6.4	7.6	14.8	10.4	7.2	11.6	43.9	14.6
Sample															
8151	0.1	0.2	168	1.81	0.689	107.1	395	3.38	5292	0.881	6.22	1.154	6.25	1.6	451.4
8152	0.2	0.1	110	5.62	0.624	84.0	281	2.61	53	0.847	5.40	0.817	6.83	2.3	224.4
8153	0.3	0.1	150	8.68	0.627	93.2	325	2.76	358	0.818	5.21	0.649	5.62	2.1	446.6
8154	0.6	0.5	86	0.59	0.058	42.4	42	1.00	705	0.293	7.80	0.837	2.49	2.0	75.5
8155	0.4	<0.1	112	5.06	0.507	49.2	236	2.13	45	0.803	5.45	0.591	6.63	3.6	384.8
8156	<0.1	<0.1	173	4.93	0.410	35.1	606	7.63	3238	0.605	4.78	1.078	3.69	0.2	212.3
8157	0.5	0.2	95	0.76	0.053	33.4	42	1.90	789	0.304	8.11	0.928	3.03	2.3	51.8
8158	0.5	0.3	87	1.34	0.041	35.2	41	1.06	806	0.262	8.18	1.119	2.80	2.2	79.9
8159	0.5	<0.1	36	5.64	0.047	26.7	17	1.78	620	0.189	5.44	1.400	2.25	1.2	41.5
8160	2.4	0.4	82	0.66	0.025	31.3	42	1.13	695	0.266	7.68	0.798	2.39	2.7	113.1
8161	0.5	0.1	66	24.04	0.160	16.5	165	3.24	1079	0.205	1.60	0.218	1.50	0.7	69.2
8162	0.6	0.1	176	5.29	0.511	41.2	480	6.25	4017	0.622	4.96	1.084	4.10	0.3	229.7
8163	0.1	<0.1	163	6.24	0.458	51.3	535	3.75	4162	0.698	5.19	1.122	3.76	0.7	351.2
8164	0.3	<0.1	52	17.96	0.061	13.1	34	0.85	626	0.187	4.08	1.146	0.89	0.8	39.9
8165	0.4	0.1	155	4.47	0.444	49.7	562	5.54	4074	0.664	5.15	1.315	3.74	0.7	343.5
8166	1.2	0.2	113	2.09	0.065	22.3	74	1.24	754	0.355	7.37	1.624	1.44	1.6	95.5
8167	<0.1	<0.1	126	5.75	0.444	48.9	347	4.80	4606	0.544	5.09	1.591	4.36	0.3	283.6
8168	<0.1	<0.1	147	5.18	0.493	49.2	346	4.85	4719	0.588	4.89	1.382	4.52	0.3	280.7
8169	0.2	<0.1	133	5.33	0.467	50.4	336	4.95	4727	0.565	4.75	1.391	4.15	0.3	284.9
8170	0.3	<0.1	64	15.89	0.122	14.9	31	0.37	677	0.198	4.58	1.348	1.05	0.7	39.6
8171	0.1	<0.1	169	7.03	0.463	29.6	834	5.46	4296	0.660	5.69	0.707	4.30	1.1	184.6
8172	0.4	0.1	119	1.80	0.059	20.5	63	1.18	747	0.318	7.01	1.632	1.52	1.3	56.1
8173	<0.1	<0.1	162	7.90	0.428	26.3	852	5.49	4029	0.657	5.46	0.546	3.85	0.3	165.9
8174	0.4	<0.1	59	21.47	0.177	19.7	33	0.92	814	0.166	3.43	0.878	0.84	0.6	44.1
8183	0.7	<0.1	463	6.67	0.100	17.1	199	3.42	243	1.482	7.02	1.746	0.80	0.3	146.9
8184	0.1	0.1	165	6.40	0.444	28.1	860	5.78	4192	0.642	5.79	0.764	6.56	0.8	179.4
8185	0.8	<0.1	459	6.61	0.093	15.7	204	3.39	225	1.451	6.71	1.647	0.75	0.4	137.2
8188	0.8	<0.1	467	6.65	0.099	16.8	189	3.46	236	1.401	6.97	1.667	0.78	0.2	152.8
8219	0.1	<0.1	165	6.64	0.505	29.6	876	5.52	4082	0.651	6.60	0.835	6.63	0.9	182.5
8229	24.2	<0.1	113	0.06	0.479	67.9	386	0.01	49	0.586	3.10	0.358	4.50	>200	40.6
8230	4.5	<0.1	51	0.14	0.063	57.0	217	0.05	3750	0.957	4.69	1.105	3.43	>200	219.2
8231	45.5	0.1	44	<0.01	0.027	6.2	78	<0.01	103	0.117	1.01	0.038	2.45	184.4	5.1
8232	0.5	0.2	95	3.25	0.170	29.5	18	0.94	229	0.363	7.89	2.181	4.70	1.0	157.1
8233	4.0	<0.1	59	0.05	0.215	62.1	421	0.02	49	0.650	3.08	0.327	3.14	>200	169.3
8234	0.2	<0.1	139	3.57	0.248	27.3	21	1.51	2644	0.436	8.02	3.684	2.85	8.0	75.6
8235	0.4	0.2	211	2.12	0.097	26.1	59	0.91	1480	0.377	8.30	2.054	2.81	2.8	81.8
8236	0.5	0.2	233	0.17	0.098	30.4	80	0.62	884	0.368	6.85	0.434	2.76	1.1	59.9
8237	1.0	0.2	203	0.23	0.096	36.8	70	0.05	1923	0.340	7.58	3.365	4.33	8.5	76.4
8238	0.8	0.8	203	2.11	0.289	33.1	132	1.87	2390	0.448	7.73	2.442	4.26	13.3	81.6
8239	2.7	0.2	171	0.21	0.107	86.8	68	0.04	4033	0.361	7.33	0.739	5.18	57.8	83.9
8240	0.3	0.3	212	1.55	0.096	22.4	64	0.85	1429	0.393	7.80	1.959	3.02	4.7	75.8
8241	0.3	0.3	226	1.35	0.105	24.4	71	0.88	1774	0.379	7.74	1.595	3.26	2.4	82.3
8242	0.5	2.0	148	3.68	0.252	24.3	60	1.72	153	0.429	7.78	2.897	4.01	4.4	133.6
8243	0.6	<0.1	186	0.27	0.095	39.9	69	0.06	2466	0.376	7.46	3.443	3.81	9.0	80.1
8244	1.4	0.6	196	1.98	0.333	38.3	147	2.33	4156	0.442	7.26	2.869	3.43	29.0	95.2
8306	0.7	<0.1	513	7.19	0.102	16.7	206	3.40	239	1.631	7.56	1.707	0.74	0.4	149.0
8307	0.8	<0.1	518	6.85	0.101	17.3	204	3.36	235	1.658	7.51	1.662	0.73	0.3	147.6
8308	0.7	<0.1	498	7.25	0.101	16.6	202	3.32	236	1.601	7.37	1.670	0.73	0.3	150.4

Appendix 4E

Element:	Ce	Sn	Y	Nb	Ta	Be	Sc	Li	S	Rb	Hf
Method:	1EX	1EX	1EX	1EX	1EX	1EX	1EX	1EX	1EX	1EX	1EX
Units:	ppm	ppm	ppm	ppm	ppm	ppm	ppm	ppm	%	ppm	ppm
MDL	1	0.1	0.1	0.1	0.1	1	1	0.1	0.1	0.1	0.1
RPD %:	6.0	23.2	4.0	5.8	7.5	23.6	1.9	13.1	0.0	9.6	4.4
RPD count:	27	27	27	27	27	20	27	27	7	27	27
APR %:	92.3	104.3	91.0	120.4	83.9	<MDL	107.1	110.9	<MDL	93.0	82.0
APR error %:	10.9	51.6	14.4	9.0	28.9		11.4	33.3		14.8	12.5
Sample											
8151	234	3.1	18.4	23.6	0.8	4	18	21.4	0.3	355.7	13.7
8152	237	2.9	21.7	22.3	0.7	3	8	11.0	3.4	324.8	6.8
8153	221	2.8	20.7	22.8	0.8	4	20	12.2	0.5	278.7	12.1
8154	82	3.0	22.6	14.9	0.8	4	10	26.8	<0.1	126.1	2.2
8155	120	2.3	10.8	22.3	0.7	4	14	14.5	3.7	270.7	10.3
8156	73	1.3	14.1	10.7	0.4	4	21	19.3	<0.1	137.2	5.4
8157	65	3.0	15.9	13.8	0.8	3	10	23.5	<0.1	163.5	1.6
8158	70	2.4	17.5	12.9	0.8	2	10	87.8	<0.1	156.9	2.4
8159	52	1.6	15.1	8.3	0.5	1	6	16.2	<0.1	77.3	1.4
8160	62	2.6	15.3	13.8	0.7	4	11	22.7	<0.1	148.6	3.0
8161	31	0.9	9.6	3.8	0.1	2	9	3.7	<0.1	56.4	1.9
8162	86	1.9	16.0	11.7	0.5	3	23	26.5	<0.1	172.3	6.0
8163	101	2.2	17.6	17.8	0.7	4	19	19.3	<0.1	172.3	9.0
8164	25	0.8	11.7	5.1	0.2	2	7	9.7	<0.1	28.8	1.0
8165	98	2.3	18.1	17.6	0.6	4	19	18.8	<0.1	178.7	8.6
8166	42	1.2	17.7	9.2	0.4	3	14	27.4	<0.1	65.1	2.2
8167	96	1.9	15.8	14.6	0.5	4	19	15.0	<0.1	172.7	7.0
8168	101	1.7	16.6	13.6	0.5	4	21	30.9	<0.1	162.0	6.6
8169	99	1.7	15.9	13.7	0.5	5	19	17.6	<0.1	172.4	7.1
8170	27	0.6	13.8	5.0	0.3	<1	7	9.6	0.2	31.4	1.1
8171	60	1.7	12.7	10.9	0.3	3	21	9.5	<0.1	196.8	4.5
8172	39	1.2	12.1	8.5	0.5	2	11	25.4	<0.1	68.6	1.6
8173	54	1.3	12.8	10.1	0.4	3	20	21.0	<0.1	204.5	4.3
8174	33	0.5	16.9	4.6	0.2	1	7	13.6	0.1	32.1	0.9
8183	38	2.2	32.4	13.8	0.7	<1	38	14.4	<0.1	22.9	4.2
8184	59	1.2	12.7	10.6	0.4	4	20	13.5	<0.1	193.3	4.7
8185	36	1.8	29.9	12.5	0.7	<1	37	16.2	<0.1	20.7	3.8
8188	38	2.1	32.2	13.3	0.7	<1	37	16.8	<0.1	21.5	4.0
8219	59	1.7	13.0	10.8	0.4	3	20	12.9	<0.1	247.6	4.6
8229	107	2.1	4.9	91.1	1.8	4	9	38.9	3.7	100.8	2.1
8230	95	1.4	6.5	109.8	3.5	4	3	32.2	0.2	94.5	8.9
8231	8	1.6	0.7	18.9	0.2	<1	<1	106.3	2.8	42.4	0.4
8232	67	2.2	15.9	17.1	0.6	2	9	8.8	1.3	89.9	4.1
8233	123	2.1	5.2	70.3	2.1	2	2	31.7	4.0	62.2	7.5
8234	57	0.9	15.0	9.6	0.4	3	13	18.4	<0.1	57.9	2.1
8235	50	0.4	15.2	13.4	0.7	2	13	32.7	<0.1	101.0	2.3
8236	57	1.4	14.4	14.4	0.7	2	12	30.0	<0.1	134.1	1.6
8237	66	1.7	17.4	15.5	0.8	<1	15	2.2	<0.1	111.8	2.1
8238	62	2.1	17.9	9.7	0.4	2	20	43.0	<0.1	115.5	2.2
8239	159	2.0	17.6	13.8	0.7	1	11	3.5	<0.1	126.8	2.2
8240	42	0.5	14.1	14.4	0.7	2	13	38.1	<0.1	105.4	2.1
8241	46	0.5	14.1	13.9	0.7	2	13	36.6	<0.1	114.2	2.2
8242	57	3.2	14.5	10.4	0.4	3	15	13.4	1.8	64.1	3.4
8243	77	1.8	16.5	16.7	0.8	<1	14	3.4	<0.1	102.8	2.1
8244	70	1.9	21.9	8.8	0.3	3	18	48.1	<0.1	108.4	2.4
8306	39	2.1	33.4	12.4	0.7	1	41	18.9	<0.1	19.7	4.2
8307	38	2.1	33.0	13.6	0.7	<1	39	18.7	<0.1	23.1	4.2
8308	38	2.1	34.0	13.2	0.6	1	40	15.6	<0.1	20.3	4.2

Appendix 4F

Element: Method: Units MDL: RPD %: RPD count: APR %: APR error %:	Sb Wgt grams 0.1 14.5 18 81.7 51.6	As INAA ppm 0.5 27.6 21 104.0 82.7	Ba INAA ppm 50 15.2 21 95.4 46.3	Br INAA ppm 0.5 33.7 15 135.0 40.0	Ca INAA % 1 5.9 15 107.8 15.9	Ce INAA ppm 3 3.3 21 97.2 10.5	Cs INAA ppm 1 9.6 13 NA	Cr INAA ppm 5 2.7 21 100.9 6.6	Co INAA ppm 1 9.2 21 97.2 9.2	Eu INAA ppm 0.2 10.5 21 88.1 19.6	Au INAA ppb 2 13.3 3 166.7 36.6	Hf INAA ppm 1 6.6 21 100.0 10.0	Ir INAA ppb 5 <MDL 21 <MDL	Fe INAA % 0.01 2.2 21 101.1 4.7	La INAA ppm 0.5 2.0 21 101.0 12.7	Lu INAA ppm 0.05 3.8 21 99.4 13.8	Hg INAA ppm 1 44.4 3 NA	
Sample																		
8151	18.21	0.2	2.5	5970	<0.5	2	250	2	561	42	3.7	<2	16	<5	6.15	121	0.28	<1
8152	14.95	0.2	2.4	4700	0.6	6	300	1	480	30	4.0	<2	8	<5	5.38	122	0.25	<1
8153	15.57	0.4	2.0	5000	<0.5	9	240	2	470	38	3.3	<2	14	<5	5.38	107	0.24	<1
8154	8.96	0.6	3.7	720	<0.5	<1	89	10	57	8	1.3	<2	6	<5	2.93	44	0.53	<1
8155	15.93	0.3	3.8	4700	<0.5	5	160	2	390	23	2.1	<2	11	<5	5.41	75.6	0.15	<1
8156	17.47	<0.1	0.7	3300	<0.5	5	78	3	883	49	1.8	<2	6	<5	6.42	38	0.18	<1
8157	17.37	0.6	3.8	810	<0.5	1	67	9	56	8	0.9	3	5	<5	3.62	34	0.47	<1
8158	15.36	0.4	1.0	880	<0.5	1	75	8	55	8	1.2	<2	6	<5	2.95	38	0.42	<1
8159	16.45	0.3	2.7	640	<0.5	6	55	3	29	4	0.8	<2	5	<5	1.39	27	0.35	<1
8160	15.05	2.4	15.0	680	3.2	<1	61	10	45	7	0.8	<2	5	<5	2.47	30	0.43	<1
8161	17.21	0.5	3.2	1100	<0.5	22	32	<1	280	17	1.0	3	2	<5	3.16	16	0.11	<1
8162	17.64	0.1	1.3	3700	<0.5	5	86	3	650	47	2.2	<2	7	<5	6.76	42	0.20	<1
8163	17.23	0.2	0.9	4100	<0.5	6	110	3	756	41	2.3	<2	10	<5	5.74	54.4	0.25	<1
8164	18.65	0.3	5.8	690	<0.5	16	24	1	52	7	0.5	<2	2	<5	2.75	13	0.22	<1
8165	16.67	<0.1	1.1	3800	<0.5	5	110	3	732	37	2.2	<2	9	<5	5.79	52.1	0.24	<1
8166	15.40	1.3	12.0	800	0.6	2	48	3	91	17	1.1	4	4	<5	3.83	24	0.36	<1
8167	17.83	<0.1	0.9	4400	0.6	6	100	2	470	29	2.1	<2	8	<5	4.85	50.4	0.19	<1
8168	16.50	0.2	1.9	4800	1.1	5	110	3	490	35	2.5	<2	8	<5	5.45	54.8	0.22	<1
8169	18.15	0.2	1.2	4700	0.7	5	110	3	490	32	2.3	<2	8	<5	5.06	53.3	0.19	<1
8170	15.45	0.4	11.0	730	<0.5	14	30	1	55	8	0.6	<2	3	<5	2.23	15	0.29	<1
8171	15.20	0.2	3.2	4000	<0.5	6	64	3	1180	47	1.5	<2	5	<5	5.50	29	0.19	<1
8172	15.44	0.4	5.4	850	<0.5	2	43	3	90	9	0.7	<2	5	<5	3.54	22	0.32	<1
8173	16.94	<0.1	<0.5	3800	<0.5	7	55	3	1210	44	1.4	<2	4	<5	4.89	27	0.14	<1
8174	15.04	0.5	21.0	820	0.5	20	36	<1	56	6	0.7	<2	3	<5	4.07	20	0.27	<1
8183	16.84	0.7	1.1	200	2.5	7	40	<1	250	46	1.9	<2	5	<5	10.70	17.0	0.54	<1
8184	15.44	<0.1	2.5	3900	<0.5	6	60	2	1170	47	1.7	<2	5	<5	5.58	29	0.16	<1
8185	14.85	0.9	3.0	190	2.3	8	41	1	260	47	1.9	12	5	<5	10.80	18.0	0.54	<1
8188	15.32	0.9	4.1	280	2.6	8	39	1	260	46	2.0	8	5	<5	10.60	17.0	0.51	<1
8219	15.19	<0.1	3.0	4000	<0.5	7	60	2	1160	47	1.5	<2	4	<5	5.37	29	0.17	<1
8229	15.11	24.7	2500.0	2600	<0.5	1	130	2	580	2	0.7	235	1	<13	9.53	90.3	0.06	<1
8230	15.21	4.0	65.1	4000	<0.5	<1	100	2	530	3	1.0	71	9	<5	0.49	63.1	0.13	<1
8231	14.78	44.2	2110.0	240	<0.5	<1	9	<1	88	<1	<0.2	959	<1	<5	6.23	6.4	<0.05	<1
8232	14.82	0.5	4.7	4600	2.0	4	100	<1	26	14	2.2	15	6	<5	2.79	44	0.31	<1
8233	15.52	3.9	502.0	2400	<0.5	<1	140	<1	666	2	1.0	27	11	<5	9.59	77.8	0.18	<1
8234	16.52	0.5	3.2	3000	1.0	4	74	5	30	14	1.8	14	4	<5	5.69	37	0.28	<1
8235	15.66	0.4	8.1	1800	1.0	2	71	5	110	4	1.1	10	5	<5	1.35	38	0.42	<1
8236	18.90	0.6	11.0	1000	<0.5	<1	79	5	120	7	1.4	<2	6	<5	1.67	43	0.48	<1
8237	14.75	1.0	35.0	2200	0.7	<1	86	1	110	8	1.2	20	5	<5	1.97	48	0.44	<1
8238	10.76	0.9	17.0	2700	<0.5	2	78	5	180	18	1.4	12	5	<5	4.92	44	0.30	<1
8239	15.58	2.7	22.0	4300	<0.5	<1	210	2	120	11	2.5	6	5	<5	2.11	113	0.39	<1
8240	20.14	0.3	17.0	1600	<0.5	1	56	6	100	4	0.9	18	5	<5	1.41	30	0.37	<1
8241	15.52	0.3	26.0	2200	<0.5	2	61	6	110	4	0.9	8	5	<5	1.23	33	0.41	<1
8242	17.09	0.6	3.8	5000	<0.5	4	76	<1	81	35	2.3	26	4	<5	4.44	35	0.22	<1
8243	14.88	0.8	20.0	3000	0.9	<1	99	<1	110	3	1.6	10	4	<5	1.59	51	0.41	<1
8244	15.68	1.5	53.6	4300	<0.5	2	88	7	230	287	2.0	16	5	<5	6.15	48	0.28	<1
8306	14.83	0.9	1.9	160	3.5	7	39	<1	250	45	1.9	<5	5	<5	10.40	17.0	0.51	<1
8307	14.71	0.6	2.4	280	2.1	7	40	<1	250	45	1.5	11	5	<5	10.20	17.0	0.51	<1
8308	16.82	0.9	3.1	270	3.2	7	40	<1	250	45	1.9	11	5	<5	10.40	17.0	0.49	<1

Appendix 4F

Element: Method: Units MDL: RPD %: RPD count: APR %: APR error %:	Mo INAA ppm 1 6.2 3 <MDL	Nd INAA ppm 5 11.0 21 98.6 35.0	Ni INAA ppm 100 20.4 6 <MDL	Rb INAA ppm 15 20.4 21 106.5 53.6	Sm INAA ppm 0.1 2.2 21 103.9 3.7	Sc INAA ppm 0.1 1.8 21 107.1 9.1	Se INAA ppm 3 <MDL 21 <MDL	Ag INAA ppm 5 <MDL 21 <MDL	Na INAA % 0.01 2.3 21 98.3 7.4	Sr INAA ppm 500 7.9 3 <MDL	Ta INAA ppm 0.5 33.1 14 120.0 40.3	Tb INAA ppm 0.5 15.5 15 95.0 30.5	Th INAA ppm 0.2 5.8 21 106.8 17.5	Sn INAA ppm 100 <MDL 21 <MDL	W INAA ppm 1 38.9 9 <MDL	U INAA ppm 0.5 16.4 19 106.7 54.8	Yb INAA ppm 0.2 3.6 21 97.1 15.5	Zn INAA ppm 50 16.7 21 120.4 17.6
Sample																		
8151	9	110	<100	390	16.8	18.6	<3	<5	1.19	1700	1.3	0.8	49.0	<100	3	13.0	1.6	120
8152	59	130	<100	340	19.8	8.3	<3	<5	0.84	1300	1.6	1.3	39.3	<100	3	34.0	1.4	100
8153	9	110	<100	320	16.8	21.0	<3	<5	0.66	1400	1.3	0.8	42.4	<100	3	13.0	1.5	99
8154	<4	39	<100	120	7.5	10.9	<3	<5	0.81	<500	1.2	0.9	13.0	<100	3	4.9	3.2	77
8155	18	67	<100	280	10.0	14.5	<3	<5	0.59	1300	0.9	0.9	36.3	<100	3	13.0	0.8	64
8156	<4	38	370	120	7.4	21.9	<3	<5	1.12	550	<0.5	<0.5	7.4	<100	<1	2.2	1.2	66
8157	<3	30	<100	150	5.8	11.4	<3	<5	0.86	<500	1.1	0.6	12.0	<100	3	4.1	2.9	93
8158	<3	30	<100	150	6.2	11.0	<3	<5	1.09	<500	1.1	0.6	13.0	<100	3	4.5	2.6	84
8159	<3	25	<100	74	4.6	5.8	<3	<5	1.33	<500	<0.5	0.7	7.8	<100	2	2.6	2.0	73
8160	8	25	<100	130	4.9	10.4	<3	<5	0.68	<500	1.0	<0.5	12.0	<100	3	5.7	2.4	51
8161	<1	16	<100	54	3.3	9.1	<3	<5	0.22	700	<0.5	<0.5	2.4	<100	<1	0.7	0.6	480
8162	<2	41	290	160	8.4	23.3	<3	<5	1.08	930	0.7	<0.5	8.5	<100	<1	3.1	1.4	100
8163	<4	52	250	190	10.0	19.4	<3	<5	1.16	1300	0.7	0.6	13.0	<100	<1	3.6	1.6	100
8164	<2	10	<100	27	2.3	6.9	<3	<5	1.09	<500	0.7	<0.5	2.9	<100	1	1.2	1.3	<50
8165	<4	50	170	170	10.0	19.2	<3	<5	1.31	1100	1.3	0.6	13.0	<100	2	3.3	1.5	99
8166	<3	23	<100	47	4.9	13.7	<3	<5	1.55	<500	<0.5	0.6	6.4	<100	<1	3.6	2.2	120
8167	<4	47	<100	160	9.1	19.0	<3	<5	1.60	1400	1.2	0.9	10.0	<100	<1	2.7	1.3	110
8168	<4	51	<100	150	10.0	21.8	<3	<5	1.44	1400	1.0	0.6	11.0	<100	<1	2.5	1.3	74
8169	<4	50	<100	170	10.0	19.7	<3	<5	1.45	1400	0.6	0.9	10.0	<100	<1	2.4	1.3	100
8170	3	12	<100	31	2.8	7.7	<3	<5	1.25	<500	<0.5	<0.5	3.7	<100	1	1.5	1.6	65
8171	<4	28	150	260	6.1	20.8	<3	<5	0.74	980	<0.5	<0.5	6.0	<100	2	2.0	1.1	81
8172	<4	21	<100	66	3.9	11.8	<3	<5	1.56	<500	1.0	0.6	6.0	<100	2	2.3	1.8	110
8173	4	28	140	250	5.6	20.1	<3	<5	0.53	860	<0.5	<0.5	5.1	<100	<1	1.5	1.1	87
8174	<3	13	<100	30	3.3	7.8	<3	<5	0.89	<500	0.9	0.6	3.3	<100	<1	1.6	1.7	<50
8183	<3	23	<100	22	6.2	39.0	<3	<5	1.70	<500	0.8	1.2	2.9	<100	2	1.3	3.4	190
8184	5	32	190	250	5.9	20.5	<3	<5	0.77	920	<0.5	0.7	5.6	<100	1	1.5	1.1	78
8185	<3	24	<100	17	6.3	39.6	<3	<5	1.73	<500	<0.5	1.1	3.0	<100	<1	1.5	3.3	210
8188	<3	18	<100	32	6.2	38.7	<3	<5	1.67	<500	0.9	<0.5	2.5	<100	2	1.0	3.5	170
8219	<3	27	280	240	5.9	20.0	<3	<5	0.74	870	0.7	0.5	5.8	<100	4	2.2	1.0	83
8229	<5	30	<100	110	4.0	9.5	<3	<5	0.37	670	1.2	<0.5	20.6	<360	320	4.3	<0.2	<50
8230	<5	32	<100	140	3.8	3.1	<3	<5	1.04	600	4.3	<0.5	25.7	<100	264	4.3	0.5	<50
8231	<3	<5	<100	35	0.3	0.3	<3	<5	0.04	<500	<0.5	<0.5	1.7	<270	171	1.7	<0.2	<50
8232	<4	41	<100	140	7.8	10.3	<3	<5	2.18	<500	1.2	0.8	9.1	<100	<1	3.0	1.7	270
8233	<3	47	<100	110	6.0	1.9	<3	<5	0.33	<500	2.2	0.6	31.2	<100	432	2.6	0.4	<50
8234	<5	33	<100	78	7.1	15.5	<3	<5	3.72	<500	1.2	<0.5	7.3	<100	10	1.8	1.7	100
8235	<5	33	<100	110	5.8	14.9	<3	<5	2.06	<500	0.6	0.6	13.0	<100	4	6.3	2.5	78
8236	<3	29	<100	150	6.4	14.9	<3	<5	0.40	<500	1.0	0.9	13.0	<100	2	5.0	2.6	<50
8237	<5	32	<100	150	6.2	17.8	<3	<5	3.32	<500	<0.5	1.0	11.0	<100	11	4.3	2.5	72
8238	<5	33	<100	160	7.1	21.6	<3	<5	2.39	<500	<0.5	0.9	8.3	<100	15	4.2	1.9	82
8239	<7	72	<100	220	10.4	13.3	<3	<5	0.75	<500	1.5	1.0	14.0	<100	74	15.0	2.2	97
8240	5	25	<100	130	4.7	14.0	<3	<5	1.87	<500	1.0	0.5	11.0	<100	6	5.1	2.2	66
8241	<5	29	<100	150	5.1	14.4	<3	<5	1.50	<500	0.9	0.6	12.0	<100	4	6.1	2.2	<50
8242	<5	31	<100	100	7.3	15.4	<3	<5	2.80	<500	<0.5	0.7	7.3	<100	5	3.5	1.6	64
8243	<3	35	<100	140	6.3	17.4	<3	<5	3.49	<500	1.6	0.8	13.0	<100	11	2.8	2.3	100
8244	15	40	350	150	8.7	19.2	<3	<5	2.82	<500	1.2	1.2	7.2	<200	32	4.3	1.7	110
8306	<3	23	<100	21	6.2	38.2	<3	<5	1.64	<500	1.0	1.0	3.0	<100	3	1.0	3.3	170
8307	<3	19	<100	22	6.2	37.6	<3	<5	1.63	<500	1.2	1.0	2.9	<200	<1	0.7	3.0	190
8308	<3	29	<100	33	6.3	38.2	<3	<5	1.66	<500	0.9	1.4	3.0	<200	<1	0.9	3.3	190

Appendix 5 – Quantitative Mineralogical Analytical Techniques

Identification of mineral phases and their relative proportions in rock samples was carried out using quantitative Rietveld X-ray diffraction (XRD) and mineral-liberation analyses (MLA) at Activation Laboratories Ltd. (Actlabs) in Ancaster, Ontario. For the quantitative mineralogical analyses, the rock samples were crushed so as to nominally pass 2 mm size. For each sample, 50 g of crushed material were pulverized for the XRD analysis and an additional 50–100 g were stage-crushed to pass 0.85 mm, and a 30 mm diameter polished section was prepared for the MLA.

The Actlabs MLA is a quantitative mineralogical technology based on an FEI Quanta600F scanning electron microscope (SEM). The method involves a combined image analysis employing atomic-number-contrast imaging from back-scattered electron (BSE)–signal intensity and energy-dispersive spectrometry (EDS) using two Bruker 5010 SDD detectors. The MLA directly identifies mineral phases and quantifies their relative proportions in polished sections using both X-ray BSE particle analysis and modal analysis by linear-intercept measurements, where points are spaced close together in the X-scanning direction, and scan lines are typically set farther apart. Chemical compositions of each mineral were assigned and assays calculated by the MLA based on comparisons of semiquantitative EDS and literature data. The identified minerals and their proportions were verified by quantitative Rietveld XRD analysis.

For the quantitative XRD analyses, portions of pulverized samples were mixed with 10 wt. % corundum and packed into standard holders. Corundum was used as an internal standard to determine the X-ray amorphous content of the samples. The quantities of the crystalline mineral phases were determined using the Rietveld method. This is based on the calculation of the full diffraction pattern from crystal structure information. The XRD analyses were performed on a Panalytical X'Pert Pro diffractometer equipped with a Cu X-ray source and operating at the following conditions: 40 kV voltage, 40 mA current, 4–80° 2 θ range, 0.02° 2 θ step, 2 seconds/step, 1° fixed-angle divergence slit, 0.2 mm receiving slit and one revolution/second sample rotation. Some mineral phases identified by the MLA but not detected by the XRD (e.g., some clays) are likely to be X-ray amorphous or poorly crystalline.

Appendix 6 – Quantitative Mineralogical Data

Rietveld X-Ray Diffraction Data

Mineral	8151	8152	8156	8162	8165	8171	8229	8231	8232	8239	8243	8244
Quartz	n.d.	n.d.	1.5	n.d.	n.d.	n.d.	20.9	50.2	n.d.	4.2	3.8	1.9
Sanidine	44.5	39.5	14.5	21.6	32.8	23.0	n.d.	n.d.	43.0	n.d.	n.d.	n.d.
Microcline/Orthoclase	n.d.	13.3	n.d.	n.d.	n.d.	n.d.	17.6	3.4	n.d.	63.3	35.0	22.2
Albite	n.d.	n.d.	n.d.	3.0	n.d.	n.d.	n.d.	n.d.	13.5	3.8	31.3	25.7
Augite	n.d.	n.d.	25.2	25.8	23.8	11.2	n.d.	n.d.	13.5	n.d.	n.d.	n.d.
Hornblende	n.d.	n.d.	n.d.	n.d.	n.d.	n.d.	n.d.	n.d.	n.d.	n.d.	n.d.	8.0
Phlogopite/Biotite	20.8	18.0	17.3	15.5	14.7	32.7	n.d.	n.d.	n.d.	n.d.	n.d.	0.9
Apatite	3.6	5.4	3.6	2.2	3.0	2.1	n.d.	n.d.	n.d.	n.d.	n.d.	n.d.
Calcite	n.d.	n.d.	n.d.	n.d.	n.d.	12.0	n.d.	n.d.	n.d.	n.d.	n.d.	n.d.
Jarosite	n.d.	0.1	n.d.	n.d.	n.d.	n.d.	15.9	10.0	n.d.	n.d.	n.d.	n.d.
Gypsum	n.d.	5.1	n.d.	n.d.	n.d.	n.d.	n.d.	n.d.	n.d.	n.d.	n.d.	n.d.
Pyrite	n.d.	n.d.	n.d.	n.d.	n.d.	n.d.	n.d.	n.d.	1.3	n.d.	n.d.	n.d.
X-ray amorphous	31.1	18.5	37.8	32.0	25.6	19.1	45.6	36.4	28.8	28.7	29.8	41.4
Total	100.0	99.9	100.0	100.1	99.9	100.1	100.0	100.0	100.1	100.0	99.9	100.1

Abbreviations: n.d., not determined. Mineral abundances are in wt %. The X-ray amorphous content includes poorly crystalline phases. Sample 8156 contains smectite (included in the X-ray amorphous content).

Mineral Liberation Data

Sample Number	8151	8152	8156	8162	8165	8171	8229	8231	8232	8239	8243	8244
Quartz	0.2	0.2	0.1	0.2	<0.1	<0.1	25.9	70.0	0.3	3.4	3.2	1.7
Amorphous silica	3.2	1.4	1.4	5.3	3.1	3.8	21.9	12.6	1.8	3.7	3.8	8.4
Potassium feldspar	47.2	39.8	10.1	11.5	32.4	23.4	15.3	3.2	57.2	73.5	33.7	27.0
Altered potassium feldspar	5.2	4.4	5.9	5.3	3.9	3.3	7.8	0.6	2.2	3.1	1.4	1.2
Plagioclase	<0.1	<0.1	0.1	3.9	n.d.	0.1	n.d.	n.d.	12.6	n.d.	n.d.	0.4
Albite	0.2	0.2	2.2	0.2	0.1	0.6	<0.1	<0.1	5.5	4.5	38.5	19.1
Augite	<0.1	<0.1	26.7	21.8	20.6	8.2	n.d.	n.d.	10.7	n.d.	n.d.	0.1
Amphibole	n.d.	9.4										
Phlogopite	18.8	16.9	15.2	17.7	10.1	31.6	n.d.	n.d.	0.3	n.d.	n.d.	5.0
Biotite	8.5	7.2	6.4	3.9	6.3	4.3	<0.1	<0.1	0.1	0.5	0.1	2.1
Clinozoisite	<0.1	<0.1	<0.1	2.2	<0.1	0.7	n.d.	n.d.	0.2	n.d.	n.d.	<0.1
Illite	n.d.	n.d.	n.d.	n.d.	n.d.	n.d.	0.4	<0.1	n.d.	0.9	1.7	n.d.
Chlorite	0.3	0.3	0.9	0.5	0.7	0.1	<0.1	<0.1	0.0	0.8	0.7	0.5
Fe-chlorite	0.4	0.3	1.8	2.6	0.8	1.0	n.d.	n.d.	0.7	n.d.	n.d.	8.8
Poorly crystalline illite-smectite clay	4.4	4.7	7.6	14.0	7.5	6.5	7.2	0.8	3.2	6.1	14.6	8.3
Saponite	0.2	0.03	9.4	1.1	1.5	n.d.						
Poorly crystalline Mg-Fe-clay	<0.1	0.1	8.0	6.2	7.3	1.5	n.d.	n.d.	0.4	n.d.	n.d.	0.9
Titanomagnetite	0.1	0.1	1.5	0.2	1.2	1.2	n.d.	n.d.	<0.1	n.d.	n.d.	<0.1
Ilmenite/Leucosene	0.4	0.8	n.d.	<0.1	<0.1	0.1	n.d.	n.d.	<0.1	n.d.	n.d.	0.3
Hematite	0.3	0.2	0.1	<0.1	<0.1	0.1	n.d.	n.d.	1.2	n.d.	n.d.	<0.1
Rutile	0.2	0.2	n.d.	n.d.	n.d.	n.d.	0.5	<0.1	0.1	0.7	0.7	0.2
Mn-oxides	n.d.	n.d.	n.d.	<0.1	<0.1	<0.1	n.d.	n.d.	<0.1	n.d.	n.d.	3.7
Goethite	1.2	2.1	0.2	<0.1	<0.1	0.5	<0.1	<0.1	0.1	2.3	1.1	0.7
Jarosite	0.5	1.5	n.d.	<0.1	<0.1	0.1	13.2	7.3	0.1	<0.1	<0.1	<0.1
Apatite	4.7	6.5	1.6	0.9	1.7	1.9	n.d.	n.d.	0.7	0.4	0.5	1.1
Phosphates	0.1	3.9	n.d.	<0.1	<0.1	<0.1	1.3	0.2	n.d.	n.d.	n.d.	n.d.
Barite	n.d.	n.d.	n.d.	n.d.	n.d.	n.d.	0.1	n.d.	n.d.	n.d.	n.d.	n.d.
Gypsum	0.1	5.2	<0.1	0.2	0.1	1.0	n.d.	n.d.	0.1	n.d.	n.d.	n.d.
Poorly crystalline Fe-sulphate	3.9	4.1	0.8	1.2	1.2	1.2	6.4	5.0	0.1	0.2	<0.1	1.2
Calcite	n.d.	0.2	0.2	0.8	0.6	7.3	n.d.	n.d.	0.4	n.d.	n.d.	n.d.
Dolomite	<0.1	<0.1	n.d.	n.d.	0.7	0.6	n.d.	n.d.	n.d.	n.d.	n.d.	n.d.
Ankerite	n.d.	n.d.	n.d.	0.4	0.3	1.2	n.d.	n.d.	<0.1	n.d.	n.d.	n.d.
Fe-rich cerussite	n.d.	n.d.	n.d.	n.d.	n.d.	n.d.	<0.1	n.d.	n.d.	n.d.	n.d.	n.d.
Pyrite	n.d.	n.d.	n.d.	0.1	n.d.	n.d.	<0.1	0.3	2.2	n.d.	n.d.	n.d.
Galena	n.d.	<0.1	n.d.	n.d.	n.d.	n.d.						
Zircon	n.d.	n.d.	n.d.	n.d.	n.d.	n.d.	<0.1	n.d.	n.d.	<0.1	<0.1	n.d.
Total	100.0											

Abbreviations: n.d., not determined. Phosphates include iron phosphates, crandallite and goyazite/gorceixite. Some quartz may include amorphous silica. Samples 8229 and 8231 also contain Fe-As-phosphate and As-bearing jarosite. Mineral abundances are in wt %.

Appendix 7 – Electron Microprobe Analytical Techniques

The chemical compositions of minerals were analyzed at the University of Alberta using a JEOL 8900 electron microprobe with five wavelength-dispersive spectrometers (WDS). Analyses were performed using 20 nA (for silicates, oxides, sulphides and some phosphates, carbonates and sulphates) and 10 nA (for feldspar, analcime, phosphates, carbonates and sulphates) beam currents, 20 kV accelerating voltage and 1–5 μm beam diameter. Peak and background count times for each element were 20 and 10 seconds, respectively. The following analytical lines and standards were used: $\text{Na}_{K\alpha}$ (albite), $\text{F}_{K\alpha}$ and $\text{P}_{K\alpha}$ (apatite), $\text{Ba}_{L\alpha}$ (barite), $\text{Ce}_{L\alpha}$ (synthetic CePO_4), $\text{La}_{L\alpha}$ (synthetic LaPO_4), $\text{Y}_{L\alpha}$ (synthetic YPO_4), $\text{Cr}_{K\alpha}$ (chromite), $\text{Si}_{K\alpha}$ and $\text{Ca}_{K\alpha}$ (diopside, except for feldspar and analcime analyses), $\text{Mg}_{K\alpha}$ (olivine, Fo_{93}), $\text{Pb}_{M\alpha}$ (synthetic glass #456_Pb), $\text{Fe}_{K\alpha}$ (hematite), $\text{Mn}_{K\alpha}$ (synthetic Mn_2O_3), $\text{Ni}_{K\alpha}$ (metallic nickel), $\text{Al}_{K\alpha}$ (pyrope, except for feldspar and analcime analyses), $\text{Ti}_{K\alpha}$ (rutile), $\text{K}_{K\alpha}$ (sanidine), $\text{S}_{K\alpha}$ and $\text{Zn}_{K\alpha}$ (sphalerite), $\text{Sr}_{L\alpha}$ (strontianite), $\text{Cl}_{K\alpha}$ (tugtupite), $\text{V}_{K\alpha}$ (metallic vanadium) and $\text{Zr}_{L\alpha}$ (zircon). The following standards were employed for feldspar and analcime analyses: plagioclase (Ca) and sanidine (Si and Al). The following peak-overlap corrections were measured using the standards and applied online to all analyses: Sr for Si (0.00420) with positive background check, V for Ti (0.00716), Cr for V (0.11075), Ba for Ti (0.00442), Ti for Ba (0.02185) and Ce for Ba (0.34262). In addition, we observed that 1) Zn and V overlapped with Na and Ce backgrounds, respectively; 2) Ba affected Cr and Ni negative backgrounds; and 3) Sr affected both Ni backgrounds. Therefore, Na and Ni could not be measured in Zn- and Sr-rich minerals, respectively. Data reduction was performed using the $\Phi(\rho Z)$ correction. The instrument calibration was deemed successful when the composition of secondary standards was reproduced within the error margins defined by the counting statistics. Multiple spots per mineral grain were analyzed in tracks across large grains (e.g., phenocrysts) from rim to rim.

Secondary-electron and back-scattered-electron (BSE) images and elemental X-ray maps were obtained using a CAMECA SX 100 electron microprobe in the same laboratory. Operating conditions of the instrument were: 15 kV accelerating voltage, 15–20 nA beam currents and $\sim 1 \mu\text{m}$ beam diameter. The elemental X-ray maps of about 1.0 mm by 1.5 mm area and resolution of $\sim 1 \mu\text{m}$ for $\text{Ca}_{K\alpha}$, $\text{Na}_{K\alpha}$, $\text{K}_{K\alpha}$, $\text{Fe}_{K\alpha}$, $\text{Mg}_{K\alpha}$, $\text{Si}_{K\alpha}$, $\text{Al}_{K\alpha}$, $\text{Ti}_{K\alpha}$, $\text{Ba}_{L\alpha}$ and $\text{Zr}_{L\alpha}$ were obtained using five WDS.

Appendix 8 – Electron Microprobe Data

Appendix 8A

Sample:	8151										8156				8168				
Mineral:	Mica										Amph	Mica				Mica			
Zone:	P-core	P-rim	P-core	P-rim	P-core	P-rim	Grm			Grm	P-core	P-rim	P-core	P-rim	P-core	P-rim	P-core	P-rim	
SiO ₂ (wt. %)	41.79	36.67	41.59	37.03	42.17	36.68	37.13	37.59	38.45	48.70	39.74	35.95	39.76	39.44	38.47	38.25	41.03	40.20	
TiO ₂	1.14	6.71	1.19	6.05	1.31	5.44	5.89	6.27	5.65	6.53	1.50	5.45	1.58	5.09	2.90	4.92	0.97	3.01	
Al ₂ O ₃	12.81	10.69	13.05	10.16	12.54	10.50	11.09	10.96	11.10	1.30	13.39	14.02	13.53	15.42	13.30	13.09	11.76	14.60	
Cr ₂ O ₃	0.78	n.d.	1.35	0.01	0.49	n.d.	n.d.	n.d.	n.d.	n.d.	0.38	n.d.	0.50	n.d.	0.12	0.06	0.77	0.03	
V ₂ O ₃	0.02	0.07	n.d.	0.07	0.02	0.04	0.07	0.09	0.05	0.16	0.03	0.07	0.02	0.07	0.06	0.06	0.02	0.06	
FeO _t	3.89	20.14	4.26	22.98	4.27	14.71	19.01	21.45	14.64	21.85	6.21	12.32	6.25	13.15	10.35	10.99	9.05	10.73	
MnO	0.03	0.22	0.06	0.31	0.05	0.14	0.20	0.24	0.12	0.44	0.04	0.14	0.06	0.14	0.08	0.09	0.07	0.09	
MgO	25.08	12.20	23.65	9.78	25.63	13.43	12.82	9.59	14.91	7.95	23.37	16.56	23.31	13.04	19.22	17.82	21.07	19.07	
NiO	n.d.	n.d.	0.30	0.07	0.10	n.d.	n.d.	n.d.	0.06	n.d.	0.37	n.d.	0.25	n.d.	n.d.	n.d.	n.d.	n.d.	
CaO	n.d.	0.03	0.02	0.03	0.06	3.77	0.01	0.02	0.04	1.75	0.03	0.09	n.d.	0.06	0.01	0.01	0.02	0.03	
Na ₂ O	0.22	0.45	0.32	0.57	0.26	0.47	0.36	0.46	0.45	8.44	0.44	0.52	0.43	0.54	0.65	0.67	0.67	0.64	
K ₂ O	10.11	8.70	8.25	8.80	7.93	8.28	8.81	9.02	9.05	2.37	9.36	8.61	9.51	8.15	9.18	9.00	8.81	9.27	
BaO	0.25	1.54	0.30	1.38	0.21	1.44	1.60	2.08	1.48	0.04	0.40	2.48	0.47	2.29	0.73	0.89	0.23	0.50	
SrO	n.d.	n.d.	n.d.	0.01	0.02	0.19	n.d.	n.d.	0.02	0.31	n.d.								
ZrO ₂	n.d.	n.d.	n.d.	0.03	n.d.	n.d.	n.d.	0.02	0.03	0.35	n.d.	n.d.	n.d.	0.02	0.02	n.d.	0.06	n.d.	
Ce ₂ O ₃	n.d.	n.d.	n.d.	n.d.	n.d.	0.08	n.d.	n.d.	n.d.	0.02	0.05	0.02	0.02	0.02	n.d.	n.d.	n.d.	n.d.	
PbO	0.03	0.01	n.d.	n.d.	n.d.	n.d.	0.01	0.03	n.d.	0.10	n.d.	0.04	0.02	0.07	n.d.	0.05	n.d.	n.d.	
ZnO	n.d.	0.03	n.d.	0.02	n.d.	0.01	0.01	0.04	0.01	0.01	0.01	n.d.	n.d.	0.03	0.01	0.02	0.01	n.d.	
SO ₃	0.04	0.02	n.d.	0.21	n.d.	0.12	0.06	0.14	0.04	0.03	0.02	0.07	n.d.	0.05	0.03	0.05	0.01	0.06	
Cl	0.01	0.03	n.d.	0.04	0.02	0.04	0.03	0.02	0.03	0.03	0.01	0.03	n.d.	0.04	0.04	0.03	0.02	0.04	
F	n.d.	n.d.	n.d.	n.d.	0.01	0.13	n.d.	n.d.	0.01	0.01	0.02	0.01	n.d.	n.d.	n.d.	0.01	n.d.	0.01	
-O ≡ F,Cl	0.00	0.01	—	0.01	0.01	0.06	0.01	0.01	0.01	0.01	0.01	0.01	—	0.01	0.01	0.01	0.00	0.01	
Total	96.20	97.48	94.33	97.54	95.08	95.40	97.09	98.02	96.13	100.38	95.35	96.36	95.70	97.62	95.17	95.99	94.58	98.32	

Structural formulas calculated on the basis of 22 (mica) and 46 (amphibole) positive charges:

Si	2.941	2.796	2.962	2.867	2.965	2.824	2.825	2.879	2.886	7.365	2.860	2.688	2.852	2.870	2.836	2.809	2.994	2.852
Al	1.062	0.961	1.095	0.927	1.039	0.953	0.994	0.989	0.982	0.232	1.136	1.236	1.144	1.322	1.156	1.133	1.012	1.221
Fe ³⁺	—	0.243	—	0.206	—	0.223	0.181	0.131	0.132	—	0.004	0.076	0.004	—	0.008	0.057	—	—
Ti	0.060	0.385	0.064	0.352	0.069	0.315	0.337	0.361	0.319	0.743	0.081	0.307	0.085	0.279	0.161	0.272	0.053	0.161
V	0.001	0.004	—	0.004	0.001	0.002	0.004	0.005	0.003	0.020	0.002	0.004	0.001	0.004	0.003	0.004	0.001	0.004
Cr	0.044	—	0.076	0.001	0.027	—	—	—	—	—	0.022	—	0.028	—	0.007	0.003	0.045	0.001
Zr	—	—	—	0.001	—	—	—	0.001	0.001	0.026	—	—	—	0.001	0.001	—	0.002	—
Ce	—	—	—	—	—	0.002	—	—	—	0.001	0.001	0.001	0.000	0.000	—	—	—	—
Fe ²⁺	0.229	1.042	0.254	1.281	0.251	0.725	1.029	1.243	0.787	2.763	0.369	0.694	0.371	0.800	0.630	0.618	0.552	0.637
Mn	0.002	0.014	0.003	0.020	0.003	0.009	0.013	0.016	0.008	0.057	0.003	0.009	0.004	0.009	0.005	0.006	0.004	0.005
Mg	2.631	1.387	2.511	1.129	2.687	1.542	1.454	1.095	1.669	1.792	2.507	1.846	2.493	1.415	2.113	1.951	2.292	2.017
Zn	—	0.002	—	0.001	—	0.001	0.001	0.002	0.000	0.001	0.000	—	—	0.002	0.001	0.001	0.001	—
Ni	—	—	0.017	0.004	0.006	—	—	—	0.004	—	0.022	—	0.015	—	—	—	—	—
Ca	—	0.002	0.001	0.003	0.004	0.311	0.001	0.001	0.003	0.284	0.002	0.007	—	0.005	0.001	0.001	0.002	0.002
Sr	—	—	—	0.000	0.001	0.009	—	—	0.001	0.027	—	—	—	—	—	—	—	—
Pb	0.001	0.000	—	—	—	—	0.000	0.001	—	0.004	—	0.001	0.000	0.001	—	0.001	—	—
Ba	0.007	0.046	0.008	0.042	0.006	0.043	0.048	0.062	0.044	0.002	0.011	0.073	0.013	0.065	0.021	0.026	0.006	0.014
K	0.908	0.846	0.750	0.869	0.711	0.813	0.855	0.881	0.867	0.457	0.859	0.821	0.870	0.757	0.863	0.843	0.820	0.839
Na	0.030	0.067	0.044	0.085	0.035	0.071	0.053	0.069	0.066	2.475	0.062	0.075	0.059	0.076	0.092	0.095	0.095	0.087
OH ⁻	1.997	1.995	2.000	1.983	1.996	1.956	1.993	1.989	1.991	1.988	1.995	1.990	2.000	1.993	1.994	1.993	1.997	1.990
Cl ⁻	0.001	0.004	—	0.005	0.003	0.005	0.003	0.003	0.004	0.009	0.001	0.003	—	0.005	0.005	0.003	0.003	0.005
F ⁻	—	—	—	—	0.002	0.032	—	—	0.003	0.003	0.003	0.003	—	—	—	0.001	—	0.002
S ²⁻	0.002	0.001	—	0.012	—	0.007	0.003	0.008	0.002	0.004	0.001	0.004	—	0.002	0.002	0.003	0.001	0.003

Abbreviations: n.d., not detected; Amph, amphibole; Grm, groundmass mineral; P-core, phenocryst core; P-rim, phenocryst rim; FeO_t, total iron expressed as FeO.

Fe³⁺ in amphiboles was calculated according to Droop (1987), and in mica assuming that the tetrahedral-site (Si+Al+Fe³⁺) is completely filled.

The content of water (OH) was calculated assuming the (OH+F+Cl) site is completely filled.

gm	8171				8232					
	Mica				Amphibole					
	P-core	P-rim								
41.63	41.61	37.51	40.36	37.59	40.48	38.82	40.54	38.66	39.52	39.43
1.18	1.07	4.75	1.53	4.81	2.35	2.21	2.23	2.09	1.68	2.26
12.15	13.43	13.33	13.23	13.43	13.27	14.00	13.09	14.20	14.38	13.97
0.45	0.79	n.d.	0.09	n.d.	n.d.	n.d.	n.d.	n.d.	n.d.	0.03
0.01	0.02	0.06	0.03	0.06	0.06	0.07	0.07	0.08	0.07	0.08
8.89	4.37	12.15	6.57	11.07	17.08	19.98	16.38	21.99	17.24	19.08
0.08	0.03	0.10	0.04	0.07	0.27	0.35	0.24	0.41	0.23	0.32
20.98	24.10	17.27	22.75	17.72	9.86	7.72	10.44	6.10	9.72	8.27
n.d.	0.04	0.34	0.05	n.d.	n.d.	n.d.	n.d.	0.02	0.04	0.11
0.03	0.04	0.09	0.02	0.09	11.13	11.01	11.09	10.84	11.36	10.91
0.68	0.27	0.39	0.32	0.42	2.28	2.25	2.31	2.30	2.32	2.20
9.14	9.18	8.76	9.65	9.03	2.07	2.13	2.07	2.16	2.02	2.09
0.26	0.25	1.94	0.37	1.86	0.17	0.20	0.19	0.19	0.09	0.20
n.d.	n.d.	0.03	n.d.	0.02	0.09	0.09	0.08	0.09	n.d.	0.05
0.02	0.03	0.01	n.d.	n.d.	n.d.	0.08	n.d.	0.08	n.d.	0.02
0.01	0.01	n.d.	n.d.	n.d.	n.d.	0.01	0.02	n.d.	0.04	n.d.
0.02	0.04	0.02	0.02	n.d.	n.d.	n.d.	n.d.	0.03	n.d.	0.05
0.04	n.d.	n.d.	n.d.	n.d.	0.02	0.02	0.02	0.03	0.03	0.02
0.04	n.d.	0.02	n.d.	0.02	0.04	0.10	0.06	0.11	0.06	0.05
0.05	0.01	0.03	n.d.	0.04	0.03	0.06	0.05	0.08	0.05	0.04
n.d.	n.d.	n.d.	0.01	n.d.	n.d.	0.01	n.d.	0.01	n.d.	0.02
0.01	0.00	0.01	0.00	0.01	0.01	0.02	0.01	0.02	0.01	0.02
95.64	95.28	96.81	95.04	96.23	99.18	99.07	98.85	99.42	98.84	99.17
3.003	2.944	2.771	2.908	2.776	6.038	5.895	6.045	5.917	5.908	5.936
1.033	1.120	1.161	1.123	1.169	2.333	2.506	2.300	2.562	2.534	2.479
—	—	0.068	—	0.055	0.419	0.500	0.472	0.424	0.567	0.539
0.064	0.057	0.264	0.083	0.267	0.264	0.252	0.250	0.241	0.189	0.256
0.001	0.001	0.004	0.002	0.004	0.007	0.009	0.008	0.009	0.009	0.010
0.025	0.044	—	0.005	—	—	—	—	—	—	0.003
0.001	0.001	0.000	—	—	—	0.006	—	0.006	—	0.002
0.000	0.000	—	—	—	—	0.001	0.001	—	0.002	—
0.536	0.259	0.682	0.396	0.629	1.712	2.037	1.571	2.391	1.588	1.863
0.005	0.002	0.007	0.002	0.005	0.034	0.045	0.031	0.053	0.029	0.041
2.256	2.542	1.902	2.444	1.951	2.192	1.748	2.321	1.392	2.166	1.856
0.002	—	—	—	—	0.002	0.002	0.002	0.003	0.003	0.002
—	0.002	0.020	0.003	—	—	—	—	0.002	0.005	0.013
0.002	0.003	0.007	0.001	0.007	1.779	1.791	1.772	1.778	1.820	1.760
—	—	0.001	—	0.001	0.008	0.008	0.007	0.008	—	0.004
0.000	0.001	0.000	0.000	—	—	—	—	0.001	—	0.002
0.007	0.007	0.056	0.010	0.054	0.010	0.012	0.011	0.011	0.005	0.012
0.841	0.829	0.826	0.887	0.851	0.394	0.413	0.394	0.422	0.385	0.401
0.095	0.037	0.056	0.045	0.060	0.659	0.662	0.668	0.683	0.672	0.642
1.992	1.999	1.995	1.998	1.994	1.970	1.948	1.961	1.947	1.956	1.952
0.006	0.001	0.004	—	0.006	0.008	0.015	0.012	0.019	0.012	0.010
—	—	—	0.002	—	—	0.004	—	0.002	—	0.008
0.002	—	0.001	—	0.001	0.004	0.011	0.006	0.013	0.007	0.006

Appendix 8B

Sample:	8151							8156											
Mineral:	Ilmenite				Unidentified Zr-Ti Phase			Titanomagnetite			Clinopyroxene						Titanomagn		
Zone:	Grm	Grm	Grm	Grm	Grm	Grm	Grm	Grm	Grm	Grm	P-core	P-core	P-core	P-rim	P-core	P-rim	Inc	Inc	Grm
SiO ₂ (wt %)	0.63	0.79	0.39	0.79	3.97	2.41	1.33	0.20	0.19	1.53	53.40	51.53	54.76	51.89	52.29	54.49	0.16	0.18	0.25
TiO ₂	51.30	51.19	50.28	52.52	76.68	79.69	88.03	7.43	5.39	6.95	0.29	0.44	0.18	0.81	0.33	0.24	3.62	3.05	7.41
Al ₂ O ₃	0.10	0.11	0.07	0.06	1.29	0.34	0.33	2.38	1.86	2.19	1.47	2.50	0.72	2.20	2.49	0.77	0.73	2.02	0.55
Cr ₂ O ₃	n.d.	n.d.	n.d.	n.d.	0.20	0.17	0.33	2.52	n.d.	0.04	0.20	n.d.	0.24	0.05	n.d.	0.26	0.29	0.50	1.91
V ₂ O ₃	0.14	0.27	0.05	0.02	0.58	0.55	1.01	0.38	0.22	0.40	0.04	0.05	0.01	0.02	0.03	0.02	0.27	0.21	0.32
FeO _t	42.33	39.66	44.41	43.20	3.02	2.47	1.49	78.58	83.45	78.97	5.63	10.21	4.04	7.23	9.21	4.13	86.09	84.17	79.84
MnO	1.09	1.95	1.85	0.78	0.01	0.01	n.d.	0.99	0.74	0.86	0.16	0.30	0.11	0.16	0.26	0.14	0.41	0.45	0.64
MgO	0.06	0.08	0.19	0.05	1.49	0.48	0.29	1.29	0.87	2.15	16.56	12.27	17.27	14.93	13.05	17.69	0.50	2.74	2.19
NiO	n.d.	0.24	0.30	n.d.	0.26	0.52	0.21	n.d.	0.47	0.30	0.30	n.d.	n.d.	n.d.	n.d.	n.d.	n.d.	0.29	n.d.
CaO	0.06	0.04	0.05	0.04	0.83	0.71	0.47	0.09	0.04	0.11	21.01	21.53	22.07	22.17	21.24	21.99	0.06	0.03	0.06
Na ₂ O	0.19	0.16	0.11	0.37	0.45	0.25	0.11	0.08	0.15	0.12	0.44	0.69	0.30	0.46	0.94	0.37	0.13	0.04	0.16
K ₂ O	0.20	0.23	0.12	0.15	0.60	0.25	0.16	0.02	0.08	0.10	n.d.	0.01	0.01	0.03	0.01	n.d.	0.11	0.03	0.01
BaO	0.74	1.43	0.26	0.71	0.26	0.32	0.25	n.d.	0.01	0.01	0.03	0.02	n.d.	0.02	n.d.	n.d.	0.03	n.d.	0.05
SrO	n.d.	0.03	n.d.	n.d.	0.03	0.07	0.01	0.04	n.d.	n.d.	n.d.	n.d.	0.02	0.05	0.02	0.01	n.d.	0.01	n.d.
ZrO ₂	0.38	0.91	0.03	0.05	6.19	7.24	2.12	n.d.	n.d.	0.04	0.10	0.05	0.03	0.16	0.03	n.d.	n.d.	0.01	0.03
Ce ₂ O ₃	n.d.	n.d.	n.d.	n.d.	n.d.	n.d.	n.d.	n.d.	n.d.	n.d.	n.d.	n.d.	0.01	0.01	n.d.	n.d.	n.d.	n.d.	n.d.
PbO	n.d.	n.d.	n.d.	n.d.	0.02	n.d.	n.d.	n.d.	0.04	0.11	0.07	0.02	0.03	n.d.	n.d.	n.d.	n.d.	0.03	n.d.
ZnO	n.d.	0.01	0.02	n.d.	n.d.	n.d.	0.02	0.11	0.10	0.12	0.01	n.d.	0.01	n.d.	0.03	n.d.	0.06	0.06	0.11
SO ₃	0.04	0.01	0.25	0.04	0.12	0.19	0.09	0.02	0.01	n.d.	n.d.	0.01	n.d.	n.d.	0.01	n.d.	0.04	0.04	n.d.
Cl	n.d.	0.02	0.01	0.02	0.02	0.01	0.01	0.01	n.d.	0.02	0.01	n.d.	n.d.	0.01	n.d.	n.d.	n.d.	0.03	n.d.
F	n.d.	0.03	0.01	n.d.	0.08	0.06	0.03	n.d.	n.d.	n.d.	0.01	n.d.	0.01	n.d.	n.d.	n.d.	n.d.	n.d.	n.d.
-O ≡ F,Cl	—	0.01	0.00	0.00	0.04	0.03	0.02	0.00	—	0.00	0.01	—	0.00	0.00	—	—	—	0.01	—
Total	97.26	97.13	98.40	98.77	96.07	95.70	96.27	94.13	93.62	94.01	99.70	99.64	99.82	100.18	99.95	100.11	92.49	93.87	93.53

Structural formulas calculated on the basis of 6 (ilmenite), 8 (titanomagnetite) and 12 (clinopyroxene) positive charges, and one silica cation (titanite):

Si	0.016	0.021	0.010	0.020				0.007	0.007	0.057	1.964	1.937	2.001	1.915	1.945	1.981	0.006	0.007	0.009
S ⁶⁺	—	—	—	—				0.00	0.00	—	—	0.000	—	—	0.000	—	0.001	0.001	—
Al	0.003	0.003	0.002	0.002				0.106	0.083	0.096	0.064	0.111	0.031	0.096	0.109	0.033	0.033	0.088	0.025
Fe ³⁺	—	—	0.049	—				1.381	1.604	1.400	0.014	0.038	—	0.055	0.049	0.010	1.745	1.715	1.479
Ti	1.002	1.007	0.968	1.007				0.210	0.153	0.195	0.008	0.012	0.005	0.022	0.009	0.007	0.105	0.085	0.211
V	0.003	0.006	0.001	0.000				0.011	0.007	0.012	0.001	0.001	0.000	0.001	0.001	0.001	0.008	0.006	0.010
Cr	—	—	—	—				0.075	—	0.001	0.006	—	0.007	0.001	—	0.007	0.009	0.015	0.057
Zr	0.005	0.012	0.000	0.001				—	—	0.001	0.002	0.001	0.000	0.003	0.001	—	—	0.000	0.001
Ce	—	—	—	—				—	—	—	—	—	0.000	0.000	—	—	—	—	—
Fe ²⁺	0.919	0.868	0.902	0.921				1.091	1.038	1.060	0.159	0.283	0.123	0.168	0.237	0.116	1.030	0.901	1.047
Mn	0.024	0.043	0.040	0.017				0.031	0.024	0.027	0.005	0.010	0.004	0.005	0.008	0.004	0.013	0.014	0.021
Mg	0.002	0.003	0.007	0.002				0.073	0.049	0.119	0.908	0.688	0.941	0.822	0.724	0.959	0.029	0.152	0.123
Zn	—	0.000	0.000	—				0.003	0.003	0.003	0.000	—	0.000	—	0.001	—	0.002	0.002	0.003
Ni	—	0.005	0.006	—				—	0.014	0.009	0.009	—	—	—	—	—	—	0.009	—
Ca	0.002	0.001	0.001	0.001				0.004	0.002	0.004	0.828	0.867	0.864	0.877	0.847	0.857	0.002	0.001	0.002
Sr	—	0.000	—	—				0.001	—	—	—	—	0.000	0.001	0.000	0.000	—	0.000	—
Pb	—	—	—	—				—	0.000	0.001	0.001	0.000	0.000	—	—	—	—	0.000	—
Ba	0.007	0.015	0.003	0.007				—	0.000	0.000	0.000	0.000	—	0.000	—	—	0.000	—	0.001
K	0.006	0.008	0.004	0.005				0.001	0.004	0.005	—	0.001	0.001	0.001	0.001	—	0.005	0.002	0.000
Na	0.010	0.008	0.005	0.018				0.005	0.011	0.009	0.031	0.051	0.021	0.033	0.068	0.026	0.010	0.003	0.011
Cl ⁻	—	0.001	0.000	0.001				0.001	—	0.001	0.000	—	—	0.000	—	—	—	0.002	—
F ⁻	—	0.002	0.001	—				—	—	—	0.001	—	0.001	—	—	—	—	—	—
S ²⁻	0.001	0.000	0.005	0.001				—	—	—	—	—	—	—	—	—	—	—	—

Abbreviations: n.d., not detected; Grm, groundmass mineral; Inc, inclusion in mica phenocryst; P-core, phenocryst core; P-rim, phenocryst rim; TiMgt, titanomagnetite; FeO_t, total iron expressed as FeO.

Fe³⁺ was calculated according to Droop (1987).

8168						8171				8232				
etite		Clinopyroxene				TiMgt	Clinopyroxene			Clino-pyroxene		Titanite		
P-rim	P-core	P-core	P-rim	P-core	P-rim	Grm	P-core	P-rim	Grm	P-core	P-rim	Grm	Grm	Grm
0.15	0.22	54.05	53.57	53.17	54.30	0.58	54.33	54.39	54.48	52.62	52.86	29.85	29.92	29.99
7.18	6.01	0.26	0.24	0.37	0.22	8.47	0.21	0.32	0.26	0.33	0.28	34.59	30.41	31.33
0.35	0.40	0.82	1.02	1.29	0.52	1.80	0.59	0.81	0.50	1.61	1.61	1.62	1.58	1.86
1.00	3.64	0.01	n.d.	0.06	0.05	0.23	0.07	0.13	0.03	0.03	0.06	n.d.	n.d.	n.d.
0.30	0.29	0.02	0.04	0.05	0.01	0.36	0.02	0.01	0.01	0.03	0.05	0.05	0.11	0.05
80.91	80.49	6.79	8.42	6.84	3.95	77.99	3.80	3.90	4.02	8.72	9.37	1.89	3.73	3.45
0.70	0.74	0.18	0.28	0.16	0.11	0.74	0.11	0.12	0.15	0.64	0.54	0.16	0.21	0.17
2.09	0.85	15.10	13.76	14.91	16.92	1.73	17.25	17.12	17.45	13.19	12.66	0.07	0.13	0.12
n.d.	0.31	n.d.	n.d.	0.26	n.d.	n.d.	0.48	0.16	n.d.	0.04	0.04	0.26	0.45	0.51
0.04	0.05	21.97	21.69	21.95	22.77	0.38	22.50	22.71	22.57	22.41	22.58	25.96	25.59	25.64
0.03	0.13	0.64	0.93	0.38	0.33	0.24	0.26	0.30	0.20	0.57	0.56	0.05	0.14	0.08
0.04	0.03	n.d.	0.01	0.01	0.01	0.08	0.01	0.03	0.02	n.d.	0.03	0.23	0.09	0.27
n.d.	n.d.	n.d.	0.01	n.d.	n.d.	0.04	n.d.	0.02	0.03	0.02	0.02	n.d.	n.d.	n.d.
0.02	0.02	0.09	0.07	0.04	0.05	0.01	0.02	n.d.	n.d.	n.d.	n.d.	n.d.	n.d.	n.d.
0.05	0.04	0.04	n.d.	0.04	0.05	0.02	n.d.	0.04	0.08	n.d.	n.d.	0.33	1.75	1.03
n.d.	n.d.	n.d.	n.d.	0.04	n.d.	n.d.	n.d.	n.d.	n.d.	n.d.	n.d.	0.71	1.30	1.06
0.13	n.d.	0.06	0.04	0.02	0.06	n.d.	n.d.	0.08	0.07	n.d.	0.02	n.d.	0.05	0.04
0.08	0.10	n.d.	n.d.	0.02	n.d.	0.08	n.d.	0.03	n.d.	0.02	n.d.	0.02	0.02	0.02
n.d.	n.d.	n.d.	0.02	n.d.	n.d.	n.d.	n.d.	n.d.	0.01	0.01	n.d.	n.d.	n.d.	n.d.
n.d.	0.01	n.d.	n.d.	0.01	0.01	n.d.	0.01	0.02	n.d.	0.01	n.d.	0.02	0.15	0.17
n.d.	n.d.	0.01	0.01	n.d.	n.d.	0.01	0.01	n.d.	0.01	n.d.	n.d.	0.03	0.01	n.d.
—	0.00	0.01	0.00	0.00	0.00	0.00	0.00	0.00	0.00	0.00	—	0.02	0.04	0.04
93.06	93.32	100.04	100.12	99.62	99.36	92.73	99.66	100.15	99.87	100.24	100.69	95.81	95.59	95.76
0.006	0.009	1.993	1.986	1.975	1.995	0.022	1.989	1.983	1.991	1.958	1.965	1.000	1.000	1.000
—	—	—	0.001	—	—	—	—	—	0.000	0.000	—	—	—	—
0.016	0.018	0.036	0.045	0.057	0.022	0.080	0.025	0.035	0.022	0.071	0.071	0.064	0.062	0.073
1.524	1.510	0.008	0.039	—	—	1.395	0.002	—	—	0.035	0.021	0.053	0.104	0.096
0.206	0.173	0.007	0.007	0.010	0.006	0.242	0.006	0.009	0.007	0.009	0.008	0.872	0.765	0.786
0.009	0.009	0.001	0.001	0.001	0.000	0.011	0.000	0.000	0.000	0.001	0.002	0.001	0.003	0.001
0.030	0.110	0.000	—	0.002	0.002	0.007	0.002	0.004	0.001	0.001	0.002	—	—	—
0.001	0.001	0.001	—	0.001	0.001	0.000	—	0.001	0.001	—	—	0.005	0.029	0.017
—	—	—	—	0.001	—	—	—	—	—	—	—	0.009	0.016	0.013
1.058	1.072	0.201	0.222	0.212	0.121	1.081	0.114	0.119	0.123	0.237	0.270	—	—	—
0.023	0.024	0.006	0.009	0.005	0.003	0.024	0.003	0.004	0.005	0.020	0.017	0.005	0.006	0.005
0.119	0.048	0.830	0.760	0.826	0.927	0.098	0.941	0.931	0.951	0.732	0.702	0.004	0.007	0.006
0.002	0.003	—	—	0.001	—	0.002	—	0.001	—	0.001	—	0.000	0.000	0.001
—	0.010	—	—	0.008	—	—	0.014	0.005	—	0.001	0.001	0.007	0.012	0.014
0.002	0.002	0.868	0.861	0.874	0.896	0.016	0.883	0.887	0.884	0.894	0.899	0.932	0.916	0.916
0.000	0.000	0.002	0.002	0.001	0.001	0.000	0.001	—	—	—	—	—	—	—
0.001	—	0.001	0.000	0.000	0.001	—	—	0.001	0.001	—	0.000	—	0.000	0.000
—	—	—	0.000	—	—	0.001	—	0.000	0.000	0.000	0.000	—	—	—
0.002	0.002	—	0.001	0.000	0.001	0.004	0.001	0.001	0.001	—	0.001	0.010	0.004	0.012
0.002	0.010	0.046	0.067	0.027	0.024	0.017	0.018	0.021	0.014	0.041	0.040	0.003	0.009	0.005
—	0.001	—	—	0.000	0.000	—	0.001	0.001	—	0.001	—	0.001	0.008	0.010
—	—	0.002	0.001	—	—	0.001	0.001	—	0.001	—	—	0.003	0.001	—
—	—	—	—	—	—	—	—	—	—	—	—	—	—	—

Appendix 8C

Sample	8151													8156			Feldspar-Group Minerals		
	Sanidine				Apatite-Group Minerals					Strontian Barite		Barian Celestine		Sanidine	Analcime		P-core	P-rim	Grm
Mineral	Grm	Grm	Grm	Grm	Grm	Grm	Grm*	Grm	Grm	Grm	Grm	Inc	Inc	Grm	Grm	Grm			
Zone	Grm	Grm	Grm	Grm	Grm	Grm	Grm*	Grm	Grm	Grm	Grm	Inc	Inc	Grm	Grm	Grm	P-core	P-rim	Grm
SiO ₂ (wt %)	62.52	63.44	63.75	62.85	0.79	0.77	0.78	2.50	0.56	0.44	1.72	1.04	1.44	64.78	54.92	55.98	64.75	62.15	61.14
TiO ₂	0.25	0.15	0.19	0.17	n.a.	n.a.	0.02	n.a.	n.a.	n.a.	0.08	0.13	0.10	0.07	0.02	n.d.	0.01	0.09	0.16
Al ₂ O ₃	15.82	16.17	16.07	15.63	0.09	0.02	0.06	0.17	0.05	0.20	0.75	0.34	0.56	18.31	22.49	22.01	18.39	18.93	18.88
FeOt	0.04	0.02	0.06	0.07	2.57	0.22	0.36	4.32	0.38	1.01	0.63	0.50	0.46	0.03	0.01	n.d.	0.01	n.d.	n.d.
MnO	0.02	n.d.	n.d.	0.01	0.03	0.04	0.02	0.04	n.d.	n.d.	n.d.	0.01	0.03	n.d.	0.02	0.01	0.01	0.04	0.03
MgO	0.03	0.02	0.02	0.04	0.30	0.37	0.44	0.33	0.07	0.07	0.14	0.51	0.97	n.d.	0.01	n.d.	0.02	n.d.	0.02
CaO	0.01	n.d.	n.d.	n.d.	46.88	53.75	50.53	27.44	27.91	0.60	0.50	0.82	1.52	0.22	0.02	0.04	0.05	0.04	0.02
SrO	0.12	0.08	0.17	0.11	1.82	0.67	0.96	17.51	25.23	22.11	16.28	40.36	48.69	n.d.	n.d.	0.02	n.d.	0.35	0.31
Na ₂ O	1.15	2.65	1.46	1.72	0.17	n.d.	n.d.	1.61	1.05	0.22	0.32	0.10	0.17	3.13	13.00	12.38	2.30	2.68	2.46
K ₂ O	14.14	12.86	14.25	13.41	0.61	0.11	0.21	0.71	0.20	0.16	0.40	0.36	0.48	11.98	0.04	0.02	13.38	11.16	11.09
BaO	1.36	0.79	0.79	1.32	0.06	n.d.	0.56	0.04	0.07	38.81	44.06	20.71	5.79	0.04	0.03	n.d.	0.32	3.58	4.73
PbO	n.d.	n.d.	0.07	n.d.	0.11	0.01	n.d.	0.02	0.06	n.d.	0.06	0.08	0.08	0.05	n.d.	0.15	0.14	n.d.	0.04
NiO	n.a.	n.a.	n.a.	n.a.	n.a.	n.a.	0.89	n.a.	n.a.	n.a.	n.d.	n.d.	n.d.	n.a.	n.a.	n.a.	n.a.	n.a.	n.a.
ZrO ₂	n.a.	n.a.	n.a.	n.a.	n.a.	n.a.	0.16	n.a.	n.a.	n.a.	n.d.	n.d.	n.d.	n.a.	n.a.	n.a.	n.a.	n.a.	n.a.
La ₂ O ₃	n.a.	n.a.	n.a.	n.a.	0.21	0.07	n.a.	1.59	1.56	0.06	n.a.	n.a.	n.a.	n.a.	n.a.	n.a.	n.a.	n.a.	n.a.
Ce ₂ O ₃	n.a.	n.a.	n.a.	n.a.	0.42	0.27	0.24	3.34	2.86	n.d.	0.10	n.d.	n.d.	n.a.	n.a.	n.a.	n.a.	n.a.	n.a.
Y ₂ O ₃	n.a.	n.a.	n.a.	n.a.	0.01	0.02	n.a.	0.13	0.02	n.d.	n.a.	n.a.	n.a.	n.a.	n.a.	n.a.	n.a.	n.a.	n.a.
P ₂ O ₅	n.a.	n.a.	n.a.	n.a.	37.61	41.02	n.a.	33.62	36.37	0.14	n.a.	n.a.	n.a.	n.a.	n.a.	n.a.	n.a.	n.a.	n.a.
SO ₃	n.d.	0.01	n.d.	0.02	1.70	0.31	0.61	0.99	0.41	31.71	37.75	34.12	35.21	n.d.	n.d.	n.d.	n.d.	0.01	0.01
Cl	0.06	0.17	0.03	n.d.	0.13	0.08	0.08	0.02	0.10	0.04	0.02	n.d.	0.01	n.d.	n.d.	n.d.	n.d.	0.02	n.d.
F	n.d.	n.d.	0.02	n.d.	2.83	3.52	3.60	1.95	1.99	0.02	n.d.	0.02	n.d.	n.d.	n.d.	0.03	n.d.	0.01	n.d.
-O ≡ F,Cl	0.01	0.04	0.02	—	1.22	1.50	1.53	0.83	0.86	0.02	0.00	0.01	0.00	—	—	0.01	—	0.01	—
Total	95.51	96.34	96.87	95.35	95.11	99.76	57.98	95.51	98.03	95.57	102.81	99.11	95.51	98.62	90.55	90.62	99.37	99.05	98.90

Structural formulas calculated on the basis of 8 cations (phosphates), 4 oxygens (sulphates), 2 positive charges (carbonates), and 12 (analcime) and 16 (feldspars)

S ⁶⁺	—	0.000	—	0.001	0.114	0.019	0.040	0.073	0.031	0.925	0.956	0.901	0.897	—	—	—	—	0.000	0.000
P	n.a.	n.a.	n.a.	n.a.	2.852	2.931	n.a.	2.793	3.055	0.005	n.a.								
Si	3.047	3.044	3.052	3.057	0.071	0.065	0.068	0.245	0.055	0.017	0.058	0.037	0.049	2.996	2.030	2.061	2.994	2.937	2.920
Ti	0.009	0.005	0.007	0.006	n.a.	n.a.	0.001	n.a.	n.a.	n.a.	0.002	0.003	0.003	0.003	0.000	—	0.000	0.003	0.006
Zr	n.a.	n.a.	n.a.	n.a.	n.a.	n.a.	0.007	n.a.	n.a.	n.a.	—	—	—	n.a.	n.a.	n.a.	n.a.	n.a.	n.a.
La	n.a.	n.a.	n.a.	n.a.	0.007	0.002	n.a.	0.058	0.057	0.001	n.a.								
Ce	n.a.	n.a.	n.a.	n.a.	0.014	0.008	0.008	0.120	0.104	—	0.001	—	—	n.a.	n.a.	n.a.	n.a.	n.a.	n.a.
Y	n.a.	n.a.	n.a.	n.a.	0.000	0.001	n.a.	0.007	0.001	—	n.a.								
Al	0.909	0.914	0.907	0.896	0.010	0.002	0.006	0.020	0.005	0.009	0.030	0.014	0.022	0.998	0.980	0.955	1.002	1.054	1.063
Fe ³⁺	0.002	0.001	0.003	0.003	—	—	—	—	—	—	—	—	—	0.001	0.000	—	0.000	—	—
Fe ²⁺	—	—	—	—	0.193	0.015	0.026	0.355	0.032	0.033	0.018	0.015	0.013	—	—	—	—	—	—
Mn	0.001	—	—	0.000	0.002	0.003	0.002	0.003	—	—	—	0.000	0.001	—	0.001	0.000	0.000	0.002	0.001
Mg	0.002	0.002	0.001	0.003	0.040	0.047	0.057	0.048	0.010	0.004	0.007	0.027	0.049	—	0.001	—	0.001	—	0.002
Ni	n.a.	n.a.	n.a.	n.a.	n.a.	n.a.	0.063	n.a.	n.a.	n.a.	—	—	—	n.a.	n.a.	n.a.	n.a.	n.a.	n.a.
Ca	0.000	—	—	—	4.499	4.861	4.739	2.885	2.967	0.025	0.018	0.031	0.055	0.011	0.001	0.002	0.002	0.002	0.001
Sr	0.003	0.002	0.005	0.003	0.095	0.033	0.049	0.996	1.451	0.498	0.319	0.824	0.959	—	—	0.000	—	0.009	0.009
Ba	0.026	0.015	0.015	0.025	0.002	—	0.019	0.002	0.003	0.591	0.583	0.286	0.077	0.001	0.000	—	0.006	0.066	0.089
Pb	—	—	0.001	—	0.003	0.000	—	0.000	0.002	—	0.001	0.001	0.001	0.001	—	0.001	0.002	—	0.001
Na	0.109	0.247	0.136	0.162	0.030	—	—	0.306	0.202	0.017	0.021	0.007	0.011	0.281	0.932	0.884	0.206	0.246	0.228
K	0.879	0.787	0.870	0.832	0.069	0.012	0.023	0.089	0.026	0.008	0.017	0.016	0.021	0.707	0.002	0.001	0.789	0.673	0.676
Cl ⁻	0.005	0.014	0.003	—	0.020	0.012	0.011	0.003	0.017	0.003	0.001	—	0.001	—	—	—	—	0.001	—
F ⁻	—	—	0.003	—	0.802	0.940	0.997	0.605	0.624	0.002	—	0.003	—	—	—	0.003	—	0.002	—
OH ⁻	n.a.	n.a.	n.a.	n.a.	0.179	0.049	—	0.392	0.359	n.a.									

* Structural formula for this groundmass fluorapatite analysis was calculated on the basis of 5 M-site cations excluding P (not analyzed), Si and S occupying the T-site in the crystal structure of apatite-group minerals (Deer et al., 1996).

Abbreviations: n.a., not analyzed; n.d., not detected; apatite, fluorapatite; grm, groundmass mineral; inc, inclusion in mica phenocryst; p-core, phenocryst core; p-rim, phenocryst rim; FeOt, total iron calculated as FeO.

The content of water (OH-) was calculated assuming the (OH+F+Cl) site is completely filled.

8168			8171						8232						
Apatite			Ferroan Magnesite			Sanidine		Apatite	Calcite			Feldspar-Group Minerals			Apatite
P-core	P-rim	Grm	P-core	P-core	P-rim	Grm	Grm	P-core	Grm	Inc	P-core	P-core	Grm	P-core	
0.21	0.21	0.45	0.04	0.04	0.05	64.92	63.10	0.09	0.07	0.10	59.11	60.01	65.00	0.29	
n.a.	n.a.	n.a.	n.a.	n.a.	n.a.	0.05	0.11	n.a.	n.d.	n.a.	0.05	0.05	0.04	n.a.	
0.03	0.01	n.d.	n.d.	0.01	n.d.	17.79	18.20	0.02	0.04	0.03	24.42	23.90	18.25	n.d.	
0.16	0.17	0.25	17.00	19.75	26.77	n.d.	0.02	0.05	1.99	1.89	n.d.	0.01	n.d.	0.22	
0.04	0.04	0.06	0.17	0.58	0.55	0.02	0.02	0.08	0.41	0.42	0.02	0.02	n.d.	0.05	
0.26	0.18	0.25	37.57	35.44	29.99	0.01	0.02	0.02	0.32	1.99	0.04	0.02	0.01	0.07	
51.51	51.08	52.42	1.88	1.81	1.96	0.04	0.25	54.25	55.96	50.47	6.16	5.41	0.11	52.69	
1.93	2.63	0.98	n.d.	0.04	n.d.	0.02	0.34	0.05	0.12	0.11	0.61	0.66	0.09	0.14	
0.11	0.15	0.19	0.07	n.d.	n.d.	2.66	2.23	n.d.	0.04	0.08	7.10	6.73	1.22	0.03	
0.01	0.01	0.01	0.01	n.d.	n.d.	12.67	13.02	n.d.	0.01	n.d.	1.06	1.92	14.20	n.d.	
0.01	n.d.	n.d.	n.d.	n.d.	n.d.	0.04	0.47	n.d.	n.d.	0.07	0.54	0.56	0.20	n.d.	
n.d.	0.08	0.02	n.d.	0.04	n.d.	0.01	0.02	0.01	n.d.	0.03	0.05	n.d.	0.01	0.03	
n.a.	n.a.	n.a.	n.a.	n.a.	n.a.	n.a.	n.a.	n.a.	n.d.	n.a.	n.a.	n.a.	n.a.	n.a.	
n.a.	n.a.	n.a.	n.a.	n.a.	n.a.	n.a.	n.a.	n.a.	0.02	n.a.	n.a.	n.a.	n.a.	n.a.	
0.06	0.09	0.03	0.03	0.01	n.d.	n.a.	n.a.	0.07	n.a.	n.d.	n.a.	n.a.	n.a.	0.11	
0.22	0.29	0.19	n.d.	0.02	n.d.	n.a.	n.a.	0.06	0.03	n.d.	n.a.	n.a.	n.a.	0.20	
0.06	0.04	n.d.	n.d.	0.04	n.d.	n.a.	n.a.	n.d.	n.a.	n.d.	n.a.	n.a.	n.a.	0.10	
41.05	40.57	40.12	0.07	0.01	n.d.	n.a.	n.a.	40.95	n.a.	0.07	n.a.	n.a.	n.a.	40.50	
0.11	0.14	0.27	0.05	0.01	0.01	n.d.	n.d.	0.13	n.d.	n.d.	n.d.	n.d.	0.01	0.14	
0.30	0.26	0.27	n.d.	n.d.	n.d.	0.01	n.d.	0.18	0.02	0.01	0.01	n.d.	0.03	0.76	
3.48	3.34	3.48	n.d.	n.d.	n.d.	0.01	0.03	3.62	n.d.	n.d.	0.01	0.01	0.01	3.49	
1.53	1.47	1.53	—	—	—	0.01	0.01	1.57	0.00	0.00	0.01	0.00	0.01	1.64	
98.00	97.82	97.47	56.89	57.80	59.33	98.24	97.80	98.01	59.01	55.27	99.17	99.30	99.17	97.17	

rs) negative charges:

0.007	0.009	0.018	0.001	0.000	0.000	—	—	0.008	—	—	—	—	0.000	0.009
3.012	2.991	2.939	0.001	0.000	—	n.a.	n.a.	2.975	n.a.	0.001	n.a.	n.a.	n.a.	2.989
0.019	0.018	0.039	0.001	0.001	0.001	3.018	2.976	0.008	0.001	0.002	2.683	2.719	3.009	0.026
n.a.	n.a.	n.a.	n.a.	n.a.	n.a.	0.002	0.004	n.a.	—	n.a.	0.002	0.002	0.001	n.a.
n.a.	0.000	n.a.	n.a.	n.a.	n.a.	n.a.								
0.002	0.003	0.001	0.000	0.000	—	n.a.	n.a.	0.002	n.a.	—	n.a.	n.a.	n.a.	0.004
0.007	0.009	0.006	—	0.000	—	n.a.	n.a.	0.002	0.000	—	n.a.	n.a.	n.a.	0.006
0.003	0.002	—	—	0.000	—	n.a.	n.a.	—	n.a.	—	n.a.	n.a.	n.a.	0.004
0.003	0.001	—	—	0.000	—	0.975	1.011	0.002	0.001	0.001	1.306	1.276	0.996	—
—	—	—	—	—	—	—	0.001	—	—	—	—	0.000	—	—
0.012	0.012	0.018	0.196	0.230	0.321	—	—	0.003	0.027	0.027	—	—	—	0.016
0.003	0.003	0.005	0.002	0.007	0.007	0.001	0.001	0.006	0.006	0.006	0.001	0.001	—	0.004
0.033	0.024	0.033	0.772	0.734	0.641	0.001	0.001	0.002	0.008	0.050	0.002	0.002	0.001	0.009
n.a.	—	n.a.	n.a.	n.a.	n.a.	n.a.								
4.784	4.767	4.860	0.028	0.027	0.030	0.002	0.013	4.988	0.955	0.911	0.300	0.263	0.006	4.921
0.097	0.133	0.049	—	0.000	—	0.001	0.009	0.003	0.001	0.001	0.016	0.017	0.002	0.007
0.000	—	—	—	—	—	0.001	0.009	—	—	0.000	0.010	0.010	0.004	—
—	0.002	0.001	—	0.000	—	0.000	0.000	0.000	—	0.000	0.001	—	0.000	0.001
0.018	0.025	0.031	0.002	—	—	0.240	0.204	—	0.001	0.003	0.625	0.591	0.109	0.005
0.001	0.001	0.002	0.000	—	—	0.751	0.783	—	0.000	—	0.062	0.111	0.839	—
0.044	0.039	0.039	—	—	—	0.001	—	0.026	0.000	0.000	0.000	—	0.003	0.112
0.954	0.920	0.952	—	—	—	0.002	0.004	0.983	—	—	0.002	0.001	0.001	0.962
0.002	0.041	0.009	n.a.	n.a.	n.a.	n.a.	n.a.	—	n.a.	n.a.	n.a.	n.a.	n.a.	—

Appendix 9 – Trace-Element Modelling Methodology

The behaviour of trace elements in the fractional-crystallization (FC) process is modelled by the Rayleigh Law (e.g., Allegre et al., 1977) as

$$C_L/C_0 = F^{(D-1)},$$

where C_0 is the concentration of a trace element in the initial magma, C_L is the concentration of a trace element in the derivative magma, F is the fraction of magma remaining and D is the bulk-distribution coefficient for the fractionating mineral assemblage. The bulk-distribution coefficient for the i^{th} element (D_i) is defined by the expression

$$D_i = \sum_{j=1}^n x_j Kd_{ji},$$

where x_j is the proportion of the j^{th} mineral in the fractionating or cumulate assemblage (X_1, X_2, \dots, X_n) and Kd_{ji} is the mineral/melt distribution coefficient for the i^{th} element in the j^{th} mineral (Allegre et al., 1977; Rollinson, 1993). The mineral proportions of the cumulate assemblage are determined by the least-squares mass-balance solutions using major elements (Table 5). The trace-element distribution coefficient (Kd) is a function of pressure, temperature and chemical composition of melt, and is defined as

$$Kd = C_{\text{mineral}}/C_{\text{melt}},$$

where C_{mineral} is the concentration of the trace element in the mineral and C_{melt} is the concentration of the trace element in the melt (McIntire, 1963). Table 6 lists published mineral/melt distribution coefficients applicable to potassic magmas, compiled from the Geochemical Earth Reference Model online database (<http://earthref.org/GERM/index.html>).

DePaolo (1981) presented the following mathematical formulation for trace-element behaviour in the assimilation–fractional crystallization (AFC) process:

$$C_L/C_0 = f' + [r/(r-1+D)] \cdot (1-f') \cdot (C_A/C_0),$$

where r is the ratio of the assimilation rate to the fractional crystallization rate, C_A is the concentration of trace element in the assimilated wall rock, C_0 is the concentration of a trace element in the initial magma, C_L is the concentration of a trace element in the derivative magma and f' is defined by the relation

$$f' = F^{-(r-1+D)/(r-1)},$$

where F is the fraction of magma remaining and D is the bulk-distribution coefficient.